DEVELOPMENT AND EXPLOITATION OF CARBON MATERIALS FROM PLANT SOURCES

A THESIS

submitted by

PULIDINDI INDRA NEEL

for the award of the degree

of

DOCTOR OF PHILOSOPHY

DEPARTMENT OF CHEMISTRY

INDIAN INSTITUTE OF TECHNOLOGY MADRAS

CHENNAI - 600 036, INDIA

DECEMBER, 2009

Dedicated

To

My Saviour and Lord Jesus Christ

My grace is sufficient for thee
II Corinthians 12 : 9

THESIS CERTIFICATE

This is to certify that the thesis entitled **"DEVELOPMENT AND EXPLOITATION OF CARBON MATERIALS FROM PLANT SOURCES"** submitted by **PULIDINDI INDRA NEEL** to the Indian Institute of Technology, Madras for the award of degree of **Doctor of Philosophy** is a bonafide record of research work carried out by him under my supervision. The contents of this thesis, in full or in parts, have not been submitted to any other Institute or University for the award of any degree or diploma.

Dr. T. K. VARADARAJAN

Research Guide

Chennai 600 036

Date:

ACKNOWLEDGEMENTS

ABSTRACT

KEYWORDS: Carbon materials, Heteropoly acids, Mesoporous silica, Gasoline additives, Fuel cell, Mercury adsorption, Adsorptive desulphurization

Synthesis of materials based on carbon has been evolving all the time. In recent times these materials have given rise to a variety of intriguing possibilities in terms of structure, morphology, texture, properties and applications. However, one of the challenging and desired aspects for carbon materials is to find ways of producing these materials from alternate (natural) sources and to tune the textural, structural, morphological and surface properties in relation to the application in mind. Activated carbon materials have been extensively exploited for a variety of applications like purification, separation, storage and as support for catalysts. The choice of the carbon precursor as well as the method of activation are the two crucial issues that determine the quality and the applicability of the activated carbon materials produced.

Activated carbon material with a high specific surface area value ($S_{BET} = 1296$ m^2/g) and uniform properties through out the material has been developed using a widely available carbon precursor, the stems of *Calotropis gigantea (Cg)*. Among different activating agents used, K_2CO_3 was found to yield carbon material (Cg carbonate 3) with superior textural properties compared to commercial activated carbon materials (Calgon and Adsorbent carbons). The carbon material, Cg carbonate 3, was employed as a support for heteropoly acid (HPW) and the supported solid acid catalyst was exploited for the production of tert-amyl methyl ether (TAME), a preferred gasoline additive. The flower spikes of *Borassus flabellifera* (Bf) were exploited as precursor for the production of

activated carbon material (C_{Bf} carbonate 1, S_{BET} = 1070 m^2/g). The carbon material thus obtained was used as support for HPW and subsequently exploited as a solid acid catalyst for the synthesis of methyl tert-butyl ether, MTBE, a well known gasoline additive. *Limonea acidissima* (Wood Apple, WA) shells were employed as carbon precursor for generating activated carbon material (S_{BET} = m^2/g) using KOH as activating agent and the same was used as support for Pt to produce Pt/C_{WA} catalyst. The catalyst Pt/C_{WA} was employed for the fabrication of anode of DMFC for the electro-oxidation of methanol. The electro-catalytic activity and stability of Pt/C_{WA} catalyst were evaluated from cyclic voltammetric and chronoamperometric studies respectively. Pt/C_{WA} catalyst exhibited better performance (improved CO tolerance and methanol oxidation current) compared to the commercial Pt/Vulcan XC 72 R catalyst.

In an attempt to develop low cost and environmentally benign sorbent for the sorption of mercury, the stems of *Ipomoea carnea* (C_{IC}), were employed as carbon precursor for the production of activated carbon. S/Hydrazine solution was used as S precursor for functionalizing carbon material with S. S functionalization (formation of C=S groups on carbon surface) has enhanced the Hg (II) sorption. The equilibrium adsorption data obtained for Hg (II) was analysed and interpreted using Freundlich and Langmuir adsorption models. The experimental adsorption data fitted well with both Freundlich (K_F = 8.3, 1/n = 0.51, R = 0.9832) and Langmuir (q_m = 55.6, b = 0.095, R_L = 0.51, R = 0.9575) adsorption models. The S functionalized carbon material has out performed various sorbents like activated carbon from *Cieba pentandra hulls*, *Phaseolus aureus hulls*, *Cicer arietinum*, Sago waste, Balluca coal, Charcoal from camel bone, clay and

vulcanized rubber. An attempt was made to develop a regenerable carbon based adsorbent to reduce S in SR diesel (CBR) from about 737 ppm to less than 200 ppm adopting the process of adsorptive desulphurization operated at ambient temperature and pressure. Among several carbon materials, calgon and adsorbent carbons showed better performance for the sorption of S compounds in the SR diesel. To further enhance the sorption of S compounds, the calgon and adsorbent carbon materials were treated with conc. HNO_3 and also subjected to thermal activation in Ar atmosphere resulting in suitable surface functionality, phase structure and pore texture for the sorption of organo-sulphur compounds. The S content of the product was analysed by using an Oxford XRF analyzer. The feed and the product diesel were also analyzed for individual sulphur compounds using a GC-PFPD. In addition to the reduction in the S content of the diesel feed to the target specifications, it was also observed that the most highly refractive compounds (C_2BT and C_2DBT) present in the feed prior to the desulphurization process were absent in the product diesel. This exemplifies the usefulness of the process in selectively adsorbing the refractory S-compounds that are difficult to desulphrize over conventional hydrotreating catalysts.

Thus, developing activated carbon materials with desired properties for energy and environmental applications has been the focus of the present work.

TABLE OF CONTENTS

CHAPTER 1   INTRODUCTION

CHAPTER 2 EXPERIMENTAL METHODOLOGY

**CHAPTER 3 CARBON MATERIALS FROM *CALOTROPIS GIGANTEA* STEMS
FOR CATALYTIC APPLICATION**

Table of Contents (Contd.)   **Page No.**

**CHAPTER 4 CARBON MATERIALS FROM *BORASSUS FLABELLIFERA*
FOR CATALYTIC APPLICATION**

Table of Contents (contd.).. **Page No.**

CHAPTER 5 CARBON MATERIALS FROM *LIMONEA ACIDISSIMA* SHELLS FOR ELECTRO CATALYTIC APPLICATION

Table of Contents (contd.).. …..**Page No.**

CHAPTER 6 CARBON MATERIALS FROM *IPOMOEA CARNEA* STEMS FOR MERCURY SORPTION

CHAPTER 7   CARBON MATERIALS FOR ADSORPTIVE
          DESULPHURIZATION

LIST OF TABLES

List of Tables (contd.)

LIST OF FIGURES

List of Figures (contd.)

List of Figures (contd.)

List of Figures (contd.)

List of Figures (contd.)

List of Figures (contd.)

List of Figures (contd.)

List of Figures (contd.)

List of Figures (contd.)

LIST OF SCHEMES

ABBREVIATIONS

BET	:	Brunauer-Emmett-Teller
CTMAB	:	Cetyl tri methyl ammonium bromide
CTEAB	:	Cetyl tri ethyl ammonium bromide
CBR	:	Cauvery Basin Refinery
C_2BT	:	Di alkyl substituted benzo thiophene
C_2DBT	:	Di alkyl substituted dibenzo thiophene
DMDBT	:	Di methyl di benzo thiophene
DMFC	:	Direct Methanol Fuel Cell
DPPH	:	Di phenyl picryl hydrazyl radical
EDAX	:	Energy dispersive X-ray Analysis
EPR	:	Electron Paramagnetic Resonance Spectroscopy
ETBE	:	Ethyl tert butyl ether
FT-IR	:	Fourier Transform Infrared
FWHM	:	Full width at half maxima
GC-PFPD	:	Gas Chromatography coupled with Pulsed Flame Photometer Detector
HDN	:	Hydro denitrogenation
HDS	:	Hydro desulphurization
HPA	:	Heteropoly acid
HPAN	:	Heteropoly anion
HPW	:	Dodeca tungsto phosphoric acid
HYD	:	Hydrogenation
MAS NMR	:	Magic Angle Spinning Nuclear Magnetic Resonance Spectroscopy
MCHT	:	Methyl cyclo hexyl toluene
MTBE	:	Methyl tert butyl ether
PEMFC	:	Proton Exchange Membrane Fuel Cell
PSD	:	Pore size distribution
S_{BET}	:	Specific surface area deduced from BET method
SBA	:	Santa Barbara Amorphous
SEM	:	Scanning Electron Microscopy
TAA	:	Tert amyl alcohol

TAME   : Tert amyl methyl ether

TAEE   : Tert amyl ethyl ether

TBA   : Tert butyl alcohol

TEOS   : Tetra ethyl ortho silicate

TG/DTA   : Thermogravimetric/Differential Thermal Analyzer

TPD   : Temperature programmed desorption

UV-vis   : Ultra violet visible spectroscopy

XRD   : X-ray diffraction

XRF   : X-ray fluorescence spectroscopy

NOTATIONS

P	: Adsorption pressure
P_0	: Saturation vapour pressure
λ	: Wave length of radiation
θ	: Diffraction angle for the peak position
Lc	: Average crystallite size along the c-axis
La	: Average crystallite size along the a-axis
K	: Shape factor
K	: Degree Kelvin
V	: Volt
A	: Ampere
P	: Plank constant
βe	: Bohr magneton of electron
H	: Magnetic field strength
ΔH	: Peak to peak separation
ν	: Micro wave frequency
N	: Spin concentration
S	: Spin number
M	: Modulation amplitude
g	: g factor of EPR signal
G	: Relative gain of the signal amplifier
h	: Hour
g	: Gram
mL	: Milli liter
C_0	: Initial concentration
C_e	: Residual concentration
R	: % Removal
K_F	: Freundlich constant (sorption capacity)
n	: Freundlich constant (sorption intensity)
q_e	: Langmuir constant (adsorption capacity)
b	: Langmuir constant (energy of adsorption)

CHAPTER - 1

INTRODUCTION

1.1 CARBON MATERIALS

Carbon materials are unique and versatile in their performance. They have major industrial significance. Typical advantages of the use of activated carbon materials include: effluent with specific standard is achievable, simplicity of the process design and ease of operation. In addition, the carbon materials being insensitive to toxic substances and corrosive (acidic and basic) environments, the regeneration is possible and easy, rendering the industrial use of activated carbon materials an economically viable option (Wang *et al*., 2008; Chen *et al*., 2002). The specific physico-chemical properties that make activated carbon materials a potential adsorbent for pollutants include: high specific surface area, porous architecture, high adsorption capacity and surface functionality (Merzougui and Addoun, 2008). Activated carbon materials, characterized by high specific surface area and tunable porosity, find utility in many vital technologies, namely, energy storage (super capacitors, batteries and hydrogen sorption), energy conversion (fuel cells and solar cells), sensors, environmental protection (regulate SO_x and NO_x emissions from fuel combustion in automobiles), production of fine and bulk chemicals and catalysis. Activated carbon is a material with highly porous structure consisting of hydrophobic graphene layer as well as hydrophilic surface functional groups making them beneficial for sorption and catalytic applications. Specific industrial applications include areas such as oil and natural gas, food, pharmaceuticals, water treatment, hydro

metallurgy and gold recovery (carbon-in-pulp, CIP, process) (Soleimani and Kaghazchi, 2008a).

Activated carbon materials are effective in removing pollutants (both gaseous and liquid). In addition to purification of gases and liquids with high adsorption potential, activated carbon materials are also used as catalysts and catalyst supports. Carbon materials play an indispensable role in almost all electrochemical devices, namely, batteries (Endo *et al.*, 2000), super capacitors (Pandolfo and Hollenkamp, 2006) and fuel cells (Dicks, 2006). The choice of carbon as the material is because of its unique properties of electrical conductivity and structural diversity. The structure of a typical microporous activated carbon is shown in Fig. 1.1. Microporous carbon materials are highly disordered. In general, the structure comprises of aromatic sheets and strips. Such sheets are often bent imitating crumpled papers and wood shavings. The voids and gaps, of molecular dimensions, between such aromatic sheets are regarded as micropores. Again the microporosity is dependent on the carbon precursor as well as the method of preparation (Stoeckli, 1990).

Fig. 1.1 Structure of activated carbon - A schematic representation (Stoeckli, 1990)

The demand for activated carbon is increasing owing to the increased utility of the carbon materials in pollution control. As a result, cost of activated carbon is also growing precluding the application. Designing ways for the production of activated carbon through economic ways is necessary. A range of low cost, easily available, carbon rich and low ash precursors and sources are being explored for the production of carbon materials.

1.1.1 Sources of activated carbon materials

Most of the commercial activated carbons are either coal based (Kruk *et al*., 2005; Lu and Zheng, 2001) or petroleum pitch based (Hayashi *et al*., 2000) which are prone to exhaustion. Their global distribution is non-uniform. As the applications of activated carbon are immense, the gap between demand and supply is ever widening. This may in due course result in scarcity of the material in addition to becoming expensive. This situation necessitates the need for the exploration of new sources of carbon materials with desired physico-chemical properties, namely, high specific surface area, micro or mesoporosity or both depending on the end application, surface functionality, thermal stability, carbon purity, adsorptive capacity and chemical composition.

Lignocellulosic materials have been and will be with mankind for ever and they hold a promise of renewable and inexhaustible supply of carbon materials provided suitable methods of production are developed.   In addition, they are more evenly distributed throughout the globe relative to either coal or petroleum. Thus, the lignocellulosic material, a regenerable natural resource, is a viable option for the

3

generation of carbon materials rather than fossil fuels. It is interesting to note that carbon has come to the rescue of even Thomas Alwa Edison, the greatest inventor of modern times, in his backbreaking toilsome efforts to invent high-resistance incandescent lamp, where in either Pt or Pt-Ir alloy failed to provide an antidote. Surprisingly, the carbon filament used was from biomass (Dickinson, 1937).

In the biological lignocellulosic material the carbohydrate (holo cellulose and cellulose) component is intimately bound to lignin. Lignin is a 3-dimensional cross linked aromatic polymer with phenyl propane units (Rials and Glasser, 1989). Next to cellulose, lignin is the major constituent of plant cell wall. Lignin possesses a complicated chemical structure with both phenolic (aromatic) as well as alcoholic (aliphatic) hydroxyl groups being present in the structure (Kubo *et al*., 1989). The main repeating unit of lignin is 3-(4-hydroxy phenyl) prop-2-eneol. Lignin is an aromatic amorphous biopolymer deposited as a reinforcing agent in plants offering mechanical support to the fibrous tissues of the plant (Sarkar and Adhikari, 2001). Thus, the main function of lignin is to impart strength and rigidity to the cell wall by acting as structural matrix. The carbon precursor as well as the method of preparation are determining factors for the textural and surface properties of carbon materials (Olivares - Marin *et al*., 2006). Taking into consideration some specific properties, like volatile matter, ash content and fixed carbon content as well as the derivable porosity, several researchers have studied the possibility of producing carbon materials from different lignocellulosic materials.

Ganan *et al*., (2006) have employed *Almond tree pruning* as precursor for producing activated carbon (S_{BET} – 959 m^2/g). A two step process of activation comprising of pyrolysis followed by catalytic air oxidation is employed. Oxides of Co and K were used as catalysts. Kazemipour *et al*., (2008) have employed *Almond (Amygodolus) shells, Apricot (Armeniaca bulgar) stones, Hazel nut (Corylus avellana), Pistacio (Pistaca) and Walnut (Jouglans regia)* as precursors for producing activated carbon materials with S_{BET} values of 1208, 861, 786, 635 and 941 m^2/g by the method of carbonization in inert atmosphere at 1073 K. The activated carbon materials from Almond shell, hazel nut and walnut were effective in the removal of 99.8 % Cu, 96.9 % Pb and 71% Zn respectively from industrial effluent water. Onal *et al*., (2007) have employed *Apricot stones* as precursor for producing activated carbon (S_{BET} – 1060 m^2/g) using $ZnCl_2$ as activating agent. The activated carbon thus produced was found to be an effective sorbent for naproxen sodium (maximum sorption capacity – 49.75 mg/g of carbon). Demirbas *et al*., (2008) have employed *Apricot stones* as precursor for producing activated carbon (S_{BET} – 560 m^2/g) at an activation temperature of 523 K in an air oven using H_2SO_4 as activating agent. The carbon material thus produced was effective in the sorption of astrazon yellow 7GL, a basic dye (adsorption capacity – 221 mg/g of carbon material). Soleimani and Kaghazchi (2008b) have produced activated carbon with a S_{BET} of 1387 m^2/g from *Apricot stone* using H_3PO_4 as activating agent. The carbon material was found to be an effective sorbent for the removal (98 % removal achieved) of gold from industrial (gold-plating) waste water. Sentorun-Shalaby *et al*., (2006) have produced activated carbon (S_{BET} – 1092 m^2/g) from *Apricot (Kabaasi) stones* using steam activation at an activation temperature of 1073 K. An inverse relationship between the S content of the carbon

precursor and the S_{BET} values was observed. The decrease in the surface area with an increase in S content was attributed to the enhanced gasification rate of the carbon material because of the presence of increased surface functional groups upon SO_2 pretreatment of the carbon precursor.

Kobya *et al*., (2005) have prepared activated carbon from *Apricot stones* using sulphuric acid as activating agent at an activation temperature of 473 K. The material (S_{BET} – 566 m^2/g) thus obtained was found to be effective in the removal of heavy metals like Cr (VI) (99.99 % at pH = 1), Cd (II) (99.68 at pH = 6), Co (II) (99.11 % at pH = 6), Cr (III) (98.99 % at pH = 6), Ni (II) (98.51 % at pH = 6), Cu (II) (97.48 % at pH = 6) and Pb (II) (99.93 % at pH = 6) from industrial waste water. Hameed *et al*., (2007) have employed *Bamboo (bambusoidae)* for producing activated carbon by adopting a physico-chemical method of activation using KOH as well as CO_2 as activating agents at an activation temperature of 1123 K. The activated carbon material with S_{BET}, total pore volume (V_p) and a pore diameter values of 1896 m^2/g, 1.109 cm^3/g and 2.34 nm was effective in the sorption of methylene blue (454.2 mg/g). Kim *et al*., (2006) have produced activated carbon from *Bamboo* using KOH activation method at 1073 K in Ar atmosphere. The activated carbon produced exhibited potential as electrode material for electric double layer capacitors. The carbon material (produced with a char to KOH (wt./wt.%) ratio of 1:3) with S_{BET} value of 894 m^2/g and the highest mesopore to micropore fraction showed the maximum value of specific capacitance. The higher capacitance was attributed to the better mobility of the electrolyte ions in the presence of larger pores (mesopores). Mohan *et al*., (2006) have employed *coconut shell fiber* as a precursor for producing activated

6

carbon (S_{BET} – 512 m^2/g) using H_2SO_4 as well as thermal means to activate the material. The activated carbon material thus produced was found to be effective in the removal of Cr (III) (sorption capacity – 16.1 mg/g). Macedo *et al*., (2008) have employed *coir pith, coir fiber and endocarp from coconut shell* to generate activated carbon material using physicochemical activation process. $ZnCl_2$ as well as CO_2 was used as activating agents at 1073 K in N_2 atm. The activated carbon produced from coir pith possessed S_{BET} value of 1880 m^2/g where as those carbon materials from coir fiber and endocarp exhibited S_{BET} value of only up to 540 m^2/g. Girgis *et al*., (2007) have employed *Peach stone shells* as precursor for producing activated carbon materials (S_{BET} – 1053 – 1404 m^2/g) using H_3PO_4 as activating agent. The carbon materials exhibited promising sorption capacities for *p*-nitro phenol (435 mg/g), methylene blue (543 mg/g) and Pb^{2+} ions (204 mg/g). Tseng and Tseng (2006) have produced activated carbon material (S_{BET} – 2300 m^2/g) from the cane pith of *sugar cane (Saccharum Officinarum)* through activation with KOH at 1053 K in N_2 atm. The high specific surface area was attributed to the catalytic smelting action of KOH which is analogous to the fermentation of flour. The carbon material showed promise in the sorption of dyes such as acid blue 74, methylene blue and basic crown.

In addition to the afore mentioned biomass sources, several other lignocellulosic materials, namely, apple pulp (Suarez-Garcia *et al*., 2002; Centeno and Stoeckli, 2006), cane bagesse (Syna and Valix, 2003; Gokam and Sankpal, 2000), corn cob (Vaughan *et al*., 2001; Cao *et al*., 2006), coconut shell (Achaw and Afrane, 2008; Li *et al*., 2008; Li *et al*., 2009) corn stalks (Zhang et al., 2008), date pits (Merzougui and Addoun, 2008; Al-

Muhtaseb *et al*., 2008), eucalyptus wood (Rocha *et al*., 2002), guava seeds (Rahman *et al*., 2003), oat hulls (Fan *et al*., 2004; Chuang *et al*., 2005), olive-stone (Rodriguez *et al*., 2008; Ugurlu *et al*., 2008), pea nut hulls (Girgis et al., 2002), pecan shell (Dastgheib and Rockstraw, 2001), pine wood (Yalcin and Sevinc, 2000), rice husk (Guo *et al*., 2005; Kalderis *et al*., 2008), rice straw (Yun *et al*., 2001; Wang *et al*., 2007; Daifullah *et al*., 2007), rock rose (Gomez-*Serrano et al.*, 1996; Pastor-Villegas and Duran-Valle, 2002), saw dust (Malik, 2004; Ismadji *et al*., 2005) and walnut wood (Gomez-Sarrano *et al*., 2005) have also been exploited by researchers for producing activating carbon materials.

1.1.2 Reactions leading to char formation from lignocellulosic carbon precursor

During pyrolytic decomposition of lignin and cellulose certain reactions result in the scission of chemical bonds leading to the fragmentation and also depolymerization of parent polymer. In addition to bond scission, formation of new bonds too takes place. Such creation of new bonds will stabilize the adjacent carbon atoms there by resulting in the formation of a non-volatile and stable carbon framework. Certain fragments formed during pyrolysis evolve as volatile products where as the other fragments gets reconnected to the carbon framework undergoing thermal reformation to form char (Makay and Roberts, 1982).

1.1.3 The factors that affect the char yield and carbon content of the activated carbon

In general, the terrestrial plants can be classified into three taxonomic groups. They are: soft wood trees, hard wood trees and the grasses. Plant tissue is made up of

lignocellulosic material. The lignocellulosic material consists of plant cell wall and also the intra cellular substances. The cell wall is made up of holocellulose which is a combination of cellulose and hemicellulose and lignin. The intracellular substances are termed as extractives based on the analytical method of extraction. The afore mentioned components, namely, lignin, cellulose and extractives are known to vary in chemical structure and initial carbon content. The cellulose is a linear polymer of glucose with a theoretical carbon content of 44.4 %. Lignin is a three dimensional polymer of aromatic alcohols with a carbon content of 60 – 63 %. As a result, the carbon content of a lignocellulosic material is dependent on the relative abundance of its constituents. Thus, it can be said that greater the carbon content of the lignocellulosic precursor greater will be the carbon content of the char. The carbon yield obtained from extractives lies between the yields obtainable from lignin and cellulose. Most of the extractives, intra cellular material, contain compounds analogous to lignin, but of relatively smaller molecular weight, and are usually termed as Brawn's lignins. Also some of the components of extractives like terpenes are relatively volatile and do not contribute to char formation during pyrolysis. Thus, the yield of carbon from each component is directly related to the carbon content of the respective components. Holocellulosic fraction with lowest carbon content results in lowest carbon yield where as lignin with the highest carbon content exhibits highest carbon yield. Thus the carbon yield upon pyrolysis of lignocellulosic material is dependent on the composition of the precursor material. In general, greater the aromaticity and molecular weight of the precursor, greater will be the char yield. The low carbon yield in the case of cellulose is due to the fact that significant amount of carbon is lost from the glucose derivatives due to

9

volatilization and as a result the char yield is low. The high yield of carbon in the case of lignin is because of the high aromatic content as well as the complex polymer structure of lignin. Interestingly, the char yield from cellulose is known to be enhanced by the presence of inorganic compounds (mineral matter). In plants Na^+ and K^+ ions are of physiological important. Plant cells are intelligent in differentiating Na^+ and K^+ by some complexing mechanism (Cotton and Wilkinson, 1976).

Increasing the inorganic content upto $2 – 15$ % (catalytic saturation limit) increases the char yield. The crystallinity of cellulose also affects the char yield. In the lignocellulosic materials, cellulose is known to be present in both crystalline and amorphous phases and the char yield was found to be higher with crystalline cellulose. Unlike cellulose, hemicellulose is only amorphous. The initial carbon content, the char yield and carbon yield from lignin were respectively 63, 53 and 76 %. On the contrary, the carbon content, the char yield and carbon yield from cellulose were 44, 18 and 40 % (Makay and Roberts, 1982). Thus, lignin contributes to higher carbon content to the activated carbon compared to cellulose.

1.1.4 Transformation of cellulose and lignin into condensed aromatic system

Tang and Bacon (1964) have provided a detailed reaction mechanism for the transformation of cellulose into a condensed aromatic system and is illustrated in Fig. 1.2. Cellulose is known to undergo thermal decomposition without the presence of a melting state resulting in the formation of a strong carbonaceous reside. The process of aromatization of cellulose involves four crucial stages. During state I, physisorbed water

molecules are removed in the temperature range of 298 – 423 K. Such a desorption of physisorbed water increases the degree of lateral order. In stage II, the structural water, involving hydrogen and hydroxyl moieties in the equatorial position, is stripped off from the cellulose in the temperature range of 423 – 513 K due to thermal excitation. Such dehydration process is essentially intramolecular. Major thermal degradation of cellulosic structure takes place in stage III at temperature above 513 K. Thermal scission of C-O and C-C bonds as well as dehydration takes place in stage III-a in the temperature range of 513 – 673 K yielding tar as well as a par of carbonaceous residue. Tar formation is supposed to be through Levoglucosan. Upon pyrolytic decomposition cellulose depolymerizes through the scission of 1, 4 glycosidic linkage. The subsequent intra molecular rearrangement of cellulosic units results in the formation of levoglucosan which leads to the formation of tar. Even though the tarry portion is a complex mixture, the main constituent of the tar was indentified to be dehydrated cellulose (mass = 144). The final breaking down of each of the cellulosic ring units takes place in Stage III c resulting in the formation of carbon residue containing four – carbon atoms (nos. 3, 4, 5 and 6).

Thus four of the six carbon atoms in each glucose monomer are retained in the char. Such four carbon atom intermediates, a very – short lived radical species, serve as "building blocks" for the repolymerization forming carbon polymer and subsequently a graphitic structure in Stage IV in the temperature range of 673 – 973 K. Both cellulose and lignin contribute to aromatic carbon content. But the precursors containing hexagonally arrayed carbon, as those found in lignin, would readily reform to stable graphitic arrays. In the case of cellulose such structural advantage is missing.
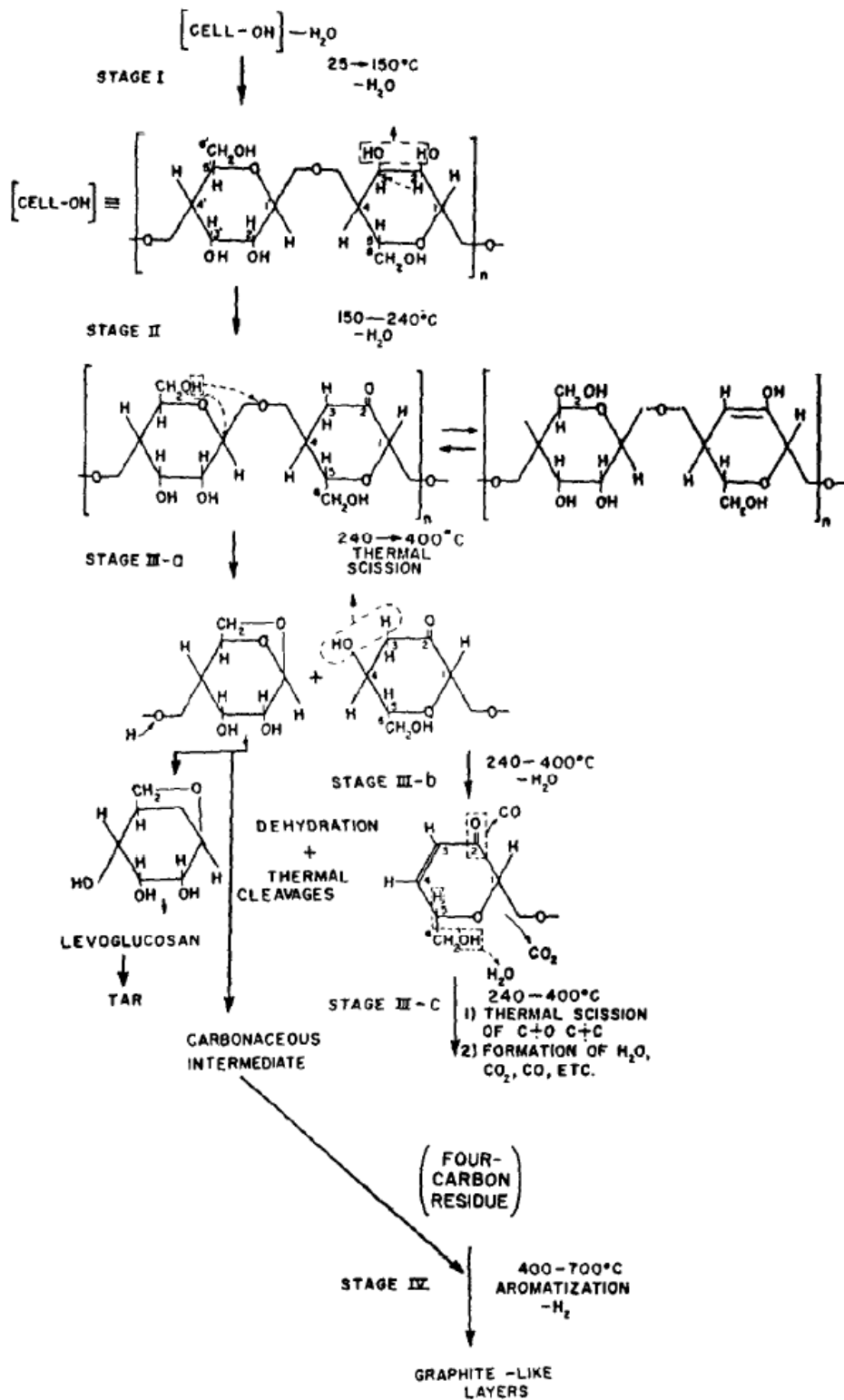
Fig. 1.2 Proposed mechanism for the transformation of cellulose to aromatic carbon (Tang and Bacon, 1964)
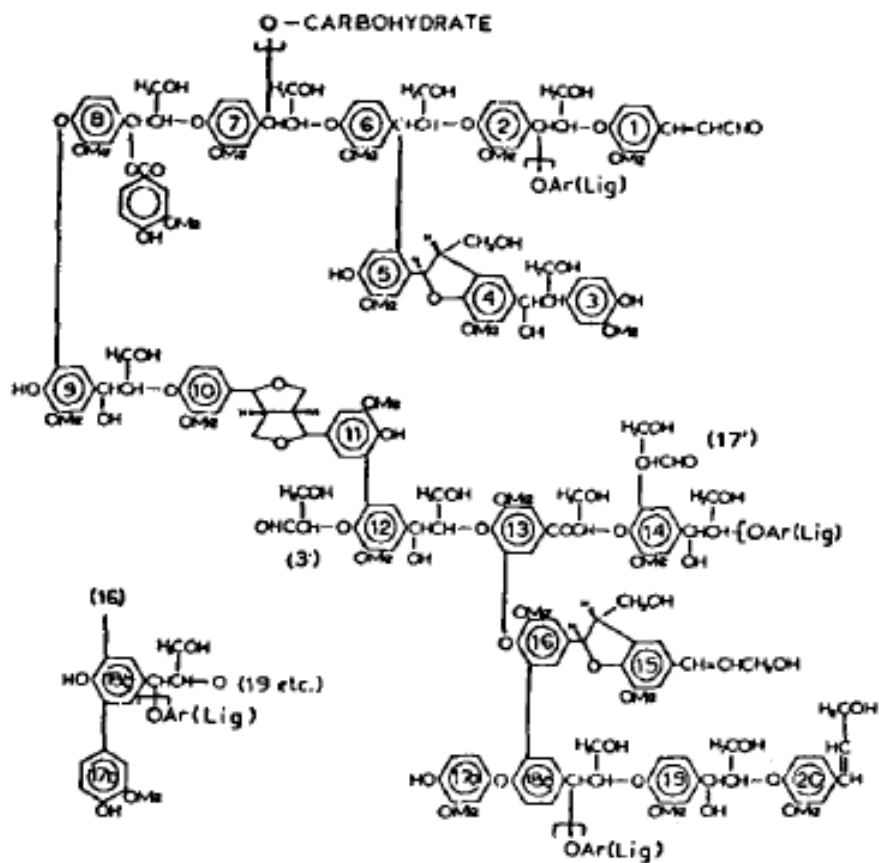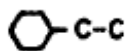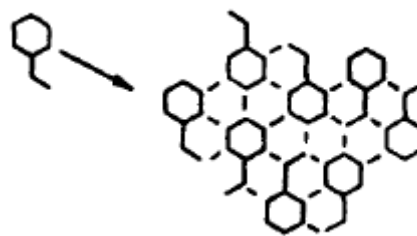
Fig. 1.3 Conceptual mechanism for the transformation of lignin to aromatic carbon: (a) typical structure of lignin, (b) basic building block of lignin structure and (c) conceptual geometry for the formation of graphite like layer from the structural units formed during pyrolysis (Makay and Roberts, 1982)

Mackay and Roberts (1982) have proposed a conceptual mechanism of aromatization of lignin upon pyrolysis as represented in Fig 1.3. The structure of lignin comprises of

13

inherent and inbuilt aromatic building blocks. Such subunits are geometrically well suited for the formation of condensed aromatic system as shown in Fig. 1.3 (c).

1.1.5 Suitable lignocellulosic materials for the production of activated carbon materials

Heschel and Klose (1995) have evaluated several lignocellulosic materials, namely, cherry stones, coconut shells, hazel nuts, peach stones, plum stones and walnut shells, to derive information regarding the specific properties of the parent lignocellulosic materials that determine their suitability for the production of activated carbon. Wood materials with a coarse cellular structure with inherent porosities greater than 35 % were found to be disadvantageous in terms of poor mechanical strength of the activated carbon derivable from such materials. Mechanical stability of the activated carbon material is desirable because sorption properties namely, adsorption capacity, hardness and granularity are mechanical strength dependent. In addition to the nature of the precursor material, the conditions of preparation have a bearing on the properties (porosity, hardness and density) of the activated carbon material. The structure of the raw material as well as the production process govern the adsorption properties of activated carbon produced. Raw materials that offer cokes with resistance to abrasion, low macroporosity and high yield are, in general, preferred and are suitable sources for the production of activated carbon. Among the materials investigated, woods are found to be of highest porosity (46 – 49 %) and nut shells and fruit stones were of lower porosity. No correlation was observed between the porosity and the chemical composition (O/C atomic ratio) of raw material where as the chemical composition of the precursor has a

bearing on the coke yield obtainable. The coke yield increased with an increase in the lignin content of the precursor. This is because lignin contains lower amount of structural oxygen compared to hemicellulose or cellulose. No correlation was found between the hardness and the O/C ratio of the coke implying that the suitability of the lignocellulosic material should not be assessed based on the O/C ratio alone. Rather the cell structure (porosity) of the plant is an important parameter in the choice of lignocellulosic materials. The morphology of the plant cell is the main factor responsible for the hardness, density and the porosity of the coke. Thus, the morphology of the plant cell with peculiar cross linking between cellulose, hemicellulose and lignin determines whether a particular lignocellulosic material is suitable for the production of activated carbon. In essence, for a lignocellulosic material to be chosen as precursor for activated carbon, the inherent porosity of the raw material should not be greater than 35 %. Also upon pyrolysis the ratio of mass loss (Δm) to volume shrinkage (ΔV) should be close to 1. Among the raw materials investigated, the order of suitability for the production of activated carbon is as follows: coconut shells > peach stones > plum stones > hezel nut shells > walnut shells > cherry stones.

1.1.6 Methods of activation of carbon precursors

A multitude of activating agents have been extensively employed for the production of activated carbon materials with desired pore structure. The purpose of activation is to create and develop (volume and size) porosity in the carbon material and thereby increase the adsorptive capacity. All the available methods of activation can be classified in to two types, namely, physical activation and chemical activation depending on whether a

gaseous or solid activating agent is used.   Each of these methods have their own merits and demerits.

Chemical activation is a single step process for the preparation of activated carbon wherein carbonization of organic precursor in the presence of chemical agents takes place.   In this method solid activating agents like alkali and alkaline earth metal containing substances and some acids are used. The activating agents employed function as dehydrating agents that influence pyrolytic decomposition inhibiting the formation of tar and there by enhancing the yield of carbon.   The temperatures used in chemical activation are lower than that used in the physical activation process. As a result, the development of a porous structure is better in the case of chemical activation method. In spite of the afore mentioned virtuous aspects, the chemical method has its own inherent drawbacks like the need for washing of the product to remove the residual inorganic material which causes pollution problem.

Physical activation involves two steps, namely carbonization of the carbonaceous precursor in an inert atmosphere and subsequent activation of the resulting char in the presence of carbon gasification reactants (gaseous) such as carbon dioxide, steam or air or a suitable combination of the afore mentioned gaseous activating agents.   In the method of physical activation, the reaction involved is between carbon atom and the oxidizing gas. It is this reaction that give rise to the pore formation and subsequent development as some parts of the char structure are reacted faster than the others. During this reaction if carbon atoms were to be removed from the interior of incipient pores

formed as a result of devolatilization during carbonization, enlargement of opened micropores and the opening up of the closed micropores takes place. If the burn off were to be from outside of the particle no new porosity results but it facilitates the reduction of particle size. Since physical activation uses gaseous activation agents and does not produce waste water this method is considered to be an environmentally benign technology. But all is not well with this process. It takes long time and much energy for producing microporous activated carbon through physical activation methods. Also, another inherent draw back of this method is that large amount of internal carbon mass is eliminated to obtain well developed pore structure. And thus, one has to satisfy with limited carbon yields if one were to go in this route.

1.1.6.1 Methods of Activation based on the chemical nature of activating agent

Chemical methods of activation utilize the micro explosion behaviour of chemical agents. Carbon nanomaterials possess unique electrical and structural properties that make them useful and indispensable in energy conversion and storage devices (as electrode material), catalytic processes (as support material) and purification technologies (sorbents). One of the main factors limiting their applicability is their low specific surface area (in the range of 200 – 300 m^2/g). Several activation methods are known to generate carbon materials with well developed porosity and high S_{BET} values.

The questions of interest are: (i) what is (are) the possible reaction(s) between carbon material (precursor to activated carbon material) and the activating agent? (ii) how does such reaction(s) contribute to evolution of porosity and an accompanied improvement in

specific surface area? (iii) how does the surface chemistry of carbon materials alter upon activation? (iv) how does the process of activation increase the sphere of usefulness of carbon materials? In spite of the availability of vast literature on various activation methods meant for improving the performance of carbon materials, detailed knowledge of the process of activation is still poor.

1.1.6.2 Activation with alkali metal hydroxides

Among the alkali metal salts, KOH is the most effective activating agent in producing activated carbon materials. Guo *et al.,* (2002a, 2002b) have proposed the following mechanism for the activation of carbon materials by KOH. In general the chemical reaction between KOH and carbon material can be written as follows:

$$4 \; KOH + C \longrightarrow K_2CO_3 + K_2O + 2 \; H_2 \quad \text{.................................(1)}$$

KOH reacts with disordered or amorphous carbon at high temperatures to form K_2CO_3 as well as the decomposition product K_2O along with the evolution of hydrogen.

Considering the decomposition of KOH into K_2O as well as the reducing ability of carbon, additional reactions do take place during the process of activation as shown:

$$2 \; KOH \longrightarrow K_2O + H_2O \quad \text{.....................................} \quad (2)$$
$$C + H_2O \; (steam) \longrightarrow H_2 + CO \quad \text{...................................} \quad (3)$$
$$CO + H_2O \longrightarrow H_2 + CO_2 \quad \text{...} \quad (4)$$
$$K_2O + CO_2 \longrightarrow K_2CO_3 \quad \text{..} \quad (5)$$
$$K_2O + H_2 \longrightarrow 2 \; K + H_2O \quad \text{..} \quad (6)$$
$$K_2O + C \longrightarrow 2 \; K + CO \quad \text{..} \quad (7)$$
$$K_2CO_3 + 2 \; C \longrightarrow 2 \; K + 3 \; CO \quad \text{...................................} \quad (8)$$
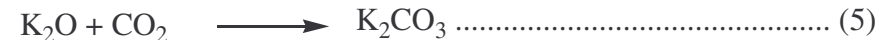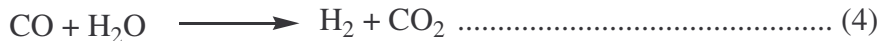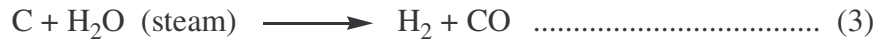
The steam generated in step (2) causes the removal of amorphous carbon as CO as shown in step (3) leading to formation of pores. Additional carbon is also consumed for

reducing K^+ to K as shown in steps (7) and (8). All these carbon losses contribute to the creation of porous network in the carbon material. It is interesting to note that KOH activation has the benefit of activating the carbon material or the carbon precursor with steam (step 3) as well as activation with K_2CO_3 (step 8). Caution should be exercised in considering reaction (8) where in amorphous carbon is gasified to CO and also yielding K which subsequently intercalates into the carbon lamella. Ji *et al.*, (2007) have proved from XRD studies that reaction (8) is only possible in ungraphitizable carbon materials but not in graphitizable carbon materials possessing structural regularity. The researchers have observed only little attenuation in the diffraction peak at the 2θ value of $26°$ (corresponding to the 002 plane of graphite crystallite) upon activation with K_2CO_3 of Meso Carbon Micro Beads (MCMB) relative to unactivated MCMB implying that there is hardly any change in the structure of the graphene layers in the original MCMB upon activation with K_2CO_3. Thus reaction (8) is not possible in graphitizable carbon materials like MCMB.

The following reaction between K_2O and silica is specific to carbon materials produced from natural sources where silica is unavoidable.

$$K_2O + SiO_2 \longrightarrow K_2SiO_3 \quad .... (9)$$
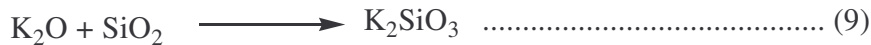
Reaction (9), where in silica is removed leaving porous structure, is important for the additional activation of carbon materials from natural sources. Thus during activation with KOH, amorphous carbon as well as silica is removed from the carbon precursor resulting in porous structure and a corresponding improvement in S_{BET} values.

Shen and Xue (2003) have inferred that during the KOH activation process, surface species (such as alkalides, -OK) as well as molecular species like K_2CO_3 and K_2O are formed. The potassium salts thus formed react further with carbon leading to the formation of K and CO. Two path ways, namely, formation of mesopores and pore widening, for the development of porosity during KOH activation were proposed. In general, the process of pore widening takes place at a higher activating agent (KOH) to carbon precursor ratio. In addition, the pore widening process is accelerated as the activation temperature is raised from 1073 to 1225 K which can be attributed to the fact that at higher temperature of activation, the melt of K_2CO_3 and K_2O as well as the vapour of K possess higher kinetic energy accelerating the pore widening process. Shen and Xue (2003) have also evaluated the effect of the amount of activating agent (KOH) on the process of activation. The activation of Meso Carbon Micro Beads (MCMBs) was carried out with different wt.%/wt. % ratios of activation agent to the carbon precursor, namely, 3, 5, 7, 8, 10 and 12. It was observed that up to a ratio (activating agent to carbon precursor, wt.%/wt. %) of 8, the S_{BET} value increased upto 3182 m^2/g. The improvement in the S_{BET} value was attributed to the extensive oxidation of carbon atoms (gasification) and the accompanied development of porosity. The micropore widening process predominates over the formation of new micropores. This is because of the availability of large number of reaction sites in the interior of the micropores rather than on the external surface. Such pore widening process results in the transformation of miroporous carbon material to mesoporous carbon material. But further increase in the ratio of the activating agent to the carbon precursor (> 8 wt.%/wt.%) results in excessive

20

carbon loss and this causes the collapse of pore wall. The mesoporosity is thus lost leading to a reduction in the S_{BET} value.

The effectiveness of KOH activation relative to either physical activation methods or activation by other chemical agents can be attributed to the ability of K to form intercalation compounds with carbon easily. In addition, the K_2O formed during the process of KOH activation, *in-situ,* can easily infiltrate into the pores. K_2O is reduced to K by carbon resulting in carbon gasification with a subsequent emission of CO_2 leading to the formation of pores. Also, the K atoms that intercalate into the lamella of the carbon crystallites widen the space between the adjacent carbon layers (intercalation phenomenon), resulting in an increase in the S_{BET} value (Ji *et al.,* 2007).

1.1.6.3 Activation with alkali metal carbonates

Even though the use of alkalimetal hydroxides like KOH and NaOH as activating agents offer the advantage of producing carbon materials with high S_{BET} values, they (alkali metal hydroxides) are corrosive, hazardous and environmentally unfriendly. Use of alkali metal carbonates such as K_2CO_3 can be a substitute to the use of alkali metal hydroxides. K_2CO_3 was found to be a better activating agent owing to the formation of atomic K during the activation process as shown in (10), which subsequently intercalates into the inter layers of adjacent hexagonal network plane of C atoms. The adjacent graphene planes were separated because of the K intercalation. Even after removal of K, either by washing with H_2O or acid, the rearranged or disordered graphene sheets of the carbon crystallite cannot go back to their original position thus leaving pores and voids.

This results in an activated carbon material with high porosity and S_{BET} value (Okada *et al.*, 2003).

Carbon reduces K_2CO_3 at elevated temperatures. As a result of the carbothermal reduction process (10) potassium vapour and carbon monoxide are formed (McKee, 1983). The occurrence of reaction (10) is verified experimentally using Knudsen cell mass spectrometry. Potassium vapour and CO were detected in the gas phase during the reaction between carbon and K_2CO_3 in vacuum at temperatures in the range of $773 - 973$ K.

$$2\,C + K_2CO_3 \longrightarrow 2\,K + 3\,CO \quad\text{.......................................} \quad (10)$$
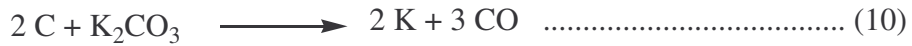
Hayashi *et al.*, (2000) have measured the weight loss rate behaviour of lignin as well as K_2CO_3 (activating agent) individually in N_2 atmosphere in the temperature range of $323 - 1273$ K at a heating rate of 283 K/min. Under identical conditions, the weight loss rate behaviour of lignin impregnated with K_2CO_3 is also measured and this is termed as experimental curve. In addition, the weight loss rate behaviour of lignin impregnated with K_2CO_3 is calculated by the summation of the values obtained from lignin and K_2CO_3 measured individually. The curve thus obtained was termed as calculated or theoretical curve. The assumption made in generating the calculated wt. loss rate curve is that there is no chemical interaction between the lignin and the activating agent. Thus the difference between the experimental and the calculated weight loss rate curves yield important insights into the chemical interaction as well as the particular weight losses resulting from the chemical reactivity between the char and the activating agent. It was

noticed that the experimental weight loss peak at around 673 K shifted to a lower temperature in comparison to the peak position in the calculated or theoretical curve. Such a shift in the weight loss rate peak towards lower temperature (lower than 673 K) was attributed to the occurrence of dehydrogenation reaction at a relatively low temperature. Such dehydrogenation reactions have not contributed to the enhancement of either S_{BET} or Vp but only indicate that the carbonization behaviour of lignin is altered or influenced by K_2CO_3 below 773 K. Also no convincing path way for the evolution of H_2 during activation in the presence of K_2CO_3 at such a low temperature (between 473 – 773 K) is illustrated.

Carbon materials are known to dehydrogenate evolving H_2 in the presence of alkali metals (Li, Na, K, Rb, Cs) at low temperatures (Mochida *et al.,* 1975; Mochida *et al.,* 1976). But the important question is that how H_2 evolution can take place in the presence of K_2CO_3 as activating agent under the reaction conditions where there is no possibility for the formation of alkali metal species. The following sequence of reactions offer a convincing pathway for the evolution of H_2 responsible for the observed weight loss rate peak at lower activation temperature (< 673 K) in the presence of K_2CO_3 as activating agent. K_2CO_3 is known to undergo thermal decomposition at a lower temperature in the presence of carbon char as shown in (11).

$$K_2CO_3 \rightleftharpoons K_2O + CO_2 \text{ .... (11)}$$
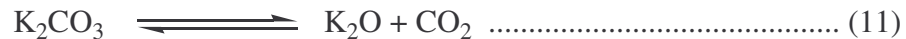
The K_2O formed in (8) reacts with the structural or crystalline water evolved in the temperature range of 473 – 623 K from the carbonization mixture to form KOH (12).

$$K_2O + H_2O \longrightarrow KOH \text{ .... (12)}$$

23

KOH thus formed in (12) reacts with CO_2 formed in (11) as well as with the carbon in the char to evolve H_2 as shown in (13). Reaction (13) is thermodynamically feasible at a temperature as low as 673 K.

$$4 \; KOH + CO_2 + C \longrightarrow 2 \; K_2CO_3 + 2 \; H_2 \quad .... (13)$$

In addition to the shift of the weight loss rate peak at a activation temperature of ≈ 673 K to a lower temperature, a huge difference in the weight loss rate behaviour is observed between the experimental and calculated curves at around 1073 K. In fact, a large peak (weight loss rate) is observed experimentally in sharp contrast to the theoretical or calculated curve where no weight loss rate peak was present. The observed weight loss rate was attributed to the release of CO by the carbothermal reduction of K_2CO_3 by carbon. Thus, K_2CO_3 acted differently in two different activation temperature ranges. Below an activation temperature of 773 K, K_2CO_3 acted as dehydrogenation agent and at an activation temperature of about 873 K, K_2CO_3 was reduced by C releasing CO and there by increasing the S_{BET} and Vp values.

1.1.6.4 Activation with transition metal salts

Recently several research groups have exploited the method of $ZnCl_2$ activation to activate carbon precursors like Rice husk (Usmani *et al*., 1994), Corn cob (Tsai *et al.,* 1998), Coffee residue (Boonamnuayvitaya *et al*., 2005), Tectona Grandis sawdust (Mohanty *et al*., 2005), Apricot stone (Basar, 2006), Cherry stones (Olivares-Marin *et al*., 2006), Sugar beet bagasse (Onal *et al*., 2007), Coconut coir pith (Namasivayam and Sangeetha, 2008) and Tamarind wood (Acharya *et al*., 2009a, 2009b). The afore-mentioned studies highlight the usefulness of $ZnCl_2$ activation in the production of activated carbon from diverse carbon precursors.

1.1.6.5 Activation with alkaline earth metal salts, acids and gases (steam, air and CO$_2$)

Apart from alkalimetal hydroxides, alkali metal carbonates and transition metal salts, activating agents belonging to the class of alkaline earth metal salts (Yamashita and Ouchi, 1982), and mineral acids, such as, H$_3$PO$_4$ (Laine *et al*., 1989; Jogtoyen and Derbyshire, 1993; Molina-Sabio *et al*., 1995, Molina-Sabio *et al*., 1996; Jagtoyen and Derbyshire, 1998; Toles *et al*., 1999; Benaddi *et al*., 2000; Puziy *et al*., 2002; Puziy *et al*., 2003; Marcias-Garcia *et al*., 2003; Molina-Sabio and Rodriguz-Reinoso, 2004; Martin-Gullon *et al*., 2004; Puziy *et al*., 2005; Rahman *et al.,* 2005; Gomez-Serrano *et al.,* 2005; Budinova *et al*., 2006; Corcho-Corral *et al*., 2006; Paredas *et al.,* 2006; Puziy *et al*., 2007; Gargis *et al*., 2007; Guo and Rockstraw, 2007; Attai *et al*., 2008; Bedia *et al*., 2009), HNO$_3$ (Battistoni *et al*., 1984; Noh and Schwarz, 1990; Vinke *et al*., 1994; Gil *et al.,* 1997; Gomez-Serrano *et al*., 1997; Shim *et al*., 2001; El-Hendaway, 2003; Zhao *et al*., 2005; Macias-Garcia *et al*., 2006) and H$_2$SO$_4$ (Caballero *et al*., 1997; Alvarez *et al*., 2007) have been extensively exploited for the chemical activation of carbon materials. Even though less advantageous, physical activation methods based on steam (Gercel *et al*., 2007; Kayembe and Pulsifer, 1976; Otto and Shelef, 1977; McKee and Chatterji, 1978; Gonzalez *et al*., 1995; Lazaro *et al*., 2007; Aranda *et al*., 2007; Salvador *et al*., 2008) air (Gonzalez-Vilchez *et al.,* 1979; Lecea *et al*., 1981; Marsh and Orchard, 1992; Kopp *et al*., 1997; Gomez-Serrano *et al*., 1999) and CO$_2$ (Rodriguez-Reinoso *et al*., 1982; Torrgrosa and Martin-Martinez, 1991; Tancredi *et al*., 1996; Carrasco-Marin *et al*., 1996; Alcaniz-Monge *et al*., 1997; Teng *et al*., 1997; Lua and Guo, 2000; Sanchez *et al.,* 2001; Tsai *et al*., 2001; Lyubchik *et al*., 2002; Lozano-Castello *et al*., 2002; Guo and

Lua, 2002; Miguel *et al*., 2003; Yang and Lua, 2003; Turmuzi *et al*., 2004; Zhang *et al*., 2004; Zabaniotou *et al*., 2004; Jasienko-Halat and Kedzior, 2005; Wu and Tseng, 2006; Paredes *et al*., 2006, Gonzalez *et al.,* 2006; Hu *et al*., 2007; and Mahamad, 2007) as activating agents have proven to be useful for the activation of carbon materials.

1.2 HETEROPOLY ACIDS (HPAs)

Heteropoly compounds (HPCs) are extensively used as homogeneous and heterogeneous acid and oxidation catalysts. HPCs are capable of bringing about many electron oxidative-reductive reactions. They exhibit unique physico-chemical properties. The structure of HPCs is well known at the molecular level. Specific variation in the acid and oxidation potentials is possible by changing the constituent elements (hetero atom, peripheral or addenda or poly atom, and the counter cation) (Konishi *et al*., 1982). Similarities in the catalytic function in both solution and in solid state are observed. Catalysts based on heteropoly compounds are active, selective, non-corrosive and environmentally benign (Kozhevnikov, 1987).

1.2.1 Molecular structure of heteropoly compounds

Heteropoly acids are polyoxo compounds. They are ionic solids with protons distributed through out the structure. Heteropoly anion is a high molecular weight cage like species The basic structural unit of the heteropoly anion comprises of metal-oxygen octahedral – (MO_6) where M is the addenda atom or peripheral atom. The heteropoly anions contain one or several hetero atoms X usually located at the centre of the anion (central atoms). The MO_6 octahedra are linked together forming an extremely stable and compact

26

skeleton of HPAN. The cations may be hydrogen, alkalimetals and other metal ions.

Among several known structural types, the compounds belonging to the saturated 12th series (M:X = 12) are of greatest significance. Such compounds possess heteropoly anions with Keggin type structure with T_d symmetry and the general formula: $XM_{12}O_{40}^{x-8}$, where X is the central atom or hetero atom (e.g., Si^{IV}, Ge^{IV}, P^V, As^V etc.,), x is the degree of its oxidation and M is the addenda atom (usually Mo and W). The Keggin type polyanion comprises of a central XO_4 tetrahedron surrounded by 12 MO_6 octahedra having common vertices and edges (Fig. 1.4). The MO_6 octahedra were grouped into four M_3O_{13} triads connected by common vertices. The radius of the HPAN is ~ 6 Å (Kozhevnikov, 1987).
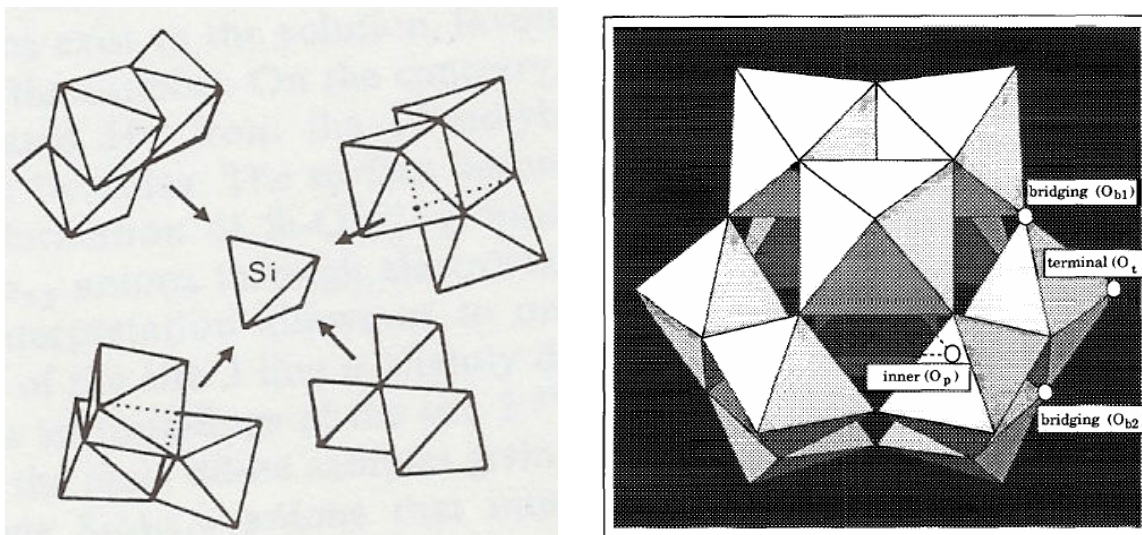
Fig. 1.4 Schematic representation of formation of the Keggin type HPAN structure with different types of oxygen atoms (Thouvenot *et al.*, 1991; Bruckman *et al.*, 1993)

Even though Keggin has first investigated the structure of such heteropoly compounds, only Brown *et al.*, (1977) have offered the complete structural analysis unraveling the

structure of hexahydrate of 12-tungstophosphoric acid ($H_3PW_{12}O_{40} \cdot 6\ H_2O$), the most stable forms of HPW among several hydrated HPWs. The protons of the heteropoly acid are in a guarded environment. It was identified that the anions ($PW_{12}O_{40}^{3-}$) are inter connected by $H_5O_2^+$ cations through hydrogen bonding of the hydrogen atoms of the water molecules to the oxygen atoms of the Keggin type anion (Hayashi *et al*., 1983). Each proton is surrounded by four water molecules. Because of the two-fold thermal disorder at any given time only two of these water molecules are hydrogen-bonded to the proton. In addition, the water molecules are hydrogen bonded to the terminal (outer) oxygen atoms of the anion structure. The structural arrangement of protons, water molecules and anions in the hexahydrate of 12-tungstophosphoric acid is depicted in Fig. 1.5 (A). (Bonardet *et al*., 1995; Ghosh *et al*., 1986; Misono, 1985; Moffat, 1985; Moffat, 1986; Moffat, 1989). The effective guarding of the acidic protons by the hydrogen-bonded water is evident in Fig. 1.5 (A). An array of four Keggin units connected by $H_9O_4^+$ nets wherein the central acidic proton (HA) of the HPW hydrogen-bonded to four water molecules through the water molecule oxygen (OW) atoms is shown in the diagram. The hydrogen atoms of these water molecules (HW) are in turn hydrogen-bonded to the terminal oxygen atoms of the Keggin anions.

Even though there are four water molecules centered around the proton, only one $H_5O_2^+$ ion exists at the site but with two possible orientations as shown in Fig. 1.5 (A) (Hayashi *et al*., 2003). Based on single-crystal X-ray and neutron diffraction studies, proton sites in the crystalline $H_3PW_{12}O_{40} \cdot 6\ H_2O$ are schematically represented as diaquahydrogen ions ($H_5O_2^+$).
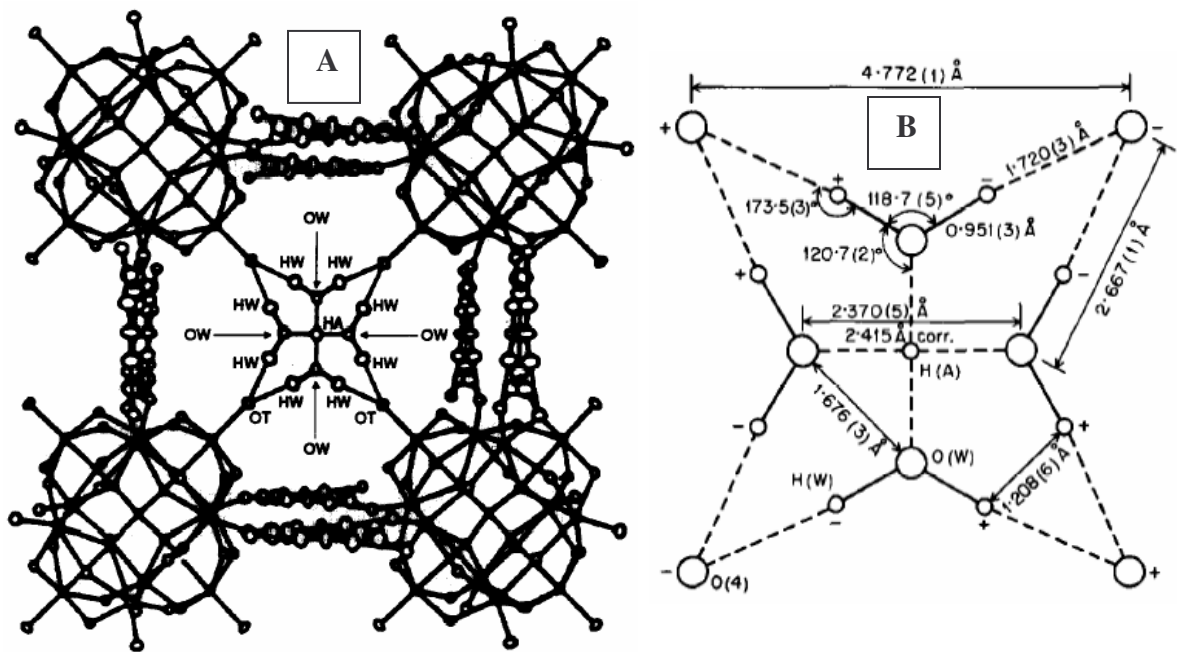
Fig. 1.5 (A) Stereoscopic drawings showing the packing of anions ($XM_{12}O_{40}^{n-}$) and
  diaquahydrogen ions ($H_5O_2^+$) (B) Structure of the diaquahydrogen ion $H_5O_2^+$ and
  its hydrogen-bonding to oxygen atoms of the Keggin Units (KUs) (Bonard et
  al., 1995; Ghosh et al., 1986; Misono, 1985; Moffat, 1985; Moffat, 1986;
  Moffat, 1989)
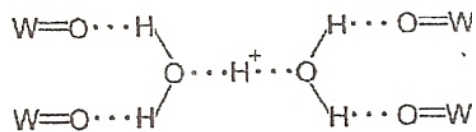
Scheme 1.1 Schematic representation of the guarded proton of the Keggin type poly
  anion (Kozhevnikov, 1994, Kozhevnikov et al., 1995)

Each such $H_5O_2^+$ species link four neighbouring HPANs through hydrogen bonding

interaction with the terminal W=O oxygen atoms as shown in Scheme 1.1.

(Kozhevnikov, 1994, Kozhevnikov et al., 1995). In anhydrous $H_3PW_{12}O_{40}$, three protons

are located on the bridge oxygen (W-O-W) of the Keggin anion (Misono and Okuhara, 1993).

The oxygen atoms of the water molecules are arranged in squares with a distance of 1.676 Å between adjacent oxygen atoms in the square and one of the protons of the acid is located at the centre of each square (Fig. 1.5 (B)). The structure may be regarded as a combination of two different inter penetrating substructures of anions and disordered $H_5O_2^+$ cations with no hydrogen bonding between these two substructures as shown in Fig. 1.6. (Janik *et al.*, 2004).
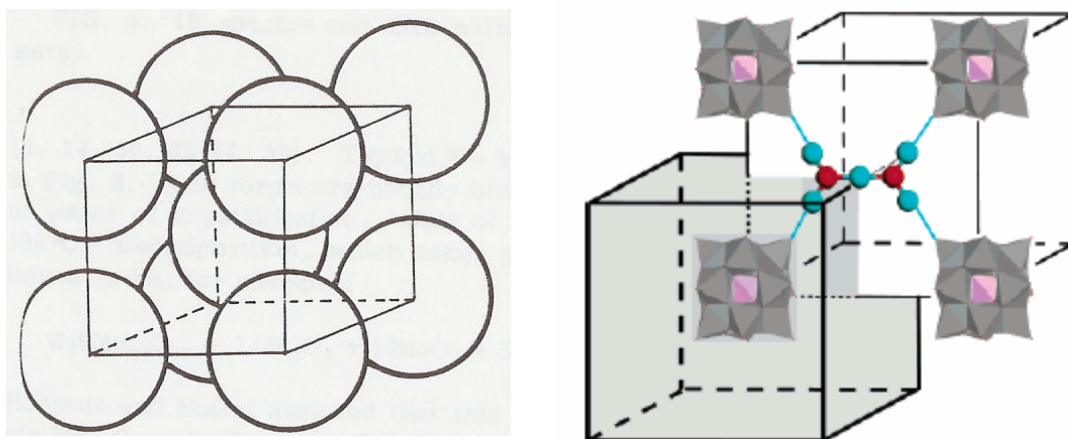
Fig. 1.6 Schematic diagram illustrating the *bcc* structure of the hexahydrate $H_3PW_{12}O_{40}$. 6 H_2O as two inter penetrating simple cubic structures. The H^+ of $H_5O_2^+$ species coordinated to the body centered Keggin units located at the midpoint of an edge of the conventional cubic cell. The Keggin units are shown in polyhedral representation (Misono, 1987; Janik *et al.*, 2004)

1.2.2 Hierarchial structure of heteropoly compounds (Misono, 1985, Misono, 1992)

In the solid state HPCs comprise of the HPAN, cation (proton or metal ions) and water and/or organic molecules. Such a three dimensional arrangement of anion, cation and

water molecules is termed as secondary structure (Fig. 1.5 (A)). The heteropoly anion itself is regarded as the primary structure (Fig. 1.4.). Unlike the stable primary structure, the secondary structure is rather a variable as the crystallization water can be easily replaced by other polar molecules leading to expansion and contraction of lattice. There are specific analytical tools yielding the structural details of the primary and secondary structures. FT-IR studies yield information on the primary structure where as the XRD studies give information on the secondary structure. The tertiary structure consists of the shape of the primary particles (crystallites), their particular aggregation that determines the specific surface area and the pore structure.

1.2.3 Chemical bonding in the Keggin type HPAN

The anion consists of 12 quasi linear M-O-M linkages between the octahedral forming part of different M_3O_{13} triads, 12 angular M-O-M linkages between the octahedral with in a single triad, 4 X-O-M bonds where the triads are joined to the central atom and 12 terminal M=O bonds (Kozhevnikov *et al.*, 1987). Different types of oxygen atoms, namely, the terminal, bridging (corner sharing, Ob1; and edge sharing, Ob2) and internal oxygens are shown in Fig. 1.7. The M-O distances are about 1.7 Å for the terminal M=O bonds, 2.0 Å for the M-O-M bridge bonds, and 2.2-2.3 Å for the M-O-X bonds, where X is the central atom (Kazanskii and Tarchenkova, 1974). The shortest M=O bond is always in the trans-position to the longest bond. The state of the O atoms in HPA is nearly close-packed (Fig. 1.7.) as the ionic radius of O^{2-} greatly exceeds the radii of M^{VI} and X^x (Kozhevnikov and Matveev, 1982). The ionic radii of Mo (VI) and W (VI) are 0.62 and 0.65 Å respectively and the ionic radius of O^{2-} is assumed to be 1.4 Å. The

striking difference between the HPCs and the usual coordination compounds is that the latter do not contain discrete ligands coordinated to the central atom. Discrete MO_6^{n-} ion does not exist in HPCs. The whole coordination sphere is regarded as one large ligand in the case of HPCs (Kazanskii and Tarchenkova, 1974).
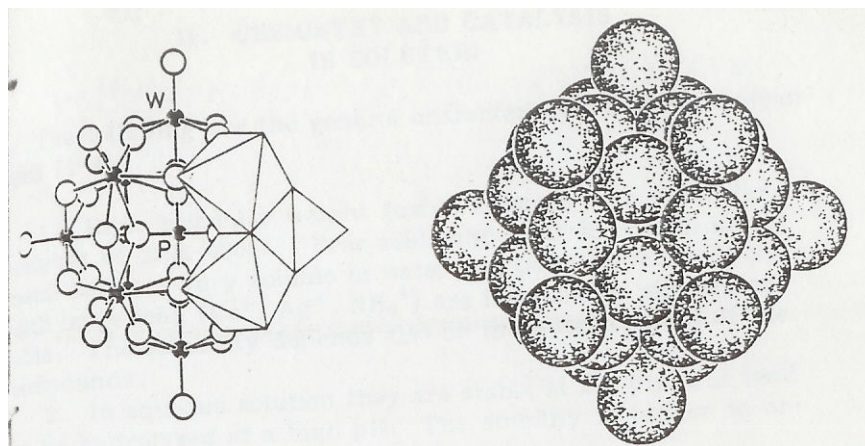
Fig. 1.7 Nearly close packed structure of oxygen atoms in the primary structure of HPW (Kazanskii and Tarchenkova, 1974)

1.2.4 Acidic properties of solid heteropoly acids (HPAs)

HPAs are strong Bronsted acids. The Bronsted acid sites are the active centers responsible for the high catalytic activity exhibited by HPAs in many catalytic reactions. The observed sequence of the acid strength of crystalline HPAs is:

$H_3PW_{12}O_{40}$ (865 K) > $H_4SiW_{12}O_{40}$ (805 K) > $H_3PMo_{12}O_{40}$ (736 K) > $H_4SiMo_{12}O_{40}$ (696 K).
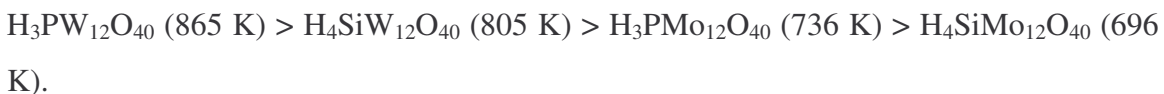
The ammonia desorption temperature in Kelvin are indicated adjacent to the formulae (Kozhevnikov et al., 1987). Anhydrous HPW has an acidity stronger than -13.16 (H_0). This value of H_0 indicates that HPW is a solid super acid. In general, a super acid is an

acid that exhibits acid strength greater that that of 100 % H_2SO_4. The H_0 value for 100 %

H_2SO_4 is - 12. The stronger acidity of HPAs is attributed to the large size of the

polyanion with a low and delocalized surface charge density. The resulting weak

interaction between the polyanion and the proton brings about the strong acidity (Misono

and Okuhara, 1993). From pyridine adsorption studies, it was established that the acidity

of HPA is of Bronsted type. Pyridine is adsorbed on strong Bronsted acid centers in the

form of pyridinium ion ($C_5H_5NH^+$). On Lewis acid sites, pyridine is adsorbed in the form

of a complex with a donor-acceptor bond. The differences in the type of adsorption of

pyridine are reflected in the FT-IR spectra. It is observed that the entire pyridine was

adsorbed on the HPA exists in the form of the pyridinium ion. A band at 1540 cm^{-1} is

characteristic of pyridinium ion which is a reflection of Bronsted acidity. The bands at

1450, 1490 and 1610 cm^{-1} represent the pyridine coordinatively bonded to Lewis acid

sites. The acid strength of P containing heteropoly acids is greater than that of Si

containing heteropoly acids and also the W containing HPAs are stronger in acidity

compared to Mo containing HPAs. The observed trend in the acid strength is in

accordance with the higher negative charge on the oxygen atoms in Mo containing HPAs

compared to the W containing HPAs. XPS studies revealed an increase in the charge on

the peripheral oxygen atoms when W is replaced by Mo (Kozhevnikov *et al*., 1987). The

peripheral metal (addenda) atoms in the anion are a dominant factor influencing the

acidic properties of the heteropoly acid rather than the central metal atom (hetero atom)

in the anion structure (Moffat, 1985). The degree of hydration dictates the proton

mobility. The protons can be transported through the hydrogen-bonded network as fast

as in a aqueous solution (Ono, 1992). The proton conductivity is dependent on the degree of the hydration and follows the following order:

$H_3PW_{12}O_{40}.29\ H_2O > H_3PW_{12}O_{40}.20\ H_2O > H_3PW_{12}O_{40}.13\ H_2O$
$H_3PMo_{12}O_{40}.29\ H_2O > H_3PMo_{12}O_{40}.18\ H_2O > H_3PMo_{12}O_{40}.13\ H_2O$

1.2.5 Pseudo liquid phase behaviour

In the presence of polar reactant molecules such as alcohols, ketones, ethers, esters and amines, solid HPAs behave analogous to the highly concentrated solutions. Not only the protons on the surface but also those present in the bulk of the poly anion participate in the catalytic reaction. Such a phenomenon unusual to heterogeneous acid catalysts is typical of HPAs and is named as pseudo-liquid phase. By virtue of this behaviour, crystalline HPAs are able to bring about the catalytic reactions involving polar molecules in the bulk of the catalyst like the reactions in homogeneous systems. Large amounts of polar molecules are sorbed into the bulk of the HPA resulting in the formation of solvates. The phenomenon is different from the adsorption in the mesopores of the usual sorbents. As a result of rapid absorption of polar reactant molecules the catalytic reactions can occur not only on the surface but also in the bulk of the HPA (Kozhevnikov, 1987). The absorption of polar molecules into the bulk of the polyanion primarily depends on the basicity and secondarily on the size of the each of the molecule that is being absorbed into the bulk. The phenomenon of absorption-desorption process of polar molecules is distinctly different from that of the diffusion of reactant molecules into the micropores as the S_{BET} values of HPAs that show pseudo-liquid behaviour are usually very small and also no such micropores are present in the HPAs in general. With the absorption of polar molecules into the bulk, the distance between the poly anions change.

The reactant molecules are absorbed in the enlarged inter-polyanion space. Increase of volume analogous to that of swelling takes place. Rapid diffusion of polar molecules, the easy rearrangement of the secondary structure and the occurance of the reaction in the internal bulk are the characteristic features of pseudoliquid phase behaviour (Misono, 1985). Unlike polar molecules, non-polar reagents, like hydrocarbons, are not absorbed into the bulk of HPA; such reactant molecules only interact on the surface of the catalyst. Soluble salts of HPAs too exhibit the phenomenon of pseudo liquid phase whereas the insoluble salts of HPA do not possess such property (Kozhevnikov *et al.*, 1987). The pseudo liquid phase behaviour endows a high catalytic activity and unique selectivity to the heteropoly compounds. As a result of this behaviour, the chemical changes taking place in the compound owing to the exposure to the reactant is not only limited to the surface but also expanded to the whole of the bulk making the spectroscopic studies of these catalysts more feasible and realistic (Misono, 1985). In addition to the pseudo liquid type behaviour, because of the presence of hierarchial structures in the case of HPCs, two other modes of catalysis, namely, surface type and bulk type II are possible as represented in Fig. 1.8. The surface type catalysis is ordinary heterogeneous catalysis taking place on the two-dimensional outer surface and the pore wall. The reaction rate is proportional to the specific surface area of the solid acid. For instance, the rate of double-bond isomerization of olefins was found to be proportional to the S_{BET} value of HPMo. More over a parallelism between reaction rates and surface acidity is observed in most of the reactions catalyzed by $Cs_3H_{3-x}PW_{12}O_{40}$ ($2<x<3$) (Mizuno and Misono, 1998).
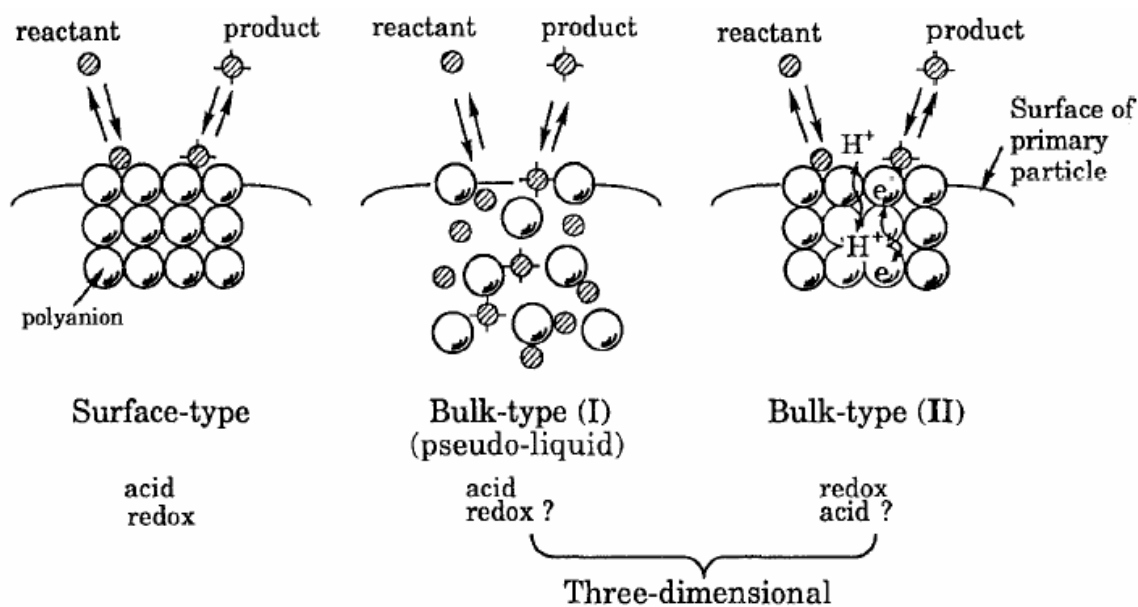
Fig. 1.8 Three types of catalysis for solid HPCs: surface type, bulk type I and bulk type II
(Misono, 1992, Misono, 2001)

In sharp contrast to the surface type catalysis, in the case of bulk type I and bulk type II catalysis, the reaction fields are two dimensional. Catalysis taking place in pseudo liquid phase is also called bulk type I. When the diffusion of reactant molecules into the solid bulk (lattice but not pores) is faster than the reaction, the solid bulk resembles a concentrated solution (pseudo-liquid phase) in which the catalytic reaction proceeds. The reactant molecules either in the gas or liquid phase penetrate in between the polyanions expanding the distance between them and react with in the bulk of the solid. The products come out of the surface and are released to the gas or liquid phase. Catalysts tend to behave like liquids (solvents) in the pseudo liquid phase. Very high catalytic activities are observed as the active sites (protons) in the bulk too participate in the reaction. Typical examples for catalytic transformation of this type include the dehydration of alcohols at low temperatures. The rate of the reaction is proportional to

the volume of the catalyst in general. Bulk type II catalysis is observed in the case of oxidation catalysis taking place at high reaction temperatures. In this type of catalysis, the redox carriers (protons and electron) diffuse into the solid bulk rapidly. The whole bulk participates in the oxidation cycle. Typical examples include oxidative dehydrogenation and oxidation of hydrogen at high temperature. The reaction rate is found to be proportional to the volume of the catalysts. Solid HPAs with cations of small ionic radii to charge ratio (H^+, Na^+, Cu^{2+}) readily absorb small polar molecules and are soluble in water. Cs^+ and NH_4 salts are scarcely soluble in water due to low salvation energy and as a result only exhibit surface – type catalysis.

1.2.6 Supported HPAs

HPAs are soluble in water and several oxygen containing organic solvents. As a result, HPAs leach out of the catalyst support in either liquid or vapour phase reactions. So it is necessary to develop supported HPA catalysts with no leaching of HPA in both liquid and vapour phase reactions. Izumi and Urabe (1981) have found activated carbon support to be capable of holding, entrapping and immobilizing HPA moieties firmly whereas silica and alkaline earth metal compounds (MgO, CaO) failed to do so. On the other hand, γ-Al_2O_3 was not a suitable as support because of its surface basicity causing the decomposition of HPAs. Owing to the microporous architecture, the activated carbon support uniquely entraps HPA moieties (Izumi and Urabe, 1981). Another drawback in the exploitation of HPAs is the low S_{BET} values of bare HPAs like HPW and HPMo usually in the range of 1-15 m^2/g. Even in the case of water-insoluble salts, the S_{BET} values are only slightly higher (100 – 200 m^2/g) (Misono 1985). In addition to the

prevention of leaching, use of the support improves the S_{BET} values of supported HPA catalysts increasing the sphere of utilization of HPAs (Kozhevnikov, 1995; Kozhevnikov, 1998).

1.3 FUEL CELLS

Fuel cell is a device that converts chemical energy into electrical energy. Fuel cells based on hydrogen, methanol and natural gas are widely used. Two most attractive features unique to fuel cells are: the high efficiency and the low pollutant emissions. Based on the operating temperature fuel cells can be classified into low and high temperature fuel cells.
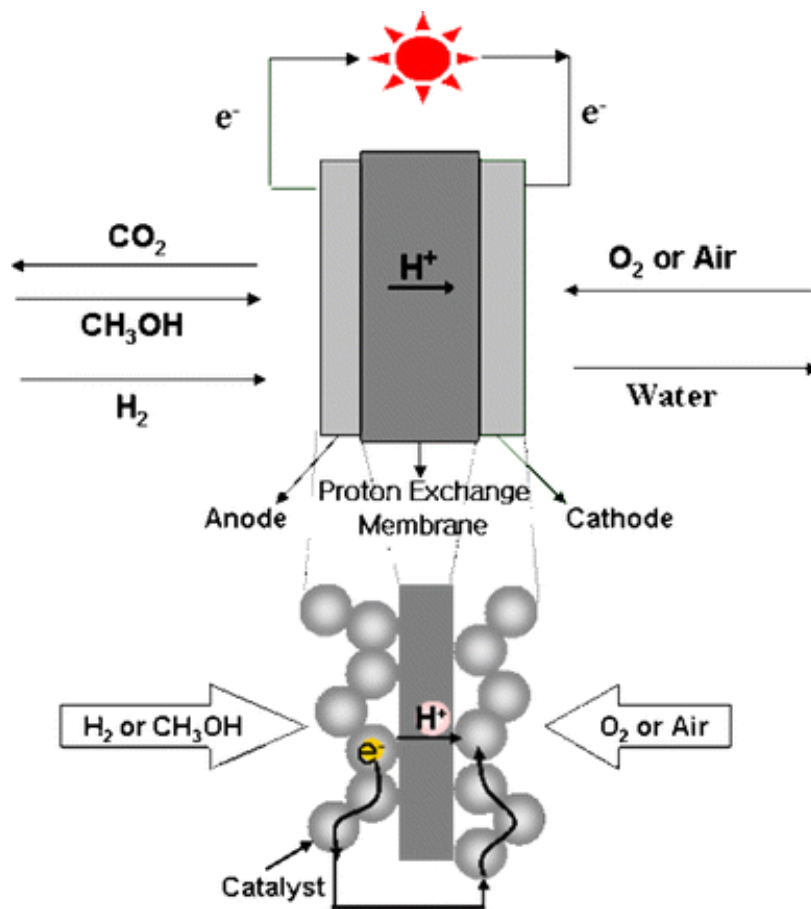
Fig. 1.9 Schematic representation of a fuel cell (Lim *et al*., 2008)

38

Proton Exchange Membrane Fuel Cells (PEMFC) and the Direct Methanol Fuel Cell (DMFC) are the most widely investigated systems operating at low temperature (333 to 373 K). Direct electrochemical conversion of fuel (hydrogen/methanol) in the presence of oxidant (air/oxygen) producing water/CO_2 takes place. A simplified version of fuel cell with the major components (electrodes and membrane) is depicted in Fig. 1.9. A thin catalyst layer is coated on one side of either of the electrodes. The fuel is fed into the anode side and the oxidant enters through the cathode side of the fuel cell. At the anode, in the case of PEMFC, hydrogen is dissociated by the catalyst into proton and an electron. The protons flow through the external circuit.

1.3.1 Electro catalytic reactions taking place at the anode and cathode of PEMFC and DMFC (Lim *et al.*, 2008)

Redox reactions taking place in PEMFC:

Anode reaction: $H_2 \longrightarrow 2\,H^+ + 2\,e^-$ $E^0 = 0.00$ V

Cathode reaction: $1/2\,O_2 + 2\,H^+ + 2\,e^- \longrightarrow H_2O$ $E^0 = 1.23$ V

Over all reaction: $H_2 + 1/2\,O_2 \longrightarrow H_2O$ $E^0 = 1.23$ V

Redox reactions taking place in DMFC:

Anode reaction: $CH_3OH + H_2O \longrightarrow CO_2 + 6\,H^+ + 6\,e^-$ $E^0 = 0.05$ V

Cathode reaction: $3/2\,O_2 + 6\,H^+ + 6\,e^- \longrightarrow 3\,H_2O$ $E^0 = 1.23$ V

Over all reaction: $CH_3OH + H_2O + 3/2\,O_2 \longrightarrow CO_2 + 3\,H_2O$ $E^0 = 1.18$ V
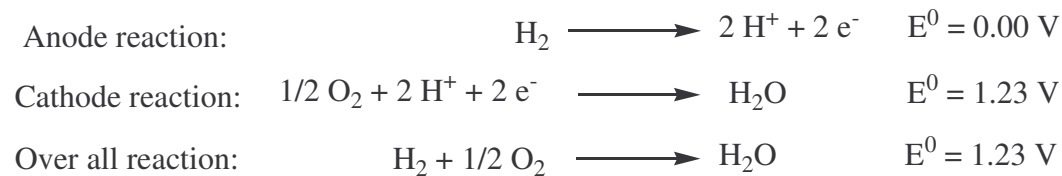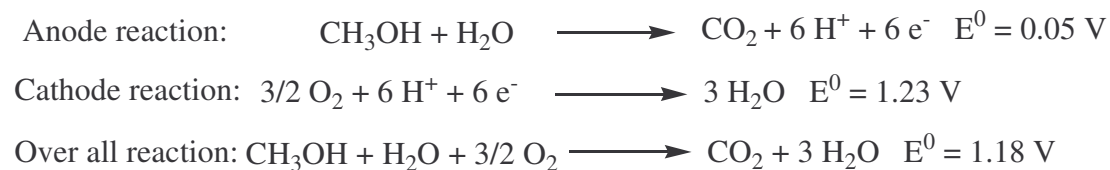
1.3.2 Mechanism of electro-oxidation of methanol

In a direct methanol fuel cell, at the anode methanol is electro-oxidised to CO_2 and at the cathode oxygen is reduced to water. Oxidation of methanol proceeds through the adsorption of methanol molecule on the catalyst surface.

$$CH_3OH + Pt\,(s) \longrightarrow Pt\text{-}CH_2OH + H^+ + e^- \tag{14}$$

$$Pt\text{-}CH_2OH + Pt\,(s) \longrightarrow Pt_2\text{-}CHOH + H^+ + e^- \tag{15}$$

$$Pt_2CHOH + Pt\,(s) \longrightarrow Pt_3\text{-}COH + H^+ + e^- \tag{16}$$

$$Pt_3COH \longrightarrow Pt\text{-}CO + 2\,Pt(s) + H^+ + e^- \tag{17}$$

$$Pt\,(s) + H_2O \longrightarrow Pt\text{-}OH + H^+ + e^- \tag{18}$$

$$PtOH + Pt\text{-}CO \longrightarrow Pt\text{-}COOH \tag{19a}$$

or

$$Pt\text{-}CO + H_2O \longrightarrow Pt\text{-}COOH + H^+ + e^- \tag{19b}$$

$$Pt\text{-}COOH \longrightarrow Pt\,(s) + COOH^+ + e^- \tag{20}$$

$$Pt\text{-}CH_2OH \longrightarrow Pt\,(s) + HCHO + H^+ + e^- \tag{21}$$

$$Pt_2CHOH + Pt\text{-}OH \longrightarrow 3\,Pt\,(s) + HCOOH + H^+ + e^- \tag{22}$$

or

$$Pt_2CHOH + H_2O \longrightarrow 2\,Pt\,(s) + HCOOH + 2\,H^+ + e^- \tag{23}$$

$$Pt_3C\text{-}OH + Pt\text{-}OH \longrightarrow 3\,Pt\,(s) + Pt\text{-}COOH + H^+ + e^- \tag{24}$$

or

$$Pt_3C\text{-}OH + H_2O \longrightarrow 2\,Pt\,(s) + Pt\text{-}COOH + 2\,H^+ + 2\,e^- \tag{25}$$
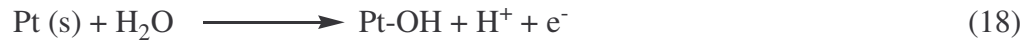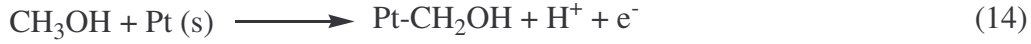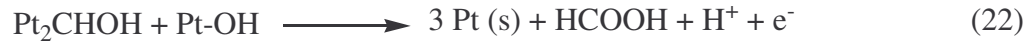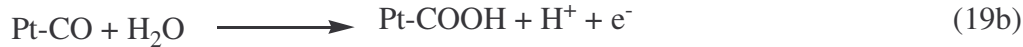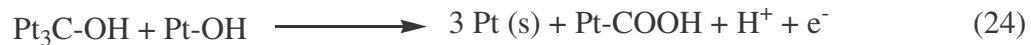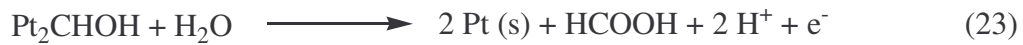
Very few electrode materials have the capacity to adsorb methanol in acidic medium. Among these, Pt based materials alone display significant stability and activity for the electro-oxidation of methanol. There are two essential features of the mechanism of electro-oxidation of methanol (Bagotzky *et al.*, 1977; Hamnett, 1997). One is the electro sorption of methanol on to the substrate followed by several steps of deprotonation

(reactions 14, 15, 16 and 17) as shown below. Also the step wise stripping of hydrogen atoms from adsorbed methanol is schematically represented in Scheme 1.2. The formation of CO during the methanol electro-oxidation is shown in Scheme 1.2. The adsorbed CO species block the catalyst surface and hinder further reaction.
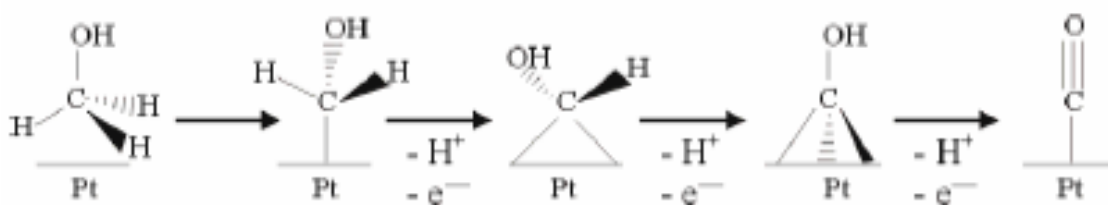
Scheme 1.2 Scheme of methanol oxidation on Pt showing the consecutive stripping of hydrogen atoms (Carrette *et al.,* 2001)

Each reaction step represents the transfer of one electron. Dehydrogenation reactions occurring during the oxidation process are shown in the direction from left to right. Oxidation by adsorbed OH occurs in the vertical direction from top to bottom. Stable compounds are located on the hypotenuse of the right angled triangle shape of the schematic representation (Scheme 1.3). The second aspect of the reaction pathway is the addition of oxygen to adsorbed carbon-containing intermediates resulting finally in the formation of CO_2 (reactions 18-25) as depicted in scheme 1.3 (Carrette *et al*., 2001). The possible reaction pathways during the electrooxidation of methanol with the accompanied products are shown in Scheme 1.3.

41

$$CH_3OH \longrightarrow \underset{X}{CH_2OH} \longrightarrow \underset{XX}{CHOH} \longrightarrow \underset{XXX}{C\text{-}OH}$$

$$\downarrow \qquad\qquad \downarrow \qquad\qquad \downarrow$$

$$CH_2O \longrightarrow \underset{X}{CHO} \longrightarrow \underset{X}{CO}$$

$$\downarrow \qquad\qquad \downarrow$$

$$HCOOH \longrightarrow \underset{X}{COOH}$$

$$\downarrow$$

$$CO_2$$
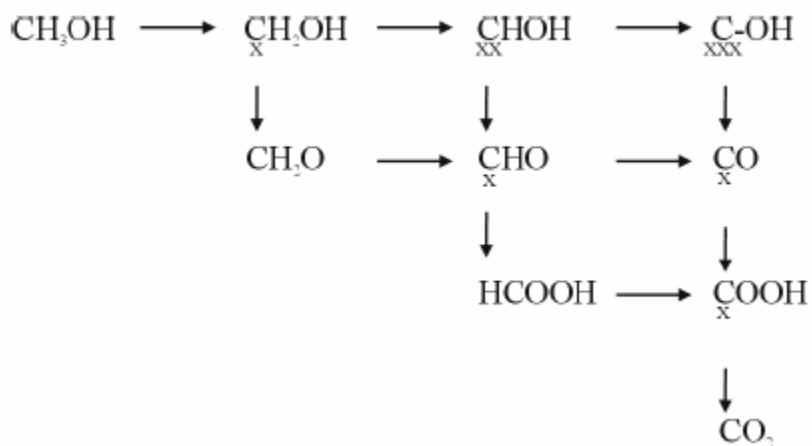
Scheme 1.3 Reaction scheme for methanol oxidation showing all the possible reaction products and possible reaction paths (each x denotes one valence bond with the surface)

Chen *et al*., (2003) have observed experimentally for the first time the formation of formate, the species proposed to be reactive intermediate responsible for the complete oxidation of methanol to CO_2, on the Pt electrode during the methanol oxidation in acidic solutions. Studies of Chen *et al*., (2003) provided deeper and clear insights into the electro oxidation of methanol on Pt electrode. To know the nature of the adsorbed surface intermediate species formed during the electrooxidation process as a function of potential in-situ surface enhanced IR absorption spectra (SEIRAS) were recorded simultaneously with the cyclic voltammograms in the solution containing methanol. Two bands were observed at 2060 and 1860 cm^{-1} at 0.05 V which are attributed to the CO molecules linearly and bridge-bonded to the Pt electrode surface respectively, unequivocally establishing the presence of adsorbed CO on Pt in both linear and bridged fashion. At more positive potential a rapid decrease in the CO band intensities and an accompanying appearance of new band around 1320 cm^{-1} was observed. The intensity of the new band increased with an increase in the potential and a maximum is observed

42

around 1.0 V. Correlation between the anodic current and IR band intensity indicated that the species related to the new peak plays a crucial role in the electro-oxidation of MeOH on the Pt electrode. It was also observed that the peak position of the band shifts from 1320 to 1328 cm^{-1} as the potential is varied from 0.60 to 1.25 V. This gives a clue that the band comes from the species that is adsorbed on the electrode. Also, the band was found to shift to 1300 cm^{-1} when CH_3OH in the solution is replaced with CD_3OH and $^{13}CH_3OH$ implying that the adsorbed species contains both H and C atoms. Endo *et al.*, (2000, 2001) have observed similar band at 1324 cm^{-1} during the oxidation of CH_3OH on Pt (111) by O_2 and UHV or ambient pressure conditions. The band was attributed to the symmetric OCO stretching mode of adsorbed formate. Endo *et al.*, (2000, 2001) have suggested the adsorbed formate to be the reactive intermediate leading to the complete oxidation of methanol to CO_2 on the Pt in the gas phase. Chen *et al.*, (2003) too have attributed the band at 1320 cm^{-1} to the formate ($HCOO^-_{ad}$) adsorbed on the Pt electrode surface. Also, the band corresponding to antisymmetric OCO mode of formate was not observed revealing the fact that the formate was adsorbed on the Pt surface with its C_2-axis perpendicular to the surface, i.e., with the two oxygen atoms bonded to the surface of Pt. Based on the experimental observations, Chen *et al.*, (2003) have proposed the CO and non-CO pathways operated in the reaction mechanism for the complete electro-oxidation of CH_3OH to CO_2 on Pt in acidic solution as depicted in Scheme 1.4.

Pt/C electro catalyst is the best material known so far to be exploited as anode and cathode in the low temperature fuel cells. The high cost of Pt based electro catalyst is one of the major problems preventing the commercialization of fuel cells. In addition,

the CO formed as reaction intermediate during the oxidation of fuel (methanol) poisons the Pt active sites and leads to reduction in the fuel cell performance. Research efforts should be thus focused not only on reducing the amount of Pt used but also on simultaneously overcoming the problem of CO poisoning.
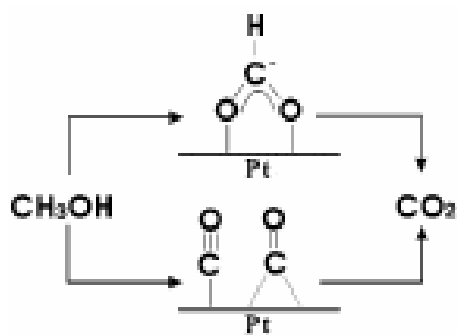
Scheme 1.4 Simplified version of reaction pathways of methanol oxidation at Pt electrode (Chen *et al.,* 2003)

1.4 MOTIVATION, OBJECTIVES AND SCOPE OF THE INVESTIGATION

1. As uniform quality activated carbon is not available indigenously, the objective of the study is to develop a viable process for the production of high surface area activated carbon materials from a widely available, inexpensive carbon precursor and also to exploit the same for energy and environmental applications.

2. Heteropoly acids (HPAs) are strong solid super acid catalysts (Viswanathan *et al.,* 1989). The limitation for the use of heteropoly acids is their low specific surface area in the solid state (≤ 10 m^2/g) (Corma, 1997). One of the ways of increasing the surface area of the HPAs is to support them on a carrier with high surface area. Activated carbon materials are suitable supports for HPAs where in the acidity is retained. Choosing an

appropriate carbon support for HPAs, for typical acid catalyzed reactions like tertiray amyl methyl ether (TAME) and methyl tertiary butyl ether (MTBE) syntheses is a challenge which has been one of the objectives of the study. When loaded on suitable support, HPAs will work as an active solid acid catalyst to be comparable with, or preferable to, the typical solid acids such as silica-alumina, supported phosphoric acid and acidic zeolites (Izumi *et al*., 1983). The study particularly gains prominence as it simultaneously addresses the issues of improving the performance of HPAs and also the production of gasoline additives such as MTBE and TAME which are well known in petroleum industry. Such oxygenates (gasoline additives) are essential to increase the oxygen content of the gasoline above 2 wt. % leading to an improvement in the burning characteristics of the fuel. Addition of oxygenates such as TAME or MTBE to gasoline not only improve the burning characteristics of fuels (Ancillotti *et al*., 1998; Boz *et al*., 2005) but also causes a reduction in CO and unburnt hydrocarbon exhaust emission.

3. Lack of efficient and inexpensive electro-catalysts for MeOH oxidation is a challenge for the large scale utility of direct methanol fuel cells. The objective of this work is to design a cost effective and highly active electro-catalyst by developing new porous carbon material as support for Pt and as an alternative to Vulcan XC 72 R. There are two major problems associated with the development of Direct Methanol Fuel Cells (DMFCs) where Pt is widely used for electrode applications. The first is poisoning of the electrode by CO (Dicks, 2006). The second problem is the high cost of the catalyst restricting the rapid and wide spread commercialization of fuel cells. There are two approaches by which one can remedy these two problems. One approach is to find suitable alternatives

(partial or complete) to the active component i.e., Pt and the second approach is to find a suitable alternative to Vulcan XC 72 R carbon black which is the carbon support material commercially used till date (Rajesh, 2002). Breakthrough in the commercialization of DMFCs is possible by the development of suitable support carbon material.

4. Removal of organo-sulphur compounds from diesel is an issue of interest from scientific, social, economic and environmental view points. Production of clean fuel is the goal of petroleum refining industry. The reduction of S below certain levels in diesel fuels become difficult due to the presence of sterically hindered S-compounds (such as 4, 6 - dialkydibenzothiophenes) that are difficult to desulfurize over conventional supported mixed sulfide catalysts. Newer technologies based on novel routes like adsorption, oxidation and chelation are being developed to remove these refractory S-compounds. Desulphurization process based on adsorption technology is a new promising approach. Desulphurization is realized at ambient temperature and pressure in this process. Development of adsorbents with a high sorption capacity and also appreciable selectivity for sulfur-containing species relative to aromatic and olefinic compounds is a stumbling block which has been addressed in the current study of "Adsorptive desulphurization process" utilizing activated carbon materials as sorbents. Oxygen containing surface functional groups are known to enhance the sorption of di benzo thiophene (DBT). Adsorption capacities were directly correlated to the density of acidic groups on the surface (Ania *et al*., 2007; Alhamed and Bamufleh, 2009, Yu *et al*., 2008). The main objective of the present study is to utilize carbon materials for the adsorptive

desulfurization of a medium S-containing straight run diesel fraction with a S content of 737 ppm, from Cauvery Basin Refinery (CBR), India.

5. Mercury is one of the most toxic elements present in the environment causing ill effects on human health (Ranganathan and Balasubramanian, 2002; Nabais *et al.*, 2006). Central nervous system, kidney function and chromosomes are adversely affected by mercury poisoning. One of the peculiar characteristics of mercury is its bioaccumulation (Madhava Rao *et al.*, 2009). Mercury is absorbed strongly into the biological tissues and the elimination of the same is extremely slow. Search for new technologies, to reduce mercury in the effluent streams whether it be water bodies or air, is necessary and is being pursued actively. 'Adsorption' based technology possess the ability to reduce contaminants (gas and liquid streams) by several orders of magnitude with the operation being relatively simple. Ordinary carbon adsorbents will not be suitable for achieving remarkable decrement in Hg levels. They possess only little capacity for mercury removal. More over, most of the commercially available carbon materials are expensive necessitating the need for the development of low cost carbon materials. Developing low cost and effective activated carbon based sorbents (modified with S) for the removal of Hg from water bodies has been one of the objectives of the study owing to the environmental significance of the issue.

CHAPTER – 2

EXPERIMENTAL METHODOLOGY

2.1 CHEMICALS AND MATERIALS USED

Carbon materials, such as, Black Pearl 2000 and Vulcan XC 72 R were purchased from Cabot Corporation; CDX 975 was supplied by Ms. Columbian Chemicals Company, USA. Nuchar activated carbon was procured from Mead Westvaco chemical division; Calgon carbon was purchased from Calgon carbon (Tianjin) Co. Ltd., China; Adsorbent carbon was purchased from Adsorbent Carbons Pvt. Ltd., Tuticorin, India; IG 18 (18 x 40 mesh), IG 12 Indo (12 x 40 mesh) and IG 8 (8 x 30 mesh) were purchased from German Carbon Limited, India; AC 4 (4 x 8 mesh, coconut shells based), AC 6 (6 x 12 mesh) and AC 12 (12 x 30 mesh) were purchased from Active Carbon India Pvt. Ltd., India; Activated carbon materials 60 CTC 12 x 30 and 60 CTC 4 x 8 were purchased from Sud Chemie India Pvt. Ltd., Graphite fine powder is purchased from Loba Chemie Pvt., Ltd., India. Heteropoly acid ($H_3PW_{12}O_{40}$ nH_2O), Tetra Ethyl Ortho Silicate (TEOS), Hexachloroplatinic acid (H_2PtCl_6), Mercuric chloride ($HgCl_2$), Potassium iodide (KI), Rhodamine 6G, Gelatin, methanol, n-butanol and tert amyl alcohol were purchased from Sisco Research Laboratory, India. 5 wt. % Nafion was purchased from Sigma Aldrich. All the chemicals and solvents used for the investigation were of analytical (AR) grade. The chemicals were used as such without further purification. The Glassy Carbon (GCdisk (0.07 cm^2) and the polishing kit were purchased from Bio Analytical Systems, USA.

2.2 CATALYTIC REACTIONS

The catalytic reactions were carried out in a fixed bed flow reactor (Fig. 2.1) working at atmospheric pressure. The reactants were fed into the reactor by means of a motor driven syringe infusion pump (Miclins syringe peristaltic pump SPO1) for accurate control of the feed flow rate. The catalytic reactor was made up of a pyrex glass tube of about 40 cm length and 2 cm diameter with the inlet tube spiraled around it over the entire length. This enabled the evaporation of the reactant and preheating of its vapours to the reaction temperature before entering into the catalyst zone. The catalyst sample was held between two glass wool plugs which were surrounded by the glass beads. The reactor was kept in a furnace which was electrically heated and its temperature was controlled by a temperature controller (Indian Furnaces, India). The temperature of the catalyst bed was measured with a chromel-alumel thermocouple placed at the centre of the catalyst bed. The effluent stream from the reactor was cooled by means of a double walled Liebig condenser and the liquid products were collected in a cold trap maintained at ice cold conditions.

2.2.1 Product analysis

Quantitative analysis of the liquid products was carried out on a gas chromatograph (Nucon 5765) using Flame Ionization Detector (FID). Nitrogen was used as the carrier gas. The reaction products were analyzed using OV 101 packed column. The products were identified by comparing the retention times of the products with that of the authentic samples.
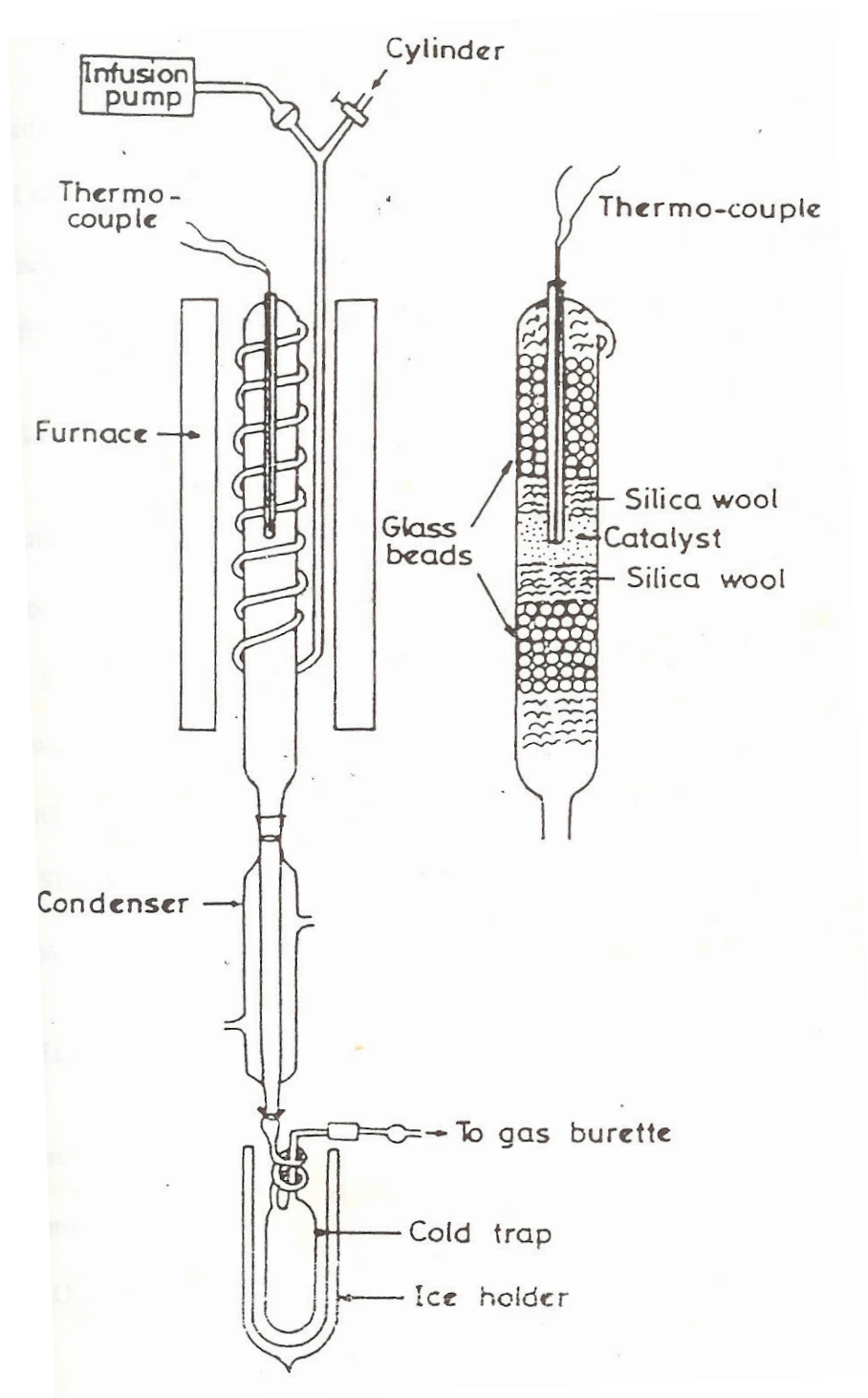
Fig. 2.1. Flow reactor used for catalytic studies

2.3 CHARACTERIZATION TECHNIQUES

2.3.1 Powder X-ray diffraction (XRD) analysis

XRD patterns of various materials were recorded using Rigaku miniflex II desktop X-ray diffractometer operated at 30 kV and 15 mA using CuKα radiation (λ = 1.5418 Å) at a scan rate of 1°/min. The diffraction profiles were obtained in the scan range (2θ) of 5 - 90°.

The interlayer spacing is calculated from the Bragg equation as shown below:

$$d = n\lambda/2Sin\theta$$

where λ is the wave length of the radiation (CuKα) used = 0.15405 nm

θ is the diffraction angle for the peak position.

Using Scherrer equation (shown below), the values of average crystallite size along the c-axis (stacking axis), L_c and along the a - axis, L_a, were determined.

$L = K\lambda/BCos\theta$ where $L = L_c$ or L_a

B is the half-width of the peak in radians and K is the shape factor. The shape factor K depends on the lattice dimension. The K values of 0.9 and 1.84 were used respectively for calculating L_c and L_a values.

2.3.2 Brunauer-Emmet-Teller (BET) sorptometry

The sorptometric analysis on various materials was carried out on Sorptometic 1990 Carbo Erba sorptometer using high pure nitrogen (99.99 %) as adsorbent at 77 K (-196 °C). Prior to the analysis, the carbon samples were out gassed (in an evacuation chamber, Carlo-Erba out gassing unit with a Pirani gauge, at a temperature of 523 K under a vacuum of 10^{-6} Torr for 12 h. The specific surface area values were derived from the

isotherm using BET method in the relative pressure range, p/p_0 (p is the adsorption pressure and p_0 is the saturation vapour pressure), of 0.05 and 0.3 where the monolayer coverage is assumed to be complete and also assuming that the surface area occupied by per physisorbed nitrogen molecule as 0.162 nm^2. The total pore volume was calculated from the amount adsorbed (liquid volume of nitrogen) at a relative pressure of 0.99.

2.3.3 FT-IR spectroscopic studies

The FT-IR spectra of various samples were recorded on Shimadzu spectrophotometer. The spectral range of analysis is 450 - 4000 cm^{-1} with a resolution of 4 cm^{-1}. The spectra were obtained in transmission mode at 20 scans. Pressed KBr pellets were prepared by grinding 200 mg of carbon samples with 0.5 g of KBr.

2.3.4 Confocal Raman spectroscopic studies

The Raman spectra were recorded on a confocal Raman microscope (Alpha-SNOM CRM 200), WITec GmbH, using Ar ion laser (514.5 nm) as irradiation source.

2.3.5 Thermogravimetric/Differential Thermogravimetric (TG/DTA) Analysis

The thermal properties of the materials were evaluated on a Perkin Elmer Diamond TG/DTA instrument. A weighed amount of the sample to be analysed was placed in a cylindrical alumina crucible mounted on one of the 2 mm diameter alumina rods. The sample was heated in a dynamic air atmosphere at a rate of 283 K/min.

2.3.6 Temperature programmed desorption (TPD) of NH_3

NH$_3$ is a probe molecule to measure the total surface acidity of catalysts. Owing to the strong basicity and small molecular size of ammonia it is possible to measure the acid surface sites inside the narrow pores. From the area under the desorption peaks the total surface acidity was obtained. The amount of NH$_3$ desorbed is an indication of the total surface acidity of the catalyst. The NH$_3$ desorption temperature is an indication of the strength of acid sites. Temperature programmed desorption spectra of ammonia on carbon supported heteropoly acids were measured using a conventional TPD apparatus. A sample of 100 mg was preheated in a TPD cell at 773 K for 1 h in a stream of helium and exposed to ammonia at 298 K for 30 min at 1 atm. The gas phase ammonia was subsequently purged with helium. TPD measurements were started from 303 K at a heating rate of 283 K/min using helium as a carrier gas (100 ml/min) up to a temperature of 773 K.

2.3.7 ^{13}C Magic Angle Spinning Nuclear Magnetic Resonance (MAS NMR) spectroscopic study

The ^{13}C MAS NMR spectrum of the carbon materials was recorded on Bruker Avance 400 spectrometer operating at 100.6 MHz (Magnetic field = 9.4 T). The experiments were carried out using silicon nitride rotors spinning at a frequency of about 5.0 to 6.0 kHz. About 1000 transients were recorded. The chemical shifts were externally referred to tetra methyl silane (TMS). Adamentane was used for setting the reference frequency.

2.3.8 Electron Paramagnetic Resonance (EPR) spectroscopic analysis

EPR spectra were recorded on a Varian E-112, X band spectrometer operating at a microwave frequency of 9.2 GHz and at room temperature using di phenyl picryl hydrazyl (DPPH) radical as the external reference to evaluate the g factor value and the spin concentrations. The experimental g-values were determined by substituting the measured values of H and ν into the following equation.

$$h\nu = g\beta H,$$

where h = Planck constant = 6.626×10^{-27} erg s

β_e = Bohr Magneton of electron = 9.274×10^{-27} erg Gauss

H = Magnetic field strength, in Gauss

ν = Micro wave frequency, in GHz

The spin concentration of paramagnetic centers in the carbon materials was calculated using the following formula:

$$N_x = A_x\, G_s\, M_s\, (g_s)^2\, (S(S+1))_s\, N_s/\, A_s\, G_x\, M_x\, (g_x)^2\, (S(S+1))_x)$$

where the subscripts s and x represent the standard (DPPH) and the carbon material under evaluation (unknown) respectively.

A is the area measured under absorption curve

M is the modulation amplitude

G is the relative gain of the signal amplifier

S is the spin number

g is the g factor of EPR signal

DPPH is used as a reference sample for spin concentration estimation.

The molecular weight of DPPH is 394.32 g/mol

Therefore the number of spins per mole of DPPH = 6.023×10^{23}

That is, the number of spins per 394.32 g of DPPH contains 6.023×10^{23} spins

Therefore the number of spins per 1 g of DPPH = $6.023 \times 10^{23} / 394.32 = 1.527 \times 10^{21}$

2.3.9 Scanning Electron Microscopy (SEM) analysis

SEM images of carbon materials were recorded using FEI QUANTA 200 FEG (field emission gun, virtual source) SEM equipped with an elemental analysis system. Carbon samples were placed on aluminum stubs using carbon tape and loaded into the microscope under ambient conditions. Care is ensured that the photographs recorded are representative of the whole of the material (sample) under study.

2.3.10 Elemental (C, H, N and S) analysis

The elemental analysis of the carbon samples was carried out on CHNS/O analyzer (Perkin Elmer Instrument, Series II). Acetanilide was used as reference for calibrating the elemental analyzer. Prior to the analysis the samples were finely ground and dried in air oven at 393 K overnight.

2.3.11 Electrochemical measurements

Cyclic voltammetric studies were carried out on a BAS Epsilon potentiast using modified glassy carbon (Bioanalytical system, USA) as the working electrode, Ag/AgCl (saturated KCl) as the reference electrode and a platinum foil (1.50 cm^2) as an auxiliary electrode. 0.50 M H_2SO_4 was employed as supporting electrolyte. The electrochemical measurements were carried out in a conventional three-electrode glass cell. The methanol oxidation reaction was carried out with 1 M CH_3OH in acid medium.

2.3.12 UV Vis spectrophotometric measurements

UV-Vis spectra of the coloured (R_2HgI_4) solutions were recorded on a Jasco V – 530 UV/Vis spectrophotometer. The residual Hg (II) concentration in the filtrate was analyzed by monitoring the adsorbances at 575 nm (characteristic of R_2HgI_4 complex) using rhodamine 6G (R) and buffered potassium iodide as reagents.

2.2.13 XRF analysis

The S content in the product diesel was analyzed by using an XRF analyzer, Oxford Instruments.

2.3.14 Gas Chromatography – Pulsed Flame Photometric Detector (GC-PFPD)

The individual sulphur compounds in the feed and the product diesel were also analyzed (in some experiments) using a Varian Gas Chromatograph (Model No. CP 3800) coupled with a sulfur specific Pulsed Flame Photometric Detector (GC-PFPD). A fused silica capillary column CP-Sil 5 CB (30 m length x 0.32 mm i.d.), with 1 µm film thickness was used.   The column temperature of 438 K and a heating rate of 275 K/min were employed.

CHAPTER - 3

CARBON MATERIALS FROM CALOTROPIS GIGANTEA STEMS FOR CATALYTIC APPLICATION

3.1 INTRODUCTION

Industrially, activated carbon materials are produced from either coal or lignocellulosic materials (Okada *et al*., 2003). In addition to several specific advantages like retention of the structural features of the original plant tissue (biotemplating feature), carbon materials produced from botanical sources possess high carbon content. The O/C and H/C ratios are lower in the case of carbon materials produced from plant sources rather than from coal. Char from botanical sources or the raw plant material lose H and O more easily than C when heat treated in inert environment (Tseng, 2007). Thus, the carbonization yield is large from lignocellulosic materials.

As uniform quality activated carbon is not available indigenously, the objective of the study is to develop a viable process for the production of high surface area activated carbon from a widely available, inexpensive carbon precursor and also to employ the same as catalyst support. *Calotropis gigantea* (Cg) is a waste land weed native of India with diverse applications. The image of the plant is shown in Fig. 3.1. The fiber from the fruit of *Calotropis gigantea* (Cg) is used as a textile fabric analogous to cotton (Tuntawiroon *et al*., 1984). The roots of the plant aids the accumulation and removal of radio nuclides like ^{90}Sr and ^{137}Cs (Phytoremediation) from nuclear waste streams (Susan *et al*., 2006). The ash from the seeds of the plant is used for the treatment of asthma (Savithramma *et al*., 2007). The flower extracts of the plant are used as a potential

analgesic (Pathak and Argal, 2007). The root extract of the plant is used as a contraceptive (Shobha *et al*., 2007). The plant is available in plenty all through the year and has not so far been explored as a source for carbon material. Exploitation of the stems of the plant for the production of activated carbon is a valuable option from economical and environmental aspects.

Fig. 3.1 Stems, leaves and flowers of *Calotropis gigantea*

3.2 EXPERIMENTAL

3.2.1 Synthesis of carbon material from Calotropis gigantea stems

The dried stems of *Calotropis gigantea* (Cg) were employed as carbon precursor. A known amount of dried stems of plant was heated in a muffle furnace at 573 K for 30 min. Volatile matter was eliminated during pyrolysis resulting in a carbon rich char (Cg as synthesized). The char was ground and sieved (200 mesh). The char is treated with

NaOH (10 wt.% aqueous solution) followed by washing with excess distilled water and drying in an air oven at 393 K. The carbon sample was further treated with conc. HCl (carbon:conc. HCl (wt./vol.%) = 1:10) followed by washing with excess distilled water and drying in an air oven at 393 K. The carbon material obtained after treatment with NaOH and HCl was designated as Cg base acid.

3.2.2 Activation of carbon material

The carbon material obtained after treatment with base and acid (Cg base acid) was subjected to activation. The process of activation involves mechanical grinding of the carbon sample (Cg base acid) and the activating agent in a mortar and pestle. The mixture (carbon and activating agent) taken in an alumina boat was placed in a tubular furnace. Inert atmosphere (N_2) was maintained in the furnace during the activation process. The temperature of the furnace was raised to 1073 K and maintained at that temperature for 2 h. The temperature of the furnace was then lowered. The contents were brought out and treated again with conc. HCl. The ratio (wt./wt.%) of Cg base acid to the activating agent was varied from 1:1 to 1:5.

3.2.3 Preparation of carbon supported heteropoly acid (HPW) catalysts ($H_3PW_{12}O_{40}$ nH_2O/Carbon)

Carbon supported heteropoly acid catalysts were prepared by the method of dry impregnation. Typical method of catalyst preparation comprised of the addition of activated carbon (1.8 g) to the aqueous solution of HPW (0.2 g) in 20 ml distilled water followed by stirring the contents on a magnetic stirrer at room temperature for 6 h

followed by evaporating the excess water to dryness in a water bath kept at 353 K. Thus 10 wt.% HPW/Carbon catalysts were prepared.

3.3 RESULTS AND DISCUSSION

3.3.1 Chemical structure of carbon material (Cg as synthesized, Char)

Useful information about the chemical changes in the original lignocellulosic composition during the initial stages of pyrolysis and the chemical environment of carbon nuclei in the condensed aromatic system (char) was obtained from ^{13}C MAS NMR spectroscopic studies.
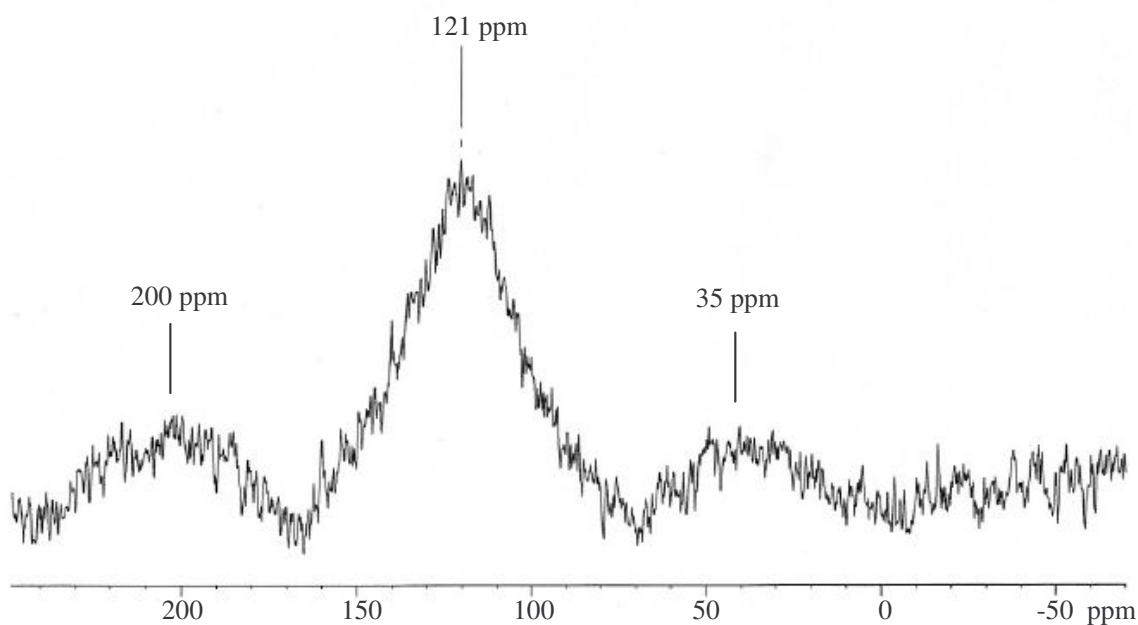
Fig. 3.2 ^{13}C MAS NMR spectrum of the char (Cg as synthesized) from Calotropis gigantea stems

The ^{13}C nuclei belonging to the aromatic carbons resonate at a frequency range distinctly different from that of the aliphatic carbon making NMR an indispensable tool for the analysis of structural (chemical) details of the carbon materials. The evolution of highly

60

aromatic structure from the pyrolysis of original lignocellulosic material (plant stems) is discernable from the high resolution ^{13}C MAS NMR spectrum of the char shown in Fig. 3.2. The strong resonance line near 121 ppm from terta methyl silane (TMS) is characteristic of carbon nuclei in the aromatic planes. In addition, two more broad resonance signals at 35 and 200 ppm attributable, respectively, to aliphatic chains of polymethylene type and ketonic carbon groups were observed in the ^{13}C MAS NMR spectrum of the char.

In general, the three main structural components of stems of plant like Calotropis gigantea are hemicellulose, cellulose and lignin. Typical structural building units of cellulose and lignin (guaiacyl unit) are shown below in Fig. 3.3.
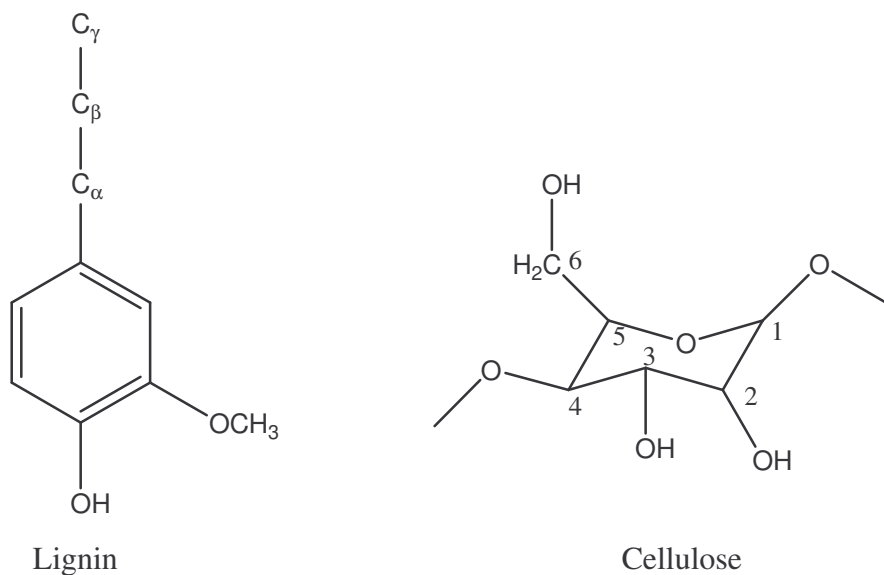
Fig. 3.3 Typical structural building units of lignin and cellulose

Among several structural components of the plant, hemicelluloses are more sensitive to temperature and they are the first to decompose in the temperature range of 473 to 533 K during pyrolysis. Cellulose is thermally more stable than hemicellulose and will decompose in the range of 513 - 673 K releasing structural water. In addition, rapture of the glycosidic linkages also takes place. Aromatization takes place subsequently. Lignin is the most thermally stable component. Decomposition of lignin takes place in the temperature range of 553 - 823 K resulting in the formation of large amount of aromatics (Freitas et al., 2001).

Typically, for lignin, a resonance line at 56.8 ppm associated with methoxy groups and also another resonance line between 115 and 150 ppm attributable to aromatic carbons are observed. The carbon nuclei from cellulose structure resonate at the following chemical shift values: C-1 at 105.8 ppm, C-2, 3, 5 at 73.2 and 75.5 ppm, C-4 at 84.4 and 89.3 ppm and C-6 at 63.5 and 65.0 ppm (Freitas et al., 2001). The carbon nuclei characteristic of hemicellulose structure results in two resonance signals at chemical shift values of 21.8 and 174 ppm respectively corresponding to the methyl and carbonyl carbon nuclei.

Thus the absence of resonance signals characteristic of cellulosic and hemicellulosic structure in the ^{13}C MAS NMR spectrum of the char (Cg as synthesized) (Fig. 3.2) indicates the break down of carbohydrate structure (cellulose and hemicellulose) as a result of pyrolysis and also the conversion of aliphatic groups into aromatic system. The broad and strong resonance signal observed at 121 ppm

corresponding to condensed aromatic system with a turbostratic graphitic structure is a contribution from the complete thermal decomposition of carbohydrate (cellulose and hemicellulose) structure and partial decomposition of lignin structure and also the subsequent reorientation of carbon containing short-lived radical intermediates to hexagonal layered structure of aromatic carbon. The undecomposed component of lignin also contributes to the intensity of the signal at 121 ppm. In fact, chars were supposed to comprise of interwoven network of carbon "ribbons" containing hexagonally arrayed carbon layers - a turbostratic structure.

3.3.2 Effect of NaOH and HCl treatment of the char on the composition of carbon material

SiO_2, oxides of alkali and alkaline earth metals (Na, K, Ca, Mg) and oxides of transition metals (Fe_2O_3) are present in the plant stems inherently. For generating pure carbon material, the inorganic matters need to be removed. Treatment with NaOH is effective in the removal of SiO_2. Mineral matters are dissolved and removed when the char (Cg as synthesised) is treated with conc. HCl (Okada *et al*., 2003).

The effectiveness of base and acid treatment in the removal of inorganic constituents in the carbon precursor is elucidated from the XRD profiles shown in Fig. 3.4. A sharp diffraction peak centered at a 2θ value of 28.7° attributable to silica (Viboon *et al*., 2008) was present in the XRD profile of the as synthesized sample (Fig. 3.4 (a)). Other additional sharp peaks above 2θ value of 28° are also seen in the Cg as synthesized sample which correspond to the presence of mineral matter. Interestingly, all the sharp

peaks corresponding to silica and other mineral matters are absent in the carbon sample (Cg base acid) treated with base and acid in succession (Fig. 3.4 (b)).
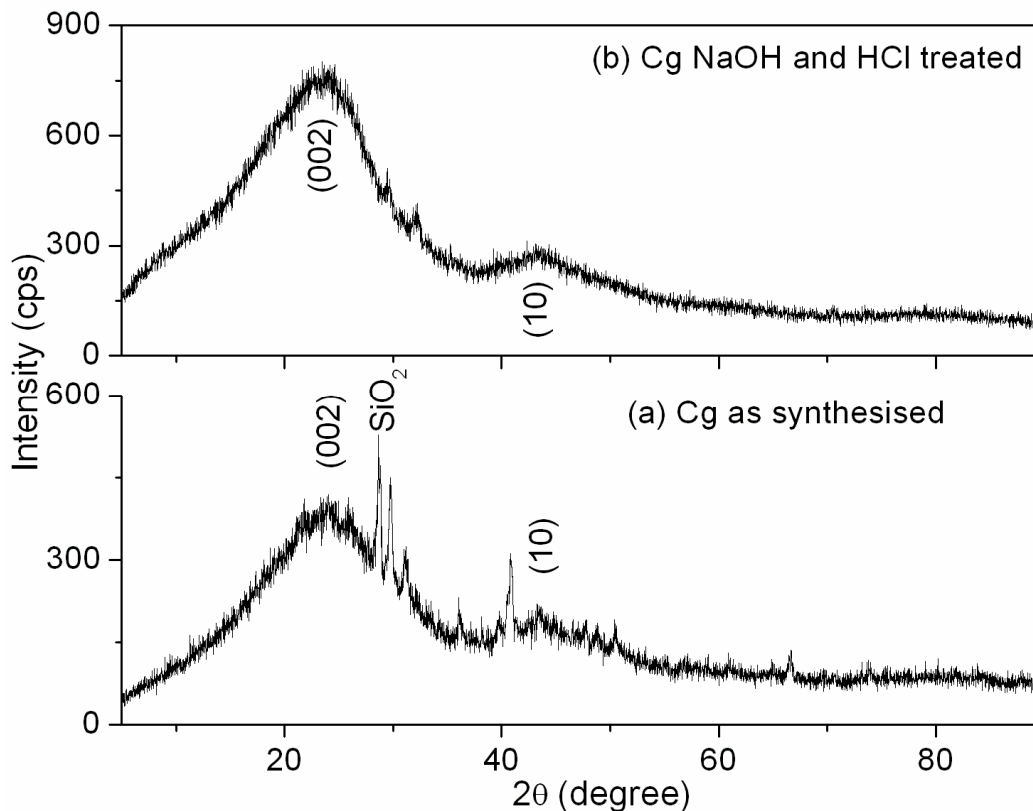
Fig. 3.4 XRD pattern of carbon materials from Calotropis gigantea (Cg) (a) Cg as-synthesized and (b) Cg base - acid treated

This indicates that the treatments with NaOH and HCl are effective in the removal of inorganic impurities present in the as-synthesized carbon material. In addition to XRD analysis, the determination of ash content also indicated the effectiveness of base and acid treatment in the removal of mineral matter. The ash content was determined by adopting ASTM standard procedure bearing the designation D2866-94. The ash content of the as synthesized carbon material decreased from 12.7 to 4.0 wt.% upon treatment with base and acid in succession. Apart from the sharp diffraction peaks corresponding to the crystalline mineral matter, the as-synthesized carbon sample also

resulted in two broad diffraction peaks centered around the 2θ values of 24 and 43°. The two peaks are indexed to the (002) and (10) planes of carbon material respectively (Jyotikusum *et al*., 2009; Devarly *et al*., 2008, Kastening *et al*., 1997, Kinoshita, 1988). The (00l) line is because of inter layer scattering where as the (hk) line is because of intra layer scattering (Ganpat *et al*., 2004; Ruland, 1990; Ruland and Smarsly, 2002).

Analogous to the as-synthesized carbon material, the carbon sample treated with base and acid also resulted in two broad diffraction peaks centered around the 2θ values of 23.3 and 43.5° (Fig. 3.4 (b)). The two peaks were respectively indexed to the (002) and (10) planes of carbon material. The interlayer spacing, d_{002}, is calculated from the Bragg equation, $d = n\lambda/2 \sin\theta$, where λ is the wave length of the radiation (CuKα) used = 0.15405 nm and θ is the diffraction angle for the peak position. The d_{002} values for the as-synthesized and base and acid treated carbon samples were respectively 0.358 and 0.396 nm. These values were higher than the d_{002} value of pure graphite (0.335 nm). This indicates that the carbon materials (as-synthesized and base and acid treated samples) have turbostratic carbon structure with the interlayer spacing value higher than that present in the pure graphitic carbon structures (Devarly *et al.*, 2008). The diffraction peaks corresponding to carbon material are more intense in the case of base and acid treated samples than the as synthesized material. This is an indication of the increase in the carbon content upon base and acid treatment. The same result was noticed from the C, H, N and S analysis shown in Table 3.7 where in the carbon content of the char has increased from 73.13 to 77.62 wt.% upon treatment with base and acid.

Removal of silica and mineral matters from Cg as-synthesized upon treatment with base and acid resulted in the generation of pores and voids which have contributed to the increase in the specific surface area value from 97 to 203 m^2/g as deduced from the N_2 adsorption – desorption isotherms shown in Fig. 3.5.
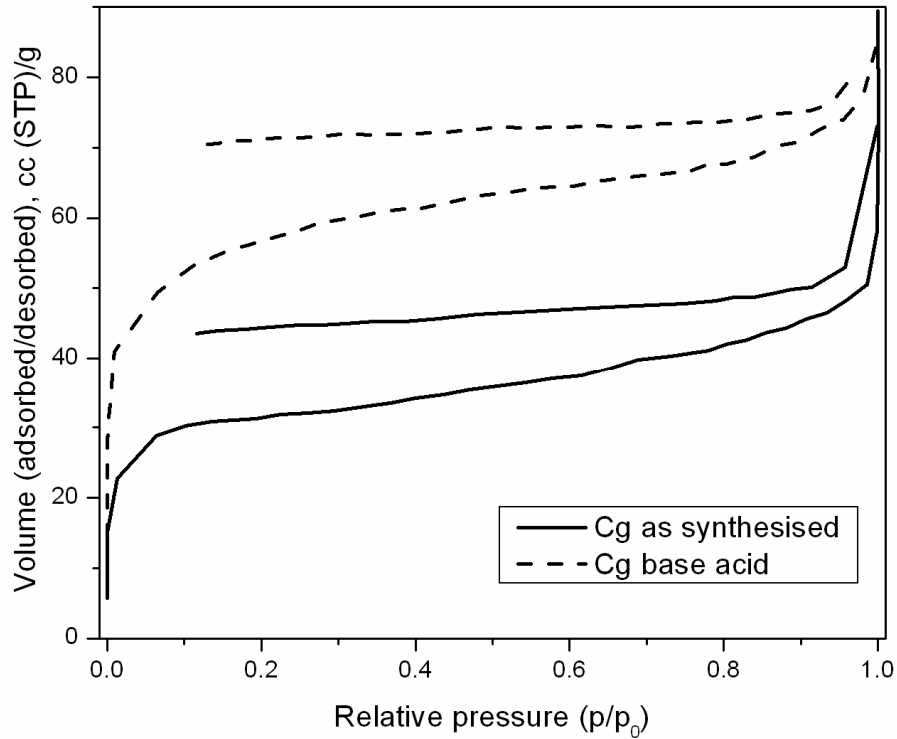
Fig. 3.5. N_2 adsorption-desorption isotherms of carbon materials prepared from Calotropis gigantea, (a) Cg as synthesized (char), S_{BET} = 97 m^2/g, V_p = 0.08 cc/g and (b) Cg base acid (NaOH and HCl treated sample), S_{BET} = 203 m^2/g, V_p = 0.12 cc/g

3.3.3 Methods of activation of carbon material (Cg base acid)

In general, activation is known to generate and develop porosity (in volume and size) in the carbon material. As a result of activation, the adsorption capacity of carbon materials increases (Hu and Vansant, 1995). Activators like transition metal salts ($ZnCl_2$, $ZnCO_3$) alkali metal halides (NaCl, NaBr and NaI), alkaline earth metal salts ($CaCO_3$, CaO,

Ca(OH)$_2$ and CaCl$_2$) and carbonates (Li$_2$CO$_3$, Na$_2$CO$_3$ and K$_2$CO$_3$) and alkali metal salts of carboxylic acids have been evaluated for the chemical activation of carbon materials.

3.3.4 Activation of carbon material (Cg base acid) with transition metal salts

Carbonization and activation are the two important stages in the manufacturing of activated carbon.   The essential reaction taking place during carbonization is the elimination of non-carbon elements (O and H are stripped-off from the carbon precursor). The residual carbon atoms are polylmerized into sheets of condensed aromatic system which are often relatively irregular and disordered.   Because of the misalignment of sheets of condensed aromatic systems relative to each other interstices or voids are formed in the char. But the voids are often blocked by deposition of tar. As a result the incipient pores will be rendered inaccessible. The process of activation is thus inevitable to generate porosity. Pore structure in the char can be developed either by physical or chemical activation (Caturla *et al.*, 1991). In general, the chemical species used for activation are normally dehydrating agents. They influence the pyrolytic decomposition of carbon precursor.   The ability of ZnCl$_2$ to activate (generate porosity) in carbon precursors is based on its dehydrating function. During the process of activation, ZnCl$_2$ eliminates hydrogen and oxygen atoms of carbon materials as water rather than as oxygenated organic compounds leading to the generation of porosity as well as enhancing the carbon content (Hu and Vansant, 1995). Even though ZnCl$_2$ has been extensively used as an activating agent, the possible use of its carbonate counter part (ZnCO$_3$) has never been explored which has been one of the aspects of the present study.

3.3.4.1 Preparation of activated carbon materials using $ZnCl_2$ as the activating agent

The process of activation with $ZnCl_2$ was carried out with varying amounts of activating agent to Cg base-acid (wt. %) ratios, namely, 1, 2, 3, 4 and 5. $ZnCl_2$ was added to the carbon (Cg base acid) in the solid state by mechanical grinding. The mixture was placed in a tubular furnace and heated at 1073 K in N_2 atmosphere for 8 h. The material thus obtained after activation was treated with conc. HCl to remove traces of metallic impurities formed as a result of decomposition of $ZnCl_2$ and subsequently washed with excess of distilled water, filtered and dried. The dried residue was the activated carbon material and is labeled as Cg zinc chloride 1, Cg zinc chloride 2, Cg zinc chloride 3, Cg zinc chloride 4 and Cg zinc chloride 5 for different (wt.%) ratios of activating agent to char, namely 1, 2, 3, 4 and 5 respectively.

3.3.4.1.1 Characterization of Carbon Materials produced by $ZnCl_2$ Activation

Details of the texture, structure and morphology of the activated carbon materials produced from $ZnCl_2$ activation were obtained from sorptometric, XRD, confocal Raman and SEM studies.

3.3.4.1.2 Textural properties of carbon materials activated by $ZnCl_2$ - BET sorptometry

According to IUPAC, porous materials can be classified into three types depending on the pore size (pore diameter). Microporous materials possess a pore size of less than 2 nm. Among micropores, those pores with size less than 0.7 nm are termed as ultra micropores and those pores with sizes ranging between 0.7 and 2 nm are called as super

micropores. Mesopores are those having pore sizes in the range of 2 to 50 nm. Materials with pore sizes greater than 50 nm are termed as macroporous materials (Gregg and Singh, 1982). Irrespective of the amount of the activating agent, all the activated carbon materials presented type I adsorption isotherm for N_2 adsorption at 77 K typical of microporous materials as shown in Fig. 3.6.
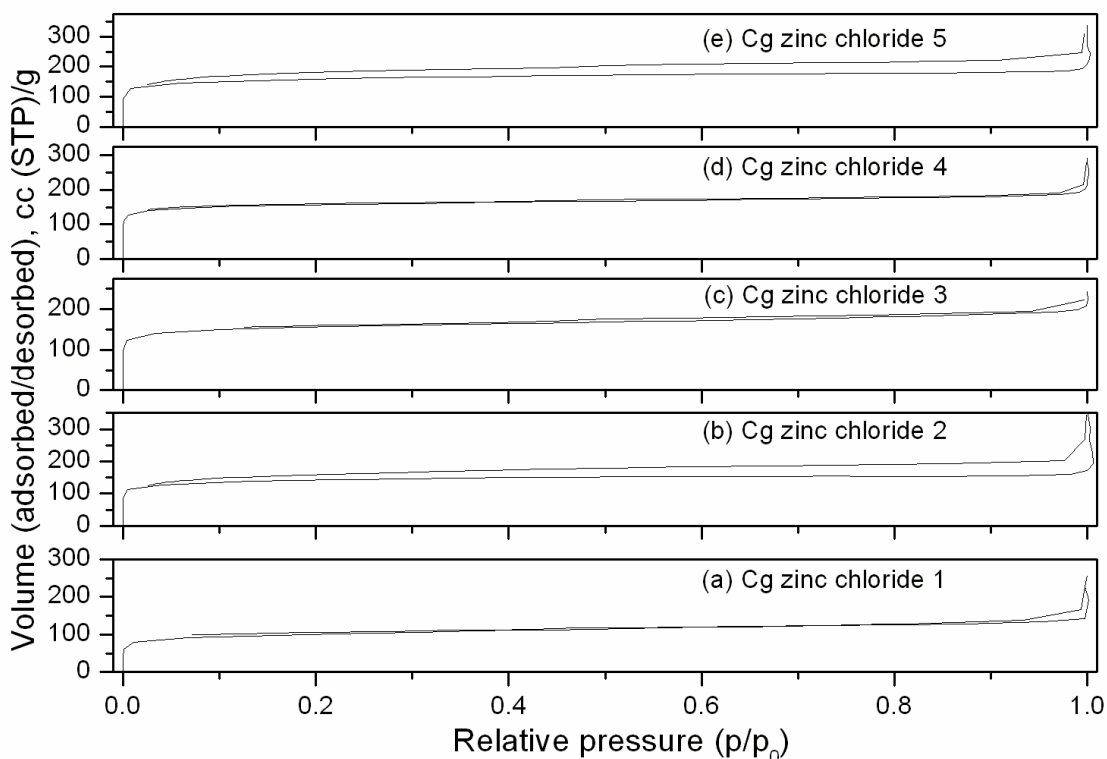
Fig. 3.6 N_2 adsorption-desorption isotherms of activated carbon materials with a Cg base acid to $ZnCl_2$ ratio (wt.%) of (a) 1:1, (b) 1:2, (c) 1:3, (d) 1:4 and (e) 1:5

The specific surface area values, total pore volume as well as the average pore diameter details deduced from the isotherms are summarized in Table 3.1. The specific surface area values of the carbon materials produced gradually increased with $ZnCl_2$ to Cg base acid (wt.%) ratio up to 4 and beyond which no increase in the S_{BET} value was observed indicating that the optimum value of $ZnCl_2$: Char ratio is 4.

Table 3.1. Effect of amount of activating agent (ZnCl$_2$) on the textural properties of
       activated carbon materials

S. no.	Carbon Material	S$_{BET}$ (m^2/g)	V$_P$ (cm^3/g)	Mean pore diameter[a] (nm)
1	Cg zinc chloride 1	356	0.21	2.36
2	Cg zinc chloride 2	493	0.25	2.03
3	Cg zinc chloride 3	564	0.30	2.13
4	Cg zinc chloride 4	573	0.29	2.02
5	Cg zinc chloride 5	553	0.29	2.1

a - Mean Pore Diameter, d = 4V/A (in nm)

where V is the total pore volume and A is the specific surface area

3.3.4.1.3 Structural (crystallographic) properties of carbon materials activated by ZnCl$_2$ – XRD studies

The crystallographic parameters of the activated carbon materials produced by ZnCl$_2$ activation of Cg base acid were obtained from X-ray diffraction studies. Three typical broad diffraction peaks centered around 2θ values of 25, 44 and 80° were visible in the activated carbons generated with the activating agent to Cg base acid impregnation ratios of 1, 2, 3, 4 and 5 (Fig. 3.7.). The two broad peaks centered around the 2θ values of 25 and 44° were indexed to (002) and (10) diffraction peaks of turbostratic carbon structure (Devarly *et al*., 2008).
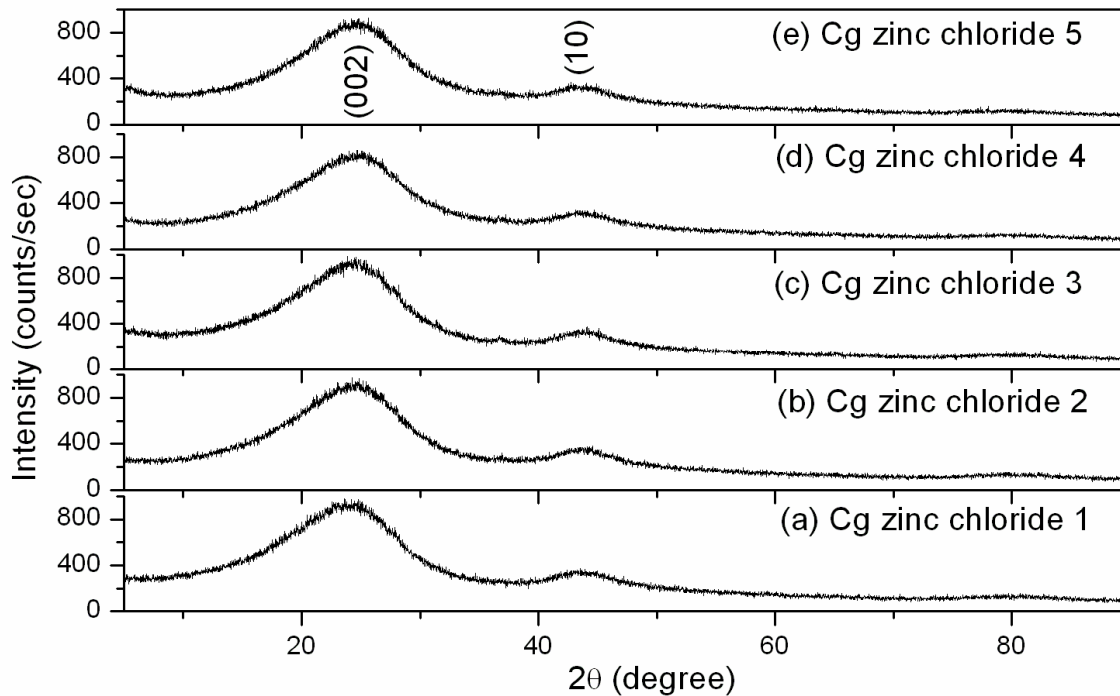
Fig. 3.7 XRD patterns of activated carbon materials prepared from Calotropis gigantea, (a) with a Cg base acid to $ZnCl_2$ ratio (wt./wt.%) of (a) 1:1, (b) 1:2, (c) 1:3, (d) 1:4 and (e) 1:5

The origin of the broad peak around 2θ value of $80°$ is not yet clearly known. The (00l) line is because of interlayer scattering where as the (hk) line is because of intra layer scattering. Thus the extent of graphitization is revealed by the appearance of general (hkl) reflections (Ganpat *et al.*, 2004; Ruland, 1990; Ruland and Smarsly, 2002). The occurrence of broad diffraction bands centered around 2θ values of 25 and $44°$ indicate better layer alignment as well as an increased regularity in the crystal structure (Yang and Lua, 2006). The interlayer spacing values, d_{002}, and the crystallite size values along the c - (L_c) and a - (L_a) axes of the turbostratic graphitic carbon deduced from the X-ray diffractograms are summarized in Table 3.2. Using the Scherrer equation, the crystallite size along the c-axis, L_c and the size of the large planes, L_a, were determined from the diffraction peaks centered at 2θ values of 25 and $44°$ respectively.

Table 3.2 Effect of amount of activating agent ($ZnCl_2$) on the structural properties of activated carbon materials

S. No.	Carbon material	d_{002} (nm)	L_c (nm)	L_a (nm)
1	Cg zinc chloride 1	0.356	1.04	3.94
2	Cg zinc chloride 2	0.356	1.02	3.50
3	Cg zinc chloride 3	0.353	1.03	3.96
4	Cg zinc chloride 4	0.356	0.91	3.72
5	Cg zinc chloride 5	0.350	0.94	3.80

The interlayer spacing values, d_{002}, almost remained unchanged with impregnation ratio of $ZnCl_2$ to char. The interlayer spacing values, d_{002}, summarized in Table 3.2. are in the range of 0.35 to 0.356 nm. These values are greater than 0.335 nm, which is the typical value of the interlayer spacing for pure graphitic carbon. L_c values for different activated carbon materials are of the order of 1 nm. A decreasing trend in the L_c value is observed with an increase in the amount of the activating agent. The L_c value is the smallest for the activated carbon with the highest S_{BET} value. The L_a values varied in the range of 3.5 to 3.96 nm. For typical graphitic carbon, the L_c and L_a values are respectively 0.06708 nm and 0.2461 nm. The magnitude of L_c and L_a values of the activated carbon materials from Calotropis gigantea (obtained by $ZnCl_2$ activation) indicate that the carbon material was made up of crystallites with dimensions of (on the average) about 15 cell lengths along the c-direction and about 14-16 cell lengths along the a - direction.

3.3.4.1.4 Order and Disorder in structure of carbon materials activated by $ZnCl_2$ - Raman Scattering Studies

The microstructural changes and the extent of crystallographic disorder (concentration of lattice defects in the graphitic structure) in the activated carbon materials produced from Calotropis gigantia by employing $ZnCl_2$ as activating agent were analysed using confocal Raman spectroscopic studies.
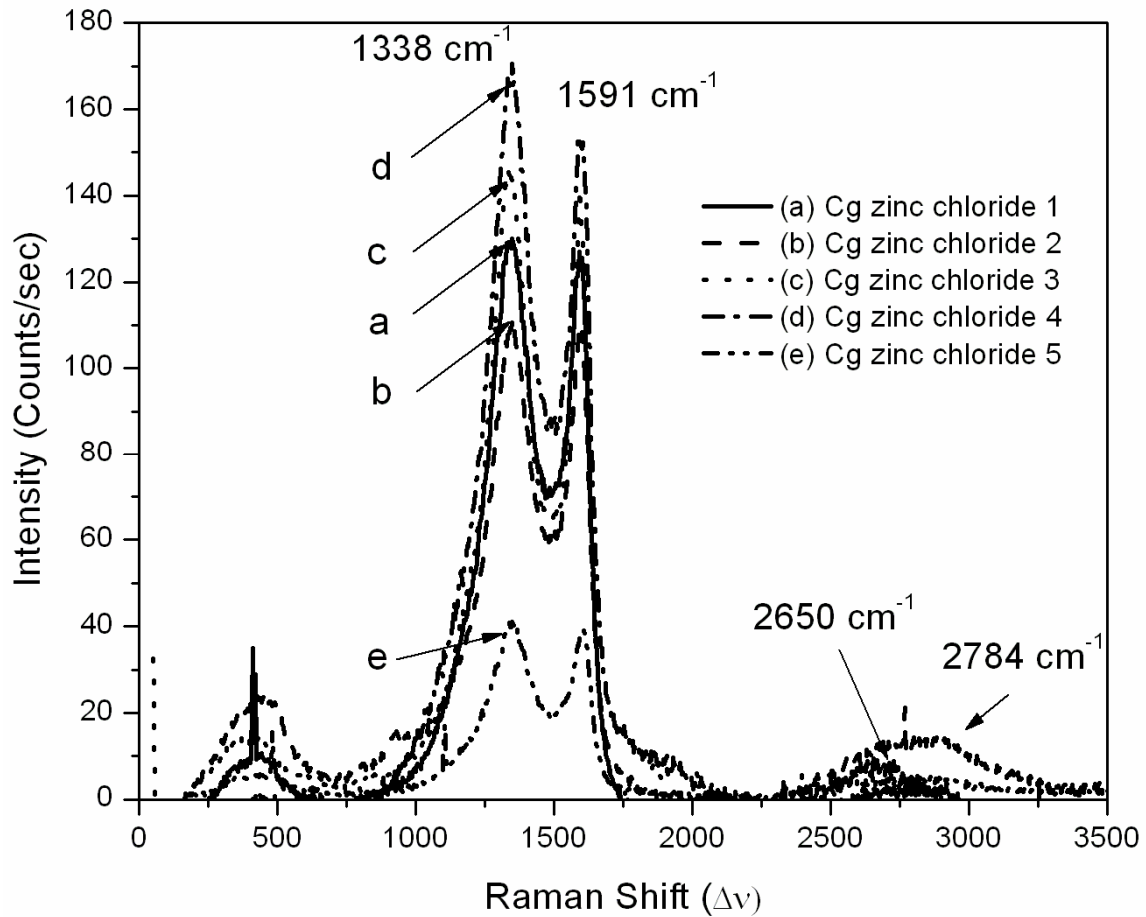
Fig. 3.8 Confocal Raman spectra of activated carbon materials prepared from Calotropis gigantea with a char to $ZnCl_2$ ratio (wt./wt.%) of (a) 1:1, (b) 1:2, (c) 1:3, (d) 1:4 and (e) 1:5

The Raman spectra resulting from activated carbon materials produced by varying the ratios of the activating agent ($ZnCl_2$) to the char (wt.%/wt.%), namely, 1, 2, 3, 4 and 5, were shown in Fig. 3.8. Irrespective of the amount of the activating agent, all the carbon materials, showed both first order (1200-1600 cm^{-1}) and second order (2400-3300 cm^{-1}) Raman lines. The information derived from the features of the first and second order Raman lines are important to access the structural order or disorder in the carbon structure and to find out whether a particular carbon material is amorphous or graphitic. First order Raman lines speak only about the structural order or disorder with in the carbon sheet or layer, i.e., carbon plane along a-axis. They are silent about the stacking order or disorder in carbon structure. On the contrary, second order lines hold information about the structural (stacking) disorder along the crystallographic c-axis (Lespade *et al*., 1982).

The two first order lines centered around 1590 (D-band) and 1348 (G-band) cm^{-1} are attributed to the graphitic and disordered carbon structure. Here the term "graphitic" means carbon atoms which are three coordinated and are bound by sp^2 type bonding orbitals and has nothing to do with the stacking of layers along c - direction. The disorder in the carbon sheet may be because of the non-planar microstructure distortions or because of the disorganized regions near the crystal edges. Lattice defects such as edge dislocation and lattice vacancies too contribute to the band at 1348 cm^{-1}. Important information extracted from the Raman spectra in Fig. 3.8. is summarized in Table 3.3. The Raman intensity ratio (R) which is a measure of the extent of disorder (quantity of defects and vacancies and dislocations) is found to decrease initially up to the activating

agent to char impregnation ratio of 3, beyond which it (R, disorder) increases. An inverse

relation is observed between the value of R and the stack width L_a (crystallite size along

a-axis). The position of the D band (peak intensity position) and the relative intensity of

the D band are found to be structure sensitive.

Table 3.3 Structural parameters (from Raman spectra) of the activated carbon materials
from *Calotropis gignatea* activated with $ZnCl_2$

S. No.	Carbon material[a]	Peak Intensity Frequency, $v_{x,}$ cm^{-1}		$R = I_D/I_G$	L_a (nm) = 4.4/R (From Raman)	L_a (nm) (from XRD)
		G band	D band			
1	Cg z c1	1591	1348	1.40	3.14	3.94
2	Cg z c 2	1591	1355	1.42	3.09	3.50
3	Cg z c 3	1591	1331	1.33	3.30	3.96
4	Cg z c 4	1587	1348	1.48	2.97	3.72
5	Cg z c 5	1606	1348	1.53	2.87	3.80

[a]: zc – zinc chloride

An increase in the frequency value of the D band is correlated with a decrease in the

crystallite size (L_a) and vice versa. A strong correlation between the structural parameters

deduced from XRD studies (Table 3.2) as well as Raman studies (Table 3.3) is observed

as the two afore mentioned techniques are mutually complimentary to each other.

Interestingly, the L_a values ($L_a = 44/R$ in Å) deduced from the relative intensity of the D

band of the activated carbon materials correlates well with the L_a values obtained from

XRD studies using the Scherrer equation (Table 3.2). But, it should be noted that the

measurement of line width from the XRD is more accurate than the measurement of the integrated peak intensity values deduced from the Raman spectra. As a result, the L_a values derived from XRD are more reliable than those deduced from the Raman spectra. In addition, the integrated intensity values from Raman spectra are sensitive to the choice of the base line. As a result, the Raman intensity ratios (R) shown in Table 3.3. are uncertain up to ± 7 %.

3.3.4.1.5 Surface morphology of carbon materials activated by $ZnCl_2$ - Scanning Electron Microscopic (SEM) Analysis

Details of the surface morphology of the activated carbon materials from Calotropis gigantea using $ZnCl_2$ activation ($ZnCl_2$ to char (wt.%/wt.%) = 1 and 3) were obtained from Field emission gun scanning electron microscopy (FEG SEM) studies. The SEM images reveal that the carbon material is composed of sheets of carbon with well aligned uniform circular pores (Fig. 3.9). In addition, the amount of activating agent has a strong impact on the pore evolution. When the amount of activating agent is lower (Cg zinc chloride 1) the pores are in the incipient stage where as with an increase in the amount of activating agent (Cg zinc chloride 3) under identical preparation conditions, the pores are fully evolved.

The porosity observed in the SEM images support the drill hole model, represented in Fig. 3.10, proposed to give some idea on the porosity and internal accessibility of the activated carbon materials.
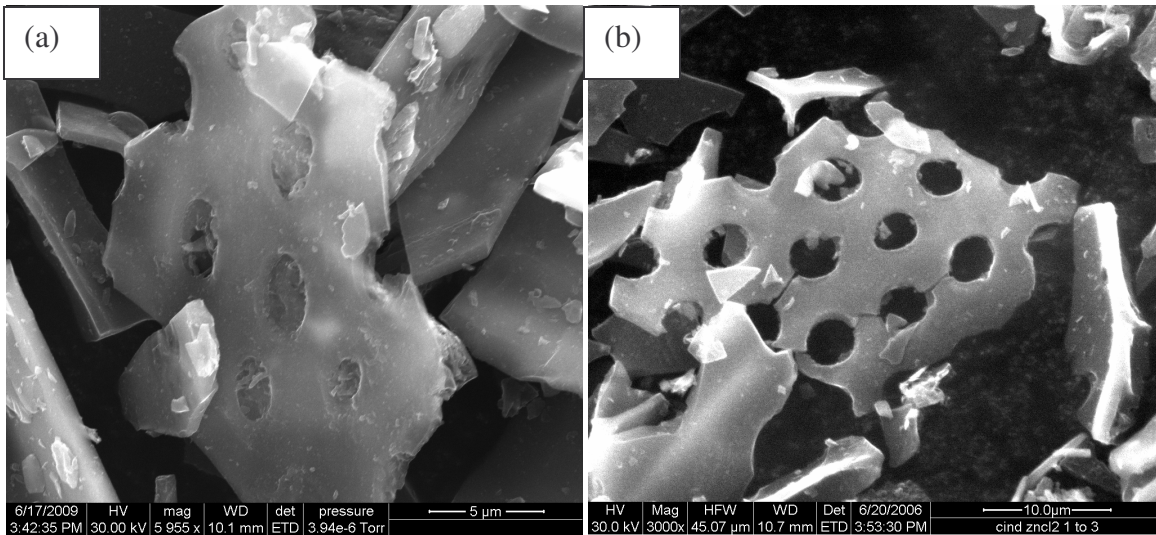
Fig. 3.9 FEG SEM images of activated carbon materials from Calotropis gigantea (a) Cg
zinc chloride 1 (5955 X) and (b) Cg zinc chloride 3 (3000 X)
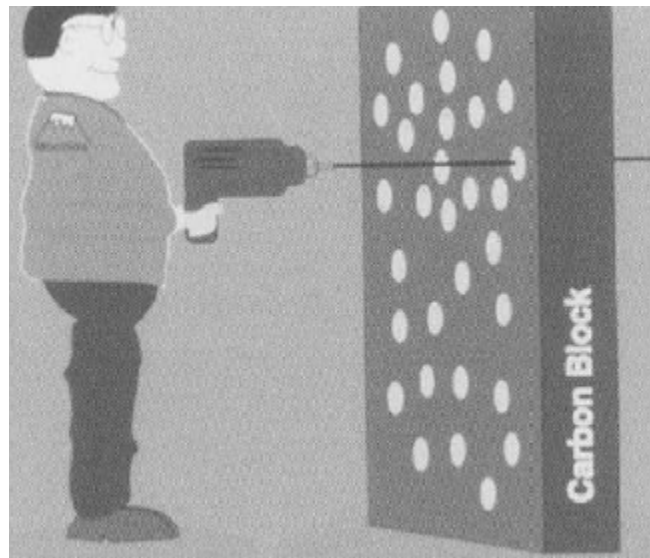
Fig. 3.10 A model of porosity in activated carbon as being isometric drill holes in a solid
(Marsh and Rodriguez-Reinoso, 2006)

3.3.4.2 Preparation of Activated Carbon Materials using ZnCO₃ as the Activating

Agent

The highest value of S_{BET} achieved with $ZnCl_2$ activation is only 573 m^2/g (Cg zinc chloride 4). To gain improvement in the properties (textural, structural and morphological) of the activated carbon material derivable from Calotropis gigantea the usefulness of $ZnCO_3$ as activating agent is evaluated. Typical process of activation with $ZnCO_3$ involves heating the mechanical mixture of Cg base-acid and activating agent ($ZnCO_3$) with a wt.% ratio of 1 in a tubular furnace at 1073 K in N_2 atmosphere for 8 h followed by treating the resulting material with conc. HCl for 1 h to remove traces of metallic impurities formed as a result of decomposition of $ZnCO_3$. The contents were subsequently filtered, washed with excess distilled water and dried in air oven at 423 K. The dried residue, the activated carbon material was labeled as Cg zinc carbonate 1. The properties of Cg zinc carbonate 1 were compared with Cg zinc chloride 1 (which was prepared under identical conditions excepting that the activating agent is $ZnCl_2$ rather than $ZnCO_3$) and also with commercial activated carbon materials, namely, calgon carbon (as received) and adsorbent carbon (as received).

3.3.4.2.1 Activation with $ZnCO_3$ and $ZnCl_2$ – A comparison

3.3.4.2.2 Comparison of the Textural properties of carbon materials activated by $ZnCO_3$ and $ZnCl_2$ – BET sorptometry

The N_2 adsorption - desorption isotherms of activated carbon materials produced by $ZnCl_2$ activation (Cg zinc chloride 1), $ZnCO_3$ activation (Cg zinc carbonate 1) and commercial activated carbon materials, namely, Calgon carbon and adsorbent carbon are shown in Fig. 3.11.
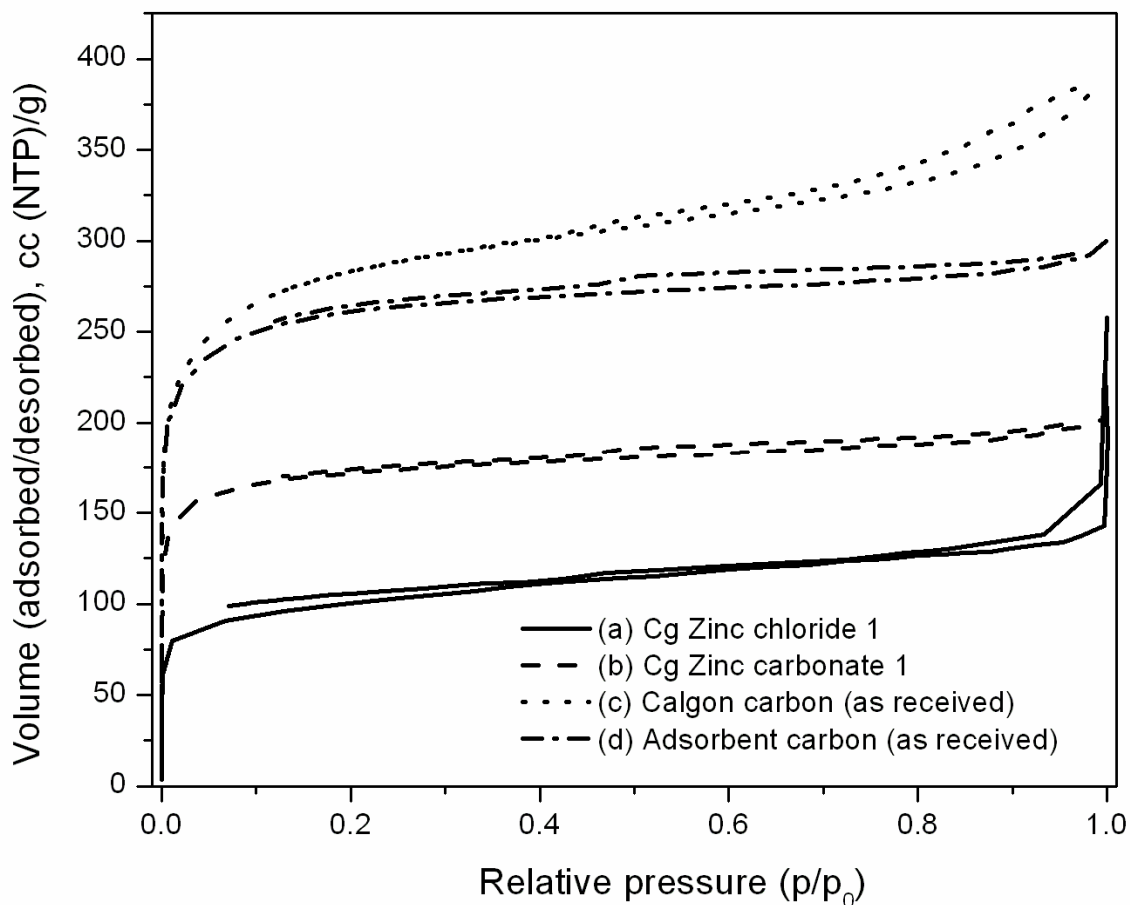
Fig. 3.11 N$_2$ adsorption-desorption isotherms of activated carbon materials (a) Cg zinc chloride 1, (b) Cg zinc chloride 1, (c) Calgon carbon (as received) and (d) Adsorbent carbon (as received)

Except calgon carbon, other three activated carbon materials exhibited type I isotherm characteristic of microporous materials as per IUPAC classification (Gregg and Singh, 1982). The afore mentioned adsorption curves rose sharply at relative pressure up to 0.10. beyond this value of p/p$_0$ the isotherms presented a plateau with increasing relative pressures. Also the adsorption and desorption branches were parallel over a wide range at higher relative pressures. This is an indication of the narrow pore size distribution in microporous materials with slit-like or plate-like pores (Qian *et al.*, 2007).

Table 3.4 Comparison of textural properties of activated carbon materials produced using $ZnCO_3$ and $ZnCl_2$ as activating agents with the commercial activated carbon materials

S. No.	Carbon Material	S_{BET} (m^2/g)	V_P (cm^3/g)	Mean Pore Diameter[a] (nm)
1	Cg zinc chloride 1	356	0.213	2.39
2	Cg zinc carbonate 1	623	0.306	1.96
3	Calgon carbon (as received)	950	0.451	1.90
4	Adsorbent carbon (as received)	1014	0.587	2.31

a - Mean Pore Diameter, d = 4V/A (in nm)

where V is the total pore volume and A is the specific surface area

The isotherm resulting from calgon carbon (as received) is of type II. Type II isotherms show an inflection in the region of $p/p_0 > 0.1$ as observed in the case of calgon carbon. Also the extent of adsorption rise rapidly at high relative pressure, $p/p_0 > 0.9$. Such isotherms represent adsorption on open surfaces with multilayer formation and are a result of the presence of micropores as well as open surfaces (Gregg and Singh, 1982). Such isotherms seen in the case of calgon carbon also indicate a pore structure which is a combination of micropores and mesopores (Puziy *et al*., 2003; Chandra *et al*., 2007). The specific surface area values, total pore volume as well as the average pore diameter details deduced from the isotherms are summarized in Table 3.4.

3.3.4.2.3 Comparison of the crystallographic structure of carbon materials activated by $ZnCO_3$ and $ZnCl_2$ – XRD studies
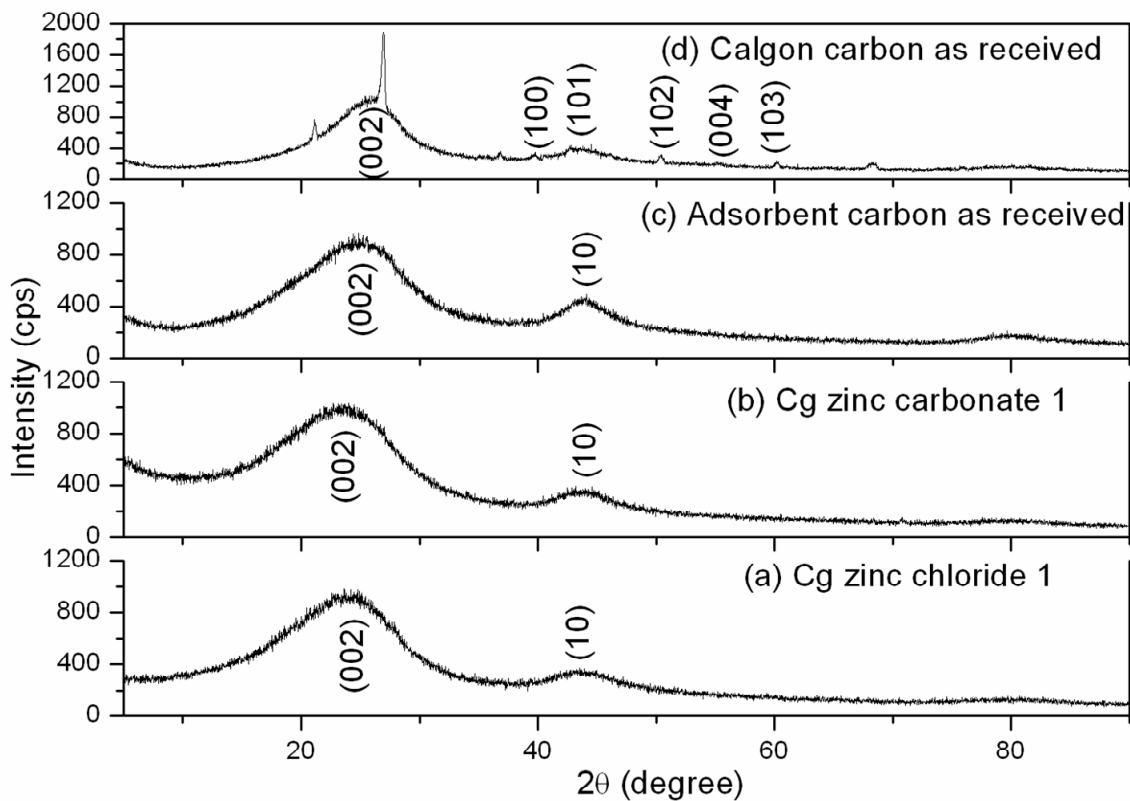
Fig. 3.12 XRD pattern of activated carbon materials (a) Cg zinc chloride 1, (b) Cg zinc carbonate 1, (c) Adsorbent carbon (as received) and (d) Calgon carbon (as received)

The X-ray diffraction patterns of activated carbon materials, namely, Cg zinc chloride 1, Cg zinc carbonate 1, Adsorbent carbon (as received) and Calgon (as received) are shown in Fig. 3.12. The XRD patterns of Cg zinc chloride 1, Cg zinc carbonate 1 were similar to that of Adsorbent carbon (as received) with three broad diffraction peaks centered around 2θ values of 25, 44 and 80°. The two broad peaks centered around the 2θ values of 25 and 44 were indexed to (002) and (10) diffraction peaks of turbostratic carbon structure. The diffraction peaks arising from Calgon carbon (as received) were indexed and are typical of graphitic carbon structure. Full width at half maxima (FWHM) of the d_{002} reflection is a measure of the crystallinity of the carbon material. The sharper the

81

peak, the greater is the crystallinity. The FWHM (d_{002} reflection) values for Cg zinc chloride 1, Cg zinc carbonate 1, Adsorbent carbon (as received) and Calgon carbon (as received) are respectively 8.80, 9.88, 8.89 and 6.39. The Calgon carbon with lowest (FWHM) value (6.39°) is highly crystalline (more graphitic) and the zinc carbonate activated sample with highest FWHM value is the least crystalline.

3.3.4.2.4 Evaluation of thermal stability of activated carbon materials obtained from $ZnCl_2$ and $ZnCO_3$ activation process - Thermal Analysis

The TG-DTA profiles of carbon materials, namely, Cg zinc chloride 1, Cg zinc carbonate 1, Adsorbent carbon (as received) and Calgon carbon (as received) are shown in Fig. 3.13. The DTA curves show exothermic peak at about 823 K for all the afore mentioned carbon materials. Weight loss is observed in the TG curves corresponding to the DTA exothermic peaks indicating that the weight loss is due to oxidation of activated carbon materials.

Okada *et al*., (2003) have observed similar thermal behaviour in the case of activated carbon material prepared from waste news paper activated by K_2CO_3 and steam. The carbon materials from Calotropis gigantea obtained by activation with transition metal salts ($ZnCl_2$ and $ZnCO_3$) were thermally as stable as commercial carbon materials, namely, Calgon carbon and adsorbent carbon.
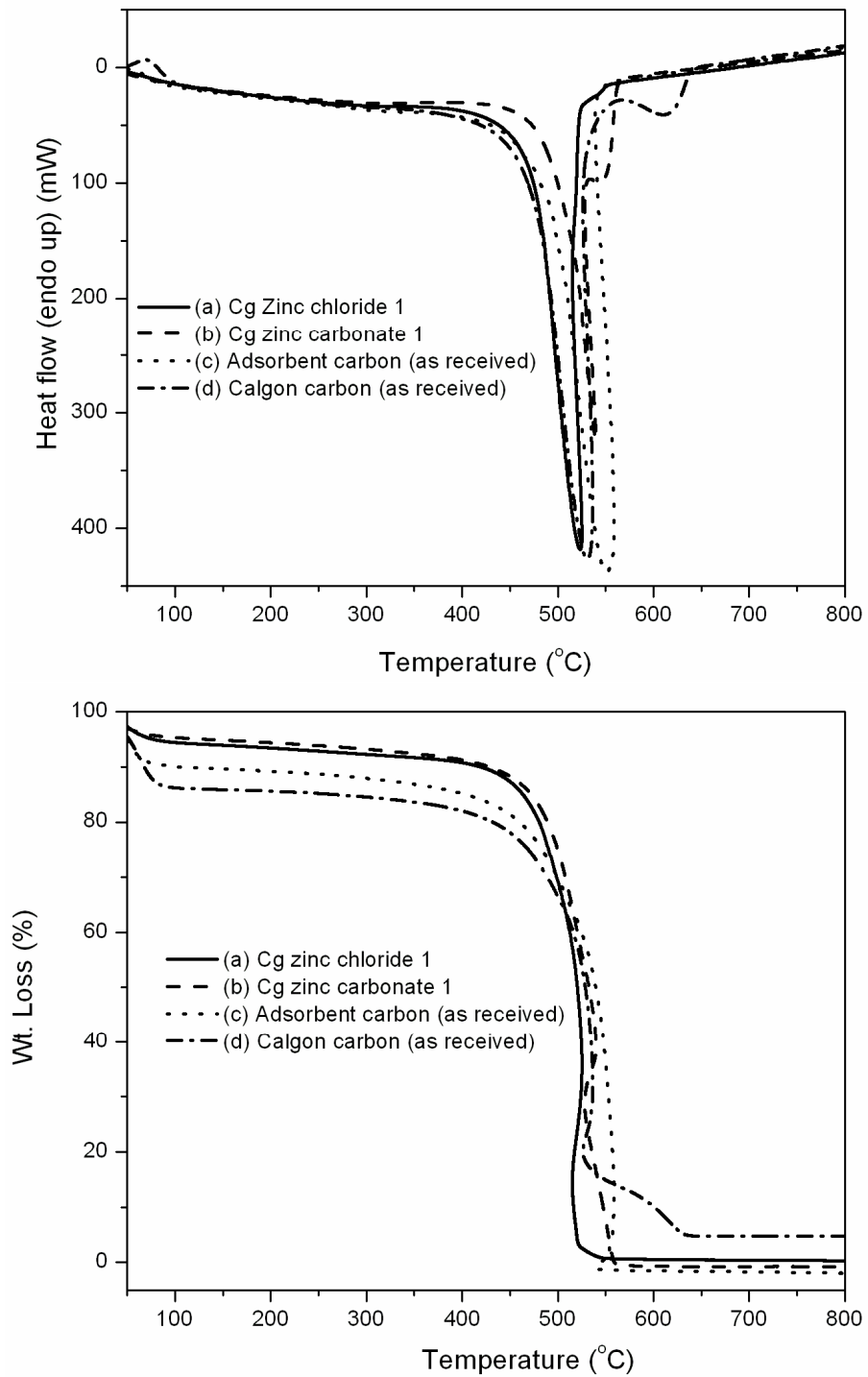
Fig. 3.13 TG – DTA curves of (a) Cg zinc chloride 1, (b) Cg zinc carbonate 1, (c) Adsorbent carbon (as received) and (d) Calgon carbon (as received)

3.3.4.2.5 Scanning Electron Microscopic (SEM) Analysis – Details of Surface Morphology

The FEG-SEM images of $ZnCl_2$ and $ZnCO_3$ activated carbon materials from Calotropis gigantea stems are shown in Fig. 3.14 (a, b, c and d). With the amount of activating agent being the same (activating agent : char = 1:1), the pores are well developed, circular and uniformly distributed through out the carbon sheet in $ZnCO_3$ activated sample (Fig. 3.14. c and d) where as the pores are only in the incipient stage with some carbon particles remaining in the pores in the case of $ZnCl_2$ activated sample (Fig. 3.14. a and b) indicating that $ZnCO_3$ serves as better activating agent than $ZnCl_2$. The CO_2 evolved during the decomposition of $ZnCO_3$ in the activation process facilitates evolution of better porosity. Also, the interaction between $ZnCO_3$ and carbon is better than $ZnCl_2$ and carbon because of the non-hygroscopic nature of $ZnCO_3$ unlike $ZnCl_2$ which is hygroscopic. Also loss of some Zn occurs in $ZnCl_2$ activation process because of the formation of volatile compounds during the activation process which retards the intensity of activation compared to $ZnCO_3$. In addition, even though ZnO is formed as decomposition product in both the cases of $ZnCO_3$ and $ZnCl_2$ activation process, the ZnO formation is not by direct decomposition in the case of $ZnCl_2$ activation but through a redox reaction between $ZnCl_2$ and carbon material. Also the ZnO formed in $ZnCl_2$ activation process is prone to sintering rendering subsequent activation process inactive. Thus $ZnCO_3$ is a better activating agent than $ZnCl_2$. For comparison the SEM images of commercial activated carbon materials, namely, Adsorbent carbon as well as Calgon carbon were shown in Fig. 3.14 (e, f, g and h).
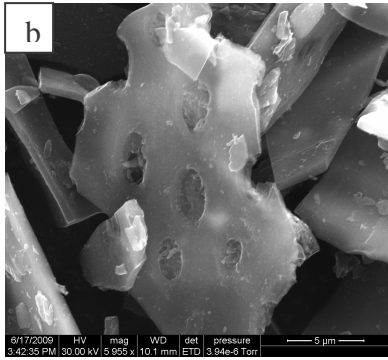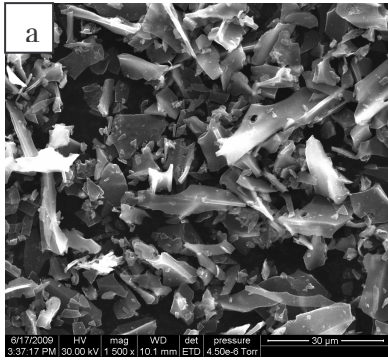
Cg zinc chloride 1

(a) 1500 X

(b) 5,955 X
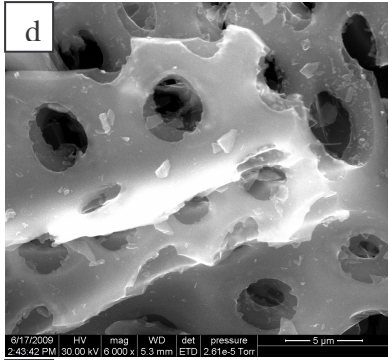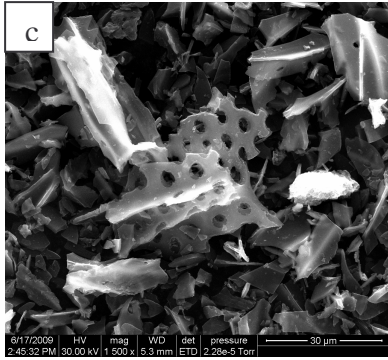
Cg zinc carbonate 1

(c) 1500 X

(d) 6000 X
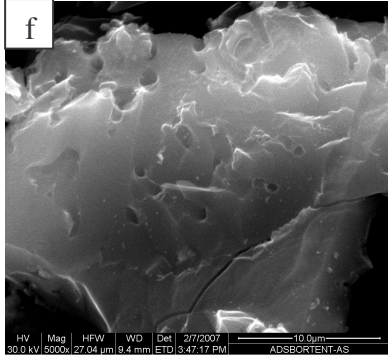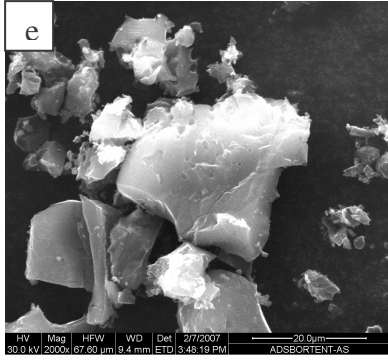
Adsorbent carbon

(as received)

(e) 2000 X

(f) 5000 X
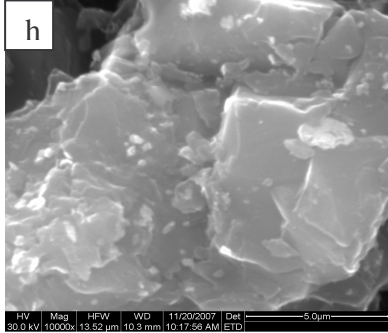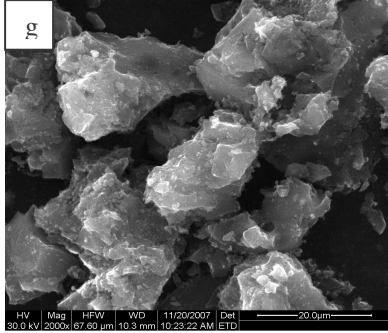
Calgon carbon

(as received)

(g) 2000 X

(h) 10, 000 X

Fig. 3.14 SEM images of activated carbon materials at different magnifications

85

Unlike the activated carbon materials from Calotropis gigantea where in intra particle pores are present, only inter particle pores are observed in the case of adsorbent carbon and calgon carbon. There is a close resemblance between the surface morphology of adsorbent carbon as received and calgon carbon as received. Both the carbon materials possess slate like particle morphology. The surface of adsorbent carbon is relatively smoother than that offered by calgon carbon whose surface is heterogeneous with steps and kinks.

3.3.5 Activation of Carbon Material (char) with Alkali metal halides

The feasibility of employing alkali metal halides as activating agents is explored by using chemicals like, NaCl, NaBr, NaI, KBr and KI as activating agents. Typical process of activation with alkali metal halides involve grinding Cg base-acid and the activating agent in 1:1 (wt.%) ratio in a mortar and pestle followed by heating the mixture in a tubular furnace in N_2 atmosphere at 1073 K for 2 h. This is followed by treating the resulting material with conc HCl for 2 h and subsequently filtering and washing the contents with excess distilled water and drying the resulting carbon material in an air oven at 423 K. The resulting activated carbon materials, designated as, Cg - activating agent - wt.% ratio of char to activating agent, were characterized using BET sorptometry to evaluate the textural properties.

3.3.5.1 Textural properties of carbon materials activated by Alkali Metal Halides – BET sorptometry

The N$_2$ adsorption – desorption isotherms of activated carbon materials (Cg sodium chloride 1, Cg sodium bromide 1, Cg sodium iodide 1) obtained using alkali metal halides, namely, NaCl, NaBr and NaI as activating agents and the char from Calotrpis gigantean (Cg as synthesized) as carbon precursor were shown in Fig. 3.15.
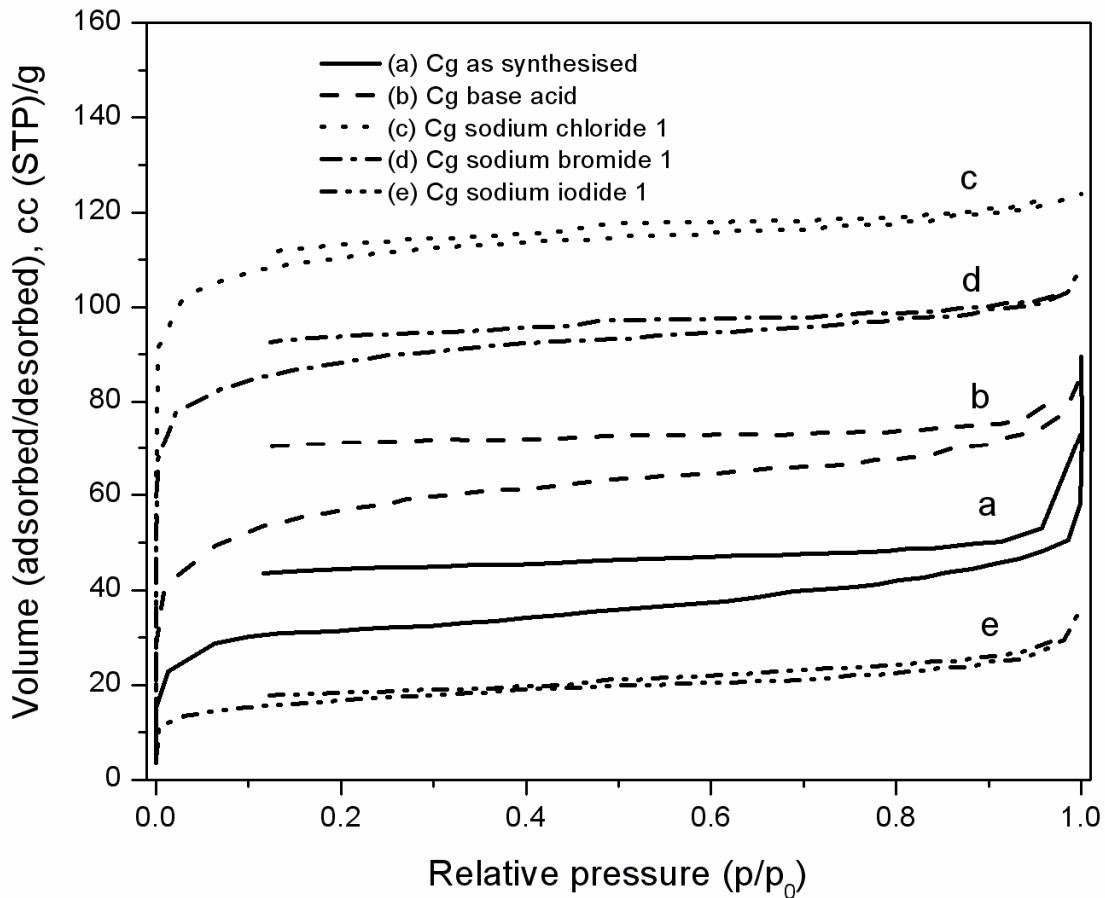
Fig. 3.15 N$_2$ adsorption – desorption isotherms of (a) Cg as synthesized, (S_{BET} = 97 m^2/g, V_p = 0.08 cc/g), (b) Cg base acid, (S_{BET} = 203 m^2/g, V_p = 0.12 cc/g), (c) Cg sodium chloride 1, (S_{BET} = 400 m^2/g, Vp = 0.2 cc/g) (d) Cg sodium bromide 1, (S_{BET} = 319 m^2/g, Vp = 0.16 cc/g) and (e) Cg sodium iodide 1, (S_{BET} = 58 m^2/g, Vp = 0.04 cc/g)

Irrespective of the nature of the activating agent all the activated carbon materials presented type I isotherm indicating that the materials are microporous. The details of textural parameters of the activated carbon materials were indicated in the caption of Fig. 3.15. Interestingly with the use of NaCl as activating agent, S_{BET} and the pore volume values were doubled compared to Cg base acid. Unlike NaCl, activation, use of NaI retarded the S_{BET} as well as the pore volume which were reduced by four times relative to Cg base acid sample under identical activation conditions.

Table 3.5 Influence of alkaline earth metal compounds on the textural parameters of activated carbon materials

S. No.	Activated Carbon Material*	S_{BET} (m^2/g)	V_p (cm^3/g)	Density (g/cc)
1	Cg calcium carbonate 1	524	0.33	0.42
2	Cg calcium oxide 1	521	0.25	0.72
3	Cg calcium hydroxide 1	189	0.11	0.51
4	Cg calcium chloride 1	156	0.09	0.46
5	Cg barium carbonate 1	170	0.10	0.54
6	Cg barium hydroxide 1	152	0.08	0.49

*Designation – Plant name – Activating agent – ratio (wt./wt.%) of activating agent to char; Activation condition: Temperature – 1073 K; Time – 2 h;

The observed trend in the decrease in the textural parameters with the use of NaCl, NaBr and NaI as activating agents is inline with the decrease in ionicity and an increase in covalency from NaCl to NaI. As a result, NaI will be strongly adsorbed on the char. More over the narrow pores which are in the incipient state in the original char will be blocked

by NaI preventing the activation of carbon material. In addition, with the same amount (wt.) of activating agent (NaCl, NaBr and NaI) the wt.% of Na in NaCl, NaBr and NaI are respectively 39.3, 22.3 and 15.3. As treatment of the activating mixture with Conc. HCl is one of the steps in the activation process, with a decrease in the Na content from NaCl to NaI the intensity of activation also decreases rendering NaI inactive for activation of carbon materials. Similar trend in the textural properties is observed when KBr (S_{BET} = 275 m^2/g, Vp = 1.0 cc/g) and KI (S_{BET} = 41 m^2/g, Vp = 0.13 cc/g) were employed as activating agents. In addition to alkali metal halides, the feasibility of employing alkaline earth metal compounds as activating agents has also been evaluated. Among various salts of calcium, calcium carbonate exhibited better performance (Table 3.5).

3.3.6 Activation of Carbon Material (char) with Alkali metal carbonates

The maximum values of specific surface area and pore volume values from $ZnCl_2$ activation are 573 m^2/g and 0.29 cc/g and the values from $ZnCO_3$ activation are 623 m^2/g and 0.306 cc/g. To attain further improvements in the textural parameters, the usefulness of alkali metal carbonates (Li_2CO_3, Na_2CO_3 and K_2CO_3) as chemical activating agents were examined. The char obtained by heating the dried stems of plant in a muffle furnace at 573 K for 30 min was ground and sieved through a 200 mesh sieve to obtain fine carbon particles. It was next ground with the alkali carbonates in the desired proportion and activated at a temperature of 1073 K for 8 h in N_2 temperature. The material thus obtained was treated with conc. HCl to remove the decomposed products of the activating

agent followed by filtering and washing with excess distilled water and drying in air oven.

3.3.6.1 Effect of K_2CO_3 activation on the textural properties of carbon materials – BET sorptometry

N_2 sorption studies provided information on the textural properties (specific surface area, pore volume, and the distribution of pores depending on the size) of carbon materials. The N_2 adsorption – desorption isotherms of the as synthesized as well as the activated carbon materials, using carbonate as activating agent, with different amounts of activating agent (K_2CO_3) were shown in Fig. 3.16. Close inspection of the isotherms gives details of the type and nature of pores present in the carbon materials. Irrespective of the amount of the activating agent, all the activated carbon materials exhibited type I isotherms according to Brunauer, Deming, Deming and Teller (BDDT) classification (Stephen *et al.*, 1940). Such type I isotherms are characteristic of microporous materials having pore diameter < 2 nm. The N_2 adsorption - desorption isotherms arising from activated carbon materials (Cg carbonate) are of typical type I isotherms in nature which are characteristic of microporous materials as per IUPAC classification (Qingrong *et al.*, 2007).

Details of textural parameters of the carbon materials deduced from the isotherms were shown in the caption of Fig. 3.16. The amount (volume) of N_2 adsorbed is the highest (Fig. 3.16. (d)) for the carbon material obtained when the K_2CO_3 to char ratio

(wt./wt.%) ratio of 3 implying the highest specific surface area value (S_{BET} = 1296 m^2/g)

for this material.
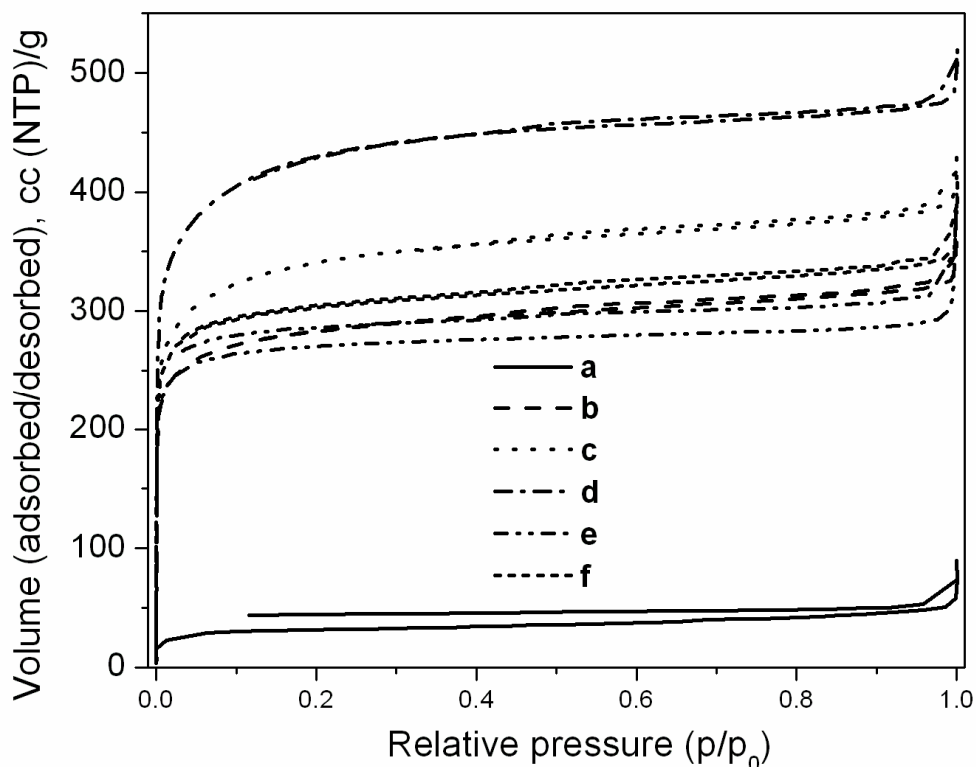
Fig. 3.16 N$_2$ adsorption-desorption isotherms of carbon materials prepared from
Calotropis gigantea, (a) Cg as synthesized (char) (S_{BET} = 97 m^2/g, V_P = 0.08
cc/g), activated carbon with a Cg base acid to K$_2$CO$_3$ ratio (wt.%/wt.%) of
(b) 1:1, Cg potassium carbonate1 (S_{BET} = 892 m^2/g, V_P = 0.5 cc/g)
(c) 1:2, Cg potassium carbonate 2 (S_{BET} = 1083 m^2/g, V_P = 0.59 cc/g)
(d) 1:3, Cg potassium carbonate 3 (S_{BET} = 1296 m^2/g, V_P = 0.73 cc/g)
(e) 1:4, Cg potassium carbonate 4 (S_{BET} = 765 m^2/g, V_P = 0.45 cc/g) and
(f) 1:5, Cg potassium carbonate 5 (S_{BET} = 922 m^2/g, V_P = 0.53 cc/g)

Thus the optimum ratio of activating agent to char is 3 (wt./wt.%) in the case of carbonate

activation. Beyond this ratio of activating agent to char, the S_{BET} as well as the pore

volume values decreased. Thus the S_{BET} (765 to 1296 m^2/g) as well as the V_p (0.45 to

0.73 cc/g) values of the carbon material are tunable as a function of the amount of activating agent.

Evaluation of the pore size distribution (PSD) is of paramount importance in the characterization of microporous materials. The PSD of the char as well as the activated carbon materials produced from different K_2CO_3 impregnation ratios using Horvath-Kawazoe method were shown in Fig. 3.17. Owing to the computational simplicity, Horvath-Kawazoe (HK) method is preferred compared to the density functional theory. The impregnation ratio is found to have a profound effect on the PSD of the activated carbon materials. With an increase in the impregnation ratio upto a K_2CO_3 to char ratio of 3, the micro pore structure (pore radius between 2 to 4 Å) as well as the mesopore volume (pore radius between 10 to 15 Å), formed by the widening of the micropores, increased resulting in an increase in the total pore volume. Beyond a K_2CO_3 to char ratio of 3, the intensity of micropore volume as well as the mesopore volume decreased due to blocking of the pores. Such pore blockage by both partial collapse of the pore wall as well as by the decomposed products of the activating agent is more pronounced in the case of activated carbon produced with a K_2CO_3 : char (wt.%/wt.%) ratio of 4 (Fig. 3.17. (e)).

Up to a K_2CO_3 to char (wt./wt.%) ratio of 3, there is a tremendous increment in the amount of N_2 adsorbed indicating an increase in pore volume and specific surface area of the carbon material as a result of evolution of pores as well as widening of the existing pores. A peculiar behaviour is observed in the textural properties of the carbon

material obtained at a char to K_2CO_3 ratio of 1:4 indicating a sort of transition being taking place at this stage.
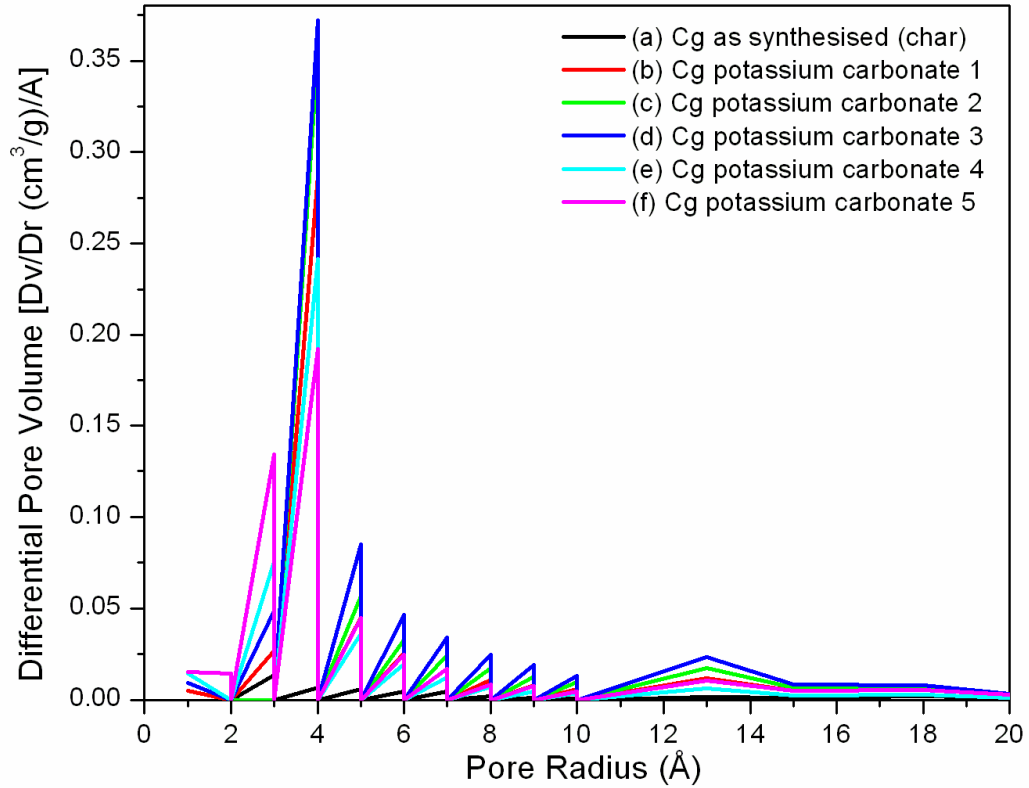
Fig. 3.17 Pore size distribution curves, based on Horvath-Kawazoe method, of carbon
materials prepared from Calotropis gigantea, (a) Cg as synthesized (char),
activated carbon with different char to K_2CO_3 ratio (wt.%/wt.%) of (b) Cg
potassium carbonate 1, (c) Cg potassium carbonate 2, (d) Cg potassium
carbonate 3, (e) Cg potassium carbonate 4, and (f) Cg potassium carbonate 5

Even though, all the carbon materials produced from activation with different amounts of K_2CO_3 exhibited type I isotherms indicating that all the carbon materials are microporous in nature there are significant differences in the shapes of isotherms offering valuable information. Firstly, the isotherm curve Fig.13.17 (e) is exactly lying parallel or horizontal to the relative pressure (p/p_0) axis (X-axis) implying that the activating carbon material obtained from a char to K_2CO_3 (wt.%/wt.%) ratio is exclusively microporous.

Major uptake occurred at a low relatively pressure (less than 0.1). This is an indication of the formation of highly microporous material with a narrow pore size distribution. Gregg and Sing (1982), have attributed such complete filling of pores at very low relative pressure in the case of microporous materials to the strong interaction potential between the adsorbent and adsorbate. Also the initial steep region was abruptly followed by a plateau. This indicates that the adsorption is stopped owing to the close proximity of the pore wall preventing the formation of multilayers. Thus mesopores and macropores are absent in the case of activated carbon produced with a K_2CO_3:Cg base acid ratio of 4.

The exclusive microporous nature and also the decrease in the micro and mesopore volumes in the afore mentioned case were observed in the pore size distribution (PSD) curve shown in Fig. 3.17. (e). In addition there is a pronounced decrease in the specific surface area value of the carbon material activated upon increasing the char to K_2CO_3 ratio from 1:3 to 1:4 (SSA decreased from 1296 to 765 m^2/g) indicating blockage of micropores as well as the mesopores. Unlike the case of activation with a char to K_2CO_3 activation with a ratio (wt.%/wt.%) of 1:4, Fig. 3.17. (e), other isotherm curves (Fig. 3.17. (b), (c), (d) and (f)) exhibited appreciable slope in the isotherm in the high pressure region. Such a marginal increase in adsorbed volume in the relative pressure range of 0.35 - 0.95 with an increase in the char to K_2CO_3 ratio (wt./wt.%) from 1:1 to 1:3 can be attributed to the formation of mesopores as a result of the pore widening. Formation of such mesopores (an increase in pore volume in the range of 20 – 30 Å (pore diameter)) is observed in the PSD curves Figs. 3.17. (b), (c), (d) and (f).

3.3.6.2 Effect of K₂CO₃ activation on the chemical environment and the concentration of unpaired electrons in carbon material –EPR spectroscopic study
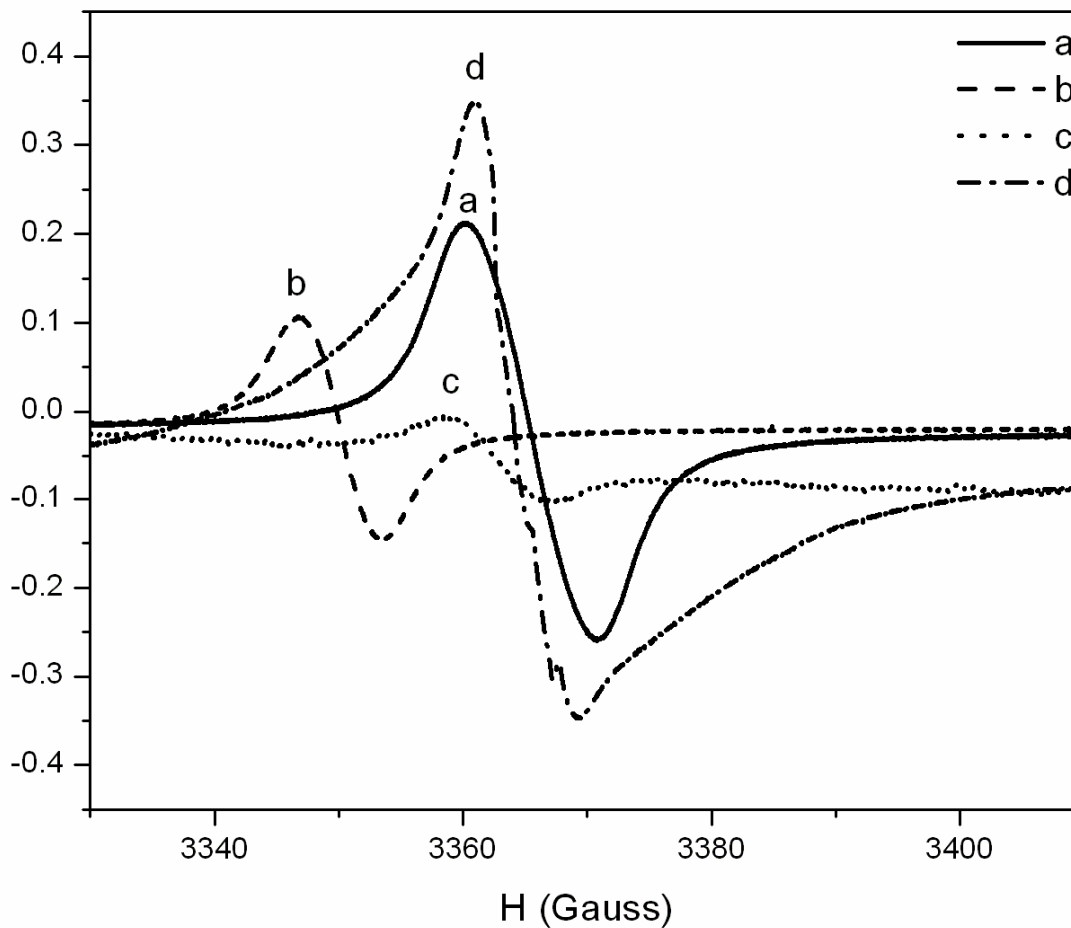
Fig. 3.18 EPR spectra of carbon materials from Calotropis gigantea (a) Cg as synthesised (b) Cg base acid (c) Cg carbonate 3

The EPR spectra of Cg as synthesized, Cg base acid and Cg potassium carbonate 3 were shown in Fig. 3.18. The g-factor values, peak to peak separation, ΔH in Gauss, and the spin concentration values were evaluated and are summarized in Table 3.6. The spin concentration values were determined by following the procedure described in reference (Sarathi *et al*., 2007).
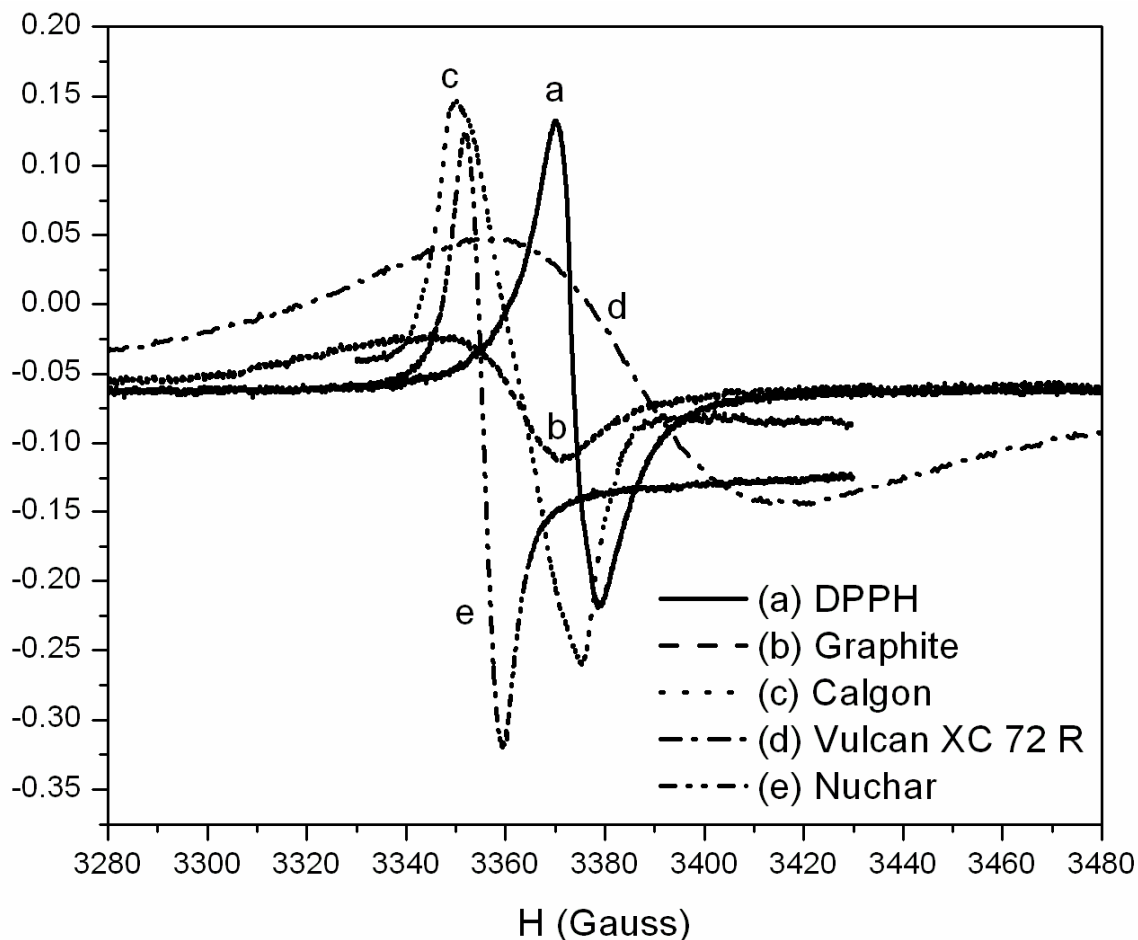
Fig. 3.19 EPR spectra of commercial activated carbon materials (a) di phenyl picryl
hydrazyl radical (DPPHP), external reference, (b) Graphite (g = 2.01805, SC =
0.14 x 10^{18} spins/g, (c) Calgon (g = 2.00050, SC = 2.3 x 10^{18} spins/g), (d)
Vulcan XC 72 R (g = 2.00839, SC = 1.6 x 10^{18} spins/g) and (e) Nuchar (g =
2.01284, SC = 0.53 x 10^{18} spins/g)

For comparison the EPR spectra of some of the well known commercial carbon materials,

namely, Graphite, Calgon, Vulcan XC 72 R and Nuchar were recorded and are shown in

Fig. 3.19. The g values as well as the spin concentration values were indicated in the

caption of Fig. 3.19. The g values of commercial carbon materials were found to be close

to that of the g value of Cg potassium carbonate 3 where as the spin concentration values

of the commercial carbon samples were found to be two orders of magnitude higher than

the value observed for Cg potassium carbonate 3.

Table 3.6 The g-factor, peak-to-peak separation (ΔH in Gauss) and concentration of
unpaired electrons in the carbon materials produced from Calotropis gigantea

Carbon Material	g-value	ΔH (in Gauss) Peak to peak separation	Spin concentration (SC) / g of carbon
Cg as synthesized	2.00092	11.0	0.73×10^{19}
Cg base acid	1.99980	6.0	0.33×10^{19}
Cg potassium carbonate 3	2.00058	9.5	0.15×10^{16}

Important details from the data derived from the EPR spectra shown in Fig.3.18 and

summarized in Table 3.6 are :

(i) The g factor values of Cg as synthesized, Cg base acid and Cg potassium carbonate 3

are close to the g value of the free electron (2.002312) with in the error of our

experiments ($\pm$ 0.002). Manivannan *et al.,* (1999), Ganpat *et al.,* (2004), Singer and

Wagoner (1968), Chauvert and Forro (1995) and Zhuo *et al.,* (1994) have made similar

observations in the case of carbon materials produced from a variety of precursors.

(ii) The peak to peak separation was found to be higher in the case of Cg as synthesized

(ΔH = 11.0 Gauss) compared to either Cg base acid or Cg potassium carbonate 3. Such a

broadness in the EPR signal is attributed to the presence of SiO_2 in the original char

which was confirmed from XRD analysis. The decrease in ΔH value upon treatment with

base and acid indicates the removal of the silica. Singer and Wagoner (1968) have made

similar observation of broadening of the EPR signal resulting from graphite because of

the presence of impurities like silica. Mrozowski has attributed the peak broadening to some changes in the structure of the carbon material (Mrozowski, 1979).

Also from the data in Table 3.6, it is observed that upon activation with K_2CO_3 the ΔH value increased from 6.0 to 9.5 G indicating the presence of traces of K in the carbon material after activation leading to the slight broadening in the EPR signal.

(iii) The concentration of unpaired electrons in the char was found to be of the order of 0.74×10^{19}/g. The origin of such spins is attributed to the generation of dangling bonds formed as a result of the extensive devolatilization from the defragmentation of the hemicellulose, cellulose and lignin structure during the preparation of the char in the muffle furnace at 573 K. Paramagnetic centers were found to be associated with the dangling bonds formed during the carbonization of carbon materials (Freitas et al., 2001). The spin concentration of the graphon black and acetylene black (Donnet et al., 1993) were 1.1×10^{19} and 3.8×10^{19} spins/g respectively which are of the same order of magnitude as that of the spin concentration value observed in the case of the unactivated char shown in Table 3.6.

Upon treatment of the char with base and acid, the spin concentration decreased from 0.74×10^{19} to 0.34×10^{19} spin/g. Nearly a three orders of magnitude reduction in the spin concentration is observed upon activation of char with K_2CO_3 (0.15×10^{16} spins/g). Such a drastic decrease in spin concentration upon activation with K_2CO_3 is because of the saturation of the dangling bonds with K metal, formed during the carbothermal reduction of K_2CO_3, resulting in the formation of surface C-K bonds which subsequently transform to C-H bonds upon final treatment with conc. HCl. Such a transformation is also

confirmed from the increase in the hydrogen content (2.63 to 3.5 wt.%) of the carbon sample activated with K_2CO_3 and subsequently treated with conc. HCl (Table 3.7). Manivannan *et al.*, (1999) have found the spin concentration values of activated carbon materials, namely, GX203 (from coconut shell precursor), P1400 (from wood precursor) and Med50 (from coconut shell precursor) to be 1.8 x 10^{17}, 5.8 x 10^{17} and 1.8 x 10^{16} spins/g respectively.

3.3.6.3 Effect of K_2CO_3 activation on the Chemical Constitution of Carbon Materials – C, H, N, S analysis

The elemental analysis of Cg as synthesized, Cg base acid and Cg potassium carbonate 3 was carried out in a CHNS/O analyzer (Perkin Elmer Instrument, Series II) and the results are presented in Table 3.7. A simple treatment of the char with NaOH (10 wt.% solution) and HCl in succession has improved the carbon content (wt.%) from 73.13 to 77.62 which is attributed to the elimination of mineral matter. Activation with K_2CO_3 has further increased the carbon content from 77.62 to 80.04 % and also the oxygen content decreased from 14.6 to 13.6 % as expected. The increase in hydrogen (2.63 to 3.5 wt.%) upon activation with K_2CO_3 is not because of activation step, but because of the subsequent treatment of the activated carbon composite (carbon material with the decomposed products of activated carbon, mainly K) with HCl and further washing with water. During the K_2CO_3 activation process surface specie such as C-O-K are formed, which upon treatment with HCl and subsequent washing with water get transformed to C-O-H groups contributing to an increase in the hydrogen content in the case of activated carbon sample relative to either Cg as synthesized or Cg base acid.

Table 3.7 Chemical composition of carbon materials from Calotropis gigantea

Element (wt. %)	Carbon Materials from Calotropis gigantea		
	Cg as synthesized	Cg base acid	Cg potassium carbonate 3
Carbon	73.13	77.62	80.04
Hydrogen	2.61	2.63	3.50
Nitrogen	0.81	0.82	0.67
Sulphur	0.36	0.33	0.36
Total	76.91	81.40	84.57
Ash content	12.7	4.0	1.8
Oxygen*	10.39	14.6	13.63

* By difference from the total amount of other constituents

3.3.6.4 Effect of the nature of cation of the alkali metal carbonate on the textural properties of Carbon Materials – BET sorptometric study

To evaluate the effect of the cation of the activating agent on the textural properties of activated carbon, the char obtained from Calotropis gigantea is subjected to activation with Li_2CO_3, Na_2CO_3 and K_2CO_3 at a temperature of 1073 K for 8 h in N_2 temperature. The (wt.%/wt.%) ratio of the activating agent to Cg base acid is 1:1. The original char as well as the activated carbon materials were subjected to sorptometric analysis. The N_2 adsorption-desorption isotherms collected over the activated carbon materials obtained from activation with Li_2CO_3, Na_2CO_3 and K_2CO_3 are depicted in Fig. 3.20.
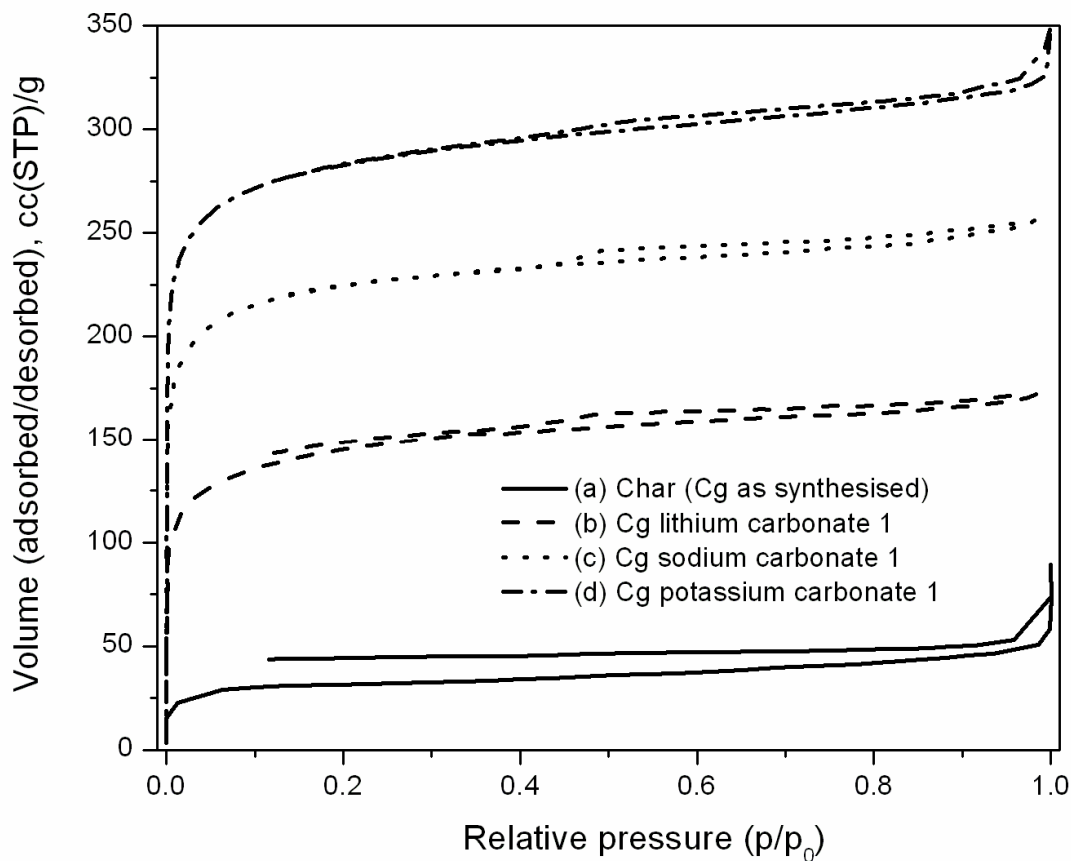
Fig. 3.20 N_2 adsorption-desorption isotherms of carbon materials prepared from
　　　Calotropis gigantea, (a) as synthesized (char) and activated carbon with a Cg
　　　base acid to activating agent ratio (wt./wt.%) of 1:1, (b) Li_2CO_3 activation (c)
　　　Na_2CO_3 activation and (d) K_2CO_3 activation

There is a steady raise in the volume of the adsorbate adsorbed on the activated carbon

material as the activating agent is changed from Li_2CO_3 to K_2CO_3 through Na_2CO_3. The

specific surface area of the activated carbon produced was found to be dependent on the

radii of the cation of the activating agent as shown in Table 3.8.

Table 3.8 Effect of nature of cation of the activating agent on the textural properties of activated carbon

S. No.	Activating agent	Ionic radii of the cation $(\text{Å})^a$	$E^0 (V)^{b, c}$	Textural parameters	
				S_{BET} (m^2/g)	Vp (cc/g)
1	Li_2CO_3	0.60	-3.0	480	0.263
2	Na_2CO_3	0.96	-2.7	811	0.395
3	K_2CO_3	1.33	-2.9	892	0.497

a. & b. Cotton and Wilkinson (1976)

b. $M+ (aq) + e \rightleftharpoons M (s)$

c. The standard redox potential of activated carbon is + 0.24 V (Adams, 1991)

3.3.7 Alkali metal salts of carboxylic acids as activating agents

The N_2 adsorption - desorption isotherms of the as synthesized as well as the activated carbon materials, using oxalate as activating agent, with different amounts of activating agent ($Na_2C_2O_4$) are shown in Fig. 3.21. Irrespective of the amount of the activating agent all the carbon materials exhibited type I isotherms indicating that the carbon materials resulting from oxalate activation are essentially microporous in nature. The textural parameters deduced from the isotherms are indicated in the caption of Fig. 3.21. Highest value of S_{BET} (785 m^2/g) and Vp (0.39 cc/g) were obtained when the char to $Na_2C_2O_4$ ratio (wt.%/wt.%) is 1:4. Also the pore volume (0.31 to 0.37 cc/g) as well as specific surface area values (647 to 785 m^2/g) are tunable with the amount of activating agent. In addition to $Na_2C_2O_4$, various other activating agents belonging to the class of carboxylic acids were evaluated to know the resulting effect on the textural parameters.

The S_{BET} and the Vp values of the resulting activated carbon materials were summarized in Table 3.9.
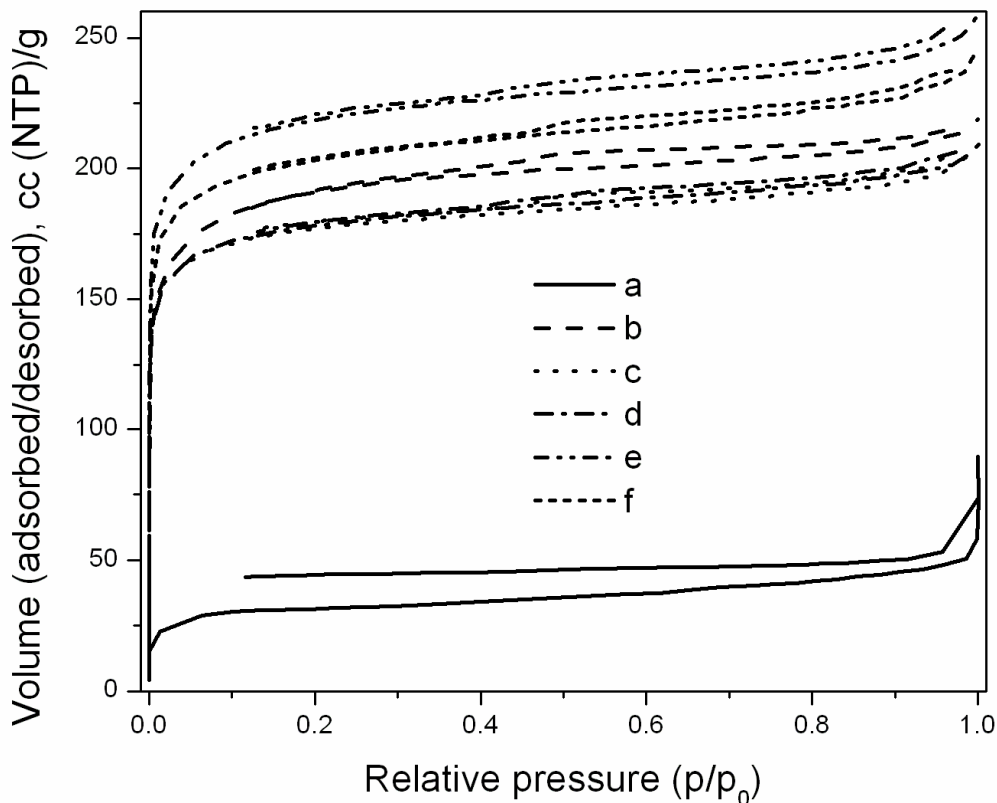
Fig. 3.21 N_2 adsorption-desorption isotherms of carbon materials prepared from
Calotropis gigantea, (a) Cg as synthesized (char) (S_{BET} = 97 m^2/g, V_P = 0.08
cc/g), activated carbon with a Cg base acid to $Na_2C_2O_4$ ratio (wt.%/wt.%) of
(b) 1:1, Cg sodium oxalate1 (S_{BET} = 707 m^2/g, V_P = 0.33 cc/g), (c) 1:2, Cg
sodium oxalate 2 (S_{BET} = 647 m^2/g, V_P = 0.31 cc/g) (d) 1:3, Cg sodium
oxalate 3 (S_{BET} = 655 m^2/g, V_P = 0.32 cc/g) (e) 1:4, Cg sodium oxalate 4 (S_{BET}
= 785 m^2/g, V_P = 0.39 cc/g) and (f) 1:5, Cg sodium oxalate 5 (S_{BET} = 734
m^2/g, V_P = 0.37 cc/g)

Table 3.9 Influence of carboxylic acids and their alkali metal salts on the textural parameters of activated carbon materials

S. No.	Activated Carbon Material	S_{BET} (m^2/g)	V_p (cm^3/g)	Density (g/cc)
1	Cg oxalic acid 1	317	0.14	0.45
2	Cg sodium oxalate 1	707	0.33	0.43
3	Cg citric acid 1	127	0.07	0.39
4	Cg sodium citrate 1	419	0.21	0.36
5	Cg tartaric acid 1	42	0.04	0.49
6	Cg di sodium tartarate 1	394	0.20	0.36
7	Cg sodium potassium tartarate 1	394	0.18	0.44

3.3.7.1 Alkali metal carbonate and oxalate as activating agents for carbon materials – A comparison

Comparison of the textural parameters of the activated carbon materials obtained from carbonate (Fig. 3.20) and oxalate (Fig. 3.21) activations indicate that K_2CO_3 (Vp = 0.73 cc/g) is twice as active as $Na_2C_2O_4$ (Vp = 0.39) in its ability to generate porosity. Since the activated carbon materials designated as (Cg potassium carbonate 3) and (Cg sodium oxalate 4) exhibited the highest S_{BET} and Vp values further structural and morphological analysis was carried out with the afore mentioned two samples. For comparison, three commercially available carbon blacks, namely, Black Pearl 2000 (Cabot Corporation), Vulcan XC 72 R (Cabot Corporation) and CDX 975 (Ms Columbian Chemicals Company) were analyzed for textural parameters.
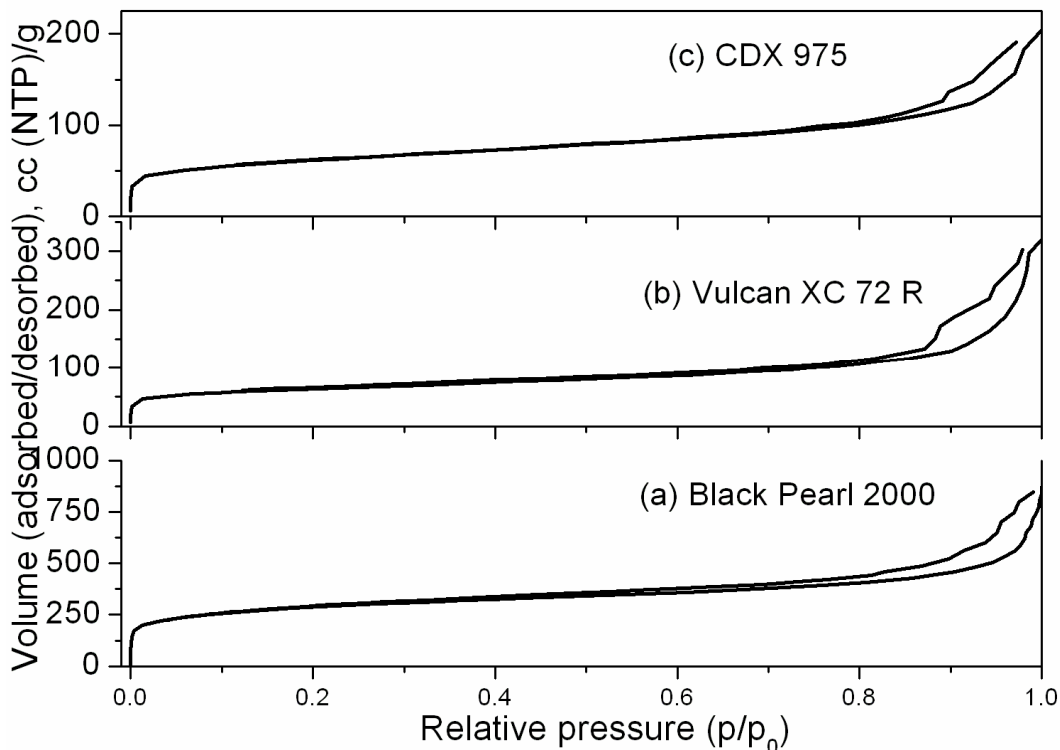
Fig. 3.22 N_2 adsorption-desorption isotherms of commercial carbon blacks
(a) Black Pearl 2000, (b) Vulcan XC 72 R and (c) CDX 975

The N_2 adsorption - desorption isotherms of these carbon materials were shown in Fig. 3.22. which are a combination of type I and type II isotherms. Such isotherms indicate the pore structure which is a combination of micropores and mesopores. The textural parameters deduced from the isotherms shown in Fig. 3.22 are summarized in Table 3.10. It is observed from the data summarized in Table 3.10. that the plant derived carbon activated with K_2CO_3 possess S_{BET} value of 1296 m^2/g which is greater than the S_{BET} value of commercial carbon black (Black Pearl 2000). In addition the activated carbon material, Cg carbonate 3 is exclusively microporous unlike the commercial carbon materials which are a combination of both micro and mesoporosity. In an analogous

manner, the plant based activated carbon, Cg oxalate 4, possess S_{BET} (745 m^2/g) value greater than that of the S_{BET} values of Vulcan XC 72 R and CDX 975 and also Cg oxalate 4 is exclusively microporous. Thus high specific surface area microporous carbon materials of varying textural parameters are derivable by suitably modulating the type and amount of activating agent.

Table 3.10 Textural parameters of commercial carbon blacks Vs Carbon materials from *Calotropis gigantea*

S. No.	Carbon Material	S_{BET} (m^2/g)	Vp (cm^3/g)
1	Black Pearl 2000	1012	1.14
2	Vulcan XC 72 R	224	0.46
3	CDX 975	215	0.28
4	Cg carbonate 3	1296	0.73
5	Cg oxalate 4	745	0.39

3.3.7.2 Effect of activation (carbonate and oxalate) on the structure of carbon materials - XRD analysis

The XRD curves resulting from the activated carbon materials from Calotropis gigantea upon carbonate and oxalate activation are shown in Fig. 3. 23. Irrespective of the type of the activating agent used the carbon materials resulted in similar XRD profiles with two broad diffraction peaks centered around 2θ values of 24 and 43° which are attributed to the reflections from the (002) and (10) diffraction peaks of carbon material respectively.
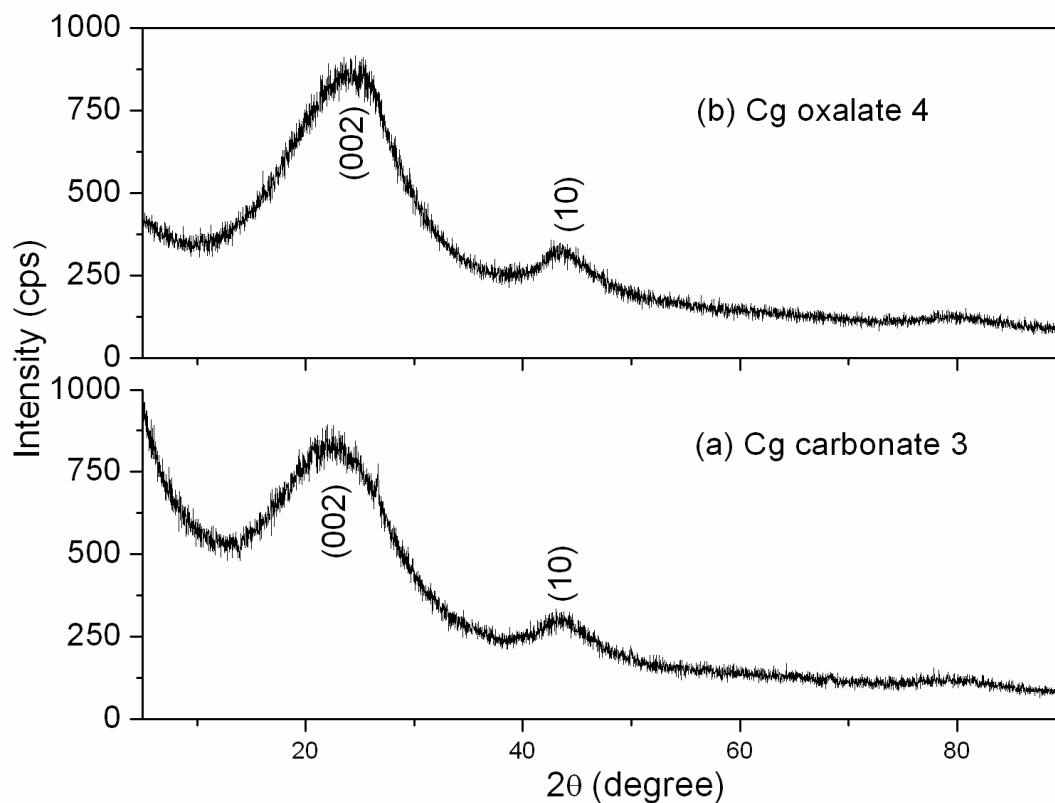
Fig. 3.23 XRD pattern of activated carbon materials from Calotropis gigantea (Cg): (a) activated with carbonate (K_2CO_3), (b) activated with oxalate ($Na_2C_2O_4$)

Crystallographic parameters of the activated carbon materials produced by K_2CO_3 (carbonate) and $Na_2C_2O_4$ (oxalate) activation were obtained from XRD studies. For comparison the XRD profiles of commercially available activated carbon materials (Black Pearl 2000, Vulcan XC 72 R, CDX 975) were recorded and are shown in Fig. 3.24. Interestingly the XRD profiles resulting from the commercial carbon black samples are exactly identical to that of the activated carbon materials produced from Calotropis gigantea by carbonate and oxalate activation. Two intense and broad diffraction peaks characteristic of carbon materials indexed to the diffraction planes of (002) and (10) were observed in the case of Black Pearl 2000, Vulcan XC 72 R and CDX 975 (Fig. 3.24). The

(002) line is a result of inter layer scattering where as the (10) line is because of intra layer scattering.
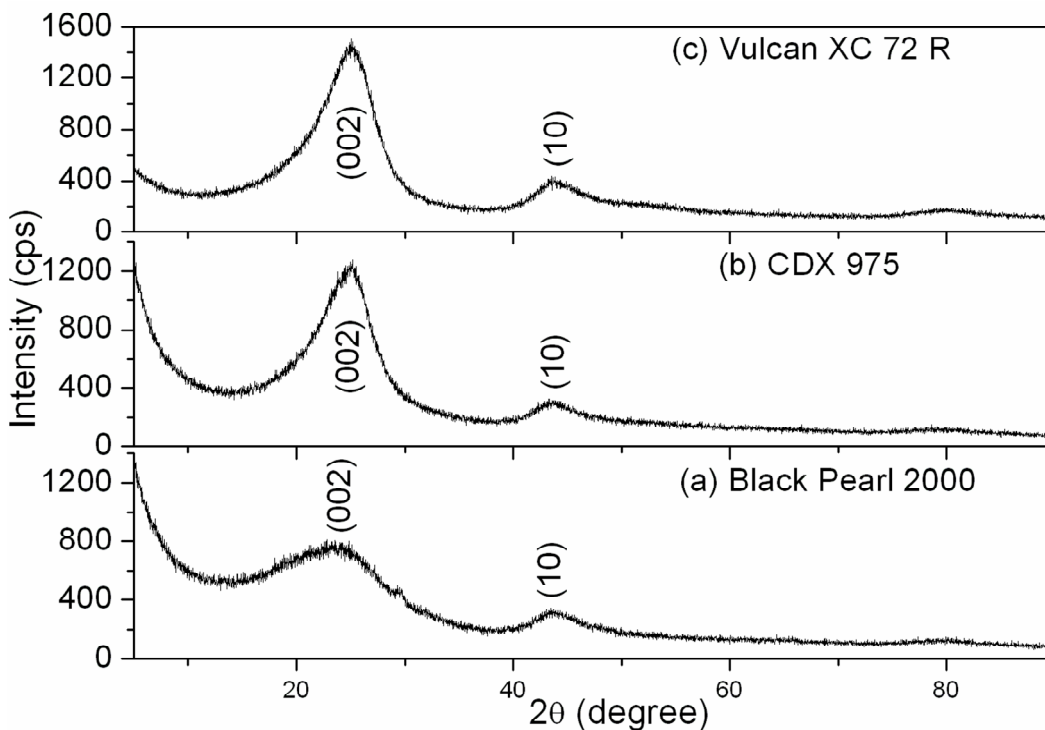
Fig. 3.24 XRD pattern of commercial carbon blacks (a) Black Pearl 2000, (b) CDX 975 and (c) Vulcan XC 72 R

Crystallographic parameters such as the interlayer spacing (d_{002}) and the full width at half maxima (FWHM) of the diffraction peak arising from (002) reflection were determined for the plant based and commercially available activated carbon materials. The structural parameters obtained were summarized in Table 3.11. The d_{002} value of carbonate (Cg carbonate 3) and oxalate (Cg oxalate 4) activated carbon materials were 0.411 and 0.385 nm respectively. The d_{002} value for pure graphitic structure is 0.335 nm. The higher values of d_{002} relative to graphitic structure indicate that both carbonate and oxalate activated carbon materials have turbo-stratic structure with the inter layer separation

greater than that of pure graphitic carbon. Such a phenomenon is more pronounced in the case of K_2CO_3 activation rather than oxalate activation owing to the severity of the activation process involving K_2CO_3 as activation agent. In addition, the value of FWHM of the (002) reflection is greater for the carbonate activated carbon sample compared to the oxalate activated sample. This too imply that carbonate activation induces structural disorder and results in the formation of amorphous carbon material similar to Black Pearl 2000 (FWHM =13.8).

Table 3.11 Effect of type of activating agent on the structural properties of activated carbon materials produced from Calotropis gigantea

S. No.	Sample	d_{002} (nm)	FWHM (002) refection
1	Cg carbonate 3	0.411	12.5
2	Cg oxalate 4	0.385	9.8
3	Black Pearl 2000	0.407	13.8
4	Vulcan XC 72 R	0.364	5.2
5	CDX 975	0.370	5.5

From the FWHM values shown in Table 3.11, it is evident that Vulcan XC 72 carbon with sharp (002) reflection is highly crystalline where as the Black Pearl 2000 with the highest value of FWHM is least crystalline. Analysis of the crystallographic parameters in Table 3.11 indicate that the plant based activated carbon materials possess structural

features (turbostratic structure) identical to that of commercial activated carbon materials but with lower crystallinity compared to either Vulcan XC 72 R or CDX 975.

3.3.7.3 Effect of activation (Carbonate and oxalate) on the morphology of carbon materials - SEM analysis

Details of the surface morphology as well as the elemental composition of the activated carbon materials from Calotropis gigantea using carbonate and oxalate activation were obtained from FEG-SEM studies. The SEM images of carbonate activated carbon, designated as Cg potassium carbonate 3 recorded at two different magnifications namely 2400 X and 5000 X were shown in Fig. 3.25. The Cg potassium carbonate 3 possess a unique morphology. The carbon materials comprise of platelet like carbon particles with evenly distributed spherical pores. Such a morphology is unique to the carbon precursor, calotropis gigantea and has not been reported previously with any other lignocellulosic carbon precursor. The energy dispersive X-ray analysis indicated a carbon content of 92.62 wt.% and an oxygen content of 7.38 wt.%.

Unlike carbonate activation, oxalate activation resulted in a distinctly different carbon morphology. Activation with $Na_2C_2O_4$ resulted in a tubular morphology. Bunches of carbon micro tubes with open ends were formed from the carbon precursor upon oxalate activation (Fig. 3.26). Energy dispersive X – ray analysis showed a carbon content of 92.49 wt. % and an oxygen content of 7.51 wt. %. Thus it is evident that the carbon morphology derivable is a function of the type of activating agent employed. Also the carbon precursor dictates the morphologies that are obtainable.
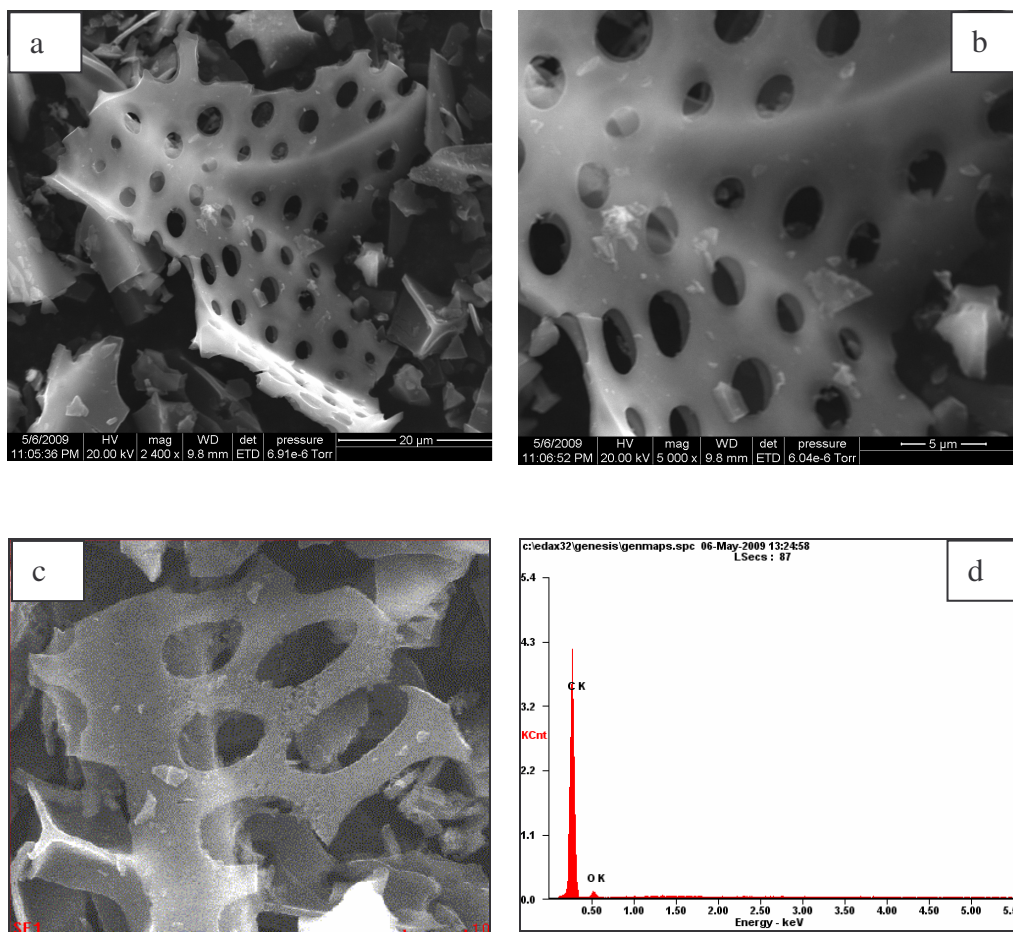
Fig. 3.25 FEG SEM images (at different magnifications) of activated (carbonate) carbon material from Calotropis gigantea, Cg carbonate 3, along with EDS (Energy Dispersive Spectroscopy) spectrum: (a) 2400 X, (b) 5000 X and (c & d) FEG SEM image with EDS spectrum

For comparison the surface morphology of commercially available activated carbon materials, namely, Black Pearl 2000, Vulcan XC 72 R and CDX 975 were recorded. The SEM images recorded on the afore mentioned carbon materials at different magnifications are shown in Fig. 3.27.
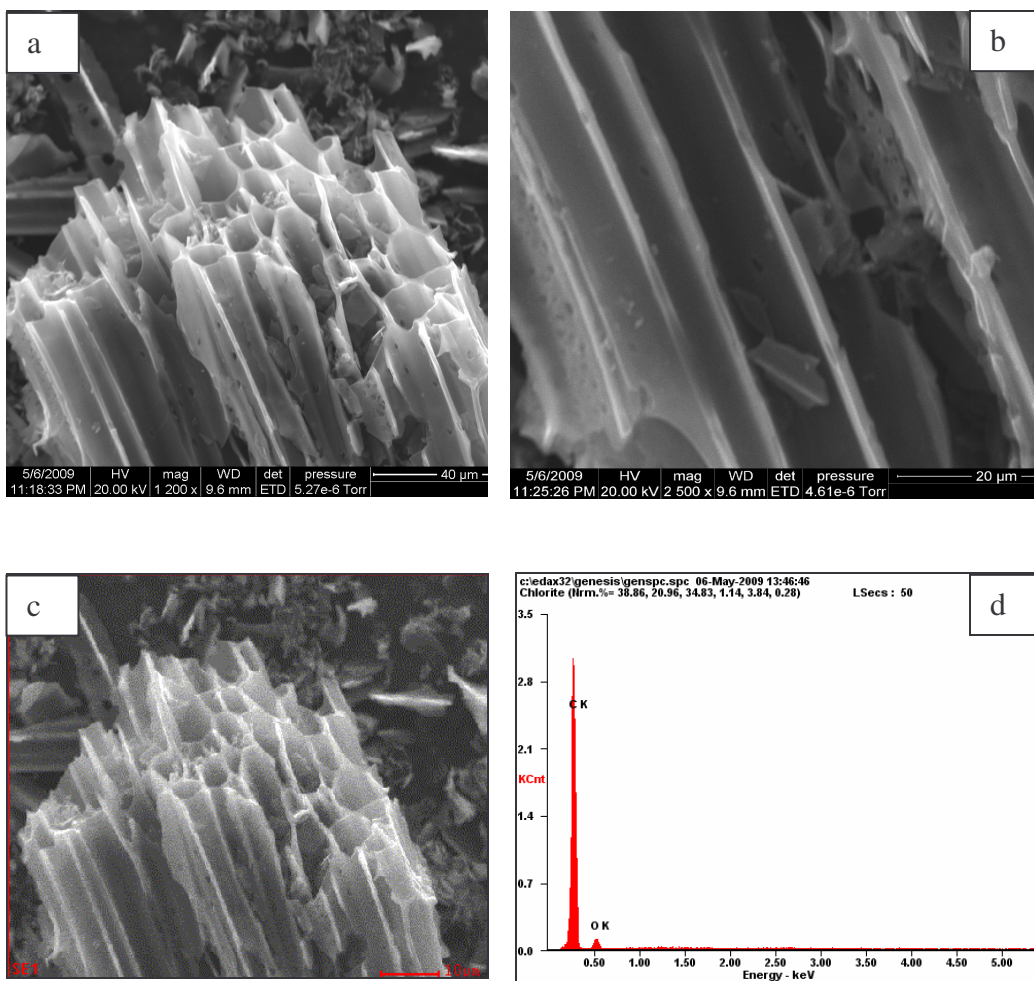
Fig. 3.26 FEG SEM images (at different magnifications) of activated (oxalate) carbon material from Calotropis gigantea, Cg oxalate 4, along with EDS spectrum: (a) 1200 X (top view), (b) 2500 X (lateral view) and (c & d) FEG SEM image with EDS spectrum

The carbon materials possessed spherical carbon nano particles. None of the commercial carbon samples examined offered the peculiar carbon morphologies derivable from the stems of Calotropis gigantea upon activation with carbonate and oxalate.
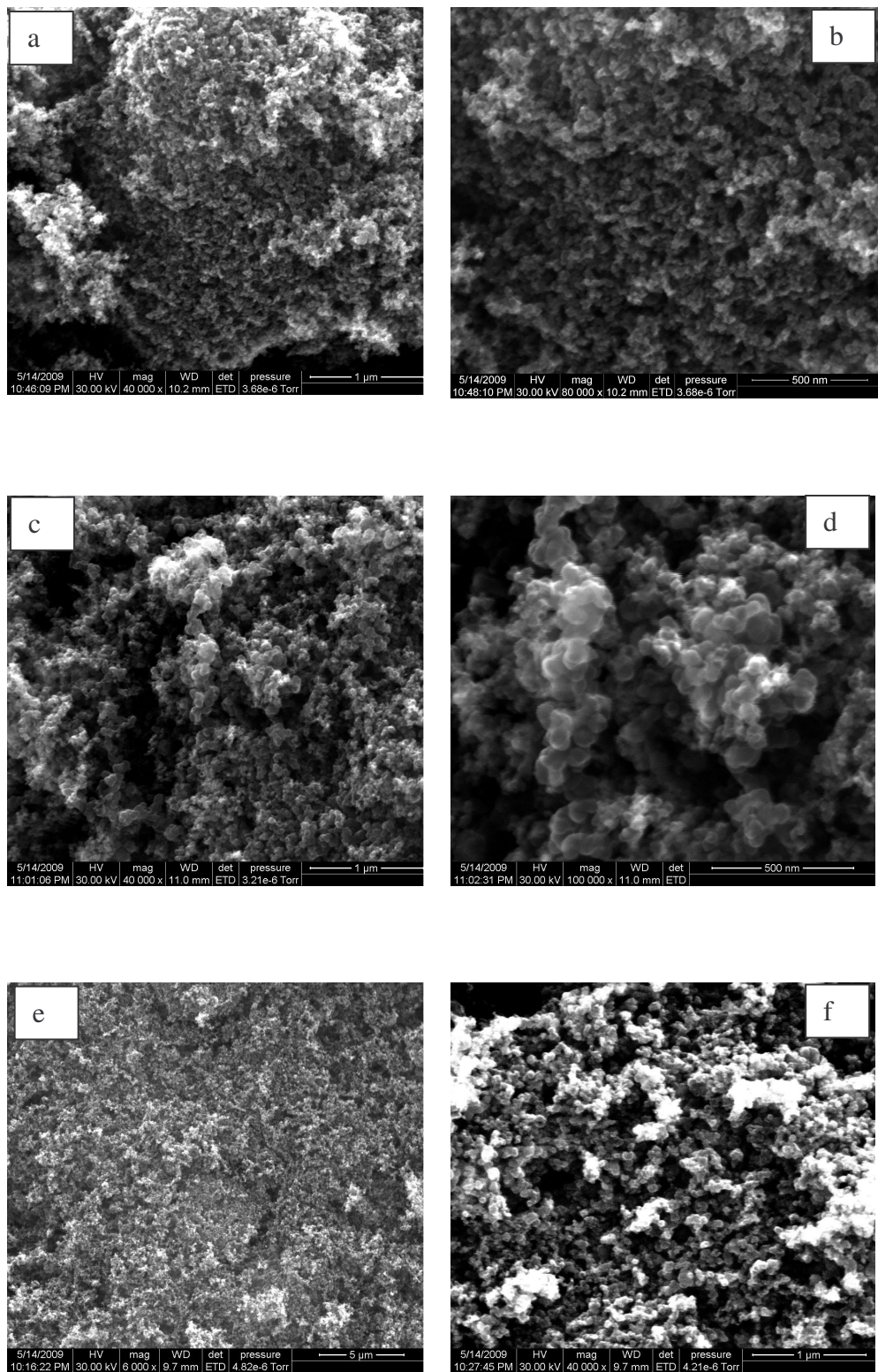
Fig. 3.27 FEG SEM images (at different magnifications) of commercial carbon

113

blacks : (a & b) Black Pearl 2000 (40, 000 X, 80, 000 X), (c & d) Vulcan XC
72 R (40, 000 X, 1,00, 000 X) and (e & f) CDX 975 (6000 X, 40, 000 X)

Commercial activated carbon materials too were analyzed by EDS and the carbon and oxygen contents present in the carbon materials are summarized in Table 3.12. The carbon content of the plant based activated carbon materials produced through simple means is comparable to that of the commercial carbon materials.

Table 3.12 Elemental analysis of carbon materials (Energy Dispersive Spectroscopy (EDS) analysis)

S. No.	Carbon Material	Element (wt. %)	
		Carbon (C)	Oxygen (O)
1	Cg potassium carbonate 3	92.62	7.38
2	Cg sodium oxalate 4	92.49	7.51
3	Black Pearl 2000	93.82	6.18
4	Vulcan XC 72 R	97.7	2.3
5	CDX 975	96.88	3.12

3.3.8 Catalytic Applications of Carbon Materials

3.3.8.1 Synthesis of tertiary amyl methyl ether (TAME)

In the condensation reaction of tertiary amyl alcohol (TAA) and methanol to form TAME, water is formed as a byproduct. The catalyst needs to be hydrophobic to resist the leaching of the active component. Carbon materials are sufficiently hydrophobic owing to the presence of graphite like chemical properties and can form an integral component of the catalyst. Acid function is the catalytic component needed to drive the etherification reaction. Heteropoly acids, particularly, dodeca tungstophosphoric (HPW)

acid is a strong super acid with a H_0 value of -13.4 (more acidic than 100 % sulphuric acid, $H_0 = -11.94$).

Four different carbon materials, namely, Cg potassium carbonate 3, Black Pearl 2000, Vulcan XC 72 R and CDX 975 with varying textural properties (Table 3.10) were employed as support materials for HPW to evaluate the effect of the nature of carbon support on the acidity and catalytic activity of the supported solid acid catalyst for the synthesis of TAME.
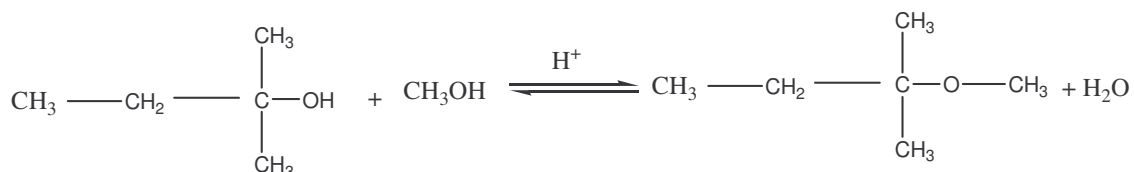
The supported catalysts (HPW/C) were investigated by sorptometry, XRD and NH3-TPD to know the texture, structure and acidity. The N_2 adsorption-desorption isotherms recorded on HPW/C catalysts were shown in Fig. 3.28. The textural parameters deduced from the isotherms are summarized in Table 3.13. Upon loading 10 wt.% HPW on carbon support, the S_{BET} values of the carbon support decreased (Table 3.10 and 3.13) and such a decrease is attributed to blocking of the fine and narrow pores by heteropoly anions. Pore blocking and the accompanying decrease in S_{BET} and Vp values is more pronounced in the case of Cg potassium carbonate 1 and this is because of the exclusive microporous nature of the support. Such blockage of micropores by heteropoly anions is a known phenomenon (Corma, 1997). As a result of pore blocking most of the poly anions do remain on the external surface of Cg potassium carbonate 3 carbon support which is evident from the XRD plot (Fig. 3.29).

115
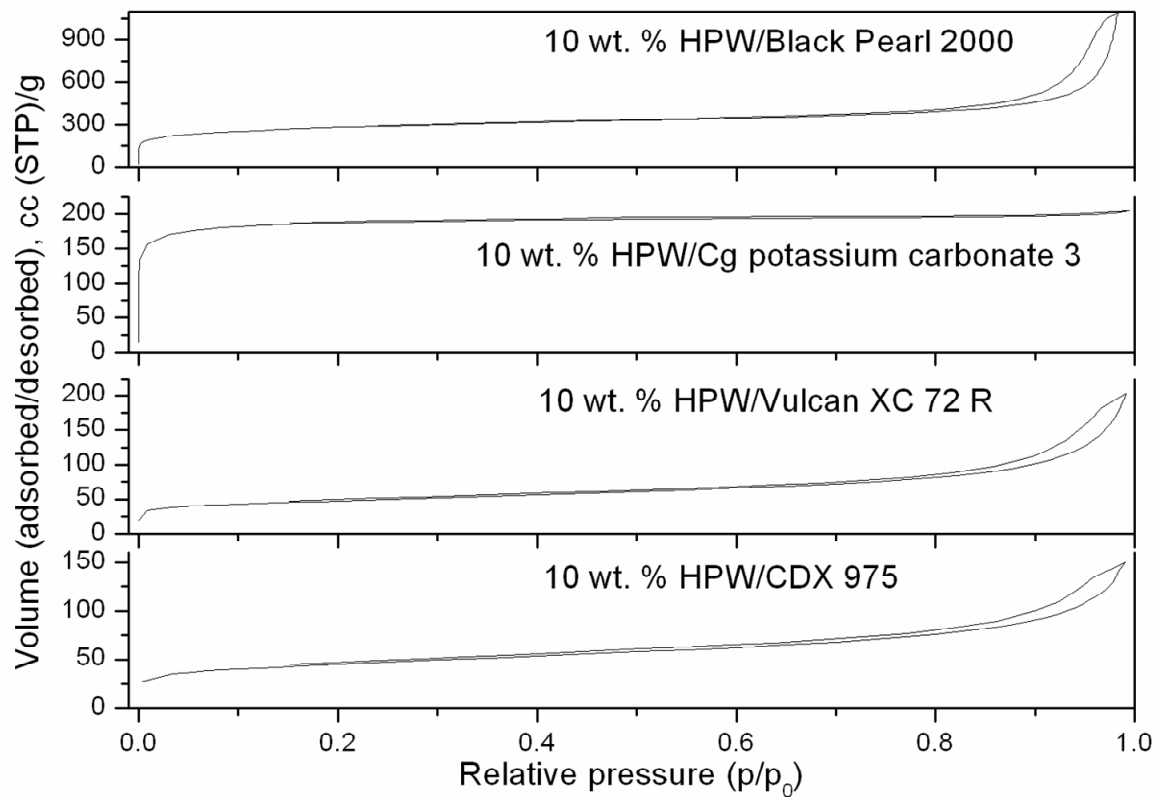
Fig. 3.28 N$_2$ adsorption-desorption isotherms of carbon supported heteropoly acids
(HPW/C)

Table 3.13 Textural properties of carbon supported heteropoly acids (HPW/C)

S. No.	Catalyst	S_{BET} (m^2/g)	Vp (cc/g)	Density (g/cc)
1	10 wt. % HPW/ CDX 975	156	0.23	0.27
2	10 wt.% HPW/ Vulcan XC 72 R	169	0.30	0.30
3	10 wt.% HPW/Black Pearl 2000	980	1.65	0.22
4	10 wt.% HPW/Cg potassium carbonate 3	711	0.32	0.38

116
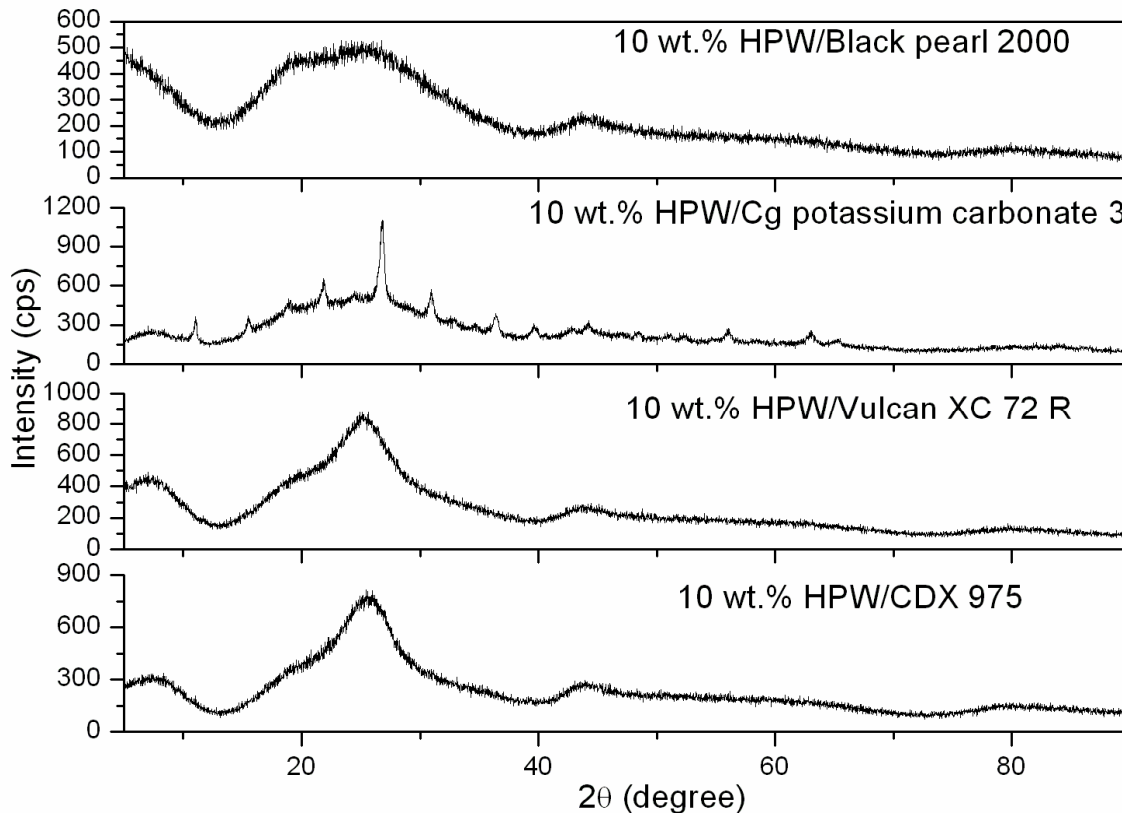
Fig. 3.29 XRD pattern of carbon supported heteropoly acid catalysts (HPW/C)

Bulk HPW show sharp peaks at 2θ values between 20 - 40° (Obali and Dogn, 2008). Features characteristic of bulk HPW are observed only in the case of HPW/Cg potassium carbonate 3 implying that the key characteristics of the primary Keggin anion structure are retained in the case of Cg potassium carbonate support. Obali and Dogn (2008) have made similar observations in the case of HPW supported on activated carbon (Kureha, Japan). The appearance of the features characteristic of Keggin anion are due to the weak interaction between the poly anion and the Cg potassium carbonate 3 support which too point out that majority of the HPW is on the external surface of the Cg potassium carbonate 3 support. Thus there is a correlation between the sorptometry result (Fig. 3.28) and the XRD result (Fig. 3.29). Unlike, Cg potassium carbonate 3 support, in the

117

case of other carbon supports no peaks characteristic of heteropoly anion are observed indicating that the polyanions are well dispersed in the porous structure of the carbon support (CDX 975, Vulcan XC 72 R and Black Pearl 2000). The carbon supported heteropoly acid catalysts were successfully exploited for vapour phase synthesis of TAME from TAA and methanol. The reaction was carried out in a down flow fixed bed reactor at atmospheric pressure at a temperature of 373 K. The liquid feed containing TAA and methanol (in the mole ratio of 1:10) was fed onto the catalyst bed through a peristaltic pump (Miclins, SPO1) at a flow rate of 10 ml/h. N_2 was used as a carrier gas (flow rate, 30 ml/min). In a typical run, 0.5 g of the catalyst was charged in the reactor. The catalyst was stacked between glass beads and ceramic wool. The reactor was maintained under isothermal conditions during all runs. The reaction products were condensed at the bottom of the reactor and analyzed for the chemical composition using a gas chromatograph equipped with an OV 101 (packed) column and a FID detector. Details of conversion of TAA and selectivity towards TAME were shown in Table 3.14. The condensation reaction between TAA and methanol over HPW/C catalysts was monitored for 3 h (Fig. 3.30). Reaction products were collected and analyzed by GC at intervals of 30 min. The catalytic activity was evaluated by monitoring the conversion of TAA with time. In situ generation of iso-amylenes (2-methyl-1- butene, 2MB1, and 2-methyl-2-butene, 2MB2) was observed during the course of the reaction. The formation of iso-amylenes is a result of the dehydration of the TAA. The iso-amylenes formed subsequently react with methanol to form TAME. Details of conversion (wt. %) of TAA and selectivity towards olefins and TAME over different HPW/C catalyst are summarized in Table 3.14.
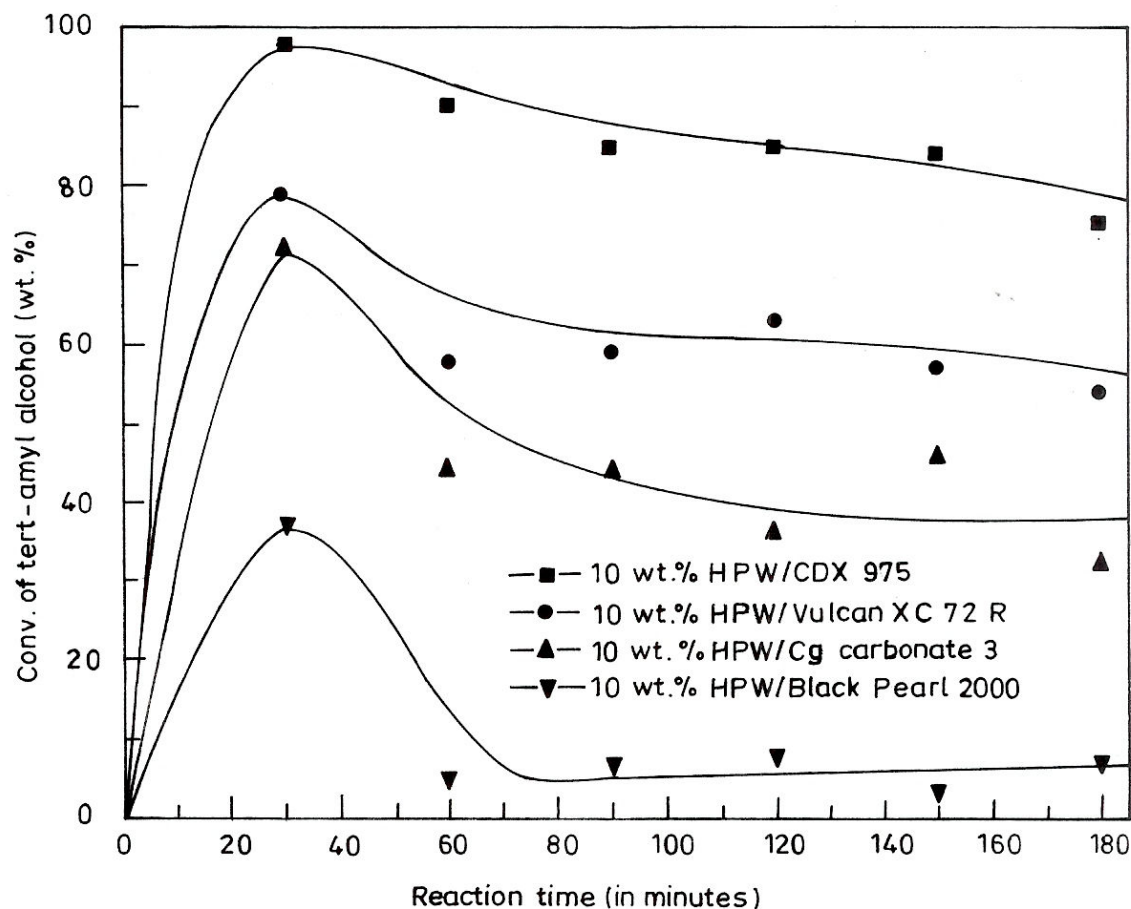
Fig. 3.30 Plot of Conversion of TAA (wt. %) Vs Reaction time (in minutes)

The results reveal that the activity and selectivity are not apparently related to the surface areas of the carbon supports (Table 3.10) or the supported catalysts (Table 3.13). Activity for the etherification could be related to many factors, such as the dispersion of HPW, the distribution of HPW in the pores, the accessibility of the active sites (through diffusion) to the reactants and the presence/absence of poisons on the surface of the support.

Table 3.14 Catalytic activity of HPW/C catalysts for the synthesis of TAME[a]

Catalyst	Conversion (wt. %)	Selectivity (%)	
		Olefins	TAME
10 wt. % HPW/ CDX 975	75	35	65
10 wt.% HPW/ Vulcan XC 72 R	54	13	87
10 wt.% HPW/Black Pearl 2000	7	47	53
10 wt.% HPW/Cg potassium carbonate 3	32	37	73

a. Reaction Conditions: Time on stream = 3 h; TAA/methanol (mole) = 1:5; flow rate of the feed = 10 ml/h; flow rate of the carrier gas = 30 ml/min; amount of catalyst = 0.5 g;

Among different supported solid acid catalysts, surprisingly, the one with the lowest S_{BET} and Vp values, 10 wt.% HPW/CDX 975, exhibited highest conversion of TAA. 10 wt. % HPW/Cg potassium carbonate 3 showed better performance compared to the Black Pearl 2000 based solid acid catalyst. The catalytic activity of the solid acid catalysts are found to be a function of the acid strength as evidenced from the NH_3 – TPD curves shown in Fig. 3.31. The NH_3 TPD spectra illustrated by the carbon supported heteropoly acids (Fig. 3.31) have two characteristic features. An intense peak with a maximum between 353 to 383 K and a shoulder at higher temperatures corresponding to the desorption of weakly held physisorbed ammonia. In addition, a wide but less intense peak appeared at even higher temperature reflecting the desorption of chemisorbed ammonia. Malnar *et al*., (1999) have observed similar features in the TPD curves resulting from the heteropoly acid catalysts immobilized in the silica matrix.
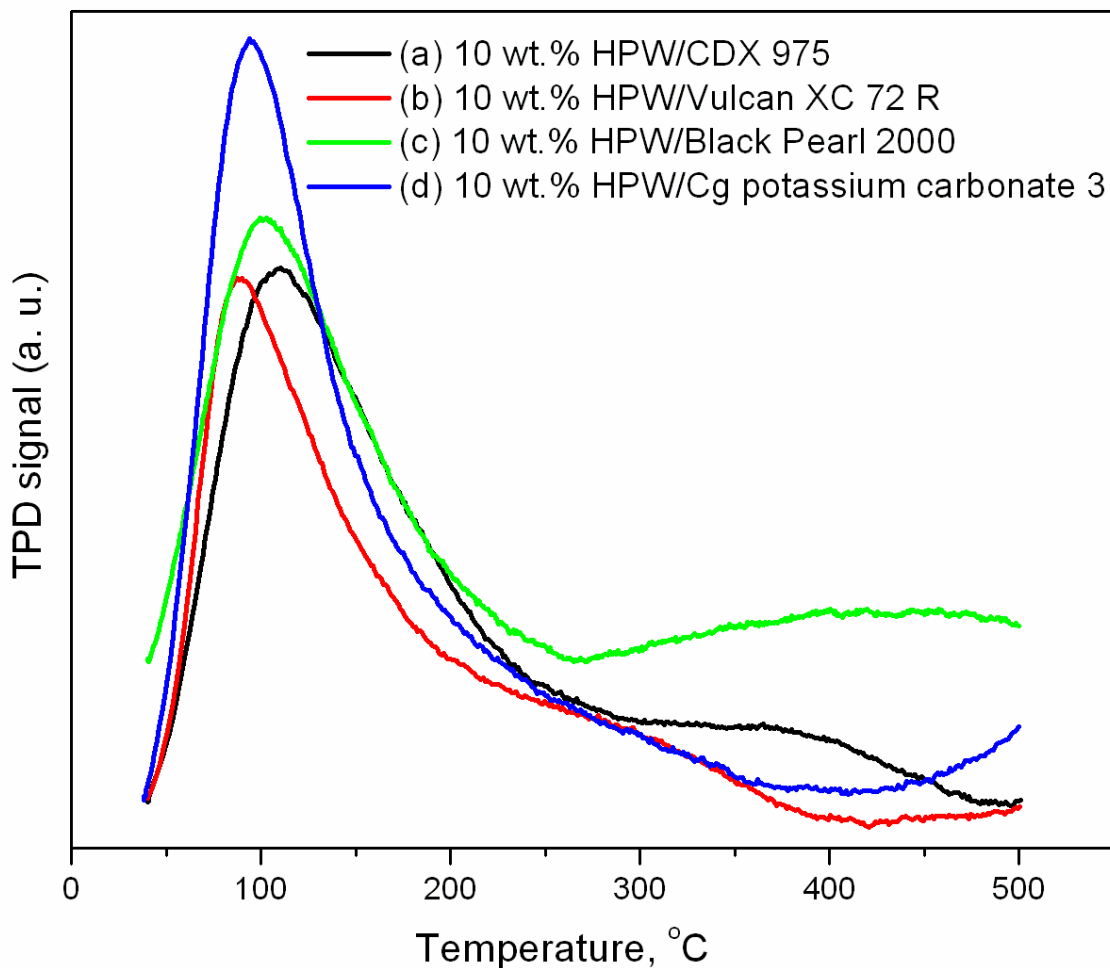
Fig. 3.31 TPD spectra of ammonia on supported HPAs: (a) 10 wt.% HPW/CDX 975, (b) 10 wt.% HPW/Vulcan XC 72 R, (c) 10 wt.% HPW/Black Pearl 2000 and (d) 10 wt.% HPW/Cg potassium carbonate 3

The NH_3 desorption temperature is a reflection of acid strength and the area under the desorption peak is a reflection of the total acidity (Izumi *et al*., 1983). For the solid acid catalysts, HPW/CDX 975, HPW/Vulcan XC 72 R and HPW/Cg potassium carbonate 3, the desorption maximum of the strongly chemisorbed ammonia appeared at 653, 601 and 581 K respectively indicating that the CDX 975 carbon support facilitated the generation of strongest acid sites among the carbon supports evaluated. In the case of HPW/Black Pearl 2000 catalyst, no desorption of NH_3 is observed beyond 523 K indicating the

complete absence of strong acid sites. The order of the acid strength of the supported catalysts is: HPW/CDX 975 > HPW/Vulcan XC 72 R > HPW/Cg potassium carbonate 3 > HPW/Black Pearl 2000. Thus a strong correlation between the acid strength and the catalytic activity for the etherification reaction is observed with the strong solid acid catalyst exhibiting higher conversion of TAA. Paakkonen *et al*., (2003) and Parra *et al*., (1998) have made similar observations where in the catalysts with higher acidic strength were the most active for the etherification reaction. Also the acid strength was found to have stronger influence on the catalytic activity rather than S_{BET} or average pore diameter values. In addition, catalyst with greater density of the acid sites was found to be more active for the etherification reaction as the reaction involves a concerted mechanism where in adjacent acid sites participate in the reaction.

3.4 CONCLUSION

Microporous activated carbon materials with a large surface area and a narrow pore size distribution have been prepared from the dried stems of Calotropis gigantea. Low ash content as well as the uniformity in properties (physical and chemical) through out the samples, were the unique advantages of activated carbon produced from Calotropis gigantea stems compared to the carbon materials produced from either coal or lignocellulosic materials. Ecological imbalance caused by Calotropis gigantea stem waste generation and disposal is solved in a productive way by transforming the waste Calotropis gigantea stems into technologically useful high specific surface area microporous carbon. Methods for tuning the textural and structural parameters of

activated carbon materials have been proposed. Many activating agents, transition metal compounds, alkali and alkaline earth compounds, alkali metal salts of carboxylic acids have been used for activation purposes. Among several classes of activating agents, K_2CO_3 has been found to be the best yielding with textural properties superior to those of commercial activated carbon materials (Adsorbent carbon, Black Pearl 2000, Calgon, CDX 975 and Vulcan XC 72 R). In addition to alkali metal carbonates, alkali metals salts of carboxylic acids, like, $Na_2C_2O_4$, have been found to be potential activating agents. The carbon material obtained from plant source, Cg potassium carbonate 3, has been successfully exploited as support for HPW and employed as a catalyst for the synthesis of TAME, a preferred gasoline additive.

CHAPTER - 4

CARBON MATERIALS FROM BORASSUS FLABELLIFERA FOR CATALYTIC APPLICATION

4.1 INTRODUCTION

Borassus flabellifera, commonly named as palmyra palm or toddy palm, is habitat of India and distributed through south-east Asia and North Australia. Borassus flabellifera is the most numerously grown palm variety in the world next to coconut palm. Almost all parts of the plant like trunk, leaves and fruit were found to be useful in some form or other except the male flower spikes (Fig. 4.1).

Fig. 4.1 Images of the (a) tree of Borassus flabellifera with fruits and (b) flower spikes derived from male tree

The fibers of the fruit of Borassus flabellifera, comprising of α-cellulose, hemicellulose and lignin, were used as reinforcement in green composites (Reddy *et al*., 2009). Kannan

and Thambidurai (2007, 2008) have produced activated carbon from the fruit seed of the plant and employed the same as adsorbent for the removal of Cr (VI) and Pb (II) from aqueous solution. Arivoli *et al*., (2007) have derived activated carbon from the bark of the plant and used the same for the sorption of copper metal ions. Yoshikawa *et al*., (2007) have isolated a steroid possessing antidiabetogenic activity from the methanol extract of the male flower spikes of Borassus flabellifera. The peculiarity of the flower spikes is the inherent porosity holding a promise of being used as a precursor for the production of activated carbon material.

Heteropoly acids (HPAs) are strong solid Bronsted acid catalysts. The strong acidity is a result of the low charge-density (extensive delocalization) on the surface of the spherical HPA molecules leading to greater mobility of proton. In solid state, HPAs are nearly 100 times stronger than sulphuric acid. In addition, HPAs offer low volatility, low corrosivity, high catalytic activity and selectivity compared to conventional mineral acids (Schwegler *et al*., 1992). But most of the HPAs are non porous with a low S_{BET} values. In heterogeneous catalysis, the catalysts are expected to be porous with high surface area values resulting in the better accessibility for reactants to the active sites and an accompanying high catalytic activity (Alcaniz-Monge *et al*., 2008). Activated carbon is a useful support for catalysts owing to its high specific surface area value and is also stable over a wide range of pH values. The source of carbon as well as the method of activation influence the hydrophilicity, hydrophobicity, the isoelectric point and the pore size distribution. Also it is possible to vary the S_{BET} and V_p values of the activated carbon material in accordance with the requirement (Schwegler *et al*., 1992). HPAs such

as HPW are known to adsorb strongly on activated carbon with the adsorption involving transfer of proton from the HPA to carbon surface (Schwegler *et al.*, 1992) resulting in a high affinity between the poly anion and activated carbon surface (Izumi and Urabe, 1981). Activated carbon appears to be the best choice as support for HPAs owing to the fact that the acid properties of HPA are retained upon supporting and also the active component is well dispersed on the support. The oxygen containing surface functional groups are known to play a role in the HPA dispersion. A variety of activated carbon materials, like, carbon black Vulcan 6, Cabot France, extra conductive carbon printex XE2 (Degussa) and Darco activated carbon, Aldrich (Liu-Cai *et al.*, 1999), Kureha activated carbon, Japan (Obali and Dogu, 2008), commercial wood based activated carbon (Chimienti *et al.*, 2001) and activated carbon produced from the timber mill of Xinhua in Shanxi (Chu *et al.*, 1996) have been employed as supports for HPAs. Exploitation of indigenously developed activated carbon (with desired properties), from an inexpensive carbon precursor (flower spikes of Borassus flabellifera), as catalyst support, in the present investigation, is an useful attempt towards the development of supported solid acid catalyst.

For comparison, in addition to the activated carbon from Borassus flabellifera, silica (mesoporous cubic SBA-1) too was employed as a support for HPA ($H_3PW_{12}O_{40}$ n H_2O) and the performance of carbon and silica supported heteropoly acid catalysts have been evaluated for the synthesis of MTBE.

Attempts to overcome the diffusion constraints offered by zeolites for the reactant molecules of large sizes to reach the active catalytic sites have culminated in the origin of mesoporous (pore size larger than 20 Å) silica materials with remarkable textural features (Taguchi and Schuth, 2005). SBA - 1 is one of the important silicious materials belonging to the class of mesoporous materials. Due to its cubic structure of the three dimensional pores SBA-1 is more desirable for the catalytic applications than one-dimensional mesoporous materials (Ji *et al.*, 2003). SBA-1 materials have been studied less often compared to MCM-48 with similar cubic structure and this is because of the fact that the synthesis of SBA-1 requires specific conditions such as acidic media, surfactant with larger head groups (alkyl triethyl ammonium surfactants) and low temperatures (Kruk and Jaronieck, 1999; Morey *et al.*, 1998; Huo *et al.*, 1996). The possibility of employing alkyl trimethyl ammonium surfactants for the synthesis of SBA-1 is also being currently explored (Kim and Ryoo, 1999). As pure silica mesoporous SBA-1 material possess a neutral frame work with limited catalytic applications, the nature of the amorphous walls is modified by the incorporation of heteroatoms such as Ti (Ji *et al.*, 2003, 2005), Mo (Dai *et al.*, 2001), Fe (Vinu *et al.*, 2007) and Cr (Zhao and Wang, 2006) widening the usefulness of the SBA-1 material.

Phasing out of alkyl lead compounds from gasoline has given imputes to the search for alternate gasoline and diesel fuel additives. The necessity of alternate fuel additives is more today than ever before as the gasoline and diesel fuel currently contain more cracked components than in the past resulting in an increase of olefin content of the fuels. Olefins are less stable to oxidation compared to paraffinic and aromatic compounds as a result of which deposits are formed in the vehicle fuel system. In addition olefins

have poor cetane quality. All these aspects, namely, the change in fuel composition and an accompanied ill-effect of the deposit formation on engine performance and life time necessitate the search for environmentally benign ways of generating potential gasoline additives. Gasoline additives are expected to improve the exhaust gas quality, fuel economy and engine performance (Owen, 1989).

Among several unleaded gasoline fuel additives, like ethyl tertiary butyl ether (ETBE), tertiary amyl methyl ether (TAME), tertiary amyl ethyl ether (TAEE), di-isopropyl ether and MTBE (methyl tertiary-butyl ether). MTBE is the most widely used quality improving additive (Ali *et al*., 2000). In addition, the production cost of MTBE is lower than other tertiary ethers. Not only the synthesis of MTBE is of industrial significance but also the decomposition as it provides a route to the production of pure isobutene. Industrially, MTBE is produced in a liquid phase reaction. The catalyst employed is a sulfonic acid resin (e.g., Amberlyst 15). The reaction temperature is of the order of 323 - 343 K and the pressure is of the order of 10 to 15 bar with a molar ratio of methanol/isobutene higher than 1:1. The disadvantage of the process is the thermal instability of the sulfonic groups of the catalyst there by resulting in corrosion problem. In addition, side products such as di-isobutenes (2-4-4 trimethyl-1- and 2-pentenes), tertiary-butyl alcohol and di methyl ether are formed. Also relatively high methanol/isobutene molar ratios are required making the recycle operation inevitable (Nikolopoulos *et al*., 1996; Collignon *et al*., 1997; Malecka *et al*., 1999; Diaz *et al.,* 2001 and Ali *et al*., 2000). More over, the reactant, isobutene employed for MTBE synthesis is currently obtained as a by-product of catalytic or steam cracking refining operation and

the supply of isobutene from these sources is insufficient to meet the future needs. So alternate catalytic routes with out the use of branched alkenes such as isobutene need to be developed. Thus the search for alternate environmentally benign, economically viable and selective catalyst is inevitable for the synthesis of MTBE.

4.2 EXPERIMENTAL

4.2.1 Synthesis of carbon material from Borassus flabellifera flower spikes

The dried flower spikes of *Borassus flabellifera* (Bf) were employed as carbon precursor. A known amount of dried flower spikes was heated in a muffle furnace at 573 K for 30 min. Volatile matter was eliminated during pyrolysis resulting in a carbon rich char (C_{Bf} as synthesized). The char was ground and sieved (200 mesh). The char was treated with NaOH (10 wt.% aqueous solution) followed by washing with excess distilled water and drying in an air oven at 393 K. The carbon sample was further treated with conc. HCl (char : conc. HCl (wt./vol.%) = 1:10) followed by washing with excess distilled water and drying in an air oven at 393 K. The carbon material obtained after treatment with NaOH and HCl was designated as C_{Bf} base acid.

4.2.2 Activation of carbon material

The char obtained after treatment with base and acid (C_{Bf} base acid) was subjected to activation. The process of activation involved mechanical grinding of the carbon sample (C_{Bf} base acid) and the activating agent (K_2CO_3) in a mortar and pestle. The mixture (carbon and activating agent in a wt/wt.% ratio of 1:1) taken in an alumina boat was placed in a tubular furnace. Inert atmosphere (N_2) was maintained in the furnace during the activation process. The temperature of the furnace was raised to 1073 K and

maintained at that temperature for 2 h. The temperature of the furnace was then lowered. The contents were brought out and treated again with conc. HCl followed by washing with excess distilled water and filtration. The material thus obtained was labelled as C_{Bf} potassium carbonate 1.

4.2.3 Synthesis of mesoporous silica (SBA-1)

The procedure employed for the synthesis was same as that reported by Kruk and Jaronieck (1999) except that cetyl trimethyl ammonium bromide (CTMAB) was used as surfactant instead of cetyl triethyl ammonium bromide (CTEAB). The SBA-1 silica material was prepared using tetraethyl orthosilicate (98 % TEOS, Aldrich) as the silica source and CTMAB as the surfactant. The molar composition of the starting mixture was, 1 TEOS : 0.2 surfactant : 56 HCl : 700 H_2O

The surfactant (3.494 g), HCl (82 mL) and distilled water (600 mL) were mixed homogeneously. The surfactant solution was cooled in an ice bath. Pre cooled TEOS (10.7 mL) was added to the surfactant solution while being vigorously stirred. The precipitation of the silica-surfactant assembly was completed with in 8 h of stirring. The precipitate formed at 273 K was aged in the reaction mixture for 2 days at room temperature to improve the cross linking of the silica frame work. As the frame work will be still weak, the precipitate was filtered as such with out any washing. The frame work was cured further through vacuum-drying at room temperature and subsequently dried in air at 433 K. The obtained material was then washed with an ethanol-HCl-H_2O mixture (1:1:15, V/V %) and subsequently air dried followed by calcination at 823 K in N_2 atm for 1 h and in air atm for 6 h.

4.2.4 Preparation of supported (activated carbon and silica) heteropoly acid (HPW) catalysts (H$_3$PW$_{12}$O$_{40}$ nH$_2$O/support)

Supported heteropoly acid catalysts were prepared by the method of dry impregnation. Typical method of catalyst preparation comprised of the addition of the support material (either activated carbon or mesoporous silica) to the aqueous solution of HPW in 20 mL distilled water followed by stirring the contents on a magnetic stirrer at room temperature for 6 h followed by evaporating the excess water to dryness in a water bath kept at 353 K. Catalysts with varying amount (10, 20, 30, 40 and 50 wt. %)) of HPW on the support (activated carbon and SBA-1) were synthesized.

4.2.5 Catalytic studies

The synthesis of MTBE from methanol and tertiary butyl alcohol (TBA) was carried out in vapour phase in a tubular reactor. N$_2$ was used as an inert carrier gas. The reaction products were analyzed using a gas chromatograph equipped with a flame ionization detector and OV-101 packed column. In a typical experiment, 0.5 g of the catalyst was placed in a tubular reactor. Various reaction parameters such as the optimum wt.% loading of the active component on the support, effect of reaction temperature and the effect of mole ratio of the reactants (methanol and TBA) on the catalytic activity and the on stream stability of the supported catalysts were evaluated.

4.3 RESULTS AND DISCUSSION

The carbon materials, mesoporous silica material (SBA-1) and the carbon and silica supported heteropoly acids were systematically characterized by a variety of physico chemical techniques to evaluate the structural, textural and morphological features. The

supported catalysts (HPW/C_{Bf} potassium carbonate 1 and HPW/SBA-1) were further exploited for the synthesis of MTBE.

4.3.1 Chemical structure of carbon material from Borassus flabellifera (C_{Bf} as synthesized, Char)

The broad peak around 128 ppm, observed in the ^{13}C MAS NMR spectrum of C_{Bf} as synthesized, is attributed to the aromatic carbon structure associated with lignin (Freitas *et al*., 2000; Solum *et al*., 1995). The features of the peak are typical of graphitic carbon powder (Freitas *et al*., 2001). Thus the graphitic ordering of carbon atoms in the C_{Bf} as synthesized is evident from the ^{13}C MAS NMR spectrum shown in Fig. 4.2.
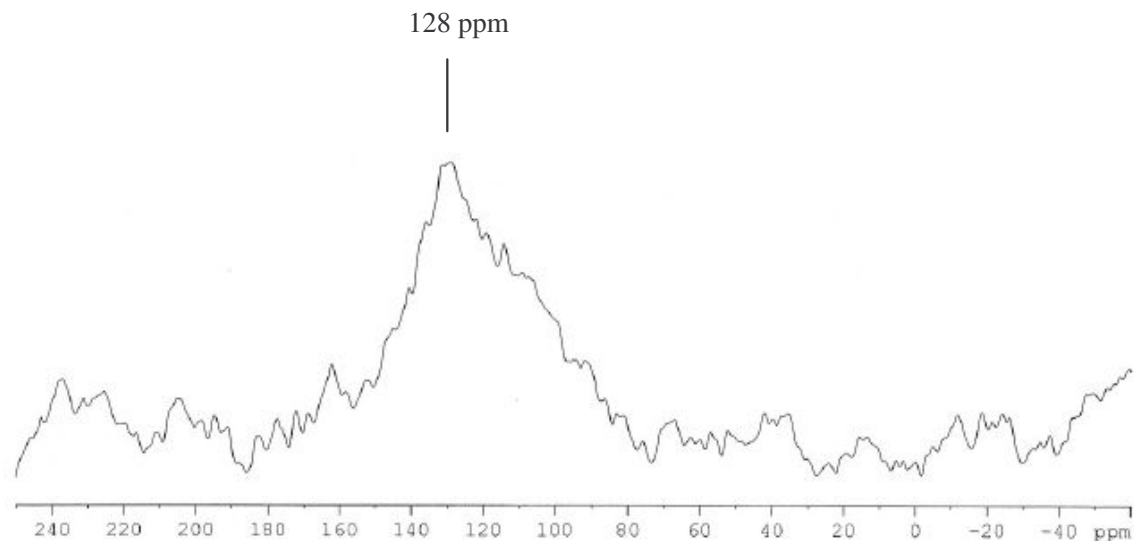
Fig. 4.2 ^{13}C MAS NMR spectrum of the char (C_{Bf} as synthesized) from Borassus flabellifera flower spikes

4.3.2 Surface morphology of activated carbon material - Scanning Electron Microscopic (SEM) Analysis
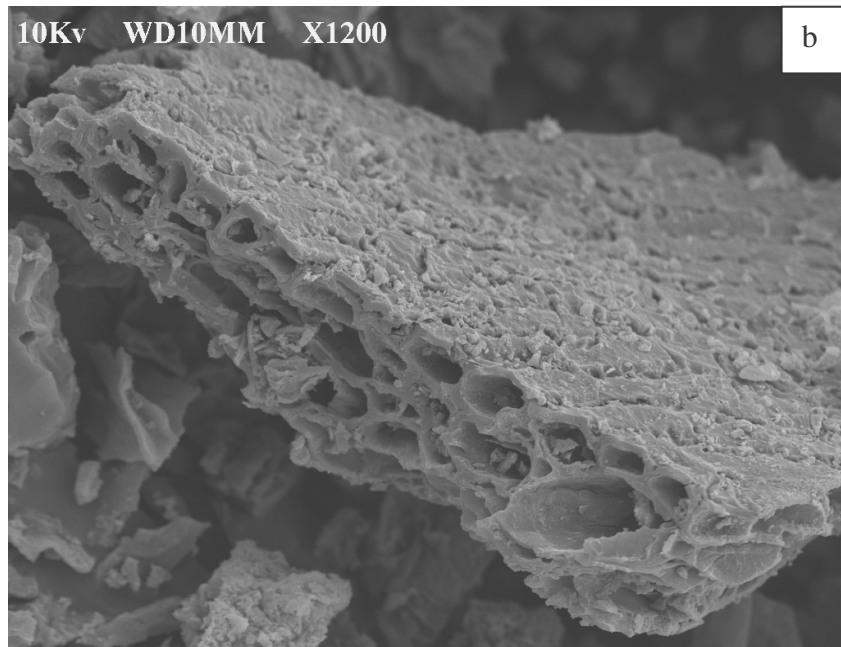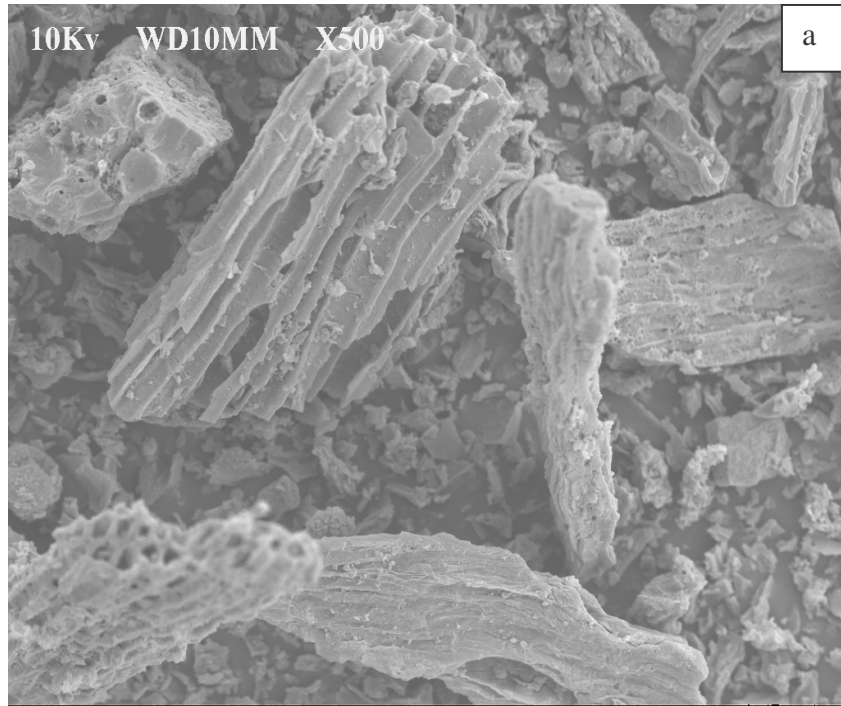
Fig. 4.3 SEM images of activated carbon from Borassus flabellifera (C_{Bf} potassium carbonate 1) at different magnifications (a) 500 X and (b) 1200 X

The surface morphology of the activated carbon material (C_{Bf} potassium carbonate 1) was

examined from SEM analysis at two different magnifications (500 X and 1200 X) and the

images are shown in Fig. 4.3. A very rough and highly porous surface is observed. The pore structure is analogous to honey comb structure with a bunch of carbon tubes in the matrix.

4.3.3 Structural (crystallographic) properties of carbon materials from Borassus flabellifera and SBA -1 - XRD studies
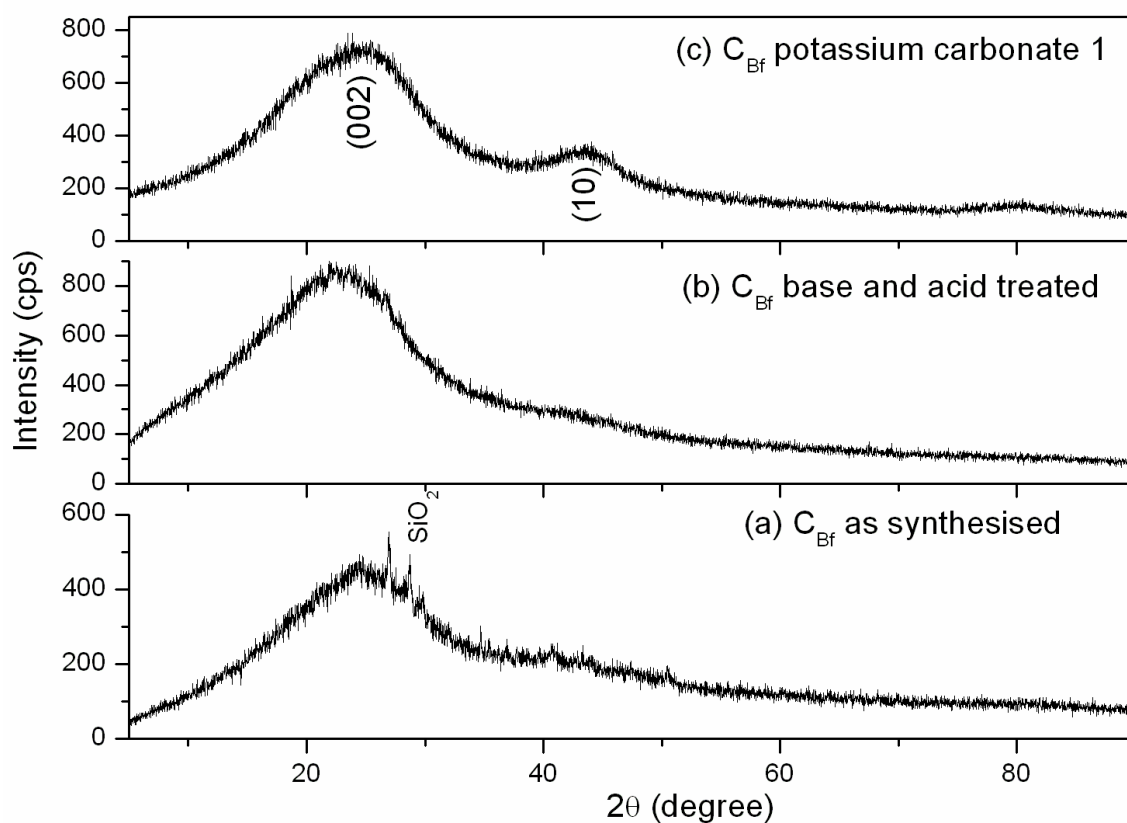
Fig. 4.4 XRD patterns of Carbon materials from Borassus flabellifera (C_{Bf}) (a) C_{Bf} as-synthesized, (b) C_{Bf} base - acid treated and (c) C_{Bf} potassium carbonate 1

The X-ray diffraction features resulting from the carbon materials (as synthesized, base and acid treated and K_2CO_3 activated) are shown in Fig. 4.4. The impurities inherently present in the as synthesized carbon material (C_{BF} as received) were effectively removed

by the treatment with base (NaOH) and acid (HCl) in succession (Fig. 4.4 (a) and (b)). Also, upon activation with K_2CO_3, the graphitic nature of the carbon material improved as evidenced from the increase in the intensity of the diffraction peak at a 2θ value of 44° (Fig. 4.4. (b) and (c)). The two diffraction peaks centered at 2θ values of 24.5 and 44° were respectively indexed to (002) and (10) diffraction peaks typical of carbon material.
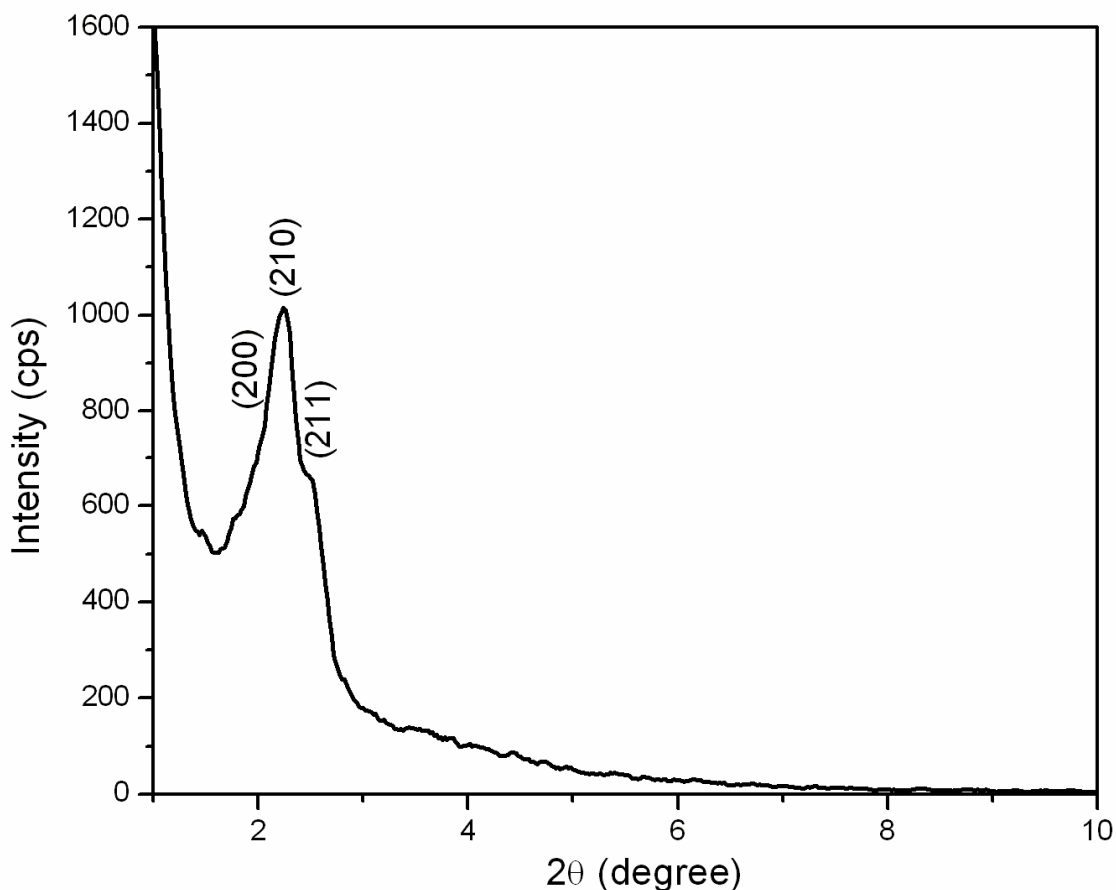
Fig. 4.5 Low angle X-ray diffraction pattern of mesoporous siliceous SBA-1 (calcined) material

The X-ray diffractogram of SBA-1 (calcined) is shown in Fig. 4.5. The diffraction peaks observed are characteristic of three-dimensional cubic mesostructure. The three peaks in the 2θ region of 2-3° are indexed to the diffraction peaks (200), (210) and (211) planes of

SBA-1 material characteristic of the cubic Pm3n space group (Huo *et al*., 1996; Dai *et al*., 2001).

4.3.4 Textural properties of carbon materials from Borassus flabellifera – BET sorptometry

The N_2 adsorption-desorption isotherms of carbon materials from Borassus flabellifera as well the carbon supported heteropoly acid catalyst are shown in Fig. 4.6. The carbon material as synthesized (C_{Bf} as synthesized) exhibited a low S_{BET} value (17 m^2/g) which upon thermal activation (heat treatment at 1073 K in N_2 atm. for 2 h) increased to 550 m^2/g. The S_{BET} value increased from 17 to 1070 m^2/g upon activation with K_2CO_3. In the case of carbon (C_{Bf} carbonate 1) supported heteropoly acids, as the wt.% loading of HPW increased from 10 to 40 wt.% the S_{BET} values decreased from 786 to 583 m^2/g because of blocking of the narrow micropores by the fine clusters of HPA. The carbon materials as well as the supported catalysts (HPW/C_{Bf} potassium carbonate 1) exhibited type I isotherms characteristic of microporous materials.

The N_2 adsorption-desorption isotherms of mesoporous silica (SBA-1) and silica supported heteropoly acid (HPW/SBA-1) catalysts with different amounts of the active component (HPW) are shown in Fig. 4.7.
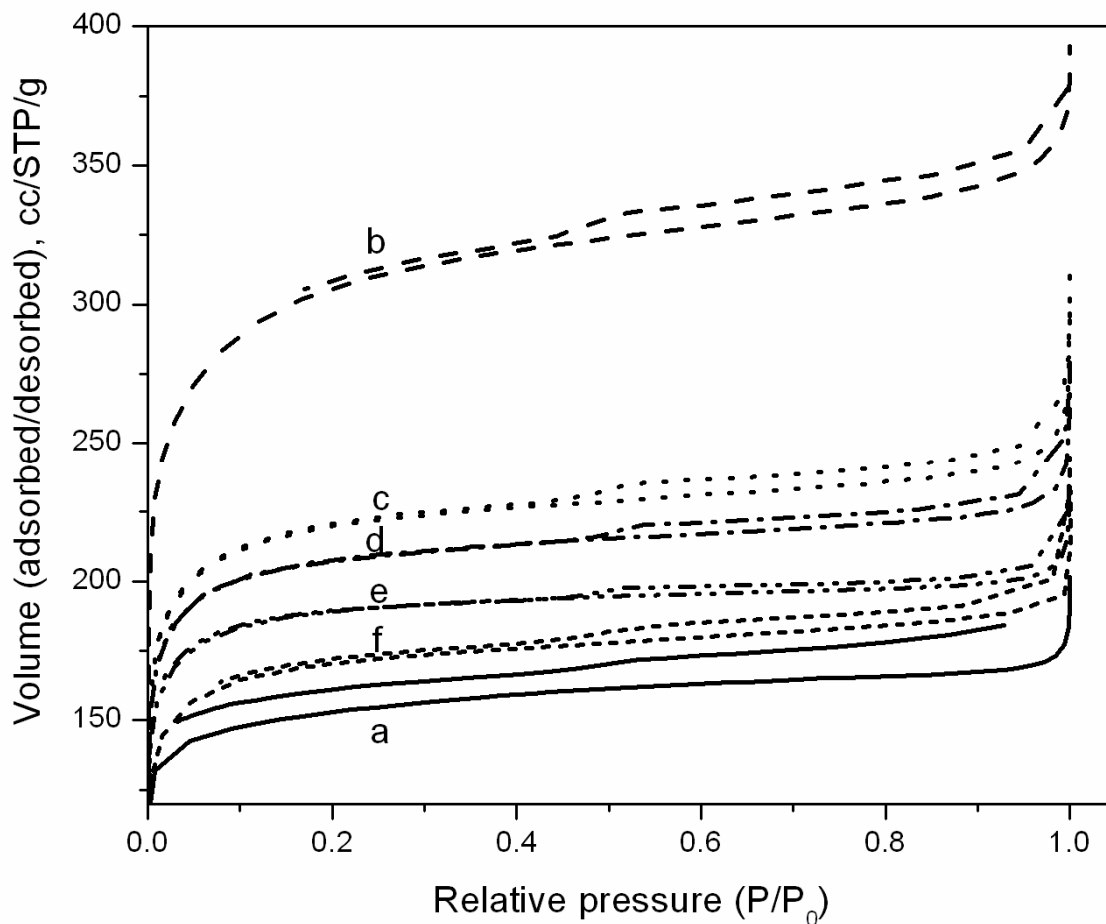
Fig. 4.6 N_2 adsorption desorption isotherms of carbon materials from Borassus
flabellifera and carbon supported heteropoly acids; (a) C_{Bf} thermal activation
(S_{BET} = 550 m^2/g and Vp = 0.28 cc/g), (b) C_{Bf} potassium carbonate 1 (S_{BET} =
1070 m^2/g and Vp = 0.55 cc/g), (c) 10 wt.% HPW/C_{Bf} potassium carbonate 1
(S_{BET} = 786 m^2/g and Vp = 0.39 cc/g), (d) 20 wt.% HPW/C_{Bf} potassium
carbonate 1 (S_{BET} = 756 m^2/g and Vp = 0.36 cc/g), (e) 30 wt.% HPW/C_{Bf}
potassium carbonate 1 (S_{BET} = 678 m^2/g and Vp = 0.31 cc/g) and (f) 40 wt.%
HPW/C_{Bf} potassium carbonate 1 (S_{BET} = 583 m^2/g and Vp = 0.29 cc/g)

The prepared SBA-1 material possessed a high S_{BET} value of 918 m^2/g. A steep increase

in the volume of nitrogen adsorbed was observed in the relative pressure range of p/p_0 =

0.15-0.25 which is attributed to the capillary condensation in the mesopores (Kao *et al.*,

2007). The isotherm could be classified as type-IV typical of a mesoporous material (Ji

et al., 2005). Even upon loading 10-50 wt.% HPW on the SBA-1 support features characteristic of a mesoporous material were observed. But the S_{BET} values decreased from 535 to 265 m^2/g as the HPW content increased from 10-50 wt.%.
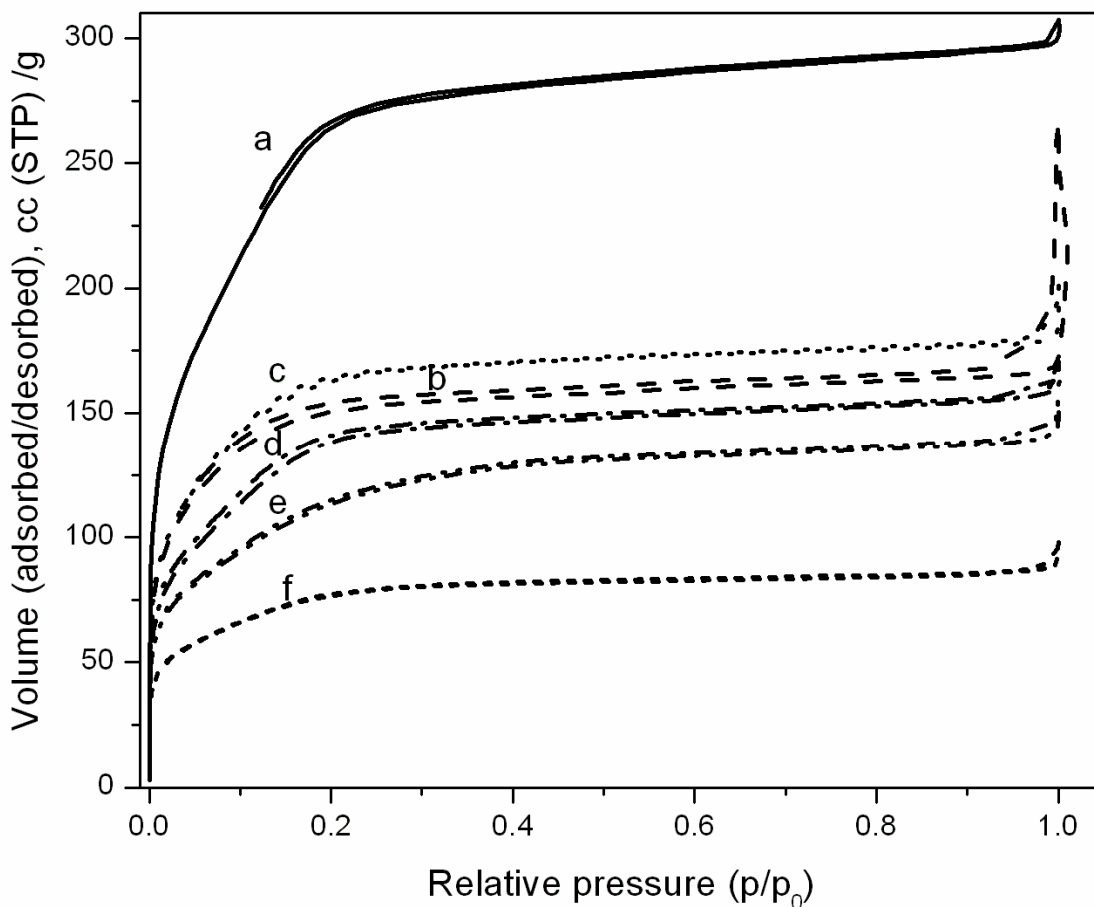
Fig. 4.7 N$_2$ adsorption desorption isotherms of mesoporous silica (SBA – 1) and SBA-1 supported heteropoly acids; (a) SBA-1 (S_{BET} = 918 m^2/g and Vp = 0.462 cc/g), (b) 10 wt.% HPW/SBA-1 (S_{BET} = 535 m^2/g and Vp = 0.28 cc/g), (c) 20 wt.% HPW/SBA-1 (S_{BET} = 567 m^2/g and Vp = 0.26 cc/g), (d) 30 wt.% HPW/SBA-1 (S_{BET} = 480 m^2/g and Vp = 0.24 cc/g) and (e) 40 wt.% HPW/SBA-1 (S_{BET} = 393 m^2/g and Vp = 0.22 cc/g) and (f) 50 wt.% HPW/SBA-1 (S_{BET} = 265 m^2/g and Vp = 0.15 cc/g)

4.3.5 FT-IR analysis of HPW/C$_{Bf}$ potassium carbonate 1 and HPW/SBA-1 catalysts
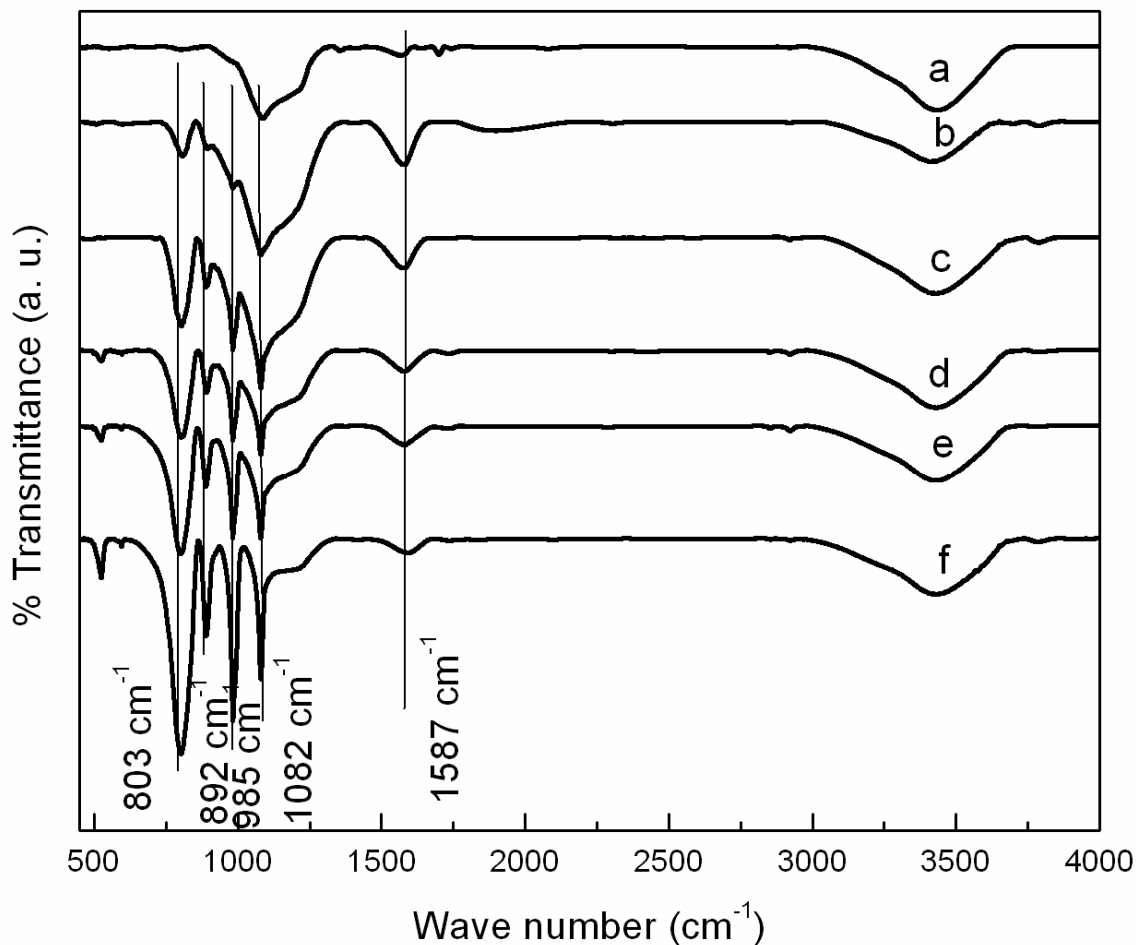
Fig. 4.8 FT-IR spectra of (a) C$_{Bf}$ potassium carbonate 1, (b) 10 wt% HPW/C$_{Bf}$ potassium carbonate 1, (c) 20 wt% HPW/C$_{Bf}$ potassium carbonate 1, (d) 30 wt% HPW/C$_{Bf}$ potassium carbonate 1, (e) 40 wt% HPW/C$_{Bf}$ potassium carbonate 1, (f) 50 wt% HPW/C$_{Bf}$ potassium carbonate 1

As the retention of primary polyanion structure of the HPA (HPW) upon loading the heteropoly acid on the carbon support is an issue of concern, the same is monitored from the FT-IR spectra of HPW/C. The FT-IR spectra of activated carbon produced from the male flower spikes of Borassus flabellifera (C$_{Bf}$ potassium carbonate 1) as well as 10, 20,

30, 40 and 50 wt.% HPW loaded on activated carbon (C_{Bf} potassium carbonate 1) catalysts are shown in Fig. 4.8.
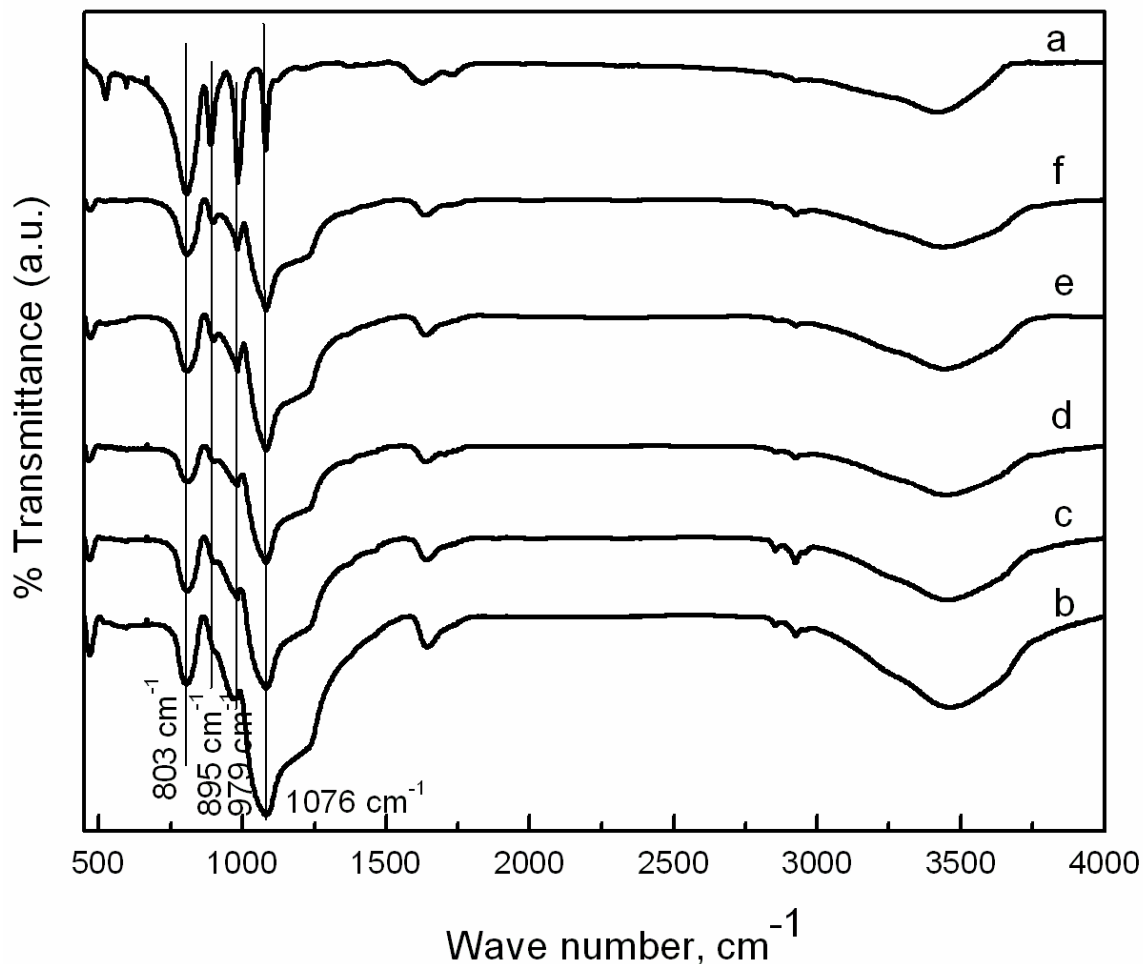
Fig. 4.9 FT-IR spectra of (a) HPW (bulk), (b) 10 wt.% HPW/SBA-1, (c) 20 wt.% HPW/SBA-1, (d) 30 wt.% HPW/SBA-1, (e) 40 wt.% HPW/SBA-1 and (f) 50 wt.% HPW/SBA-1

The primary Keggin type structure comprises of mainly four different types of oxygen atoms depending on their bonding to metal atoms (central as well as addenda atoms). The absorption at $\nu = 1080\text{-}1081$ cm^{-1} is attributed to the excitation of P-O bond; the band at $\nu = 976\text{-}995$ cm^{-1} is attributed to the excitation of the W=O $_{terminal}$ bond; the band at $\nu =$

890-900 cm^{-1} was attributed to the excitation of the W-O$_{corner}$-W bond and the band at ν = 805-810 cm^{-1} is typical of the W-O$_{edge}$-W. Interestingly in all the spectra (HPW/C) shown in Fig. 4.8, the transmittances fall in the regions typical of Keggin type structure and so it can be said that the primary poly anion structure is retained upon loading HPW (10 to 50 wt.%) on activated carbon support. FT-IR spectra of silica (SBA-1) supported HPW catalysts are shown in Fig. 4.9. For comparison the FT-IR spectrum of bulk HPW is also shown. It is observed that the features characteristic of Keggin type poly anion are retained and the primary structure remain undecomposed when HPW is supported on SBA-1 for all the wt. % loadings of HPW (10 to 50 wt. %).

4.3.6. Synthesis of MTBE over HPW/carbon and HPW/silica catalysts

To evaluate the optimum amount of the active component (HPW) in HPW/SBA-1 catalytic systems, MTBE synthesis was carried on catalysts with different amounts of active component (10, 20, 30, 40 and 50 wt. %) over SBA-1 mesoporous silica (Fig. 4.10).

The reaction was carried out at a temperature of 373 K with a methanol to TBA molar ratio of 10:1. The flow rates of the feed and the carrier gas were 10 mL/h and 30 ml/min respectively. The reaction was monitored for 300 min with the reaction products being collected for every 30 min and analysed by a GC. 20 wt.% HPW on SBA-1 mesoporous silica was found to be the optimum HPA loading over the silica support

resulting in higher conversion of TBA compared to catalysts with various other amounts of HPW (10, 30, 40 and 50 wt.% HPW/SBA-1).
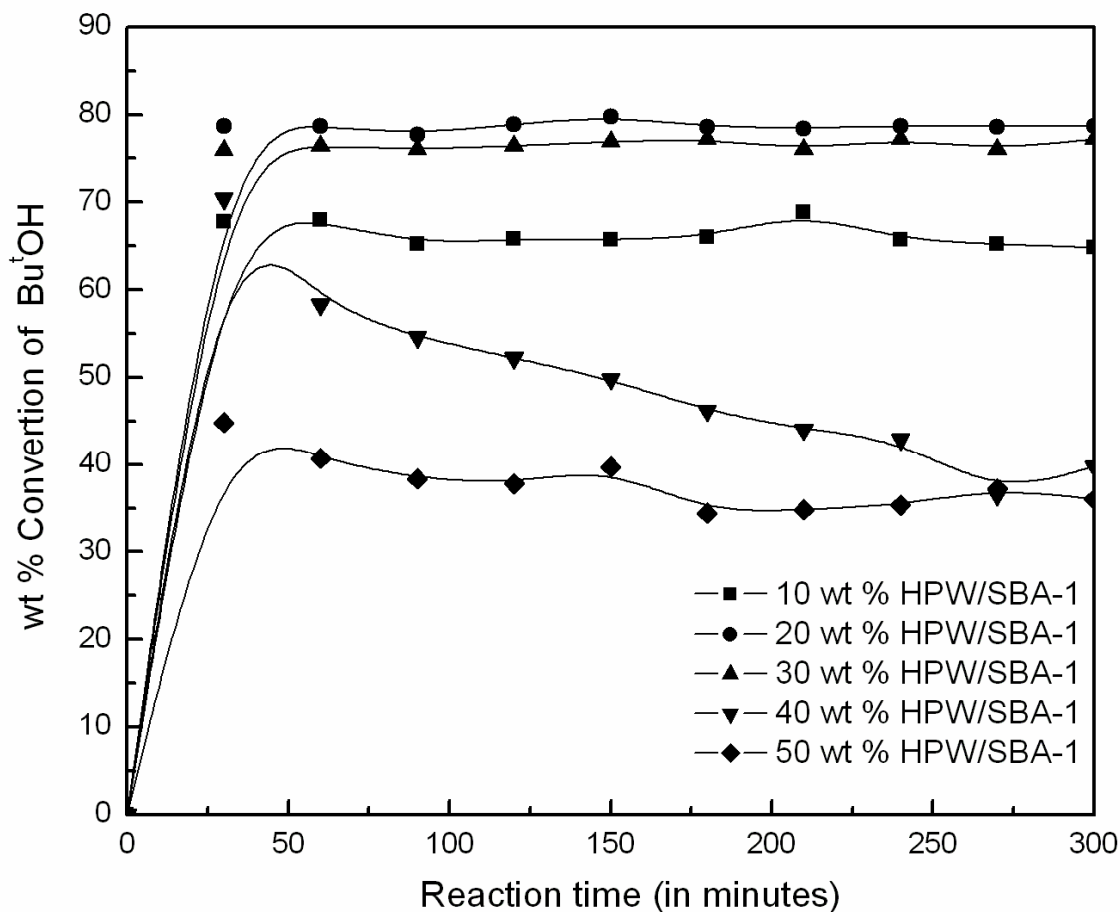
Fig. 4.10 Time course of MTBE synthesis from methanol and TBA over HPW/SBA-1 at different wt.% loadings of the active component (HPW) (a) 10 wt.% HPW/SBA-1, (b) 20 wt.% HPW/SBA-1, (c) 30 wt.% HPW/SBA-1, (d) 40 wt.% HPW/SBA-1 and (e) 50 wt.% HPW/SBA-1

4.3.6.1 Effect of reaction temperature

MTBE synthesis was carried out over 20 wt.% HPW/C_{Bf} potassium carbonate 1 and 20 wt.% HPW/SBA-1 catalysts at different reaction temperatures, namely, 353, 363, 373 and 393 K. The mole ratio of methanol to TBA is 10:1.

142
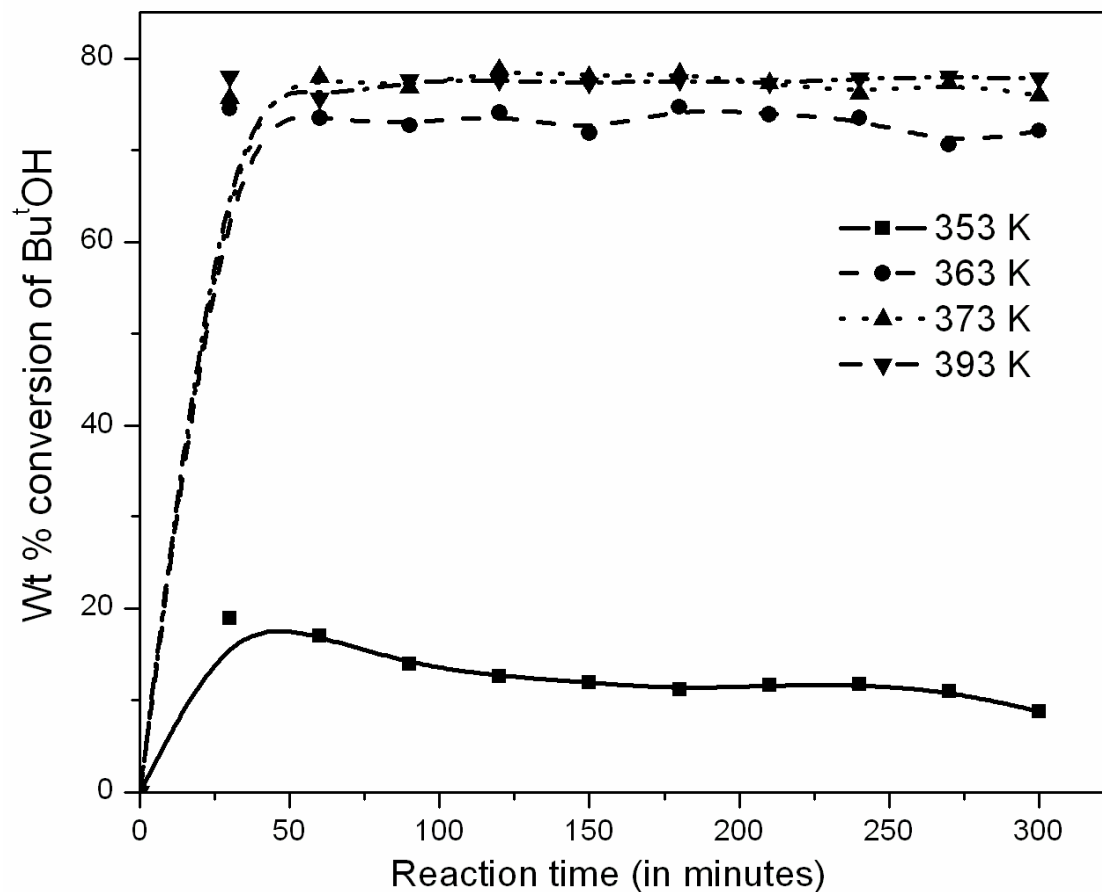
Fig. 4.11 Time course of MTBE synthesis from methanol and TBA over HPW/CBf
potassium carbonate 1 at different temperatures (a) 353 K, (b) 363 K, (c) 373 K
and (d) 393 K

Irrespective of the nature of support, the conversion of TBA to MTBE increased with
temperature and reached a maximum of nearly 80 % at a reaction temperature of 373 K
beyond which a slight decrease in the conversion of TBA was noticed (Figs 4.11 and
4.12).

Obali and Dogu (2008) have also made similar observations. The decrease in
conversion with an increase in temperature was attributed to the role of porous support
being acting as a reservoir for the adsorbed reactants. As a result, there will be a decrease

in the adsorbed concentration of reactants with an increase in temperature and an accompanied decrease in the conversion of TBA. In addition, as the synthesis of MTBE is an exothermic reaction, lower reaction temperatures are favoured.
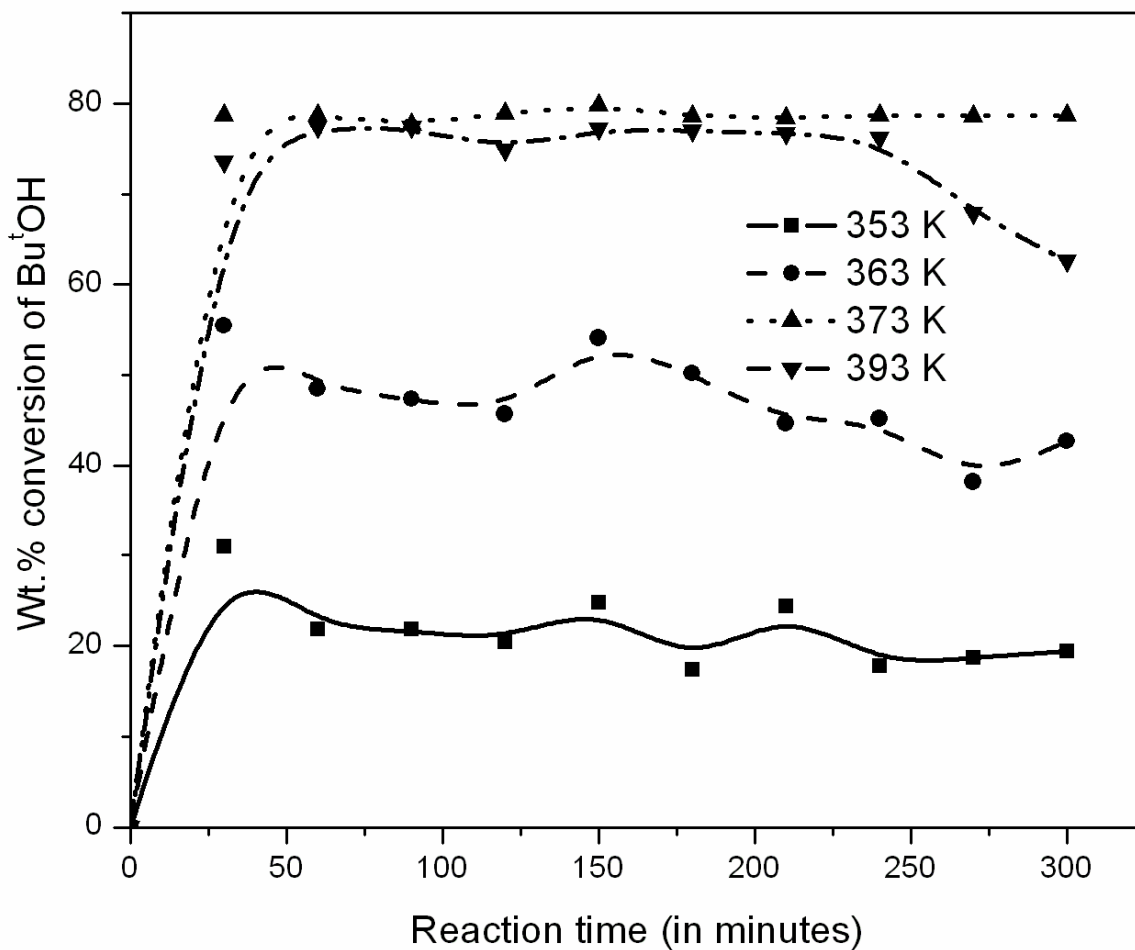
Fig. 4.12 Time course of MTBE synthesis from methanol and TBA over HPW/SBA-1 at different temperatures (a) 353 K, (b) 363 K, (c) 373 K and (d) 393 K

4.3.6.2 Effect of mole ratio of the reactants

In addition to the amount of the active component (HPW) on the support and the reaction temperature, the mole ratio of the reactants (methanol:TBA) was also found to be crucial.
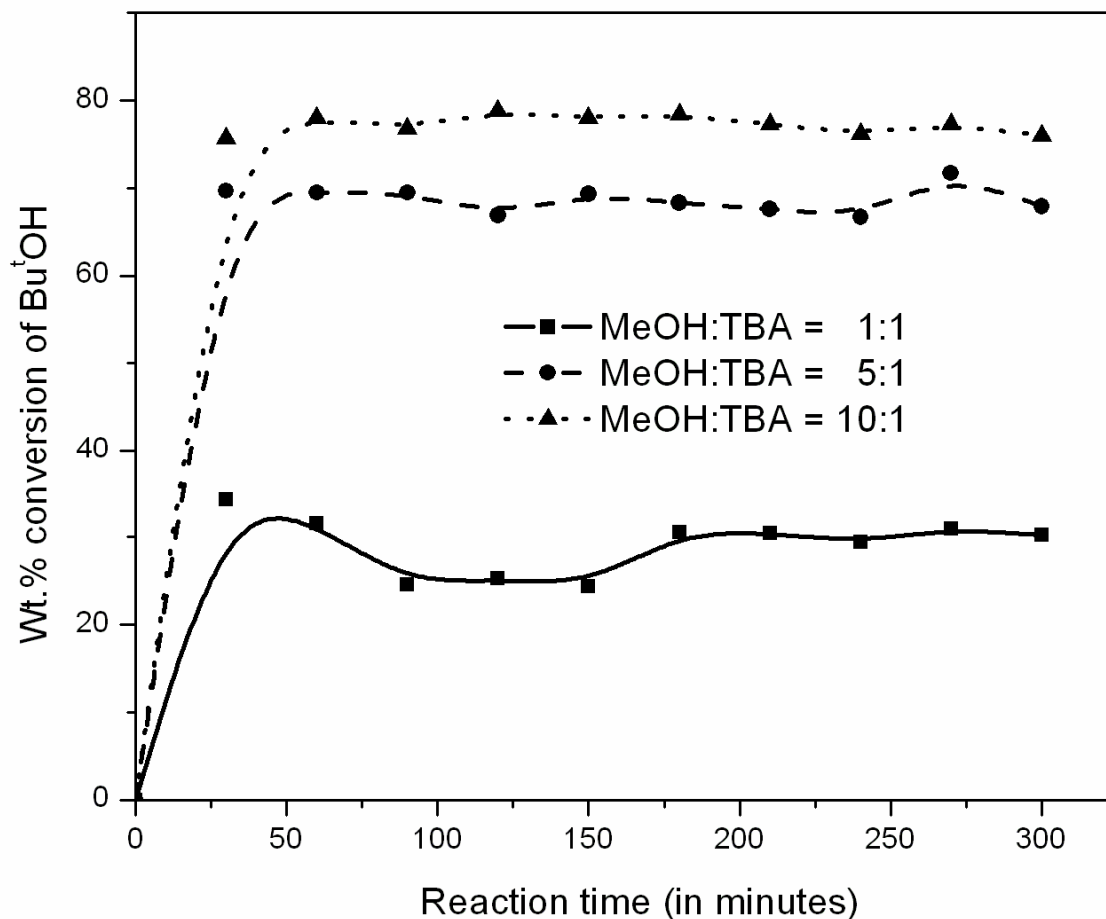
Fig. 4.13 Time course of MTBE synthesis from methanol and TBA over HPW/C$_{Bf}$ potassium carbonate 1 at different mole ratios of methanol to TBA (a) 10:1, (b) 5:1 and (c) 1:1

The synthesis of MTBE was carried out at three different mole ratios of methanol and TBA (10:1, 5:1 and 1:1) with other reactions conditions remaining constant (Figs. 4.13 and 4.14). Maximum conversion of TBA to MTBE was achieved with a methanol to TBA mole ratio of 10:1 implying that the adsorption coefficient of methanol over the catalyst is 10 times lower and to compensate the same a relatively higher amount of methanol compared to TBA need to be employed for attaining the highest conversion

values possible. It is interesting to note that the reaction course followed a similar trend on carbon and silica supported HPW catalyst as a function of mole ratio.
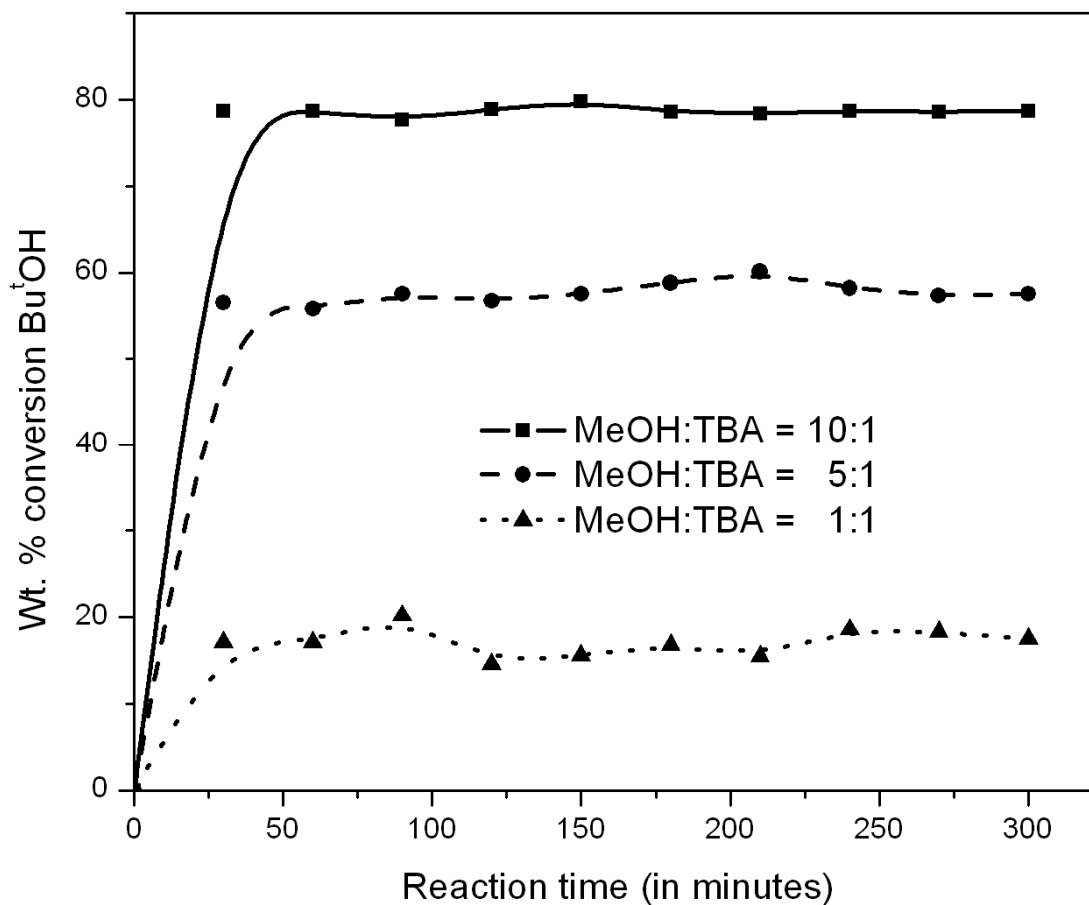
Fig. 4.14 Time course of MTBE synthesis from methanol and TBA over HPW/SBA-1 at different mole ratios of methanol to TBA (a) 10:1, (b) 5:1 and (c) 1:1

4.3.6.3 Evaluation of stability of HPW/C Vs HPW/SBA-1 acid catalysts for MTBE synthesis

The on-stream activity and stability of 20 wt.% HPW/C and 20 wt.% HPW/SBA-1 were illustrated in Fig. 4.15.

146
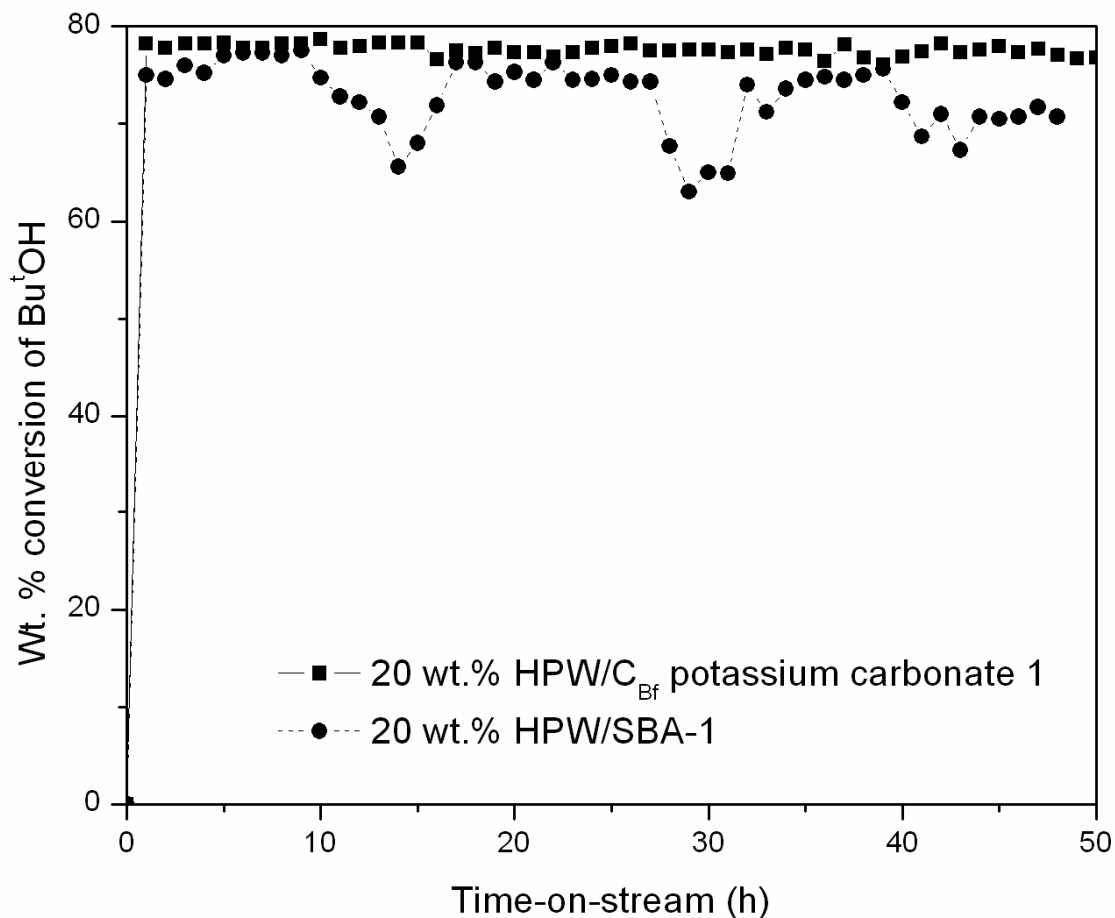
Fig. 4.15 Comparison of the stability of on-stream 20 wt. % HPW/C_Bf potassium
carbonate 1 and 20 wt.% HPW/SBA-1 catalysts for the gas phase synthesis of
MTBE

The reaction was carried out under optimal reactions conditions, namely, at a reaction

temperature of 373 K with a MeOH to TBA molar ratio of 10:1 and the flow rates of the

carrier gas and the feed (solution of MeOH and TBA) being 30 mL/min and 10 mL/h

respectively. With an increase in the time-on-stream to 50 h, the highly selective

coversion of Bu^{t}OH to MTBE hardly changes in the case of either HPW/Carbon or

HPW/SBA-1 indicating the excellent stability of these catalysts. The aforementioned

comparison illustrates the potential of carbon material from plant source to assist as a

suitable support for HPW. Moreover, the activated carbon material prepared from an

147

inexpensive source and by adopting simple method is found to perform on par with the well acclaimed mesoporous silica (SBA-1) support for the synthesis of MTBE.

4.4. CONCLUSION

Flower spikes of Borassus flabellifera are a potential precursor for high specific surface area (1070 m^2/g) activated carbon material with a peculiar porous (bunch of carbon tubes) morphology. The activated carbon material prepared was found to be a suitable support for heteropoly acid (HPW). The carbon supported heteropoly acid catalysts exhibited appreciable conversion of tertiary butyl alcohol (TBA) to MTBE and also a unique selectivity towards MTBE in the etherification reaction of methanol and TBA. The optimal reaction conditions for the vapour phase MTBE synthesis over HPW/C_{Bf} potassium carbonate 1 were found to be as follows:

Reaction temperature – 373 K; Mole ratio of Methanol to TBA – 10:1; flow rate of the feed – 10 ml/h; flow rate of the carrier gas – 30 ml/min.

The activity, selectivity and stability of carbon supported HPW catalyst were found to be on par with the well acclaimed mesoporous silica (SBA-1) supported HPW solid acid catalysts. Thus, an environmentally benign, economically viable and industrially adoptable carbon supported heteropoly acid (HPW) catalyst has been developed.

CHAPTER - 5

CARBON MATERIALS FROM LIMONEA ACIDISSIMA SHELLS FOR ELECTROCATALYTIC APPLICATION

5.1 INTRODUCTION

Energy sources are inevitable for the sustenance, progress and prosperity of mankind. There is an abrupt need for long lasting and human friendly energy sources in view of the fast depleting fossil fuel based non renewable energy resources. Energy security and energy independence are the two challenges before any nation in this new millennium. Global demand for energy is vast and recurring. The two challenges for human society in the 21st century are the speedy transition towards a clean and sustainable energy source and also to ensure effective utilization of natural resources available across the globe. Fuel cells appear to be one of the promising and clean energy sources for utility in near future.

5.1.1 Fuel cells as clean energy sources

In a fuel cell, the chemical energy of the fuel is directly converted to the electrical energy through a chemical reaction (Viswanathan and Aulice Scibioh, 2006). Electric current can be generated by the direct electrochemical oxidation of methanol. The electro oxidation reaction of methanol at the anode can be represented as follows (Ren *et al.*, 2000):

$$CH_3OH + H_2O \longrightarrow CO_2 + 6\,H^+ + 6\,e^- \qquad E^0 = 0.05\ V$$
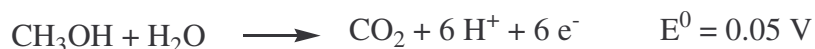
The electro oxidation of methanol bears technological significance in the operation and exploitation of Direct Methanol Fuel Cells. DMFCs hold promise as a clean energy

source for future transportation demands. Typical stationary and mobile applications of fuel cells include electrification of residences, providing power to mobile phones, lap top computers and other portable electronic devices (Sania *et al*., 2007).

5.1.2 Challenges in the development of fuel cell anode electro catalyts

Platinum group metals (PGM's) are most widely used for electrode applications in fuel cells. There are two major problems associated with the development of DMFC. The first is poisoning of the electrode by CO (Dicks, 2006). Phosphoric acid fuel cells can with stand up to 2 % CO in the fuel stream. But Proton Exchange Membrane Fuel Cells can only withstand ppm levels of CO. The second problem is the high cost of the catalyst restricting the rapid and wide spread commercialization of fuel cells. There are two approaches by which one can solve these two problems. One approach is to find suitable alternatives (partial or complete) to the active component i.e., Pt and the second approach is to find suitable alternative to Vulcan XC 72 R carbon black which is the best carbon support material commercially used till date (Rajesh, 2002). For example, Samant *et al*. (2005) have generated a catalyst more active than 10 wt.% Pt/Vulcan XC 72 R just by changing the support i.e., by replacing Vulcan XC 72 R with mesoporous carbon produced by a sol-gel method.

In general, high specific surface area carbon material is employed as support for Pt for fuel cell electrode applications. The carbon support facilitates the dispersion of the stable metal crystallites with favourable electronic and metal support interaction (Viswanathan, 2009). The carbon support influences the electrochemical properties and

150

in turn the performance of Pt-based electro catalysts. The nature of carbon material (oxygen surface functional groups, electronic conductivity, pore structure, morphology, electrochemically accessible surface area) determines the electrochemical performance of electrode catalysts. Electronic conductivity, surface area (electro active as well as BET), porosity, micro structure, macro morphology, corrosion resistance and cost are some of the important issues that determine the suitability of a carbon material for electrode applications. Any breakthrough in the commercialization of DMFCs is possible only by significant improvements either in the replacement of active Pt metal or the support carbon material.

Activated carbon materials from natural sources (lignocellulosic materials) have been widely exploited for sorption and catalytic applications. Such materials have remained unexplored for energy conversion device applications. Activated carbon material was synthesized from Limonea acidissima (wood apple) shells using KOH as activating agent. The carbon material (C_{WA}, Carbon from wood apple shell) obtained was used as support for Pt. The electro catalyst Pt/C_{WA} was employed for the fabrication of anode for the electro oxidation of methanol for fuel cell application.

5.1.3 Carbon material from Limonea acidissima shell by KOH activation

Limonea acidissima (Wood Apple) Shells were conceived for the first time as a source for activated carbon. The fruit, Limonia acidissima, (Fig. 5.1.) is native to India and other Asian countries. Limonia acidissima is also called as Feronia elephantum, Feronia limonia, Hesperethusa crenulata, Schinus limonia, Wood apple, Elephant apple and Curd

151

fruit. The shells of Limonia acidissima (wood apple) have features bearing close resemblance to that of coconut shells. Activated carbon from Limonea acidissima is produced by the chemical activation method using KOH as activating agent.

Fig. 5. 1 Wood apple (Limonea acidissima) fruits

5.1.4 Fabrication of Anode Electro catalyst with the carbon material obtained from Limonea acidissima shell for DMFC Application

Lack of efficient and inexpensive electro catalysts for methanol oxidation is a challenge for the large scale utility of direct methanol fuel cells. The objective of this work is to design a cost effective and highly active electro catalyst by developing new porous carbon material as support for Pt, as alternative to Vulcan XC 72 R.

5.2 Experimental

5.2.1 Synthesis of carbon material

Typical method of synthesis of carbon material involves the soaking of a known amount (50 g) of dried shells of Limonea acidissima in 100 mL of 50 wt.% KOH solution for 2 h. Excess KOH solution is then decanted. The shells soaked in KOH solution are then dried in an air oven at 423 K followed by subjecting the same to thermochemical activation in a N_2 atmosphere at 1073 K for 2 h. The char thus obtained is subsequently treated with conc.HNO_3. The char to conc. HNO_3 ratio (wt.%/wt.%) is 1:5.

5.2.2 Preparation of Pt/C catalysts

Pt supported carbon catalysts have been prepared by impregnating hexa chloro platinic acid in carbon material followed by reduction of Pt (4+) to Pt (0) in hydrogen atmosphere at 450 ºC for 2 h. Catalysts with different wt.% loadings, namely, 5, 10 and 20 wt. %, of active component (Pt) on the carbon support (C_{WA}) were prepared by adding the requisite amounts of a H_2PtCl_6 solution to the carbon support (C_{WA}) and drying at 383 K. 20 wt. % Pt/Vulcan XC 72 R prepared under identical conditions was employed as a reference for comparing the performance of C_{WA} carbon material relative to that of Vulcan XC 72 R carbon black.

5.3 RESULTS AND DISCUSSION

5.3.1 Characterization of activated carbon material from Limonea acidissima shells

The textural, structural and morphological features of activated carbon material from Limonea acidissima shells were thoroughly investigated using BET sorptometry, XRD, FT-IR, confocal Raman, EPR spectroscopy and SEM and the insights obtained are summarized below.

5.3.1.1 Textural properties of Carbon Material - BET sorptometry

N_2 adsorption – desorption isotherms obtained for the activated carbon from Limonea Acidissima are shown in Fig. 5.2. The corresponding pore size distribution curve (BJH) is also shown in the insert of the figure. The isotherm in Fig. 5.2 is of type I, characteristic of a microporous material. The pore size distribution reveals that the pore dimension is less than 2 nm suggesting that the activated carbon material is micorporous in nature.
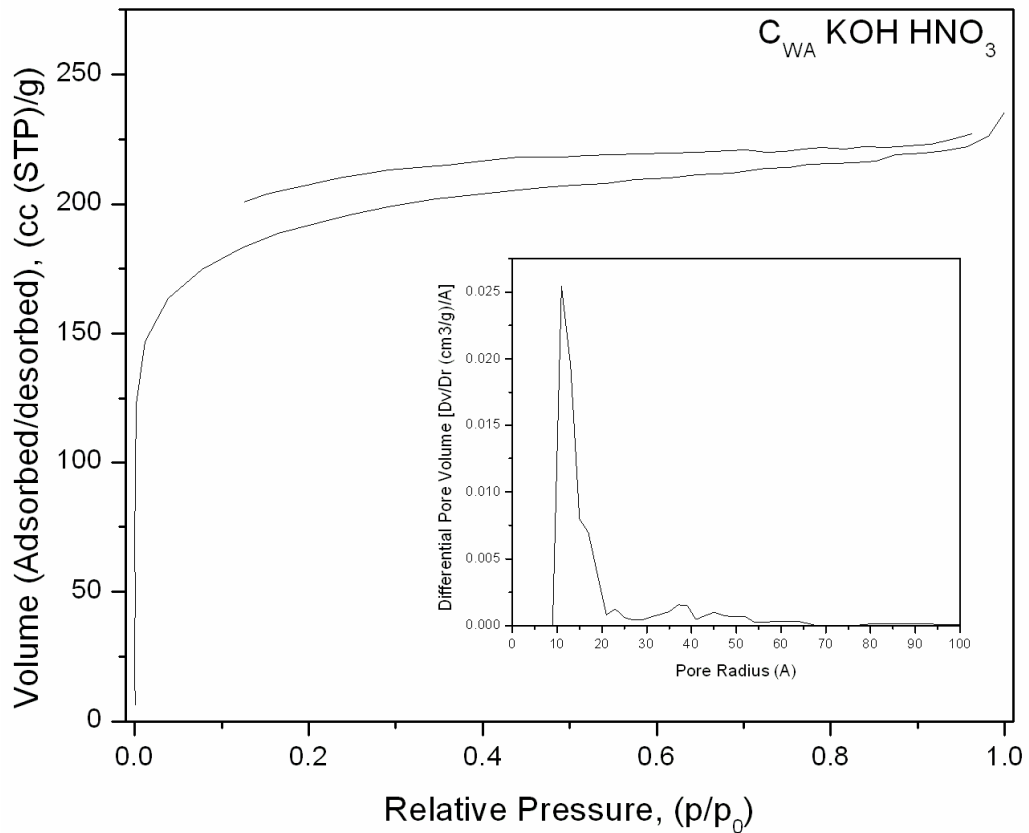
Fig. 5.2 N_2 adsorption-desorption isotherm of carbon material prepared from Limonea acidissima; the corresponding pore size distribution of the activated carbon material is shown in the insert; S_{BET} = 698 m^2/g; Pore volume (V_p) = 0.35 cm^3/g; and mean pore diameter = 2.0 nm (Pore size distribution of C_{WA} KOH HNO$_3$ is shown in the insert)

5.3.1.2 Structural (crystal) details of carbon material - XRD Studies

The X-ray diffraction pattern obtained for the activated carbon material from Limonea acidissima shells is shown in Fig. 5.3.
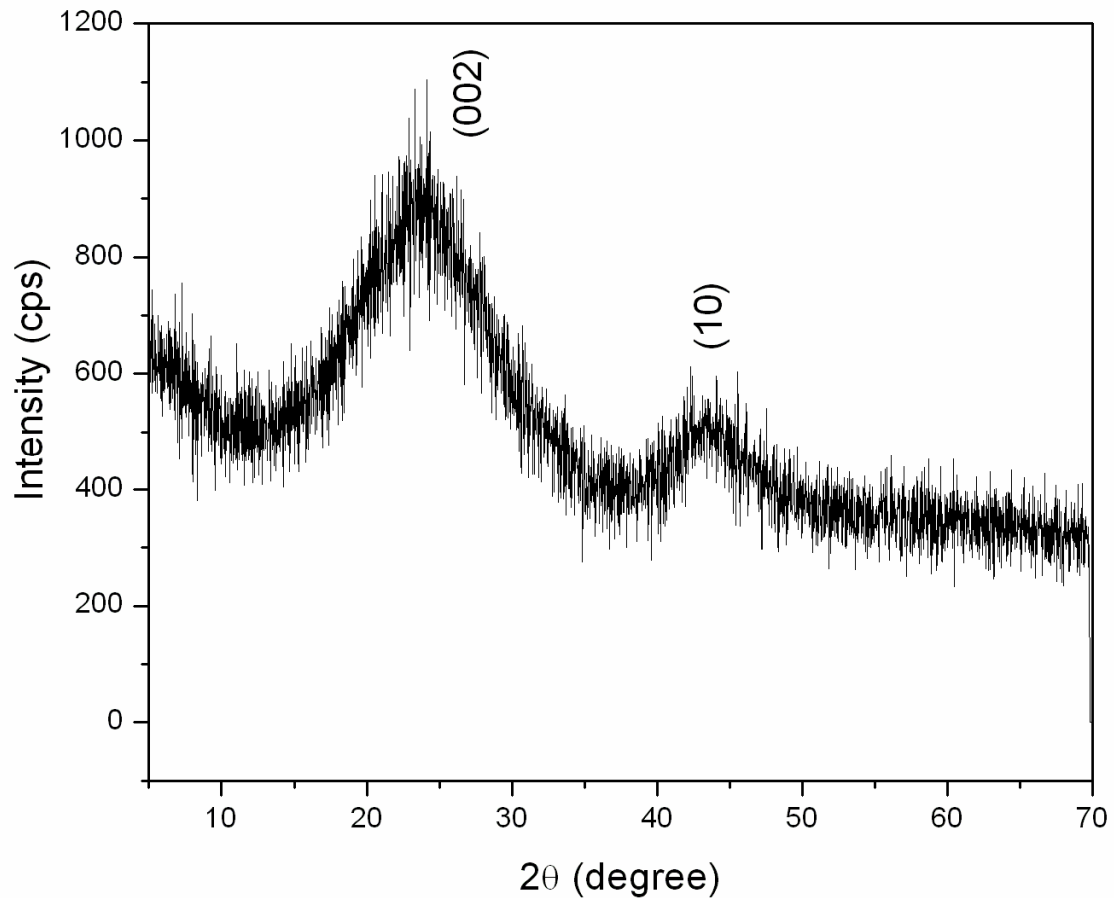
Fig. 5.3 XRD pattern of carbon material prepared from Limonea acidissima shells by KOH activation method followed by treatment with conc. HNO_3

Two broad diffraction peaks centered around 2θ values of 24 and 43° which are, respectively, attributed to the reflections from the (002) and (10) planes (the hk line is because of intra layer scattering) of the carbon material. The values of average crystallite sizes along the c-axis (stacking axis) and the a - axis were determined using the Debye –

Scherrer equation. Shape factor, k, values of 0.89 and 1.84 were employed for the calculation of values of L_c and L_a values respectively.

The diffraction angles as well as the value of full width at half maximum corresponding to the diffraction planes of (002) and (10) were employed for the calculation of values of L_c and L_a values respectively. The values of L_c and L_a were found to be of the order of 1.1 nm and 3.656 nm respectively. The values of L_c and L_a for typical graphitic carbon structure are 0.0670 nm and 0.2461 nm respectively (Mohindar and Pavlovic, 1993; Suresh and Seehra, 1996). The magnitude of the values of L_c and L_a of the activated carbon materials from Limonea acidissima (obtained by KOH activation and treatment with conc. HNO_3) indicate that the carbon material contained roughly about 16 cell lengths along the c-direction and nearly 15 cell lengths along the a - direction.

5.3.1.3 Surface functional groups - FT – IR spectroscopic studies

Fourier transform infrared (FT-IR) spectroscopy provides evidence for the presence of specific functional groups on the surface. Several characteristic bands were observed in the FT – IR spectrum of activated carbon from Limonea acidissima, C_{WA} shown in Fig. 5.4 and each of the bands has been assigned to specific functional group based on the assignments reported in literature. Even though a cluster of functional groups are present on the carbon surface, the prominent among them are: a sharp and intense band centered around 1637 cm^{-1}, which is attributed to the carbonyl (C=O) stretching vibration of quinone.
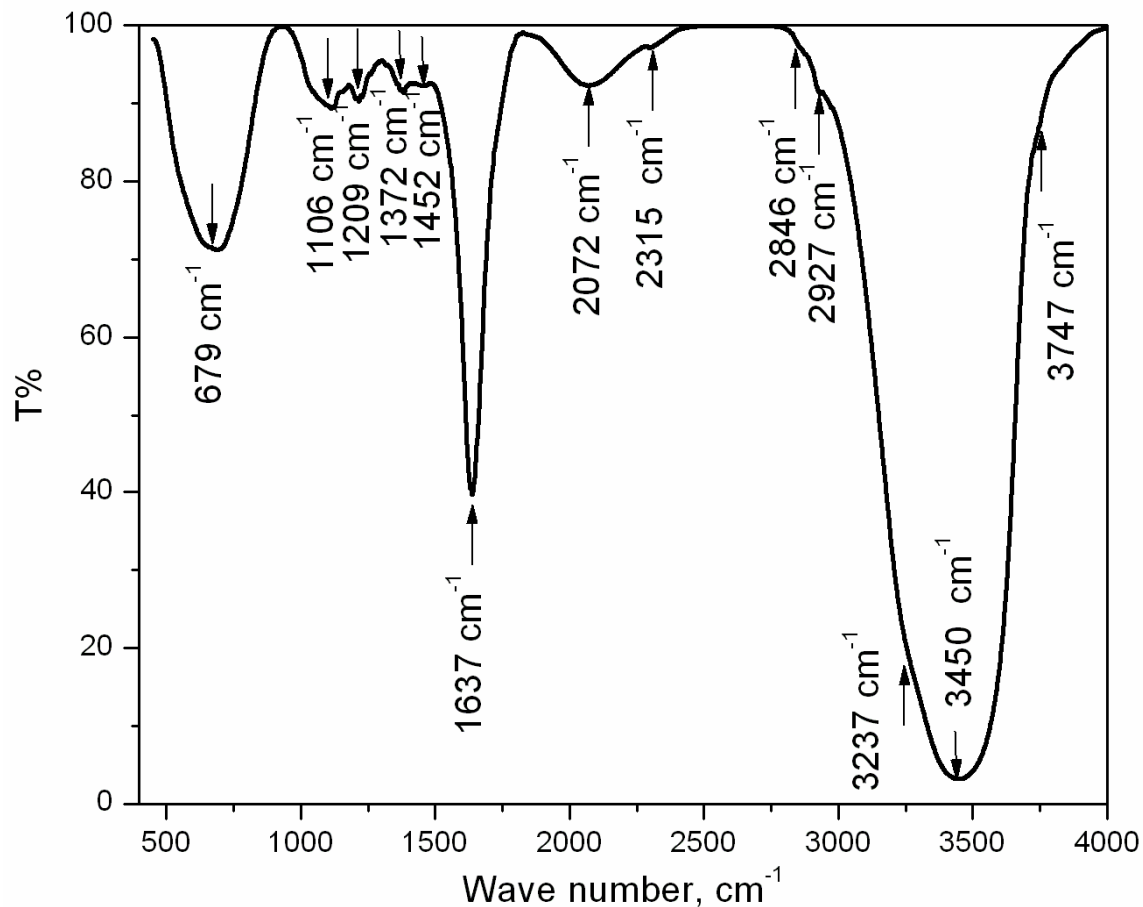
Fig. 5.4 FT – IR spectrum of activated carbon produced from Limonea acidissima Shells using KOH activation followed by treatment with conc. HNO_3

The carbon surface is oxidized by treatment with conc. HNO_3 leading to the generation of such quinone type carbon functional groups, which bear significance in the redox chemistry of carbon materials. Such carbonyl functional groups are known to be pronounced in the case of oxidized carbon materials rather than the original parent carbon material. In addition, a broad and intense band is observed in the range of 3200 – 3600 cm^{-1}, centered at 3450 cm^{-1} attributable to the O-H stretching vibration of surface hydroxylic groups as well as to the adsorbed water. The asymmetry of this band (a

shoulder at a lower wave number, 3237 cm^{-1}) indicates the presence of strong hydrogen bonding interactions.

5.3.1.4 Structural (crystal, order, disorder, defect) details of Carbon Materials - Confocal Raman Spectroscopic Studies

Details of structural disorder as well as the crystallographic parameter of the activated carbon material produced by KOH activation of the shells of Limonia acidissima were obtained from the confocal Raman spectrum shown in Fig. 5.5. Two characteristic Raman peaks centered around 1348 and 1591 cm^{-1} were observed in the confocal Raman spectrum. These two bands were designated as D (disordered) and G (graphitic) bands and were attributed to the A_{1g} and E_{2g} Raman active C-C vibration modes with in the graphitic layer. The Raman peaks at 1348 and 1591 cm^{-1} are called the first order Raman peaks. The other details deduced from the Raman spectrum are: R (I_D/I_G) = 1.408; L_a = 4.4/R = 3.125 nm. This value is comparable to the value of L_a deduced from XRD pattern (3.656 nm). The Raman intensity ratio (the ratio of the integrated intensities of the D and G bands) (I_D/I_G) is a measure of the extent of disorder with in a carbon layer. The R value for the activated carbon material from Limonia acidissima was found to be 1.408 which is typical of disordered carbon materials like glassy carbon. The slight variation ($\approx$ 5 Å) in the L_a value obtained between confocal Raman spectrum and X-ray diffraction pattern is attributed to the $\pm$ 7 % error involved in the calculation of the integrated intensity values under the D band and G band. Since line width from XRD is more accurately determined compared to the integrated intensity values under the D and

G bands in the confocal Raman spectrum, the L_a value obtained from wide angle X-ray studies is more reliable.
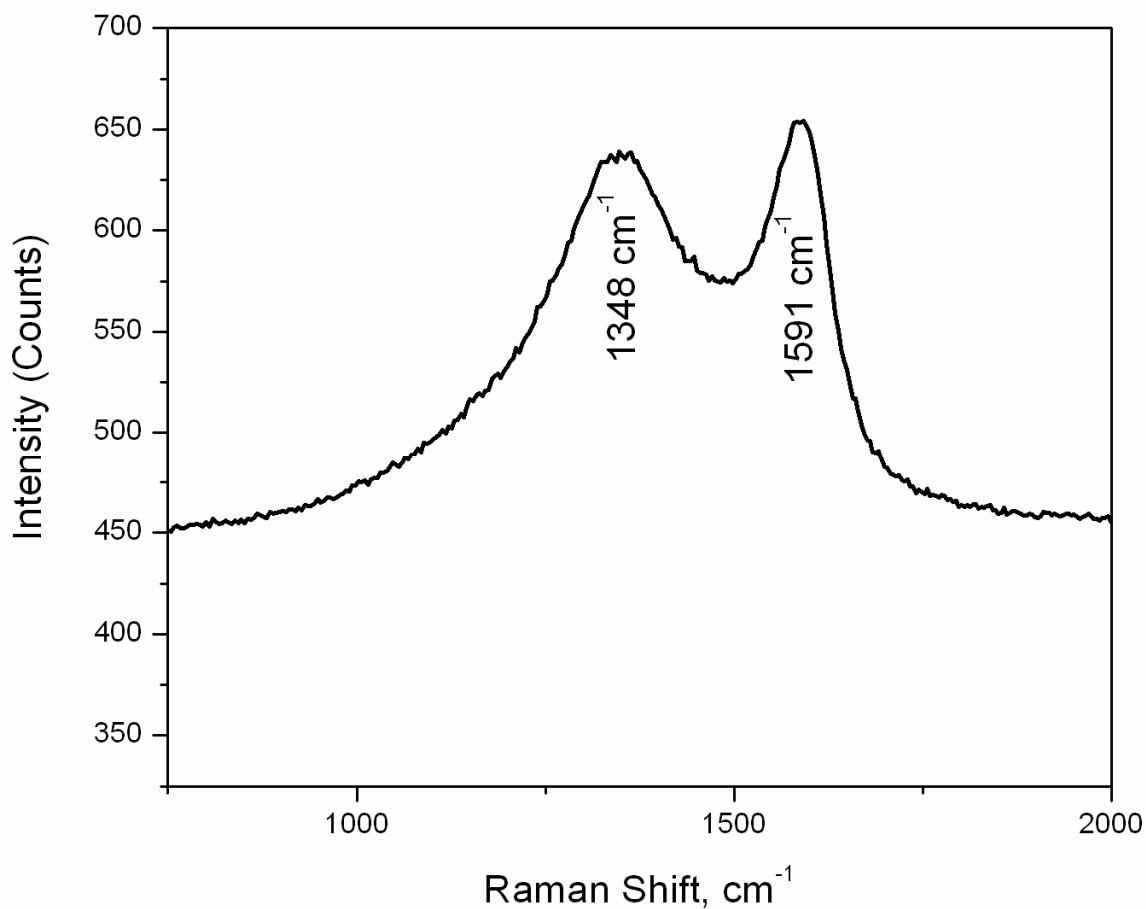
Fig. 5.5 Confocal Raman spectrum of activated carbon produced from Limonea acidissima by KOH activation followed by treatment with conc. HNO_3

5.3.1.5 Dangling Bond Concentration on the Surface of Carbon - Electron Paramagnetic Resonance Spectroscopic Studies

The Electron Paramagnetic Resonance (EPR) spectrum of activated carbon from Limonea acidissima, C_{WA} KOH HNO_3, is shown in Fig. 5.6. The g value of the resonance signal for the activated carbon is 2.03095 which is close to the free electron g value.
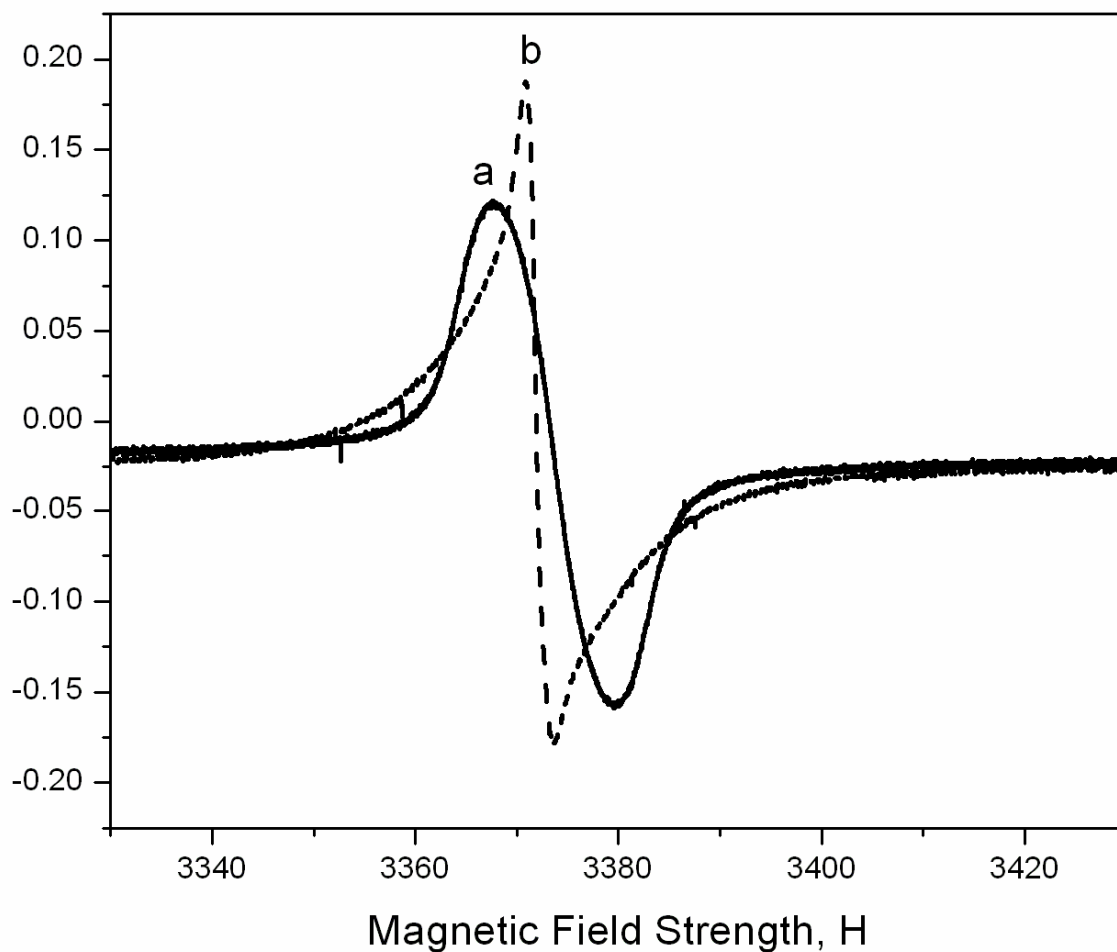
Fig. 5.6 EPR spectrum of activated carbon from (a) Limonea acidissima by KOH
     activation followed by treatment with conc. HNO_3 and (b) DPPH (reference)

The origin of the EPR signal is attributed to the presence of dangling bonds in the carbon

structure. The concentration of unpaired spins was found to be 1.3×10^{18} spins/g of the

carbon material. The spin concentration value of activated carbon from the stems of

Limonea acidissima (C_{WA}) is an order of magnitude lower than that of the spin

concentration values reported for commercial acetylene based carbon (3.8×10^{19}) and

graphon (1.1×10^{19}) (Timothy and Glasser, 1989). The lower spin concentration in our

sample is because of the saturation of the dangling bonds with potassium, formed during the carbothermal reduction of K_2CO_3, resulting in the formation of surface C-K bonds which subsequently transform (partially) to C-H bonds upon final treatment with conc. HNO_3. The formation of C-K type bonds is also confirmed by the presence of 0.45 wt.% K (from EDAX analysis) in the activated carbon material even after treatment with conc. HNO_3 (Fig. 5.7). The transformation is also confirmed from the appearance of C-H bonds in the FT – IR spectrum shown in Fig. 5.4.

5.3.1.6 Morphology and Elemental Composition - Scanning Electron Microscopy and Energy Dispersive X-ray Analysis

Details of the surface morphology as well as the elemental composition of the activated carbon material were obtained using High resolution Scanning Electron Microscopy (HR SEM, FEL, Model: Quanta 200) equipped with Energy dispersive X-ray analysis facility. Scanning electron microscope images are obtained at a magnification of 4000 x and 10, 000 x and at a scanning voltage of 30 kV. A highly heterogeneous and rough surface with a continuous porous net work is viewed on the surface of the activated carbon produced from Limonea Acidissima. The porous network is clearly viewed at the higher magnification (10, 000 x) (Fig. 5.7 (a & b)).

The chemical composition of the activated carbon material was determined using energy dispersive X-ray analysis. A high carbon content of 74.84 wt.% was found. In spite of treatment with HNO_3, 0.45 wt.% K was inevitably present in the activated carbon. The oxygen content was found to be 24.7 wt.% (19.83 atomic %).

(a)

(b)

(c)

(d)
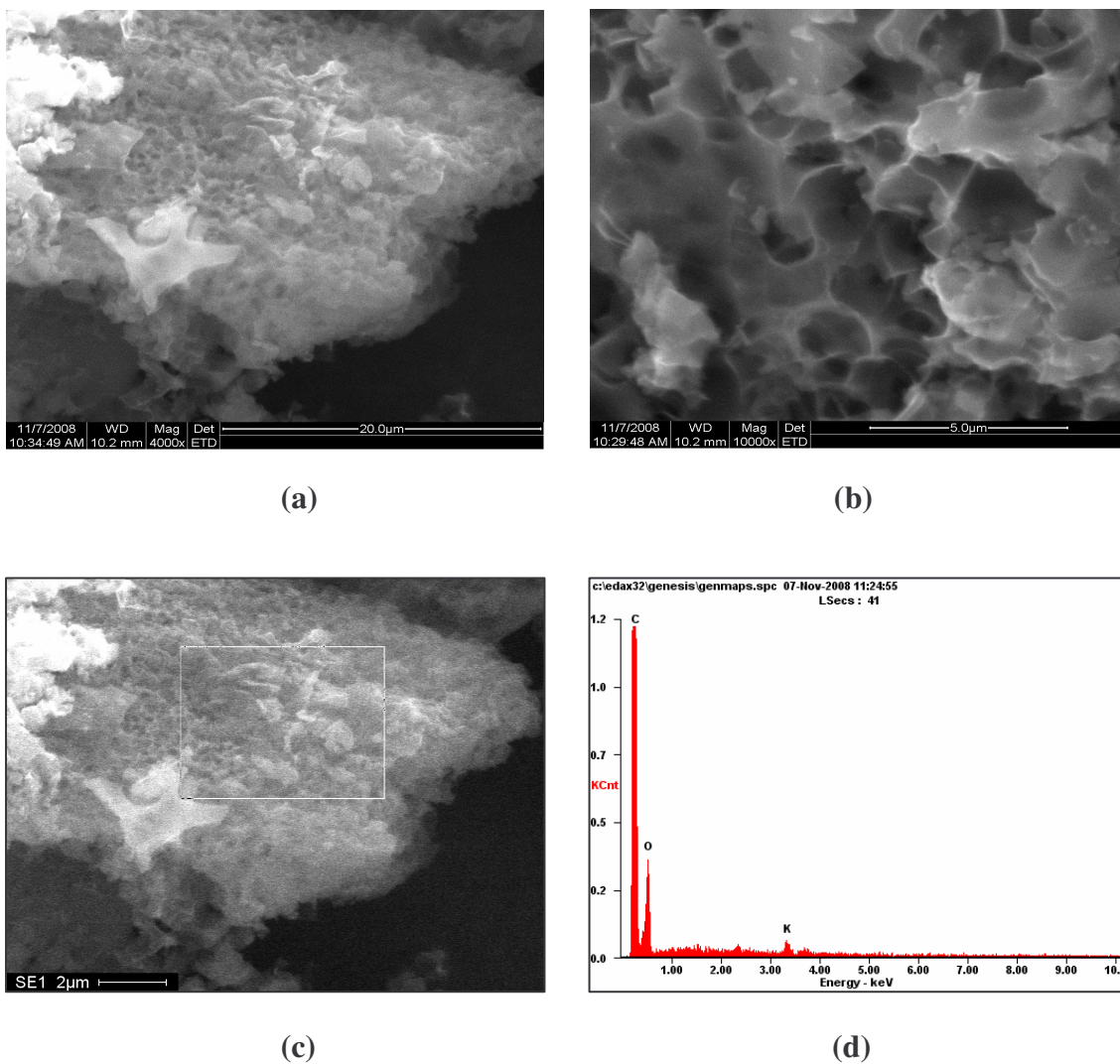
Fig. 5.7 SEM images and EDAX spectrum from the activated carbon material from Limonea acidissima using KOH activation; at a magnification of (a) 4000 x, (b) 10, 000 x, (c) selected region for elemental analysis and (d) energy dispersive X-ray analysis spectrum

5.3.2 Mechanism of KOH Activation

The sequential reactions involved in the activation of carbon precursor with KOH were discussed in Section 1.1.5.2.

5.3.2.1 Role of HNO₃ Activation

There are two advantages in treating the char with HNO_3: The advantages are the effective removal of traces of mineral matter in the char, traces of activating agent and its decomposed products and also the generation of oxygen rich surface functional groups (Cuerda – Correa *et al*., 2006)

5.3.3 Evaluation of Electro catalytic Activity of Pt/C Catalysts

5.3.3.1 XRD analysis of Pt/C catalysts

The X-ray diffractograms of 5, 10, and 20 wt.% Pt on carbon material obtained from the shells of Limonea acidissima (wood apple) are shown in Fig. 5.8. For comparison the XRD pattern of 20 wt.% Pt/Vulcan XC 72 R is also shown in Fig. 5.8. Diffraction peaks characteristic of Pt metal with a face centered cubic lattice are observed and the peaks are all indexed as (111), (200), (220), (311) and (222) (JCPDS file No. 87-0647). The crystallite size of Pt calculated using Debye-Scherrer equation (West, 1984) and the lattice parameter values of Pt metal in the case of each of the catalysts (Pt/C_{WA} and Pt/Vulcan XC 72 R) was calculated. The broad diffraction peak centered around a 2θ value of 24° corresponds to the (002) reflection of the carbon support with a turbostratic graphitic structure. The lattice constant value of ~ 0.39 nm correlates well with the FCC lattice of Pt metal supported on carbon materials [JCPDS file No. 87-0647]. The lattice constant value of Pt metal is (0.3923 nm) (Liu *et al*., 2004). Reflection from the (220) plane of Pt metal was used for the calculation of the crystallite size as it is away from the region of the broad diffraction peak (from (002) plane) of the carbon support.
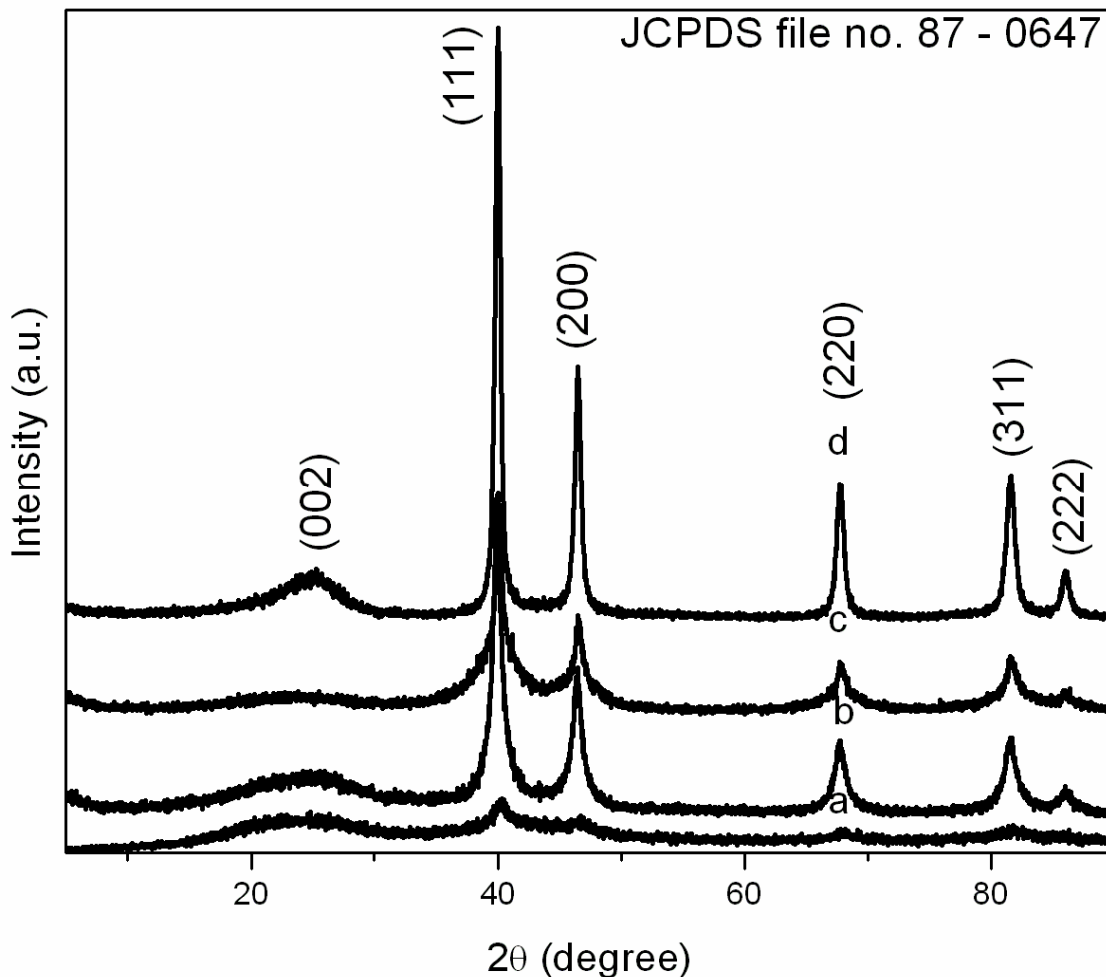
Fig. 5.8 X-ray diffraction patterns of (a) 5 wt. % Pt/CWA (crystallite size ~5.0 nm) (b) 10 wt. % Pt/CWA (crystallite size ~10.2 nm) (c) 20 wt. % Pt/C_{WA}) (crystallite size ~10.4 nm) and (d) 20 wt. % Pt/Vulcan XC 72 R (crystallite size ~13.1 nm)

The crystallite size of Pt is found to be dependent on the Pt loading and also on the nature of the carbon support. With the same amount of Pt loading (20 wt.%), the crystallite size of Pt on carbon produced from Limonea acidissima shell is smaller (10.4 nm) than on Vulcan XC 72 R (13.1 nm) indicating better dispersion of Pt on the C_{WA} support due to the enhanced surface oxygen functional groups as well as the higher value of specific surface area. Also, the Pt crystallite size was found to be the least (5 nm) in the case of 5 wt.% Pt/C_{WA}.

5.3.3.2 Textural properties of the Pt/C catalysts - BET sorptometric studies

In addition to the structural properties, crystallite size of the Pt dispersed on carbon, the textural properties of the electro catalyst (Pt/C$_{WA}$) too have an effect on the electro catalytic activity of the supported catalysts. The textural properties (specific surface area, total pore volume, mean pore diameter) of the Pt/C$_{WA}$ catalysts are investigated by sorptometry. All the catalysts exhibited typical type I isotherms characteristic of microporous solids. This indicates that the pore texture of the support is retained and no collapse of pore texture has taken place upon impregnating Pt on to the support up to a loading of 20 wt.%. Another important observation is that the volume of N_2 (adsorbate) adsorbed, decreased drastically as the wt. % loading of Pt increased from 10 wt. % to 20 wt.%. 10 wt. % Pt/C$_{WA}$ showed similar sorption capacity of the adsorbate as that of 5 wt.% Pt/C$_{WA}$ even though it is expected to show lower sorption for N_2 compared to 5 wt.% Pt/C$_{WA}$. The observed discrepancy is because of the fact that, in the case of 5 wt. % Pt/C$_{WA}$ catalyst, the small crystallites of Pt (5.0 nm) were very finely dispersed over the whole of the carbon support surface. Even though the dispersion of the nano crystallites of Pt is advantageous, these small crystallites partially block the accessibility of the micropores to the adsorbate (N_2) and this phenomenon is more severe in the case of 5 wt.% Pt/C$_{WA}$. The non accessibility of the micropores to the adsorbate is also evident from the micro surface area value of 5 wt.% Pt/C$_{WA}$ (267 m^2/g) which is lower than that of the micropore surface area of 10 wt. % Pt./C$_{WA}$ (318 m^2/g).

The micropore values were deduced from t-plots. Even though no quantitative estimation of the dispersion of Pt over carbon support is made, an appropriate guess can

be made about the extent of dispersion from the relative crystallite sizes of Pt in the case

of 10 wt.% Pt/C_{WA} (10.2) and 5 wt.% Pt/C_{WA} (5.0 nm). The details of textural properties

and parameters deduced from corresponding isotherms were summarized in Table 5.1.

Table 5.1 Textural properties of carbon supported Pt catalysts

S. No.	Electro catalyst	S_{BET} (m²/g)	[i]$S_{Micropore}$ (m²/g)	[ii]V_P (cm³/g)	Mean Pore Diameter[iii] (nm)
1	5 wt. % Pt/C_{WA}	505	267	0.289	2.28
2	10 wt. % Pt/C_{WA}	526	318	0.288	2.19
3	20 wt. % Pt/C_{WA}	195	102	0.119	2.44
4	20 wt. % Pt/Vulcan XC 72 R	123	0	0.29	9.43

i. Micropore area deduced from t-plot

ii. Total pore volume

iii. Mean pore diameter, d = 4V/A (in nm)

where V is the total pore volume and A is the BET specific surface area

The textural properties of the Pt/C_{WA} catalysts were investigated by BET sorptometry. At

all loadings the Pt/C_{WA} catalysts exhibited typical type I isotherms characteristic of

microporous solids. An important observation was that the surface area and the volume

of N_2 (adsorbate) adsorbed decreased drastically as the wt. % loading of Pt increased (5

wt.% Pt/C_{WA} [S_{BET} = 505 m²/g, V_p = 0.289 cm/g], 10 wt.% Pt/C_{WA} [S_{BET} = 526 m²/g, V_p

= 0.288 cm³/g] and 20 wt.% Pt/C_{WA} [S_{BET} = 195 m²/g, V_p = 0.115 cm³/g]. For

comparison the textural properties of 20 wt.% Pt/Vulcan XC 72 R catalyst are: (S_{BET} = 123 m^2/g, Vp = 0.294 cm^3/g).

5.3.3.3 Electro oxidation of methanol - Cyclic voltammetry

The cyclic voltammograms recorded with electrodes fabricated using 5, 10 and 20 wt.% Pt supported on carbon material C_{WA} are shown in Fig. 5.9. For comparison, the cyclic voltammetric response from the electrode fabricated with 20 wt.% Pt supported on Vulcan XC 72 R is also shown in Fig. 5.9. The feature common to all the cyclic voltammograms is that one anodic peak is observed in the forward scan and another in the reverse scan. The anodic peak in the forward scan is attributed to oxidation of methanol (Manohara *et al*., 1992; Liu *et al*., 2004; Sevilla *et al.,* 2007; Niu *et al*., 2007; Lei *et al*., 2008; Zheng *et al*., 2007). The anodic peak in the reverse scan is attributed to the removal of the incompletely oxidized carbonaceous species (mostly in the form of linearly bonded Pt=C=O) formed in the forward scan (Manohara *et al*., 1992).

The critical parameter that determines the usefulness of an electrode is the onset potential. A less positive value of the onset potential is preferred. A lower onset (less positive potential) potential value implies the requirement of lower energy for the methanol oxidation reaction to take place (Sobkowski *et al*., 1992). The onset potential value is related to the breaking of the C-H bond of methanol which is the primary step involved in the mechanism of electro oxidation of methanol (Wu *et al*., 2007). The onset potential values for the electro oxidation of methanol deduced from the cyclic voltammograms obtained over different electrodes, along with peak potential and current

values corresponding to the methanol oxidation (anodic peak in the forward sweep) as well as the oxidation of the intermediate species formed during the oxidation of methanol (anodic peak in the reverse sweep) are summarized in Table 5.2. Liu *et al.*, (2004) have reported the onset potential values of 0.27 V and 0.28 V, respectively, on Pt/Vulcan XC 72 R and Pt/CNT's for the electro oxidation of methanol in 1 M H_2SO_4 and 2 M CH_3OH at a scan rate of 50 mV/sec.

The onset potential being a little lower (0.21 V) than the commercial vulcan carbon (0.25 V), 5 wt.% Pt/C_{WA} showed a higher current density which is an indication of higher electrochemical catalytic activity. Such high current values derivable from the modest wt.% loadings of Pt is an indication of the effective utilization of Pt over the C_{WA} support. The improved performance of the electro catalyst, 5 wt.% Pt/C_{WA}, is attributed to the high electro catalytic activity of the Pt nano crystallites (5.0 nm) finely dispersed over the carbon support. The ratio of the anodic peak current densities in the forward (i_f) and reverse (i_b) scans too gives a measure of the catalytic performance. A higher i_f/i_b ratio indicates superior oxidation activity of methanol during the anodic scan and less accumulation of carbonaceous species on the nano catalyst surface and thus an indication of better CO tolerance. The i_f/i_b value in the case of 5 wt.% Pt/C_{WA} catalyst is 14.4 which is an order of magnitude higher than that of either 20 wt.% Pt/C_{WA} or 20 wt.% Pt/Vulcan XC 72.
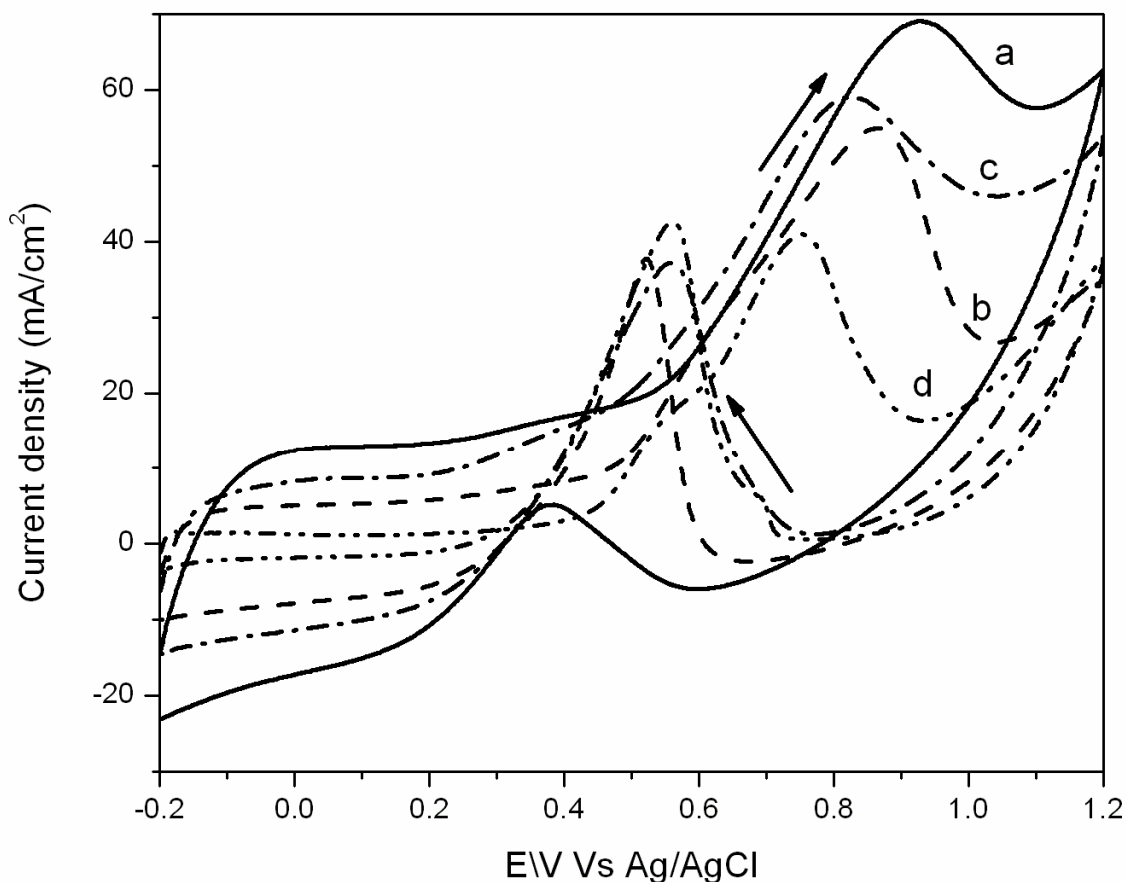
Fig. 5.9 Cyclic Voltammetric response of (a) GC/C$_{WA}$ - 5 wt.% Pt - Nafion electrode (b) GC/C$_{WA}$ - 10 wt.% Pt - Nafion electrode (c) GC/C$_{WA}$ - 20 wt.% Pt - Nafion electrode and (d) GC/Vulcan XC 72 R - 20 wt.% Pt - Nafion electrode in 0.5 M H$_2$SO$_4$ and 1 M CH$_3$OH, at a scan rate of 25 mV/sec between -0.2 to 1.2 V Vs Ag/AgCl

The i_f/i_b value of the electro catalyst produced from commercial fuel cell grade Vulcan XC 72 carbon was found to be 0.96. At all the loadings of Pt, the electrodes fabricated using C$_{WA}$ carbon materials showed an i_f/i_b value greater than 0.96 (value obtained for Vulcan XC 72 R based catalyst). For comparison, the i_f/i_b value for 20 wt.% PtRu/C catalyst of commercial Johnson Matthey sample is 1.33 (Lin *et al*., 2008). Lei *et al*., (2009) have observed the i_f/i_b values of 2.22, 1.47, 1.33, and 1.11 on 20 wt.% Pt supported on nitrogen containing ordered mesoporous carbon heat treated at 873, 973,

1123 and 1173 K. The afore mentioned catalysts were prepared by wet chemical reduction method. For comparison, Lei et al., (2009) have evaluated the performance of 20 wt. % Pt/Vulcan XC 72 under identical conditions and observed an i_f/i_b value of 0.89. The aforementioned value is close to the value shown in Table 5.2.

Table 5.2 Effect of Pt loading and the nature of the carbon support on the electro catalytic activity of methanol electro oxidation of Pt/C_{WA} and Pt/Vulcan XC 72 R

S. No.	Electrode	Onset Potential, V	i_f/i_b	Activity*			
				Forward sweep		Reverse sweep	
				I (mA/cm^2)	E (V)	I (mA/cm^2)	E (V)
1	GC/C_{WA}-5 % Pt-Nafion	0.21	14.4	69.0	0.92	4.97	0.37
2	GC/C_{WA}-10 % Pt-Nafion	0.18	1.45	55.0	0.86	37.6	0.52
3	GC/C_{WA}-20 % Pt-Nafion	0.18	1.60	58.9	0.82	37.28	0.51
4	GC/Vulcan XC 72 R-20 % Pt-Nafion	0.25	0.96	40.9	0.75	42.6	0.56

*Activity evaluated in 0.5 M H_2SO_4 and 1 M CH_3OH, at a scan rate of 25 mV/sec between -0.2 to 1.2 V Vs Ag/AgCl

5.3.3.4 Methanol Electro Oxidation – Effect of Scan Rate

The effect of scan rate on the electrochemical performance (current out put) of different electrodes, namely, 5, 10 and 20 wt. % Pt/C_{WA}/GC at the scan rates of 5, 10, 15, 20 and 25 mV/sec in 0.5 M H_2SO_4 and 1 M CH_3OH between – 0.2 to 1.2 V Vs Ag/AgCl is

evaluated. For comparison the current response to variation in scan rate for the electrode

fabricated using Vulcan XC 72 R as support with 20 wt.% Pt loading was also studied.
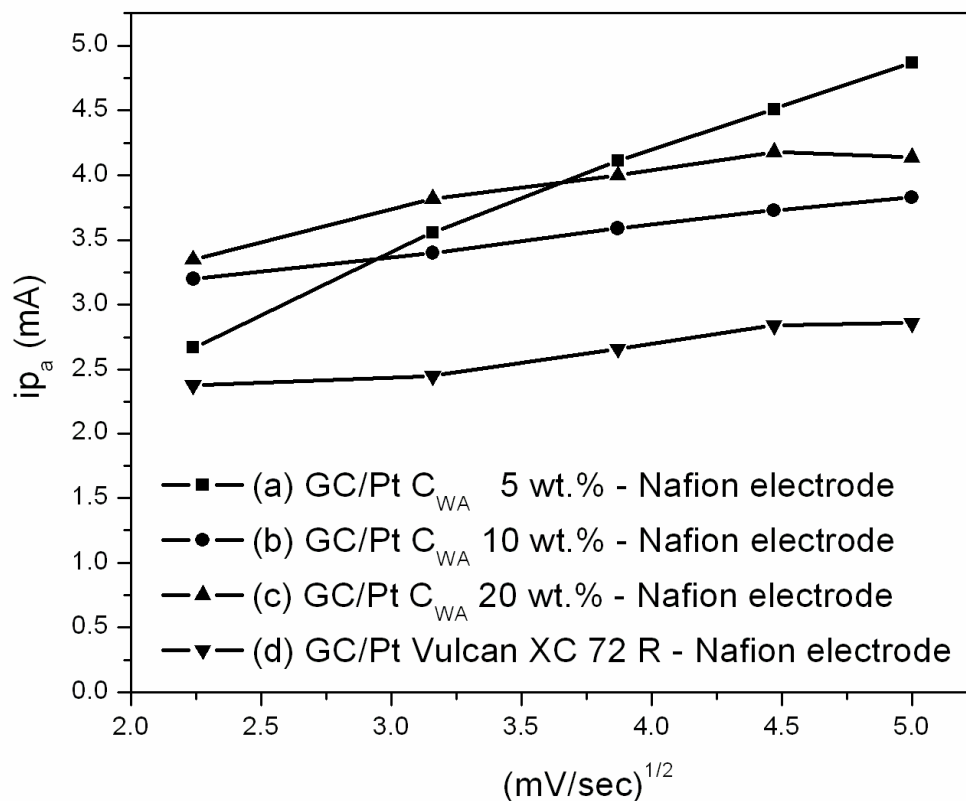
Fig. 5.10 Dependence of peak currents on the square roots of scan rates for (a) GC/Pt
C_{WA} 5 wt.%- Nafion electrode, (b)   GC/Pt C_{WA} 10 wt.%- Nafion electrode, (c)
GC/Pt C_{WA} 20 wt.%- Nafion electrode and (d) GC/Pt Vulcan XC 72 20 wt.% -
Nafion electrode in 0.5 M H_2SO_4 and 1 M CH_3OH, at different scan rates (5,
10, 15, 20 and 25 mV/sec) between -0.2 to 1.2 V Vs Ag/AgCl

It was observed that the peak current density values due to the methanol oxidation

increased as the scan rate increased from 5 to 25 mV/sec irrespective of the nature

(amount of active compound or the type of carbon support) of the catalyst. A small

increment in the peak potential with an increase in the scan rate is also observed. The

peak currents were found to be linearly proportional to the square root of scan rates as

shown in Fig. 5.10. in all the cases. Such a linear proportionality relationship between the current response and square root of scan rate indicate that the electro oxidation process of methanol is controlled by diffusion (Wang *et al.*, 2006).

5.3.3.5 Evaluation of stability of the electrode for Methanol electro oxidation – Chronoamperometry
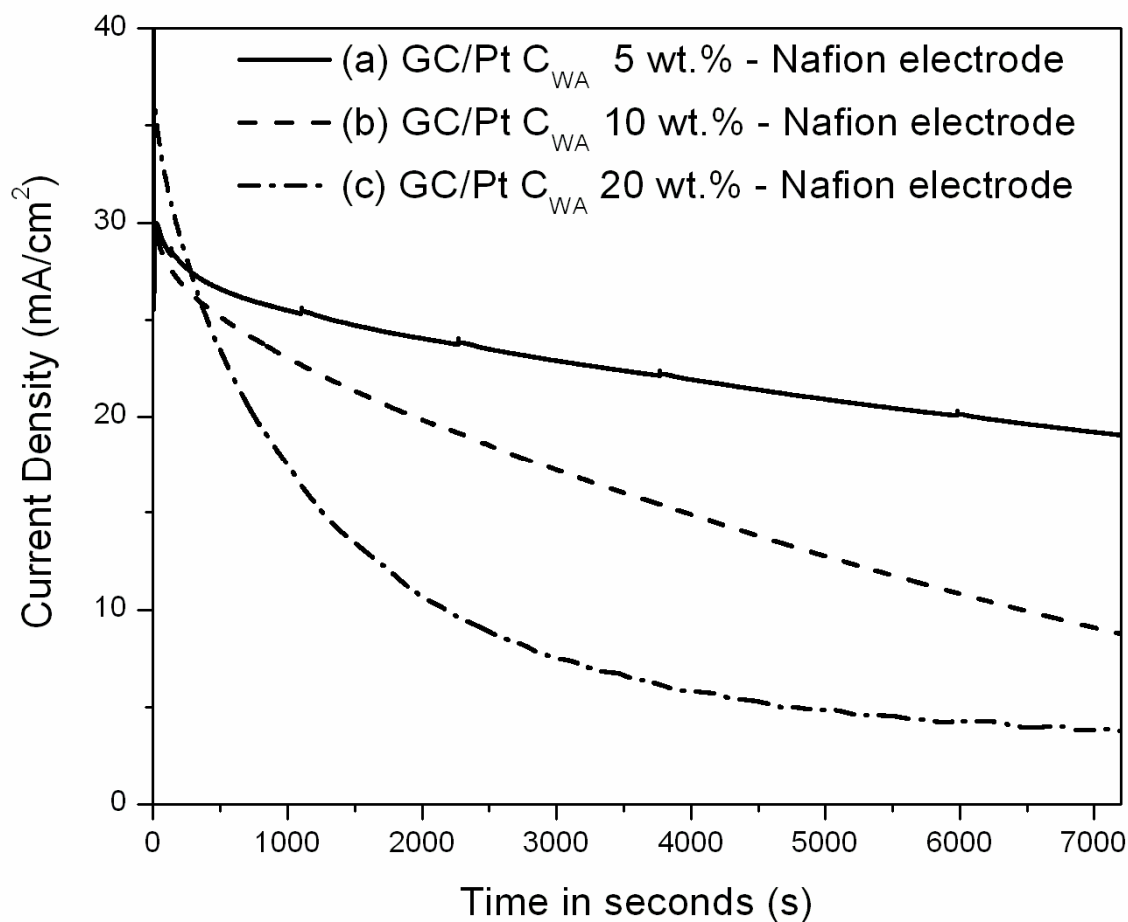
Fig. 5.11 Chronoamperometric response of (a) GC/C_{WA} - 5 wt.% Pt - Nafion electrode (b) GC/C_{WA} - 10 wt.% Pt - Nafion electrode and (c) GC/C_{WA} - 20 wt.% Pt – Nafion electrode polarized at + 0.6 V Vs Ag/AgCl in 0.5 M H_2SO_4/ 1 M CH_3OH for 3 hours

The long term stability of the fabricated electrodes was evaluated by chrono amperometric studies carried out for a duration of 3 h with the electrode being polarized at + 0.6 V Vs Ag/AgCl in 0.5 M H_2SO_4 and 1 M CH_3OH. The current density Vs time plots derived from the electrodes based on 5, 10 and 20 wt.% Pt/C_{WA} are shown in Fig. 5.11. The initial and final (after 3h) current density values derivable from the electrodes fabricated from 5, 10 and 20 wt. % Pt/C_{WA} electro catalysts are summarized in Table 5.3. The percentage decrease of the activity of the aforementioned electrodes after 3 h is also shown in Table 5.3.

Table 5.3 Evaluation of the stability of C_{WA} based electrodes for the electro oxidation of Methanol in half cell mode

S. No.	Electrode	Activity*		% Decrease in activity after 3 h at + 0.6 V
		Initial (I), $mAcm^{-2}$	Final (I), $mAcm^{-2}$	
1	GC/C_{WA}-5 % Pt-Nafion	25.2	19.1	24
2	GC/C_{WA}-10 % Pt-Nafion	29.7	19.0	36
3	GC/C_{WA}-20 % Pt-Nafion	36.1	3.7	89

*Activity evaluated in 0.5 M H_2SO_4 and 1 M CH_3OH for 3 h with the electrode being polarized at + 0.6 V Vs Ag/AgCl

Among the electrodes studied, the 20 wt. % Pt/C_{WA} catalyst based electrode showed least stability with a 89 percentage decrease of initial activity at the end of 3 h. In sharp contrast, as expected, the electrode fabricated using 5 wt.% Pt/C_{WA} possessing the

smallest Pt crystallites (5.0 nm) as well as high i_f/i_b ratio showed highest stability. Only 24 % loss in the initial activity is observed at the end of 3 h in the case of the GC/C_{WA} – 5 % Pt – Nafion electrode. Thus, it is clear that the stability of the electrode is based on the smaller crystallite size of Pt as well as the high CO tolerance (high i_f/i_b ratio value).

5.4 CONCLUSIONS

The activated carbon material produced from Limonea acidissima by KOH activation is a promising support for Pt for the electro oxidation of methanol. The excellent performance of 5 wt. % Pt/C_{WA} is attributed to the increase in the extent of utilization of Pt metal. Thus the use of carbon material from Limonea acidissima as support for Pt offers the promise of effective utilization of Pt, high electro oxidation (methanol) activity, high CO tolerance and long term stability. A strong correlation was found between the Pt crystallite size and the electro oxidation activity and stability of the carbon supported Pt catalysts.

CHAPTER – 6

CARBON MATERIALS FROM IPOMOEA CARNEA STEMS FOR MERCURY SORPTION

6.1 INTRODUCTION

6.1.1 Mercury in Environment – Health hazards

Mercury is one of the most toxic elements present in the environment causing ill effects on human health. Mercury is carcinogenic, mutagenic, teratogenic and promotes tyrosinemia (Zhang *et al*., 2005). Mercury induces cellular toxicity by binding to intracellular sulfhydryl groups. Even though the inorganic form of mercury is the most prevalent in aquatic ecosystem, it gets readily transformed to more toxic methyl mercury by the action of microorganisms (Inbaraj *et al*., 2009). Central nervous system, kidney function and chromosomes are adversely affected by mercury poisoning. Mercury can easily pass through the blood-brain barrier and exposure to the same is more harmful for the developing fetuses and children under the age of four as it interferes with the normal brain development. Chest pain, difficulty in breathing, vomiting, diarrhea, fever, skin rash, limb weakness, loss of appetite, irritability, headache and loss of memory are other adverse effects of mercury poisoning. One of the peculiar characteristics of mercury is its bioaccumulation. Mercury is absorbed strongly into the biological tissues and the elimination of the same is extremely slow (Madhava Rao *et al*., 2009). The poisonous compounds of mercury are absorbed through the gastro intestinal track, skin and lungs and are circulated in the blood and stored in the liver, kidneys, brain, spleen and bones causing health problems like paralysis, intestinal and urinary complications and even death. Ingestion of a mercury dose of less than 0.5 g is fatal (Nabais *et al*., 2006).

6.1.2 The Minamata disaster in Japan - An ecological accident

Severe mercury poisoning causes Minamata or Chisso-Minamata disease which was first discovered in 1956 in the city Minamata (Japan). Minamata disease is a neurological syndrome resulting in numbness in hands and feet, muscle weakness, damage of hearing and speech, narrowing of field of vision and leading even to coma and death. It all started in the year 1932, when Chisso-Minamata factory of Japan started the production of acetaldehyde. The same year 210 tons of acetaldehyde was produced. Mercury sulphate was used as catalyst for the production of acetaldehyde. With in a span of nearly two decades, i.e., by 1951, the production of acetaldehyde rose from 210 tons to 6000 tons. One of the side reactions of the catalytic process for the production of acetaldehyde employing mercury sulphate as catalyst resulted in the formation of small amount of methyl mercury which is the most toxic compound of Hg. The industrial waste water containing mercury compounds was dumped by Chisso corporation factory into the Minamata Bay, Japan. The highly toxic methyl mercury compound bioaccumulated in the fish of the Bay. More than 10, 000 people were affected with Minamata disease when they have consumed the fish in which the toxic compound was bioaccumulated. This tragedy caused nations to recognize the environmental pollution and the damaging effects of mercury. From then on several permissible limits were set up by World Health Organization (WHO) to discharge heavy metals into the environment. According to the WHO report between 25, 000 and 1,25,000 tons of mercury were released into the environment in 1976. Severe regulations on mercury release into the environment have been imposed. The permissible limit of mercury in waste water is nil according to the

USAs Environmental Protection Agency (EPA) where as the same is 0.01 mgL^{-1} according to the Bureau of Indian Standards (BIS). According to the Indian Standard Institution (ISI), the permissible or tolerance limit of Hg (II) for drinking water is 0.001 mgL^{-1} (Namasivayam and Kadirvelu, 1999; Kadirvelu *et al*., 2004).

6.1.3 Sources of Hg emissions and the need for controlling pollution caused by Hg

Chloralkali (chlorine manufacturing), switch gear/batteries, pulp paper, oil refining, electrical, rubber processing, fluorescent lamps and fertilizer industries and dental wastes from hospitals, agricultural chemicals, pharmaceuticals are the major contributors of mercury emission into the atmosphere. Flue gases from coal combustors (for electricity generation) do contain mercury (Hassan *et al*., 2008, Madhava Rao *et al*., 2009). Alarming quantities of mercury (600 ton/annum) were emitted into the environment from coal-fired power plants in the world (Yaji *et al*., 2008). During the production of nuclear fuel (uranium purification and separation of U^{235} and U^{238}) large quantities of Hg are released into the environment (Hassan *et al*., 2008).

Owing to the harmful nature of mercury, it is imperative and inevitable to remove the Hg (II) from waste waters before they are discharged into the environment. Among several methods for reducing the Hg (II) content in industrial waters, for instance, chemical (sulphide) precipitation, solvent extraction, ion exchange, membrane separation (electro dialysis and reverse osmosis), alum and iron coagulation, lime softening, activated carbon adsorption, electro deposition, photo reduction and some biological process, the adsorption based processes employing activated carbon materials as sorbents

has been the most widely used. Operational difficulties are associated with conventional methods like sulphide precipitation, ion exchange and coagulation. There has been only limited success with adsorbents like fly ash, low rank coal and clay minerals (Meenakshi and Amutha, 2008; Hassan *et al.*, 2008). Processes other than adsorption require either high-energy or large quantities of chemicals necessitating the development of suitable methods of reduction of pollution caused by mercury. Among several physical and chemical methods, Adsorption seems to be an effective and simple technique for the removal of mercury from wastewater (Zhang *et al.*, 2005; Anirudhan *et al.*, 2008; Skodras *et al.*, 2008). Even though activated carbon is the best sorbent, the material is expensive. There is a need for the development of low cost activated carbon based adsorbent for Hg (II) sorption. Commercially available activated carbons are expensive. So there is an urgent need for the development of methods for the production of activated carbons for controlling environmental pollution. The adsorbent should possess high sorption capacity, regenerability and also should be disposable (Kadirvelu *et al.*, 2004). There is a growing need to develop low cost activated carbon adsorbent materials from inexpensive and locally and widely available biomass. Activated carbon produced from several novel precursors like coal, onion skin, waste rubber, coconut husk, photo film waste sludge has been widely used for the removal of mercury from solution (Inbaraj and Sulochana, 2006). Other low cost adsorbents tested for Hg (II) sorption include fly ash, tree bark, human hair, fertilizer waste, used tea leaves, waste rubber, rich husk ash and oil shale (Hassan *et al.*, 2008). Search for new technologies, to reduce mercury in the effluent streams whether it be water bodies or air, is the need of the hour. 'Adsorption' based technology possess the ability to reduce contaminants (gas and liquid streams) by

several orders of magnitude. Selective Adsorption Associates Inc. (SAA) and NUCON International Inc., have recommended 'Adsorption' as the technology of choice. Activated carbon materials have large specific surface area values (≈ 1000 m^2/g). In spite of the high specific surface area value their potential to adsorb mercury is only low. Ordinary carbon adsorbents will not be suitable for achieving remarkable decrement in Hg levels. They possess only little capacity of mercury removal. Carbon materials modified with sulphur are proposed to be suitable sorbents for Hg removal. Even in nature Hg occurs as HgS (in Cinnabar). Thus the affinity of Hg for S could be suitably exploited so as to bring down the Hg levels in the waste water streams. Carbon sorbents when modified with S become potential to chemically react with mercury, through S, forming insoluble mercury sulfide. With suitable contact time between the adsorbent and the effluent water, extremely low mercury concentrations could be achieved. Use of sulphur impregnated activated carbon, MERSORB$^{\circledR}$ LW mercury adsorbent indicated the feasibility to achieve effluent mercury levels of < 100 ng/kg (parts per trillion). The best available technology economically achievable for the removal of mercury from waste water is based on chemical precipitation with sulphide compounds, followed by filtration where in mercury is removed as insoluble mercury sulphide as indicated in the equation below:

$$Hg^0 + Hg_2{}^{2+} + Hg^{2+} + 2\,S^{2-} \rightarrow 2\,Hg^0 + 2\,HgS\downarrow$$

Recently Holtra Chem adopted, adsorption as a post sulfide treatment process. Even though many new technologies are emerging to bring down mercury levels to the order of magnitude required by new discharge limits, most of them were still experimental

179

(Tonini *et al*., 2003). Madhava Rao *et al*., (2009) have observed that the adsorption capacities are 25.88, 23.66 and 22.88 mg Hg/g of the activated carbon prepared from agricultural by-products, namely, Ceiba pentandra hulls, Phaseolus aureus hulls and Cicer arietinum respectively. The initial Hg (II) concentration was 40 mL/L. Nabais *et al*., (2006), have reported an unusually high Hg sorption value in the range of 290 – 710 mg Hg/g of activated carbon prepared from acrylic textile and a commercial carbon material prepared from the polymerization of phenol and formaldehyde. The high Hg uptake by the sorbents was attributed to the modification of the sorbents with elemental sulphur or by treatment with H_2S at 600 and 800 °C. S in the range of 0.68 – 6.27 wt.% is introduced into the carbon materials. The authors have proposed that it is not the total amount of S but only the type of sulfur functional groups on the carbon surface that are most important for Hg uptake (Nabais *et al*., 2006).

The objective of the investigation is to develop low cost and effective activated carbon based sorbent from the stems of *Ipomoea carnea* (Fig. 7.1.) for the removal of Hg from water bodies for the benefit of industries (oil refining and chloralkali) releasing Hg into the environment.

Ipomoea carnea is an exotic weed with prolific growth potential distributed in tropical countries of Asia and America. In India, the plant grows profusively and gregariously in wastelands even in most unfavourable habitats (Bhalerao and Chaphekar, 2009). The common names of the plant is besharam and thutu kada. The plant is toxic to cattle. Goats fed with the plant showed signs of anorexia, dullness and loss of body

weight. Cerebrum, cerebellum and spinal cord are chiefly affected by the consumption of Ipomoea carnea (Srilatha *et al*., 1997). Karthikeyen *et al*., (2007) have employed the activated carbon material produced from the stems of Ipomoea carnea for the sorption of basic red dye (sorption capacity, 49.84 mg/g). The leaves of the plat (both dry and fresh) were used for the production of biogas (Singh and Jain, 2002; Marsonia and Goswami, 1994). The stems of the plant hold a promise for the production of pulp and paper (Shukala *et al*., 1991; Agarwal *et al*., 1992; Behera and Tiwari, 1980).

Fig. 6.1 Image of stem, leaves and flowers of Ipomoea carnea

6.2 EXPERIMENTAL

6.2.1 Synthesis of Carbon Materials

6.2.1.1 Carbon material as synthesized from Ipomoea carnea stems (C_{IC} N_2 400)

Dried stems of Ipomoea carnea (22.434 g) are pyrolysed in N_2 atmosphere at 400 °C for 8 h. Devolatilization and subsequent carbonization took place. The yield of the carbon material as synthesized is 8.88 g (39.6 %). The obtained carbon material is designated at $C_{IC} N_2$ 400.

6.2.1.2 Base treatment of carbon material as synthesized (C_{IC} N_2 400)

Carbon material as synthesized (C_{IC} 400 N_2, 4.3 g) is treated with 43 mL of 10 wt.% NaOH solution for 1 h. The contents are then filtered through a 200 mL G4 sintered funnel. The yield of the base treated carbon material is 3.636 g (84.5 %). The loss in wt. after NaOH treatment is 0.664 g (15.4 %) which corresponds to the impurities (SiO_2) soluble in NaOH. The carbon material obtained after base treatment is designated as C_{IC} N_2 400 B.

6.2.1.3 Acid treatment of base treated Carbon material ($C_{IC} N_2$ 400 B)

Base treated carbon material (C_{IC} N_2 400 B, 3.636 g) is treated with 36 mL of conc. HCl for 1 h. The contents are then filtered and washed with excess distilled water. The yield of the carbon material after acid treatment is 3.246 g (89.4 %). The weight loss of 0.39 g (10.7 %) corresponds to metal impurities soluble in Conc. HCl. The carbon material from Ipomoea carnea thus obtained after base and acid treatment is designated as C_{IC} N_2 400 B A.

6.2.2 Sulphur functionalization on carbon material (C_{IC} 400 N_2 B A)

The carbon material is functionalized with S by a simple method where in N_2 gas is bubbled through a solution of elemental sulphur dissolved in hydrazine monohydrate. The process of S functionalization is carried out in a tubular furnace at 400 °C in quartz tube. 6.0 g of carbon material (base and acid treated) to be functionalized with S is taken in an alumina boat. The alumina boat with the carbon sample is placed in a tubular furnace. N_2 gas is bubbled through a solution of S (24.05 g) dissolved in hydrazine monohydrate (60.05 g) (the method of preparation of S solution in hydrazine is given below). The process of S functionalization is carried out for 4 h. The initial volume of the solution of S in hydrazine is 42 mL and the final volume after 4 h treatment of the carbon material is 32 mL implying that 10 mL of S in hydrazine monohydrate solution is consumed during the process of impregnation. The yield of the S impregnated carbon material is 4.567 g (76 %). The material thus obtained is designated as C_{IC} 400 N_2 B A S.

6.2.2.1 Preparation of S solution in Hydrazine monohydrate (Vecht *et al*., 1998)

Hydrazine hydrate (60.05 g, 58.47 mL, d = 1.027 g/mL, Mol. Wt. = 50.06 g) is taken in a beaker. placed in a trough with ice cubes. Magnetic pellet is placed in the beaker. The contents in the beaker are subjected to stirring. Sulphur (24.05 g, Mol. wt. of S = 30.06 g) is added slowly to the hydrazine hydrate ($NH_2NH_3^+OH^-$). Since the reaction between hydrazine and sulphur is exothermic, the reaction is carried out under ice cold conditions. The solution of S/hydrazine thus obtained is placed in a bubbler connected to a tubular furnace. N_2 gas is passed though the bubbler into the furnace where the carbon material to be impregnated with S is placed.

6.2.2.2 Nature of the S species present in hydrazine/S solution

Saraswathi *et al.*, (1997) have confirmed the formation of sulphide ions by the dissolution of S in hydrazine hydrate. Cyclic voltammetric studies were carried out on sulphur dissolved in 4-8 % hydrazine hydrate in an acetate-supporting electrolyte at a pH of 9.0 in the scan range of -0.3 V to – 1.0 V versus SCE. A single anodic wave at - 0.7 V is seen. The anodic as well as the cathodic peak potentials are constant with the change in concentration of sulphur and the scan rates indicating the reversible nature of the electrode reaction. The peak potential difference (Ep,a/Ep,c) is around 30-35 mV, indicating a two-electron oxidation process. Also the plot of current Vs $V^{1/2}$ deviated from linearity at very low scan rates indicating that the electrode reaction is not diffusion controlled. The anodic waves observed in the 4-8 % hydrazine hydrate were attributed to the oxidation of mercury by the sulphide formed as a result of the dissolution of sulphur in hydrazine hydrate.

$$Hg + H_2S \rightleftharpoons HgS + 2 H^+ + 2 e^-$$

The mercuric sulphide is reduced to hydrogen sulphide as shown below resulting in the cathodic peak in the cyclic voltammogram.

$$HgS + 2 e^- + 2 H^+ \longrightarrow Hg + H_2S$$

It all started with the surprising finding of the unexpected and spontaneous formation of an yellow precipitate when the metal salt, $ZnCl_2$, was added to the hydrazine/sulphur solution. The intention was to alter the rate of proton exchange by interaction with the nitrogen lone pair electrons while investigating the nature of the species present in the hydrazine/sulphur solution (Vecht *et al.*, 1998). On heating the yellow precipitate at 900 C in an inert atmosphere, crystalline white powder was formed which is a very good

specimen of ZnS. Afterwards, the action of such hydrazine/sulphur solutions on a range of solutions of metal salts were employed as a method for the preparation of metal sulfides and selenides. A cluster of reactions do take place when sulphur is dissolved in hydrazine hydrate. The following two reactions are the predominant among several other possible reactions.

$$H_2NNH_3{}^+OH^- + 2\,S \longrightarrow 2\,H_2S + N_2 + H_2O$$

$$2\,H_2NNH_3{}^+OH^- + S \longrightarrow 2\,NH_3 + H_2S + 2\,H_2O$$

Polarographic studies of hydrazine/chalcogen solutions have concluded that polysulfide ions ($S_n{}^{2-}$) are formed in such solutions. The polysulfide ions are characterized by visible colours from red for $S_4{}^{2-}$ to blue for $S_6{}^{2-}$. Thus the red colour of low sulphur concentration solutions in hydrazine and the darkening of the solution by the addition of more chalcogen is explained by the presence of $S_4{}^{2-}$ and $S_6{}^{2-}$ species in the hydrazine/S solutions.

6.2.3 Batch mode Hg (II) sorption studies

Removal of Hg (II) using activated carbon prepared from the stems of Ipomoea carnea was carried out by batch method. The influence of various experimental parameters such as the effect of pH, contact time, activated carbon dose and initial sorbate concentration was studied. For each experimental run, 100 mL of the metal ion solution of known concentration was taken in a 250 mL stoppered reagent bottle. The pH was adjusted to the desired values using dilute solutions of HCl and NaOH. A known amount of activated carbon (sorbent) was introduced into the reagent bottles. The solutions in the bottles were agitated at room temperature using a mechanical shaker for a prescribed time to

185

attain equilibrium. At the end of the predetermined time intervals, the samples were taken out and the solutions were separated from the activated carbon by filtering through a sintered funnel. Blank solutions were also treated similarly (without adsorbent) and the concentration was taken as initial concentration. The effect of pH was studied in the range of 1 – 10 by adjusting the pH with the addition of dilute aqueous solution of HCl or NaOH and buffer solutions. The effect of adsorbent dose was studied in the range of 20 – 200 mg. The effect of contact time on the process of adsorption was determined at different time intervals of 1-10 h. Adsorption isotherms and the effect of initial concentration were studied by varying the initial metal ion concentration from 10 mg/L to 70 mg/L and keeping the carbon dosage at a constant level. All the batch experiments were carried out in duplicate. The values reported are the average of the two readings.

The % removal of mercury (R) was calculated according to the following equation:

R = $[(C_0 – C_e)/C_0]$ x 100, where C_0 and C_e are the initial and residual concentrations (mg/L) of mercury (II) respectively.

Adsorption capacity of the carbon sorbent was evaluated using the following equation:

q_e (mg/g) = V/m $(C_0 - C_e)$, where V is the total volume of mercury (II) solution in L,

m is the mass of the adsorbent in g,

C_0 is the initial concentration of mercury (II) solution (mg/L) and

C_e is the residual concentration of Hg (II) in solution (mg/L).

6.2.3.1 Reagents used

Mercury (II) solution

Dissolved 1.354 g of mercury (II) chloride and 10 g NaCl in water and diluted to 1000 ml. Diluted appropriate volumes of this stock solution (1 mg mL^{-1}) with water to prepare 10, 20, 30, 40, 50, 60 and 70 mg/L solutions which were used for Hg (II) sorption studies using carbon materials as adsorbents. Presence of NaCl provide sufficient chloride ion concentration to hold the mercury (II) in the solution as anionic complex $HgCl_4^{2-}$. The reduction of Hg (II) to Hg (I) by activated carbon sorbent is avoided by bringing all the Hg (II) ions into the anionic form (tetra chloro mercurate (II)) (Huang and Blankenship, 1984).

The aqueous solution chemistry of metal ions, in general, is so complex that quantitative adsorption studies are difficult. Most of the mercury exists in the form of complex species, either positive, neutral or negative, depending on the composition as well as the pH of the solution. Fortunately, in the case of adsorption of Hg (II) species the complexity is surmounted by the fact that the composition of the solution (type and amount of the mercury species) can be fixed by controlling the concentration of Cl$^-$ ion. The type and the amount of various mercury species that exists in solution as a function of Cl$^-$ concentration (pCl) is shown in Fig. 6.2 (Carrott *et al*., 1998). At high chloride ion concentration (> 0.1 molL^{-1}) as in the present case (~ 0.2 molL^{-1}) the predominant species in solution is the tetra chloro mercurate (II) complex, $HgCl_4^{2-}$, and the fractional concentration of the same is independent of pH even in highly basic solutions (Carrott *et al*., 1998). Thus care is taken to ensure that there exists essentially only one type of mercury species in the solution ($HgCl_4^{2-}$) reducing the complexity of the adsorption studies.
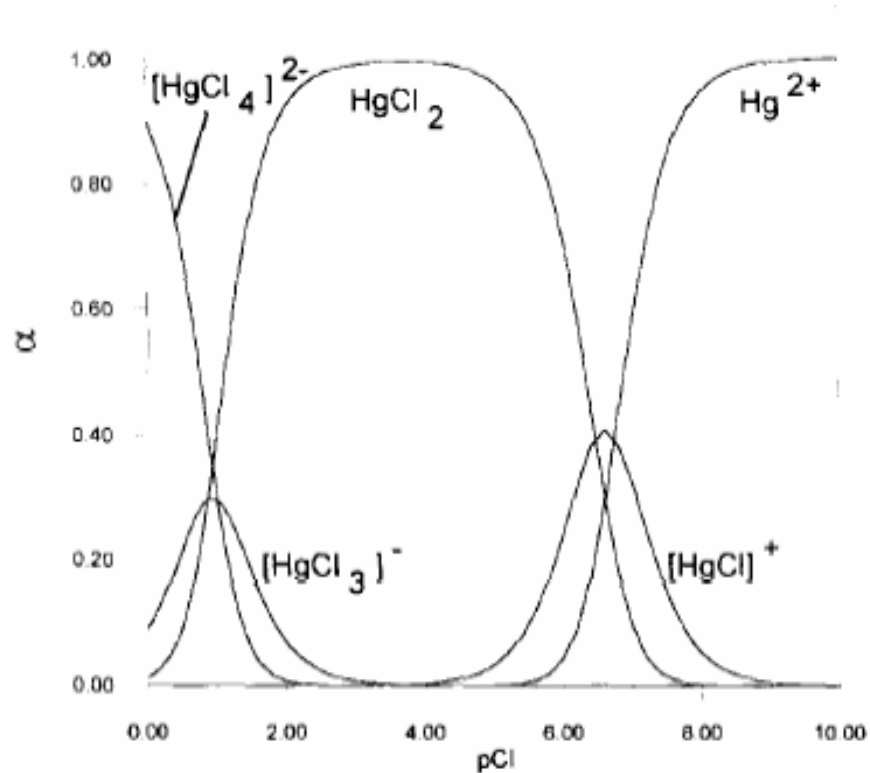
Fig. 6. 2 Effect of Cl⁻ concentration on the fractional composition of mercury (II) species (Carrott *et al*., 1998)

Buffered potassium iodide solution: Dissolved 5 g of potassium iodide and 5 g of potassium hydrogen phthalate in water. Added a few crystals of sodium thiosulphate and diluted to 250 ml with water.

Rhodamine 6G solution (0.005 wt.%): Dissolved 0.05 g of the reagent in water and diluted to 1 liter.

Gelatin solution (1 % (wt./vol.): Dissolved 1 g of gelatin powder in water for 15 minutes on a magnetic stirrer at 60 °C and diluted to 100 mL.

6.2.3.2 Method of estimation of residual Hg (II) in the filtrate (Ramakrishna *et al.*, 1976**)**

Transferred a suitable aliquot (up to 10 ml) of the sample solution containing not greater than 25 μg of mercury to a 25 ml volumetric flask. Added with mixing 5 mL of the buffered potassium iodide and 5 mL of the Rhodamine 6 G solution followed by addition of 1 mL of 1 % (wt./vol.) gelatin solution. Diluted the solution to the mark with distilled water and measured the absorbance at 575 nm against a blank reagent using spectrophotometry.

6.3 Results and Discussion

6.3.1 Characterization of carbon materials prepared from Ipomoea carnea

6.3.1.1 Structure of carbon materials - X-ray diffraction (XRD) studies

The structural features of the carbon materials (as synthesized, acid (HCl) and base (NaOH) treated and S functionalized) were studied by X-ray diffraction and the corresponding XRD patterns are shown in Fig. 6.3. Two broad diffraction peaks at 2θ values of 24.5° and 44.5° respectively indexed to (002) and (10) diffraction peaks characteristic of carbon materials are observed in the case of the three afore mentioned carbon materials. In addition, treatment with HCl followed by NaOH treatment effectively reduced the mineral contaminants (Na, K, Mg, Ca, Si) in the as synthesized carbon sample (Fig. 6.3. (a)) which will be in general intimately associated with the biomass. Also S functionalization carried out at 400 °C in inert atmosphere has not altered the original micro structure of the carbon material (Fig. 6.3 (c)).
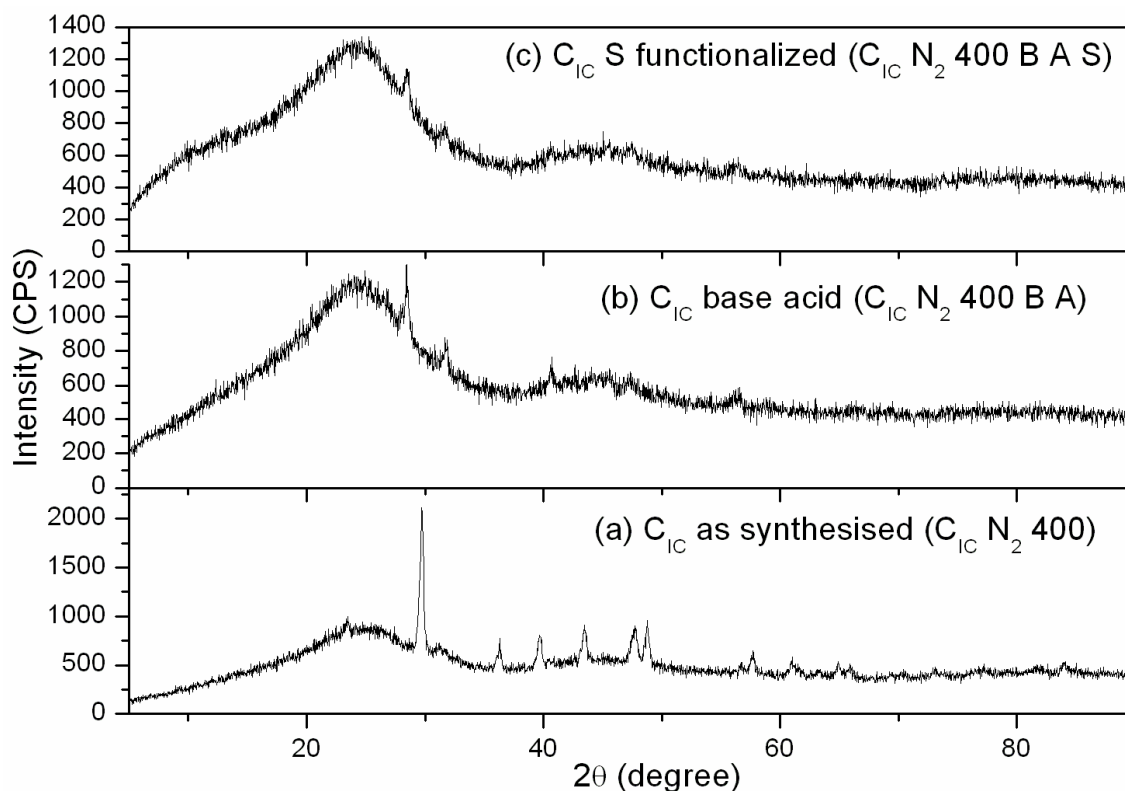
Fig. 6.3 XRD pattern of carbon materials from Ipomoea carnea, (a) as synthesized, (C_{IC} N_2 400 as syn), (b) base and acid treated, (C_{IC} N_2 400 B A) and (c) base and acid treated and sulphur functionalized, (C_{IC} N_2 400 B A S)

6.3.1.2 Surface functional groups on carbon materials - FT-IR spectroscopic studies

The nature of surface functional groups present on the carbon materials (as synthesized, acid (HCl) and base (NaOH) treated and S functionalized) was studied by FT – IR spectroscopy and the corresponding spectra were shown in Fig. 6.4. A band at 1165 cm^{-1} is observed in the S functionalized carbon materials alone (C_{IC} N_2 400 BAS) and is characteristic of the presence of C=S functional group (Valix *et al*., 2008; Inbaraj and Sulochana, 2006) and this indicates the effectiveness of the sulphurization process adopted for generating S containing functional groups on carbon surface which are known to enhance the sorption of Hg (II) ions from aqueous solutions. In addition, a

shoulder at 1693 cm^{-1} is observed in the case of the S functionalized carbon sample characteristic of C=O absorption in carboxylic acids.
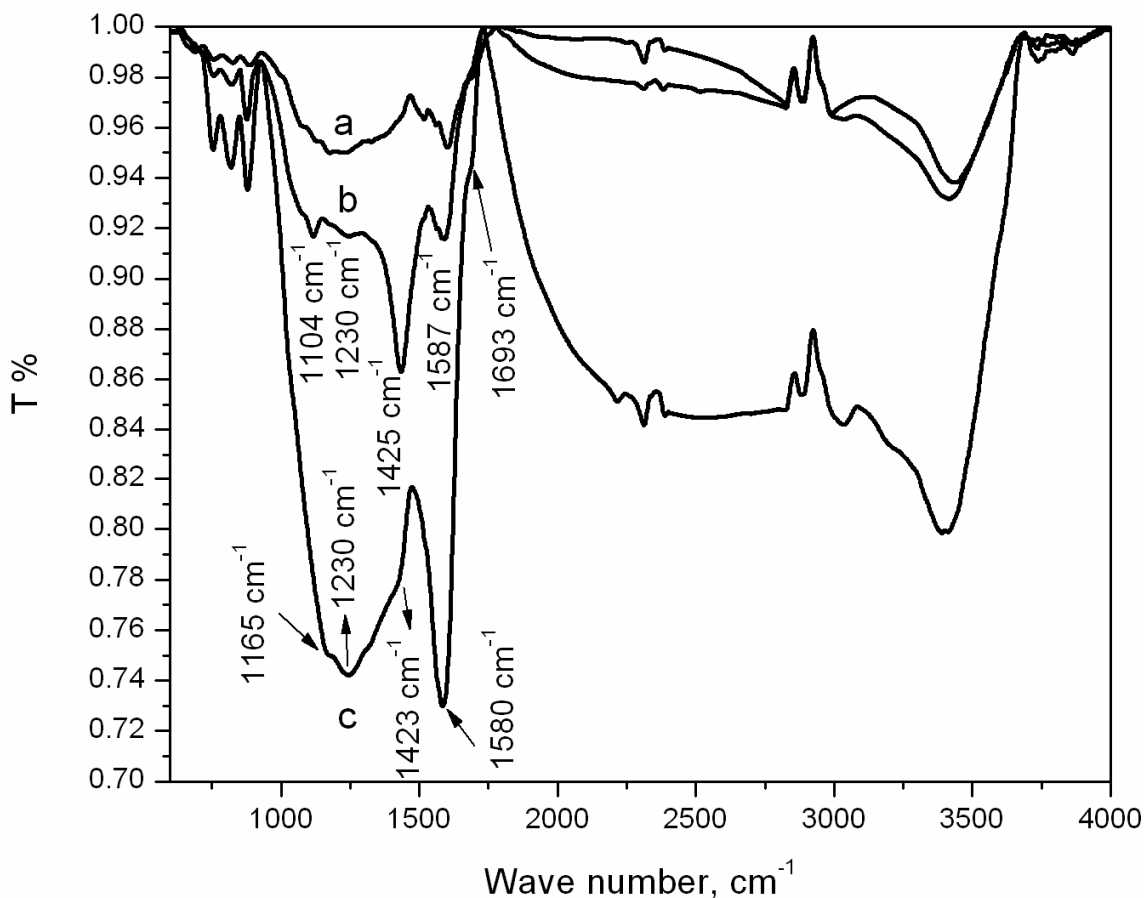
Fig. 6.4 FT-IR spectra of carbon materials from Ipomoea carnea (a) as synthesized (C $_{IC}$ N$_2$ 400 as syn) (b) base and acid treated (C $_{IC}$ N$_2$ 400 B A) and (c) base and acid treated and S functionalized, (C$_{IC}$ N$_2$ 400 B A S)

The relatively low frequency of the band indicates conjugation of C=O to the aromatic ring system (Puziy *et al.,* 2005). The small intensity of this peak suggests that a relatively low content of carboxylic groups are present as compared to other functional groups on the surface. Bands near 1230, 1420 and 1580 cm^{-1} are common to both the acid-base treated (Fig. 6.4 (b)) and S functionalized carbon materials (Fig. 6.4 (c)) which

are attributable to C-O stretching in acids, alcohols, phenols, ethers and esters (Puziy *et al.*, 2003), symmetrical C=O stretching vibration and the asymmetrical C=O stretching vibration of the carboxyl group (Anirudhan *et al.*, 2008).

6.3.1.3 Chemical environment and the concentration of unpaired spins in carbon material - EPR spectroscopic study
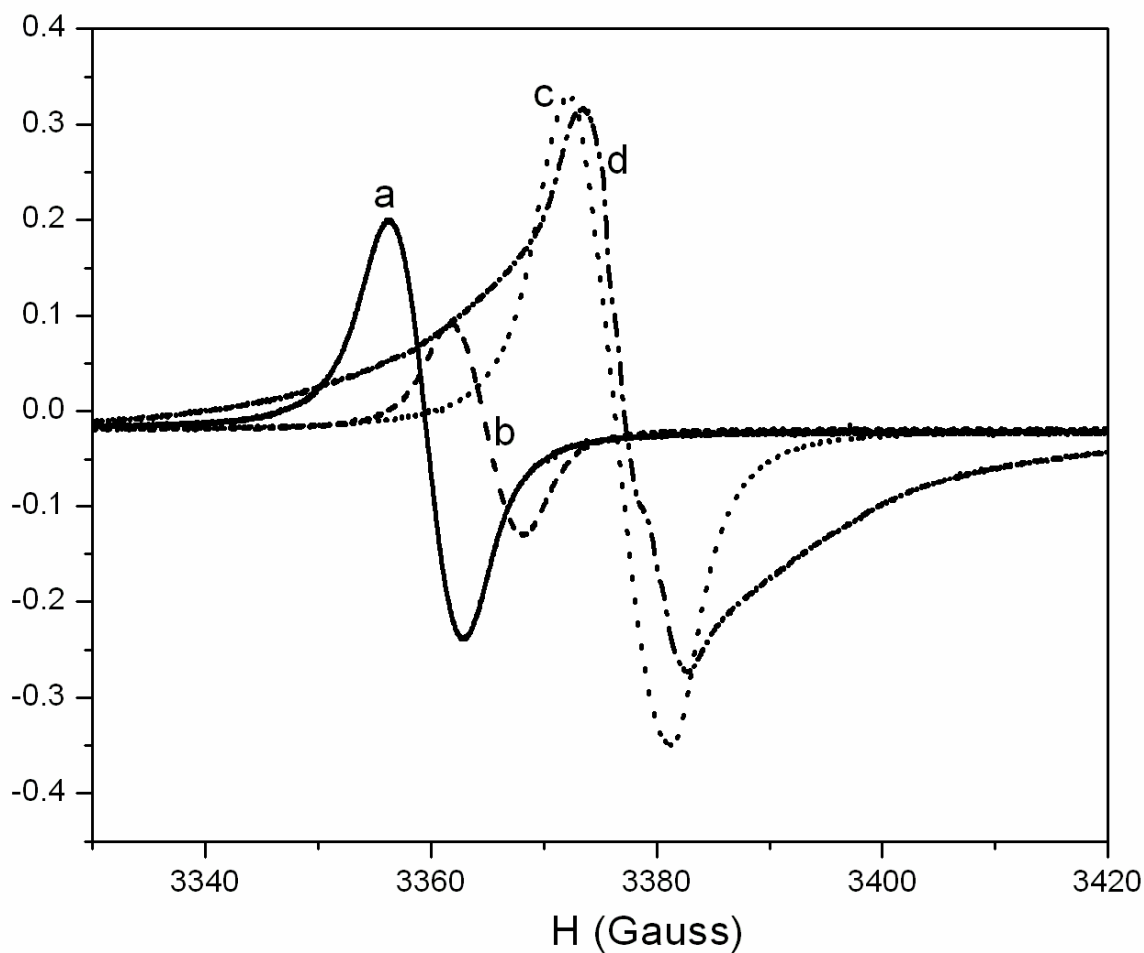
Fig. 6.5 EPR spectra of carbon materials from Ipomoea carnea, (a) as synthesized (C $_{IC}$ N$_2$ 400), (b) base and acid treated (C$_{IC}$ N $_2$ 400 B A), (c) sulphur functionalized (C $_{IC}$ N$_2$ 400 B A S) and (d) DPPH (standard)

The presence of paramagnetic spins originating from the dangling bonds is evident from the signal emanating from the carbon materials (as synthesized, acid (HCl) and base (NaOH) treated and S functionalized) as shown in Fig. 6.5. The g values and the spin concentration values deduced from the EPR signals are summarized in Table 6.1. The g values were found to be close to that of a free electron g value (2.00232). Also the spin concentration value was found to decrease upon treatment with acid and base which is a result of the saturation of dangling bonds.

Table 6.1 g factor and electron spin concentration values of carbon materials prepared from Ipomoea carnea

S. No.	Carbon Material	g value	Spin Concentration (spins/g)
1	Carbon material as synthesized (C_{IC} 400 N_2 as syn)	1.99832	5.75×10^{19}
2	Carbon material treated with base followed by acid (C_{IC} 400 N_2 B A)	1.99916	2.39×10^{19}
3	Sulphur functionalized carbon material (C_{IC} 400 N_2 B A S)	2.00082	9.83×10^{19}

A four fold enhancement in the spin concentration value is observed upon functionalization of the acid and base treated carbon sample with S as evident from the increase in the intensity of the EPR signal relative to either as synthesized sample or the base and acid treated carbon material. The spin concentration values of the carbon materials from Ipomoea carnea were found to be of the same order of magnitude as those

193

derived from acetylene, 3.8 x 10^{19} (Donnet *et al*., 1993) and coconut shell, 1.2 x 10^{19} spins/g (Manivannan *et al*., 1999).

6.3.1.4 Study of morphology of carbon materials - SEM analysis
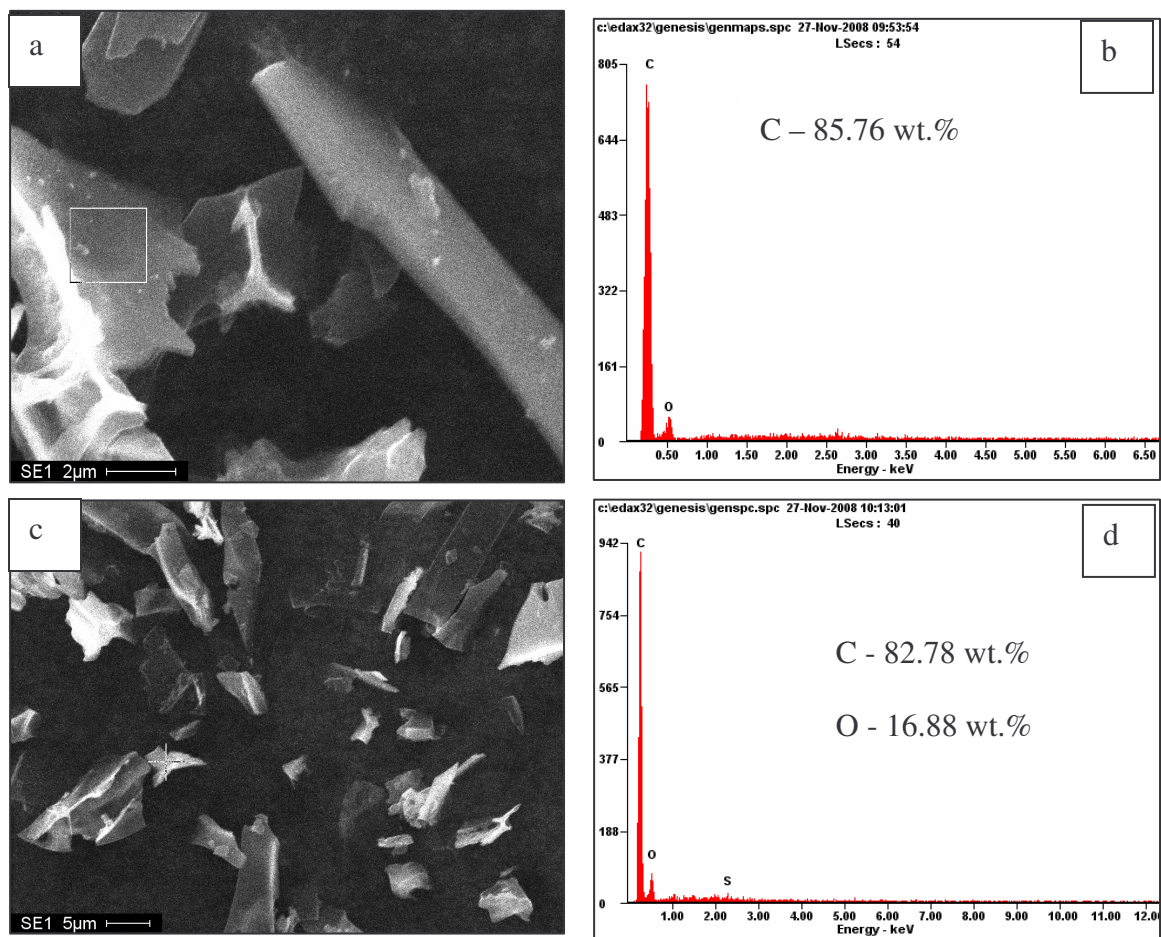
Fig. 6.6 SEM images with EDX spectra of (a & b)) base and acid treated carbon, C_{IC} N$_2$ 400 B A, and (c & d) sulphur functionalized carbon C_{IC} N$_2$ 400 B A S

The surface morphology as well as the chemical composition of the carbon materials from Ipomoea carnea is evaluated by scanning electron microscopy and energy dispersive X-ray analysis. Slate like particle morphology is observed in the case of acid and base

treated (Fig. 6.6 (a)) as well as sulphur functionalized (Fig. 6.6 (b)) carbon materials. The presence of S (0.34 wt. %) in the S functionalized carbon material is confirmed from the EDAX analysis (Fig. 6.6 (d)).

6.3.2 Hg (II) sorption studies on bare (C_{IC} N_2 400 B A) and S functionalized (C_{IC} N_2 400 B A S) carbon materials produced from Ipomoea carnea

6.3.2.1 Preparation of calibration plot

1. The calibration plot for the estimation of Hg (II) concentration (in the filtrate after treating the Hg (II) solutions with carbon adsorbents) is obtained from measuring the absorbances of the Hg (II) solutions containing 6, 8, 10, 12, 14, 16, 18, 20, 22 and 24 µg Hg (II) in 25 mL.

2. The Hg (II) solutions with 6, 8, 10, 12, 14, 16, 18, 20, 22 and 24 µg of Hg (II) per 25 ml were prepared by diluting 0.3, 0.4, 0.5, 0.6, 0.7, 0.8, 0.9, 1.0, 1.1 and1.2 ml of 1 x 10 $^{-4}$ M mercury solution.

3. To each of the 25 ml volumetric flask containing 0.3, 0.4, 0.5, 0.6, 0.7, 0.8, 0.9, 1.0, 1.1 and 1.2 ml of 1 x 10 $^{-4}$ M mercury solution, added 5 ml of buffered KI, 5 mL of Rhodamine 6 G reagent and 1 mL of 1 % (wt./vol.) and then the solutions are made up to the mark using distilled water which yielded 6, 8, 10, 12, 14, 16, 18, 20, 22 and 24 µg of Hg (II) in 25 mL.

4. The solutions are shaken thoroughly. Dark pink colouration is developed by the formation of R_2HgI_4 complex which absorbs at 575 nm. The UV-Visible spectra are recorded for the 10 sample solutions prepared (Fig. 6.7) and a calibration plot is drawn as shown below (Fig. 6.8).

The colour reaction of Rhodamine 6 G with tetra iodo mercurate (II) (HgI_4^{2-}) was distinctive. The complex species formed, R_2HgI_4 or $RHgI_3$ (λ_{max} = 575 nm), is pink in colour in contrast to the red colour of the reagent, Rhodamine 6 G (λ_{max} = 530 nm). The absorbance of the complex remained unchanged at 575 nm for at least 24 h by the addition of gelatin (anticoagulation agent). Addition of gelatin retarded the precipitation of the complex even on leaving the solutions overnight.
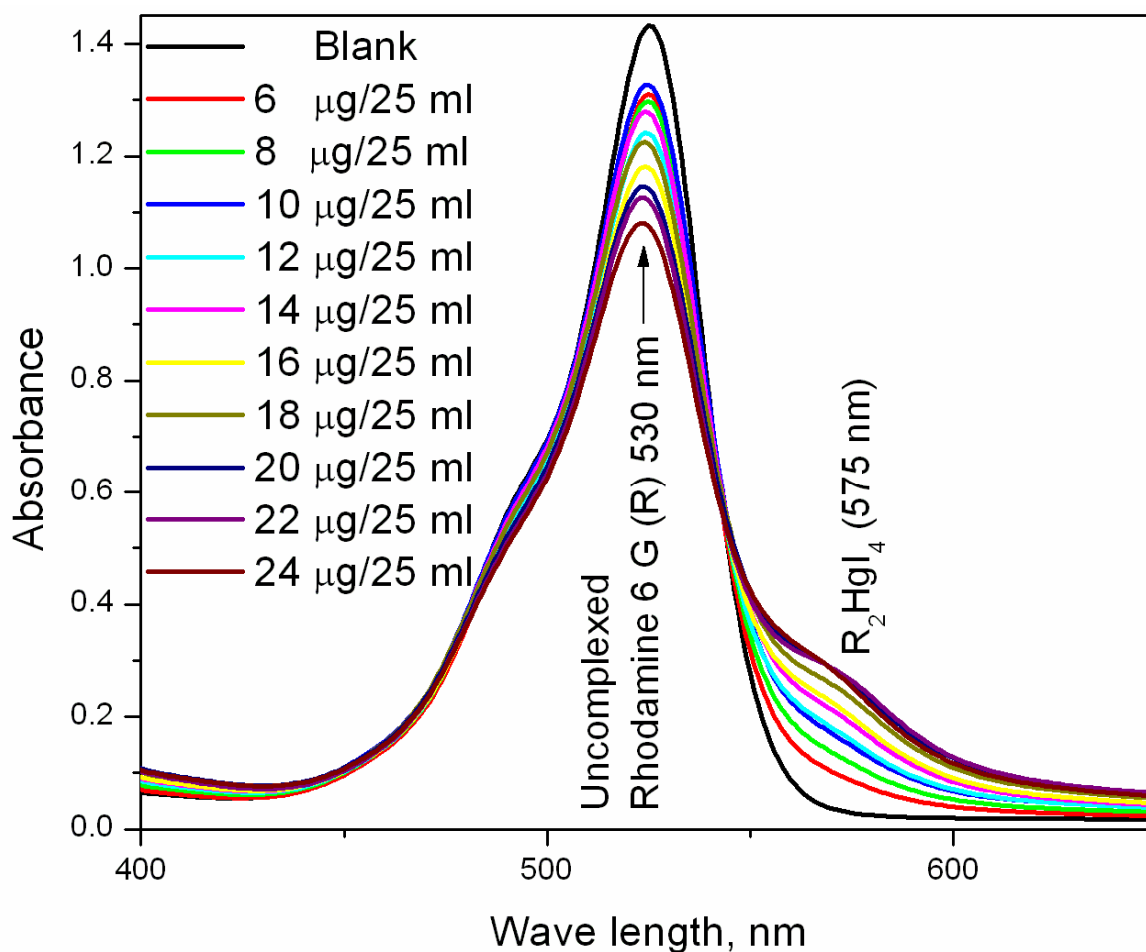
Fig. 6.7 Absorption spectra (total volume 25 ml): 5 ml of 0.005 wt.% Rhodamine 6 G and 5 mL of buffered KI solution with 1 ml (1 wt/vol %) gelatin (Blank). (6 – 24 µg Hg (II) : As in the blank with the addition of 0.3, 0.4, 0.5, 0.6, 0.7, 0.8, 0.9, 1.0, 1.1, 1.2 ml of 1 x 10^{-4} M mercury solution

Linearity (correlation coefficient, R = 0.9966) in the relation between Hg (II) concentration and absorbance of $RHgI_3$ or R_2HgI_4 complex is observed up to 25 µg Hg (II)/25 mL concentration beyond which the Beer Lambert's law is not valid. Blank, 6, 8, 10, 12, 14, 16, 18, 20, 22 and 25 µg Hg (II) in 25 mL volumetric flasks were used as standard solutions to obtain the calibration plot. The standard solutions were prepared from the stock solution of 1×10^{-4} M Hg (II).
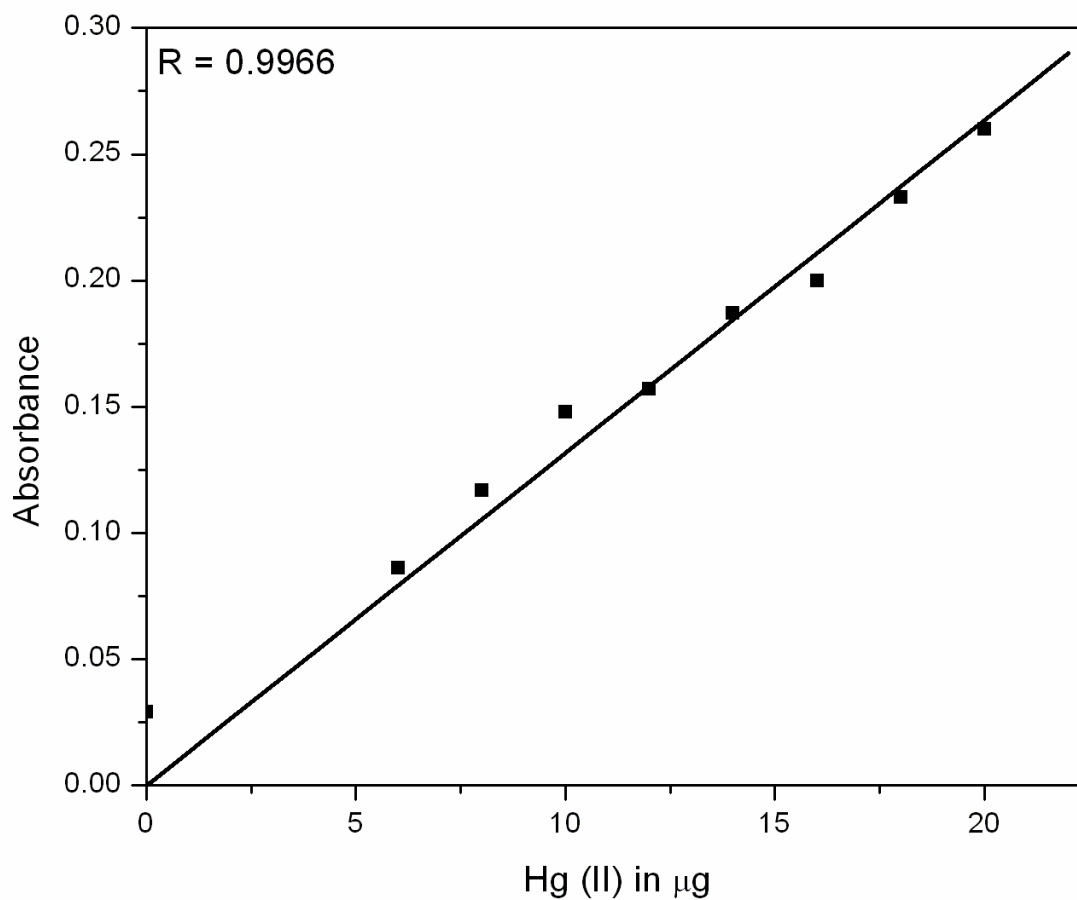
Fig. 6.8 Calibration plot of Hg (II) conc. in µg Vs absorbance of R_2HgI_4 at 575 nm

6.3.2.2 Evaluation of effect of pH on the sorption of Hg (II) on bare and sulphur modified carbon materials (C_{IC} N_2 400 B A Vs C_{IC} N_2 400 BAS)

To evaluate the most suitable pH for the removal of Hg (II) the sorption studies were carried out at varying pH values in the range from 1 – 10. Taken 100 mL of 10 mg/L Hg(II) with 10 g/L NaCl solutions in polyethylene reagent bottles (250 ml capacity). Dilute solutions of 1 M HCl and 1 M NaOH were used for adjusting the pH. Added 0.1 g of the sorbent (C_{IC} N_2 400 B A or C_{IC} N_2 400 B A S) to each of the 10 reagent bottles. The solutions were equilibrated for 24 h. The contents were filtered after 24 h. The filtrate was tested for the presence of Hg (II) and the amount of Hg (II) adsorbed was estimated.

As expected S functionalized carbon material (C_{IC} N_2 400 B A S) exhibited better performance compared to the carbon material (C_{IC} N_2 400 B A) with out S containing (C=S) functional groups. At all pH values sulphur functionalized carbon material showed superior performance compared to the bare carbon material (Fig. 6.9). Enchancement in the removal of Hg (II) as a result of the presence of S containing functional groups of the carbon surface can be explained on the basis of Pearson's theory of acids and bases (Pearson, 1988) According to which hard acids prefer to coordinate with hard bases and soft acids to soft bases. Hg (II) ions ($HgCl_4^{2-}$)are soft Lewis acids and as a rule they prefer to complex with protonated form of S containing functional groups of carbon surfaces which act as soft bases ($C=SH^+$) (Madhava Rao *et al*, 2009; Danwanichakul *et al*., 2008; Zhang and Itoh, 2003).
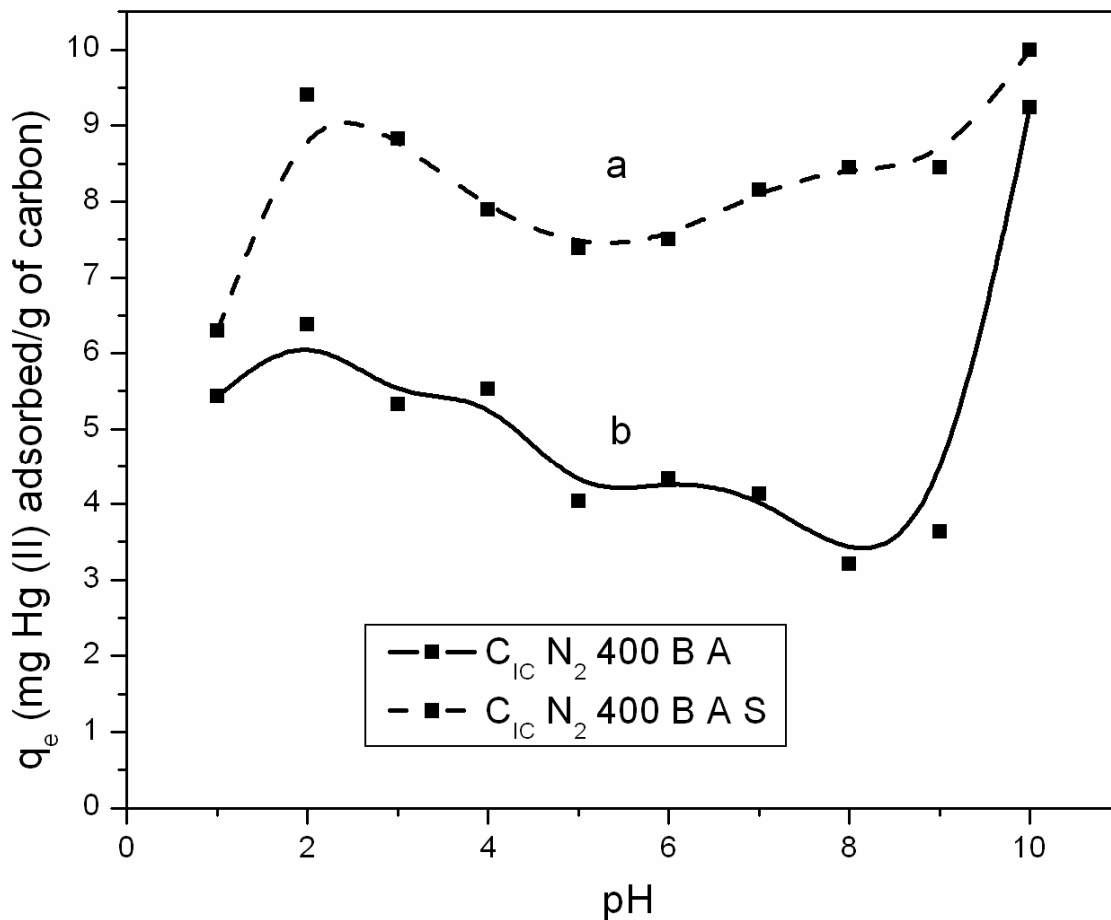
Fig. 6.9 Effect of pH on the removal of Hg (II) using carbon materials as sorbents (a) S functionalized carbon material (C_{IC} N_2 400 B A S) and (b) bare carbon material (C_{IC} N_2 400 B A)

Filho *et al*., (1995) have attributed the high affinity between S on carbon surface and the Hg (II) species in solution to the formation of a strong metal - sulphur (donor atom) bond. Krishnan and Anirudhan (2002) have also observed enhancement in the adsorption of Hg (II) species owing to the presence of S containing functional groups on the carbon surface. Meng *et al*., (1998) have observed high adsorption capacity of Hg (II) in the case of tyre rubber particles containing a variety of S groups such as poly sulfides (-CH_2-S_x-S_y-CH_2-) and thiocarbonyls (N-C-S-). Gomez-Serrano *et al*., (1998) have observed

high chemical affinity between the adsorptive (Hg (II) species) and surface functional groups (sulphur and oxygen groups) of sulphurized activated carbon samples.

A peculiar trend in the variation of the amount of Hg (II) adsorbed as a function of pH is observed. Whether it be S containing or the bare carbon material two extreme cases of adsorption of Hg (II) as $HgCl_4^{2-}$ do exist. The adsorption of Hg (II) is the least at a pH value of 1 owing to the presence of excess Cl- ions which compete with anionic Hg (II) species such as $HgCl_4^{2-}$ for the active sites of adsorption ($C=SH^+$, soft base). Another extreme case where in maximum amount of Hg (II) is adosorbed on the surface of the carbon material do exist at a pH value of 10. Carrott *et al.*, (1998) have observed a similar trend in the adsorption of $HgCl_4^{2-}$ species on Norit AZO activated carbon where in the amount of Hg (II) adsorbed is higher at a pH value of 10.2 and the lowest at a pH value of 0.2. At a pH value of 10.2 each protonated basic site (SX^+) provoke the adsorption of slightly more than one complex ion ($HgCl_4^{2-}$) resulting in a sudden enhancement in the amount of Hg (II) adsorbed on the carbon surface (Carrott *et al.*, 1998). At pH values between 2 and 9 there is no significant change in the amount of Hg (II) adsorbed in the case of S functionalized carbon sample where as a slight decrease in the Hg (II) adsorption is noticed in the case of bare carbon material (C_{IC} N_2 400 B A). The soft bases like the surface functional groups on the S functionalized carbon surface (C=O and C=S) do result in the ionized carbon surface according to the following equilibrium:

$$B + H^+ \rightleftharpoons BH^+$$

As the only mercury species present in solution is the negatively charged tetra chloro mercurate (II) complex, the $HgCl_4^{2-}$ species adsorb on the carbon surface due to the protonated basic sites with the following stoichiometry:

$$HgCl_4^{2-} + b\ BH^+ \rightleftharpoons HgCl_4B_bH_b^{(b-2)+}$$

($BH^+ \cong C=SH^+$ or $C=OH^+$ type protonated basic sites generated from the surface functional groups on the carbon)

6.3.2.3 Evaluation of effect of adsorbent dosage on the sorption of Hg (II)

Adsorbent dosage is a necessary parameter in sorption studies as it determines the sorption capacity of the adsorbent for a given initial concentration of metal ion solution. With an increase in the adsorbent dosage from 20 to 200 mg the percent removal of Hg (II) increased up to ~ 99 % (Fig. 6.10).

The increase in the percent removal of Hg (II) with an increase in the adsorbent dosage is expected as the number of active sites (surface functional groups) increase with the dosage. Similar trend in the sorption of Hg (II) as a function of adsorbent dosage was reported when activated carbon materials from agricultural wastes (Madhava Rao *et al.*, 2009) and sago waste (Kadirvelu *et al.*, 2004) were employed as sorbents. Anirudhan *et al.*, (2008) have observed an increase in the percentage Hg (II) adsorption from 62.3 to 99.9 % with an increase in the dosage of coconut coir pith base ion exchange from 0.5 to 5 g/L. Nearly 1.6 g of the sulphur functionalized carbon material (C_{IC} N_2 400 B A S) is required for the complete removal of Hg (II) from 1000 ml of Hg (II) solution with an initial concentration of 10 mg/mL.
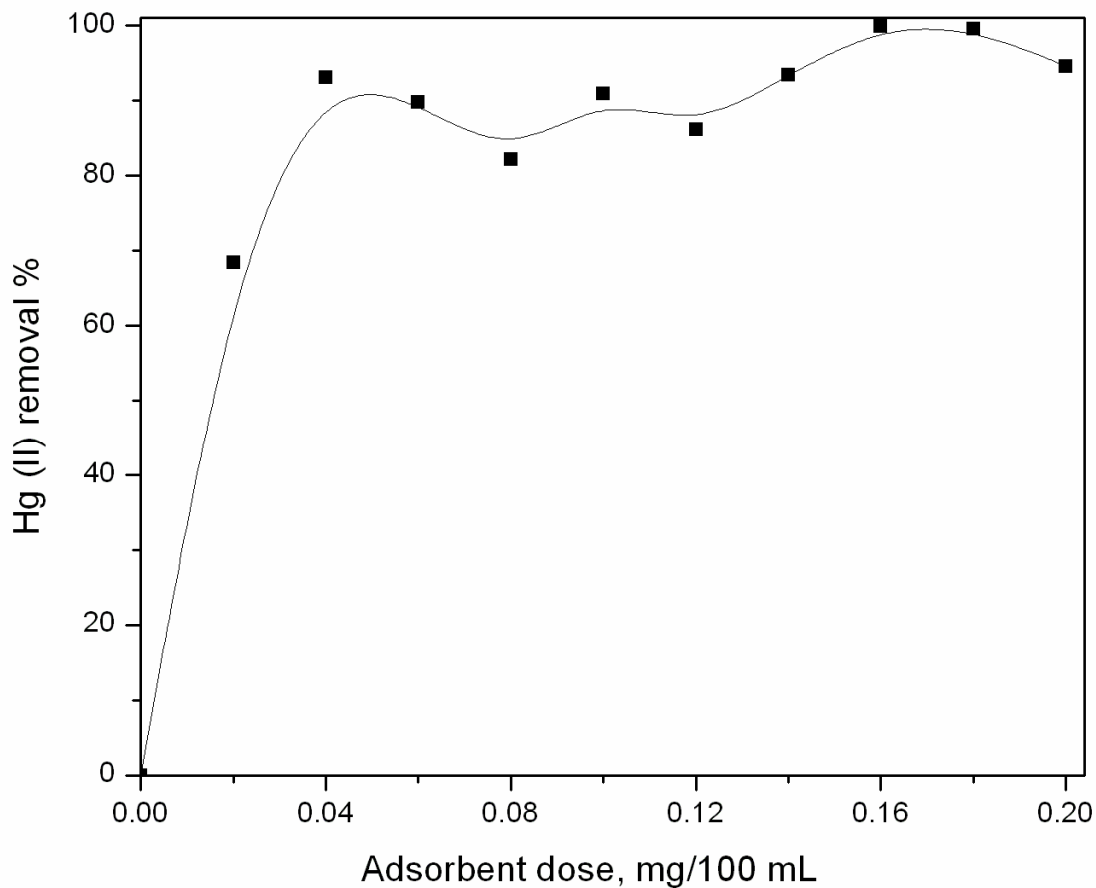
Fig. 6.10 Effect of adsorbent dose for the removal sorption of Hg (II) onto S
functionalized carbon material (C_{IC} N_2 400 B A S) (Initial Hg (II) concentration
= 10 mg/L with 10 g/L NaCl; pH = 6.0; contact time = 24 h)

6.3.2.4 Effect of contact time on the removal of mercury

The effect of contact time on the removal of Hg (II) from an aqueous solution with an
initial concentration of 10 mg/L is evaluated for a period of 24 h. An increase in the
removal of Hg (II) with time is noticed and equilibrium is attained in 1 h of agitation
(mechanical shaking).

6.3.2.5 Effect of initial metal ion concentration on the sorption of Hg (II)

The effect of initial mercury concentration (10 – 70 mg Hg (II)/L) in the aqueous solution on the removal of Hg (II) by the S functionalized carbon material (C_{IC} N_2 400 B A S) is shown in Fig. 6.11. An increase in the removal capacity with an increase in the initial concentration of Hg (II) is observed. The removal of Hg (II) increased from 7.1 to 45.7 mg/g when the initial concentration of the Hg (II) was increased from 10 to 70 mg/L.
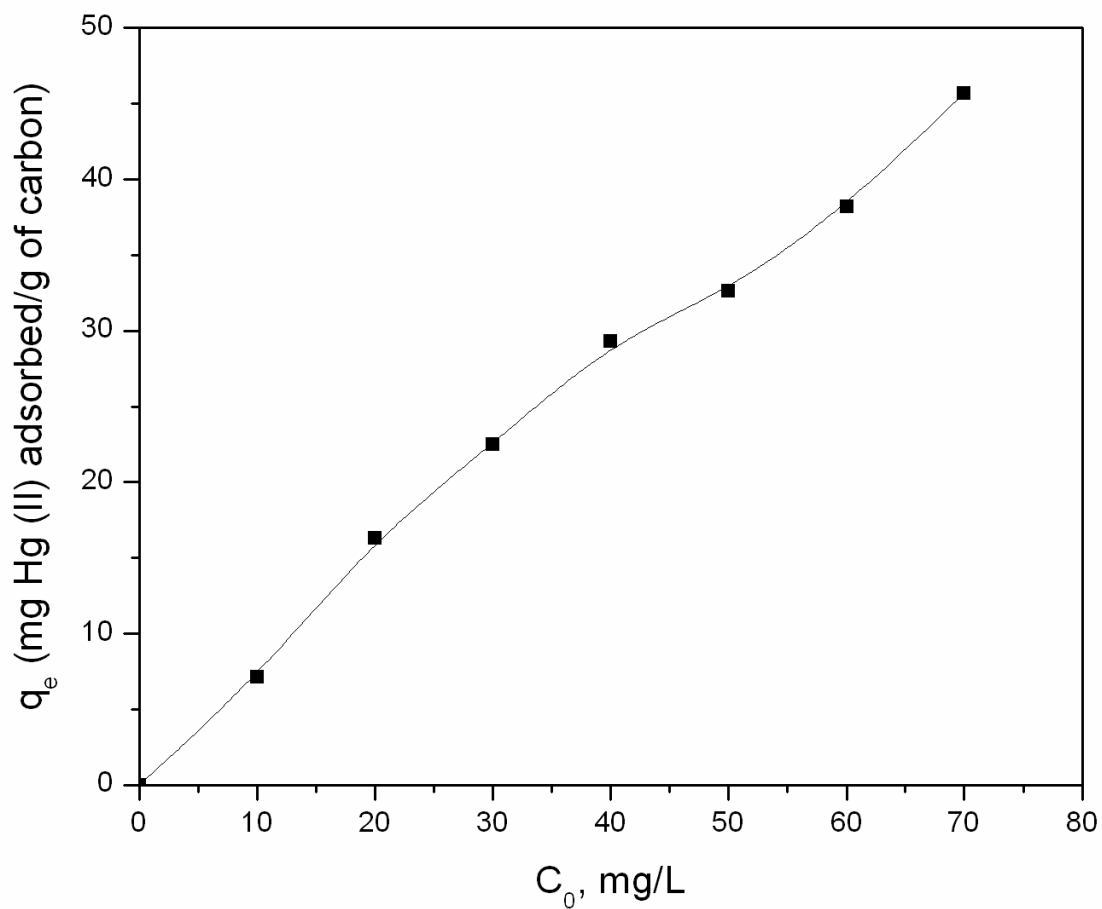
Fig. 6.11 Effect of initial concentration of metal ion on the removal of Hg (II)
(Sorbent : C_{IC} N_2 400 B A S; Dose: 0.1 g/100 mL Hg (II) solution; pH = 6; equilibration time – 1 h)

6.3.2.6 Adsorption isotherm

Adsorption isotherm for the removal of Hg (II) by sulphur functionalized carbon materials was depicted in Fig. 6.12. The two most commonly used equilibrium models, namely, Freundlich and Langmuir adsorption models were applied for analyzing and interpreting the equilibrium adsorption data and also to evaluate which model best fits the experimental data.
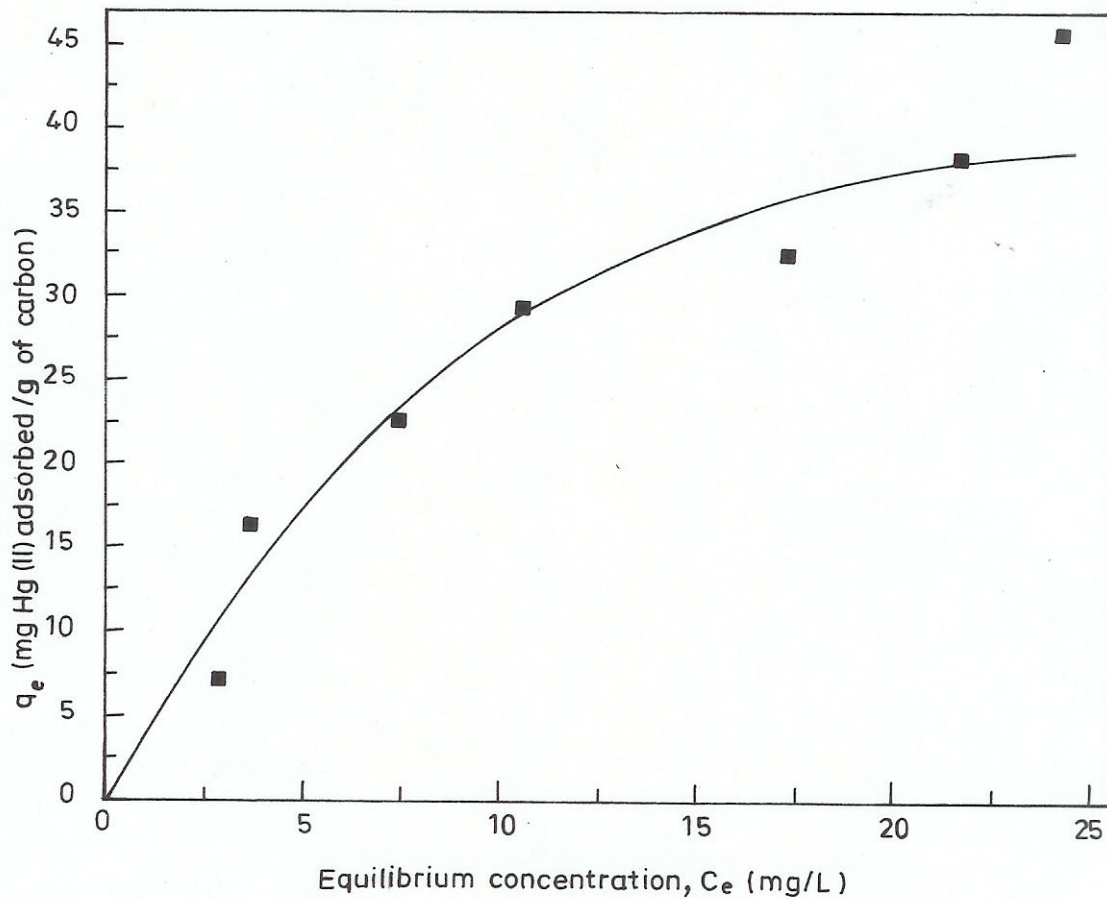
Fig. 6.12 Adsorption isotherm of Hg (II) sorption (Sorbent : C_{IC} N_2 400 B A S; sorbent dose: 0.1 g/100 ml Hg (II) solution; pH = 6; equilibration time – 1 h)

Freundlich isotherm is the most widely used non-linear sorption model and is given by the general equation:

$$q_e = K_F \, C_e^{\, 1/n}$$

where K_F and n are the Freundlich constants related to the sorption capacity

($mg^{1-1/n}L^{1/n}g^{-1}$) and n to the sorption intensity respectively.   Thus higher values of K_F

indicate higher adsorption capacity. q_e is the amount of the adsorbate adsorbed at

equilibrium (mg/g) and C_e is the equilibrium concentration of the adsorbate is solution

(mg/L).

The logarithmic form of the above equation is generally used to fit the data from batch

equilibrium studies.

The logarithmic form of Freundich equation is shown below:

$logq_e = logK_F + 1/n \ logC_e$

A plot of $logq_e$ Vs $logC_e$ is shown in Fig. 6.13.   A straight line indicates that the

adsorption follows Freundlich isotherm model and the equilibrium data were fitted well

by the Freundlich isotherm model. The Freundlich constants, K_F and 1/n, were calculated

from the intercept and slope of the plot of $logq_e$ Vs $logC_e$.   High value of correlation

factor close to 1 (R = 0.9832) indicate that the adsorption follows Freundlich isotherm

model perfectly. The K_F and 1/n values were 8.3 and 0.51 respectively. The value of 1/n

lying between 0 and 1 (1/n = 0.51) is an indication of the heterogeneity of the carbon

surface. In general smaller value of 1/n (close to zero) and larger value of K_F indicate

that the sorbent possess greater intensity of mercury adsorption and higher adsorption

capacity respectively (Zhang *et al*., 2005). Thus the ultimate adsorption capacity of the

adsorbent (C_{IC} N_2 400 B A S) can be calculated from the isothermal data substituting the

required equilibrium concentration in the Freundlich equation (Anirudhan *et al*., 2008).

For a K_F value of 8.3, 1/n value of 0.51, assuming the equilibrium concentration of Hg (II) to be 1.0 mg/L, each gram of adsorbent can remove 8.3 mg of Hg (II) at 30 °C.
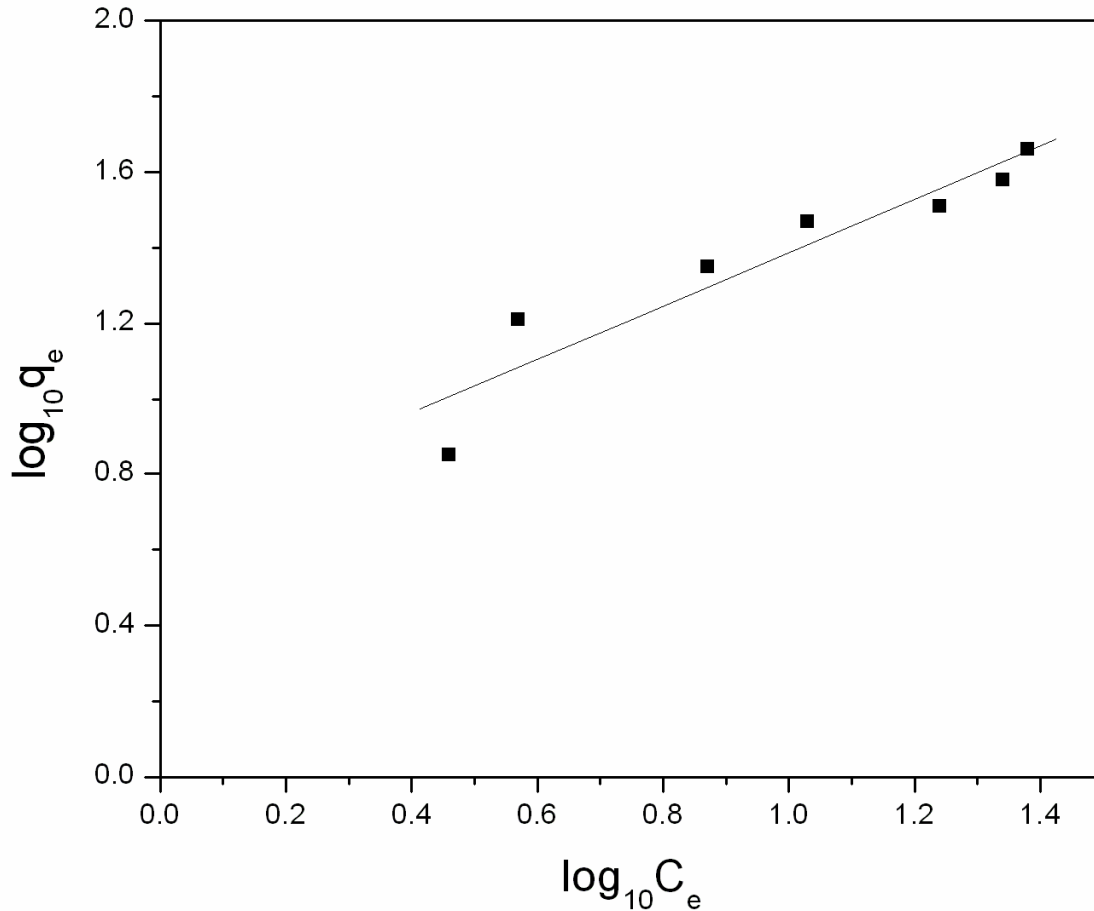
Fig. 6.13 Freundlich plot of mercury (II) adsorption

The Langmuir adsorption model is one of the first theoretical treatments of non-linear sorption. The model has been successfully applied to a wide range of systems that exhibit limiting or maximum sorption capacities. The model assumes uniform energies of adsorption onto the surface and also no transmigration of the adsorbate in the plane of the surface (Langmuir, 1918)). The Langmuir isotherm is given by the following equation:

$q_e = q_m \, b \, C_e \, /(1 + bC_e)$

where q_m and b are the Langmuir constants related to the adsorption capacity and the energy of adsorption respectively. q_m is the maximum adsorption capacity of the adsorbent corresponding to the complete monolayer coverage (mg/g). q_m gives the limit towards which adsorption of pollutants from the solution tends (Laszlo *et al.*, 1997). 'b' is the adsorption coefficient and is a measure of the energy of adsorption (L/mg). C_e is the equilibrium metal ion concentration in solution (mg/L) and q_e is the amount of Hg (II) adsorbed at equilibrium on the sorbent surface (mg/g).

The linear form of Langmuir equation is shown below:

$C_e/q_e = C_e/q_m + 1/bq_m$

The above equation is used to analyze the batch equilibrium adsorption data. The values of qm and b were determined from the slope and the intercept of the plot of C_e/q_e Vs C_e as shown in Fig. 6.14. A good representation of the Langmuir's dependence is observed. The high value of the correlation coefficient close to 1 (R = 0.9575) suggests that the experimental data can be represented by the Langmuir sorption model (Budinova *et al*, 2008). From the correlation coefficient values and the Freundlich and Langmuir plots, it can be concluded that the fit is better with Freundlich model (R = 0.9832) rather than with Langmuir model (R = 0.9575). As the Freundlich type adsorption isotherm is an indication of surface heterogeneity of the adsorbent (Madhava Rao *et al.*, 2009), it can be deduced that the carbon adsorbent (C_{IC} N_2 400 B A S) is made up of small heterogeneous patches (comprising of specific S and O surface functional groups).
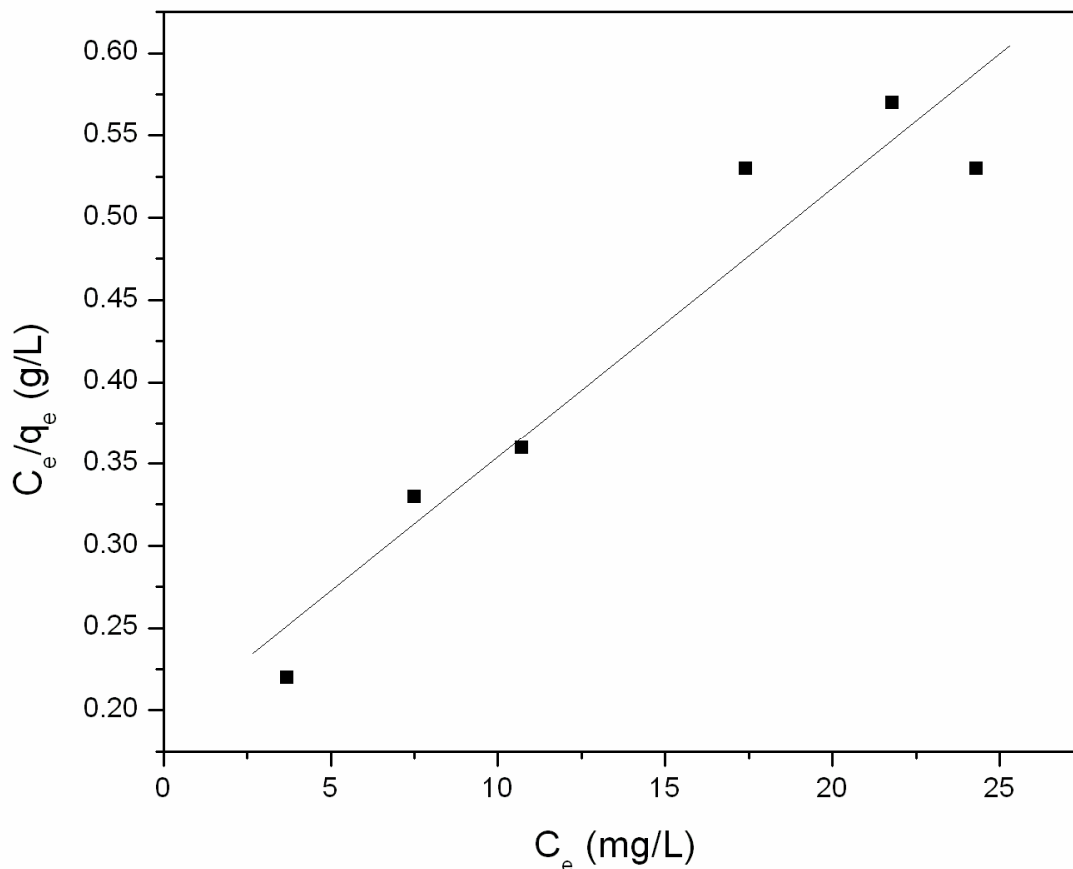
Fig. 6.14 Langmuir plot of mercury (II) adsorption

For Langmuir type adsorption process, a dimensionless separation factor is defined to determine if the adsorption is favourable or not. The essential features of the Langmuir isotherm can be expressed in terms of R_L. R_L is an equilibrium parameter defined as follows:

$R_L = 1/(1+bC_0)$, where C_0 is the initial metal ion concentration (mg/L) and b is the Langmuir constant (L/mg). This type of isotherm is said to be unfavourable, linear, favourable and irreversible if the values of R_L are respectively as follows: $R_L > 1$, $R_L = 1$, $0 < R_L < 1$ and $R_L = 0$ (McKay *et al*., 1982; Ekinci *et al*., 2002; Inbaraj and Sulochana, 2006; Oubagarauadin *et al*., 2007; Madahava Rao *et al*., 2009) In the case of the S

functional carbon adsorbent (C_{IC} N_2 400 B A S), the value of R_L is 0.51 ($0 < R_L < 1$) indicating that the isotherm (adsorption process) is favourable on the adsorbent developed for Hg (II) sorption.

The equilibrium adsorption data fitted well with both Freundlich and Langmuir adsorption models. The Freundlich and Langmuir constants corresponding to the adsorption process of S functionalized carbon material from Ipomoea carnea (C_{IC} N_2 400 B A S) were compared with several other well studied adsorbents and a comparison of the same is summarized in Table 6.2.

Table 6.2 Comparison of Freundlich and Langmuir constants of the adsorbent developed
in the current study with several adsorbents reported in literature

Adsorbent	Freundlich constants	Langmuir constants	Reference
S functionalized activated carbon	K_F = 8.3 1/n = 0.51 R = 0.9832	q_m = 55.6 b = 0.095 R_L = 0.51 R = 0.9575	Present study
Activated carbon from Cieba pentandra hulls	K_F = 11.24 1/n = 0.24 R = 0.9686	q_m = 25.88 b = 0.45 R_L = 0.06 R = 0.8167	Madhava Rao *et al.*, 2009
Activated carbon from phaseolus aureus hulls	K_F = 9.51 1/n = 0.27 R = 0.9661	q_m = 23.66 b = 0.51 R_L = 0.04 R = 0.9016	Madhava Rao *et al.*, 2009
Activated carbon from	K_F = 8.36	q_m = 22.88	Madhava Rao *et al.*, 2009

Cicer arietinum	1/n = 0.275 R = 0.966	b = 0.36 R_L = 0.05 R = 9273	
Fullers earth (clay)	K_F = 0.375 1/n = 0.334 R = 0.996	q_m = 1.145 b = 0.359 R_L = 0.053 R = 0.991	Oubagaranadin *et al.*, 2007
Activated carbon (Merck)	K_F = 10.464 1/n = 0.487 R = 0.997	q_m = 69.44 b = 0.104 R_L = 0.161 R = 0.967	Oubagaranadin *et al.*, 2007
Activated carbon from Sago waste	K_F = 3.58 1/n = 0.53	q_m = 55.6 b = 0.375 R = 0.9871	Kadirvelu *et al.*, 2004
Carbon cloth	K_F = 5.25 1/n = 0.21	q_m = 37 b = 0.0068	Meenakshi and Amutha, 2008
Ind Carb 50 (wood based carbon)	K_F = 7.58 1/n = 0.25	q_m = 111 b = 0.0409	Meenakshi and Amutha, 2008
GAC – 1240 Norit (peat based carbon)	KF = 8.71 1/n = 0.34	q_m = 120 b = 0.08	Meenakshi and Amutha, 2008
GAC – R (peat based carbon)	K_F = 50.12 1/n = 0.6	q_m = 143 b = 0.117	Meenakshi and Amutha, 2008
Char coal from camel bone	K_F = 14.457 1/n = 0.283 R = 0.9637	q_m = 28.24 b = 1.09 R = 0.9901	Hassan *et al.*, 2008
Activated carbon from Terminalia catappa shell	K_F = 38.25 1/n = 0.25 R = 0.9128	q_m = 94.43 b = 0.49 R = 0.9956	Inbaraj and Sulochana, 2006
Vulcanized rubber C 30 EV	K_F = 3.9 1/n = 0.23	-	Danwanichakul *et al.*, 2008

Cation exchanger from coconut coir pith	$K_F = 13.73$ $1/n = 0.451$	**-**	Anirudhan *et al.*, 2008
Activated carbon from sewage sludge	$K_F = 10.1$ $1/n = 0.96$ $R = 0.9972$	-	Zhang *et al.*, 2005
Activated carbon from sewage sludge (H_2SO_4 activation)	$K_F = 13.6$ $1/n = 0.91$ $R = 0.9901$	**-**	Zhang *et al.*, 2005
Activated carbon from sewage sludge (H_3PO_4 activation)	$K_F = 16.0$ $1/n = 0.86$ $R = 0.9869$	-	Zhang *et al.*, 2005
Activated carbon from sewage sludge ($ZnCl_2$ activation)	$K_F = 42.6$ $1/n = 0.32$ $R = 0.9926$	**-**	Zhang *et al.*, 2005
Gauva bark	$K_F = 0.2394$ $1/n = 0.635$ $R = 0.999$	-	Lohani et al., 2008
Steam pyrolyzed activated carbon from bagasse pith	**-**	$q_m = 172.4$ $b = 0.0072$	Anoop Krishnan *et al.*, 2002
Used tyre rubber	**-**	$q_m = 14.6$ $b = 4.71$	Meng *et al.*, 1998
Activated carbon (from Mengen coal)	-	$q_m = 92$ $b = 0.34$	Ekinci *et al.*, 2002
Activated carbon (from Seyitomer coal)	-	$q_m = 56$ $b = 1.46$	Ekinci *et al.*, 2002
Activated carbon (from some coal)	-	$q_m = 105$ $b = 1.19$	Ekinci *et al.*, 2002
Activated carbon (from Bolluca coal)	-	$q_m = 37$ $b = 0.18$	Ekinci *et al.*, 2002
Activated carbon	-	$q_m = 153$	Ekinci *et al.*, 2002

(from Apricot stones)		b = 0.23	
Activated carbon (from furfural)	-	q_m = 174 b = 1.4	Ekinci *et al.*, 2002
Activated carbon from antibiotic waste	-	q_m = 129 b = 0.5 R = 0.9949	Budinova *et al.*, 2008

6.4 CONCLUSION

A botanical source, Ipomoea carnea, is exploited for the production of activated carbon which is used as sorbent for Hg (II). For the first time S/Hydrazine solution is exploited as a S precursor for functionalizing carbon material with S. S functionalization has enhanced Hg (II) sorption by carbon material from Ipomoea carnea stems. The equilibrium adsorption data fitted well with both the Freundlich and Langmuir adsorpion models. Observation and comparison of the Freundlich and Langmuir constants corresponding to various adsorbents reveal the fact that the S functionalized carbon material produced from Ipomoea carnea out performed various sorbents like activated carbon materials produced from Cieba pentandra hulls, Phaseolus aureus hulls, Cicer arietinum, sago waste, Bolluca coal and also adsorbents other than activated carbon like the fuller's earth (clay), char coal produced from camel bone, guava bark, used tyre waste and vulcanized rubber. Improvement in the sorption capacity of C_{IC} N_2 400 B A S is anticipated with an increase in the density of C=O and C=S surface functional groups.

CHAPTER - 7

CARBON MATERIALS FOR ADSORPTIVE DESULPHURIZATION
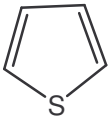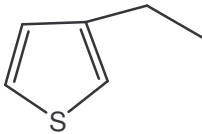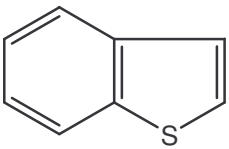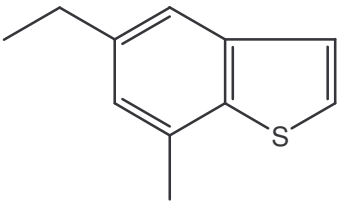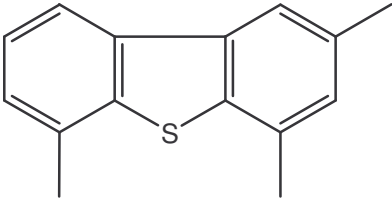
7.1 INTRODUCTION

Removal of organo-sulphur compounds from diesel is of interest from scientific, social, economic and environmental view points. Production of clean fuel is the goal of the petroleum refining industry. The reduction of S below certain ppm levels in diesel fuels becomes difficult due to the presence of sterically hindered S-compounds (such as the 4, 6 - dialkydibenzothiophenes) that are difficult to desulfurize over conventional supported mixed sulfide catalysts. Hence, newer technologies based on novel routes like adsorption, oxidation and chelation are being developed to remove these refractory S-compounds. Any breakthrough achieved in desulphurization technology will have its impact on human well being.

Burning of fuel (gasoline or diesel) with S contents beyond permissible limit causes ill effects on human health. Current world demands zero sulphur fuel. Even though the production of clean fuel is the goal of petroleum refining industry, the refinery itself is engulfed now in the vicious circle of a host of problems that include environmental legislation, crude oil quality variation, product state demand, economic imbalances, energy uptake, safety and process efficiency (Babich and Moulijn, 2003). It should not be mistaken that conventional HDS can be a panacea to the recurring problem of S specification in the transportation fuels. Newer technologies, if found promising,

should be given place and adopted. Typical S containing compounds present in petroleum fractions are shown in Table 7.1.

Table 7.1 Some S containing compounds present in petroleum fractions

S. No.	S Compounds
1	R-SH (Thiol, Mercaptan)
	R-S-R' (Sulfide)
	R-S-S-R' (Disulfide)

Thiophene

Substituted thiophene

Benzothiophene

Substituted benzothiophene

Substituted dibenzothiophene

Hydroprocessing is one of the most important steps in the petroleum refining industry. Hydroprocessing refers to a variety of catalytic processes aimed at the removal of S, N, O and aromatic compounds present in the gasoline and diesel feed stocks. $\gamma - Al_2O_3$ supported sulfided NiMo oxide is the best known commercial catalyst for hydrodenitrogenation (HDN) where as the sulfided CoMo oxide supported on $\gamma - Al_2O_3$

in the industrial catalyst for hydrodesulphurization. As the name of the processes suggest, the catalyst should possess strong hydrogenation function as hydrogenation is the prime reaction in both HDN and HDS processes. Sulphur in the oil streams is removed as H_2S from the petroleum streams in the process of hydrodesulphurization (HDS) under severe conditions of reaction temperature and hydrogen pressure. Even though the oxides of sulfided CoMo and NiMo supported on $\gamma - Al_2O_3$ showed excellent performance for HDS and HDN reactions respectively, the afore mentioned catalysts need to be sulfided a priori to achieve the active site formation. The sulphidation process is usually carried out by exposing the catalyst to the sulphur containing feed itself. There are several ways in which the sulfided CoMo and NiMo based catalysts lose their activity. Factors that cause the loss of activity are: sintering of the active phases, decomposition of the active phases, covering of the active sites by reactants or products, coking, formation of deposits of metal sulfides. Owing to the afore mentioned problems, in addition to the necessity of H_2 as well as the severity of the operation conditions, there is an urgent need for the development of alternate methods of desulphurization with efficiency towards the removal of refractory compounds.

4, 6 dimethyl dibenzothiophene (4, 6 DMDBT) with alkyl groups close to 'S' atom is highly refractory compound to be desulphurized. 'S' species in such 'sterically' inaccessible environment are too difficult to be removed. Two parallel reaction path ways, namely, the direct desulphurization as well as involving the hydrogenation step followed by desulphurization, are possible for the desulphurization of 4, 6 DMDBT on commercial oxide catalyst (either NiMoS/Al or CoMoS/Al) as depicted in Scheme 7.1.

4, 6 DMDBT

Direct Desulphurization

Hydrogenation

4, 6 - THDMDBT
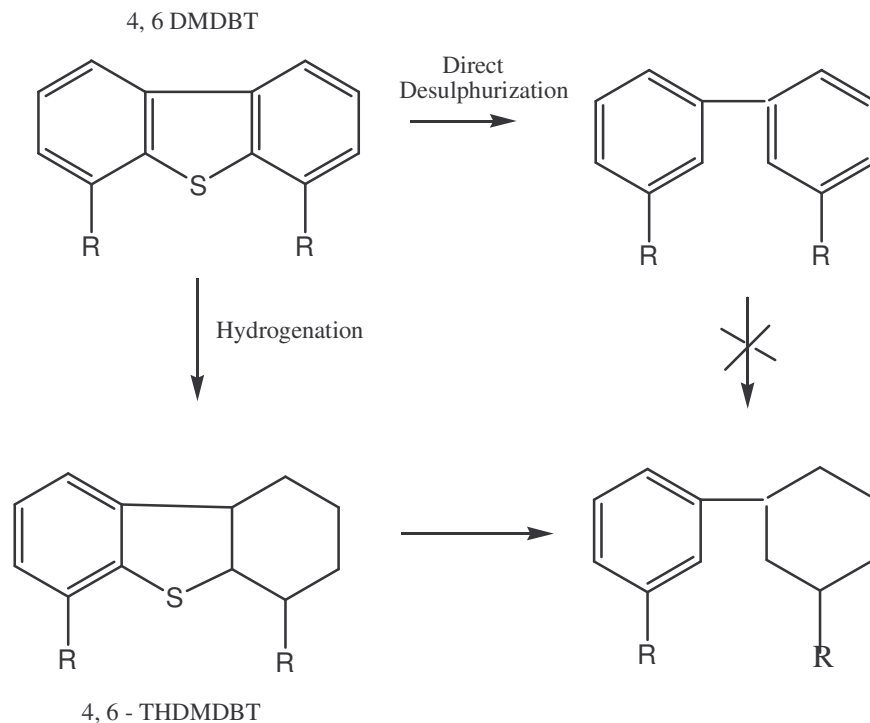
Scheme 7.1 Hydrodesulphurization of 4, 6 – DMDBT (R – CH_3) involving direct route

and hydrogenation route (Manoli *et al*., 2004)

Direct desulphurization of 4, 6 DMDBT yields dimethyl di phenyl. Hydrogenation route initially yields dihydrobenzothiophene which subsequently desulphurizes to form methyl cyclohexyl toluene (MCHT). It was found that around 80 % of the HDS of 4, 6 – DMDBT proceeds via the hydrogenation route where in the adsorbed 4, 6 – DMDBT is first hydrogenated and then the hydrogenated compound is desulphurized (Manoli *et al*., 2004). Breysse *et al*., (2003) have proposed the following reaction mechanism for the hydro desulphurization of substituted (2, 4 di alkyl) dibenzo thiophene which is the most highly refractory compound (difficult to get desulphurized).

216
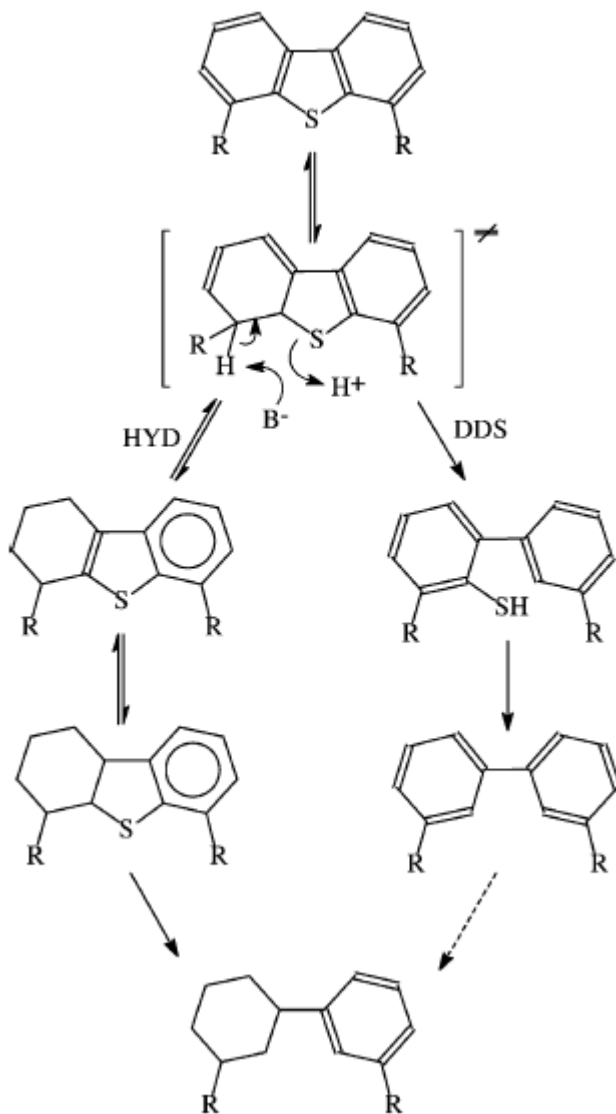
Scheme 7.2 Mechanism of desulphurization of substituted dibenzo thiophene (Breysse *et al.*, 2003)

The origin of refractory behaviour in compounds such as highly substituted dibenzothiophenes, 4, 6 DMDBT in particular, is related to the steric hindrance encountered for the breaking of the C-S bond. The desulphurization of 2, 6 DMDBT proceeds via two routes, namely, the hydrogenation (HYD) and the direct desulphurization (DDS) as shown in Scheme 7.2. The partial hydrogenation reaction of

4, 6 DMDBT is a common as well as the primary reaction for either the HYD route or for the DDS route. After the formation of partially hydrogenated products, the C-S bond is cleaved in the DDS route with out any further hydrogenation. Unlike the DDS route, in the path through hydrogenation (HYD route), complete hydrogenation of atleast one of the aromatic rings is inevitable for the C-S bond to cleave. The presence of substituents at 4 and 6 positions of DBT hinders the β – elimination step which is necessary for the desulphurization to take place. Presence of refractory sulphur compounds like, 4, 6 dimethyl dibenzothiophene, necessitate the severe operation conditions.

In most of the diesel fuels, 4, 6 DMDBT, the most difficult S containing compound to be desulphurized, is present in amounts > 100 ppm. In view of the increasing process severity of diesel HDS units to meet the upcoming stringent specifications of permissible S content, alternate methods of desulphurization are being explored. To over come the problem of refractory compounds, in addition to hydrodesulphurization (Ng and Milad, 2002; Manoli *et al*., 2004; Hubaut *et al.,* 2007 and Pinto *et al*., 2008) various strategies for desulphurization, namely oxidation (Collins *et al*., 1997; Mei *et al*., 2003; Yu *et al*., 2005; Toteva *et al*., 2009; Jia *et al*., 2009; Dai *et al*., 2007; Ukkirapandian *et al*., 2008), adsorption (Davini, 1999; Alhamed and Bamufleh, 2009; Yu *et al*., 2008; Aburto *et al*., 2004; Castro et al., 2001; Sano *et al*., 2004; Ma *et al*., 2005; Ngamcharussrivichai *et al*., 2008; Zhang *et al*., 2008; Rheinberg *et al*., 2008; Sano *et al*., 2005; Agueda *et al*., in press; Cao *et al*., 2008; Sotelo *et al*., 2007; Selvavathi *et al*., 2009), chemical (Borah, 2005; Osbaldiston and Markel, 1994; Brader *et al*., 1989; Eisch *et al*., 1985), biochemical (Pandey *et al*., 2004; Labana *et al*., 2005; Bhadra *et al*.,

1987), photochemical (Zhao *et al.*, 2008) and pervaporation (Lin *et al.*, 2008; Lin *et al.*, 2007) methods are being developed.

The process of oxidative desulphurization is selective in converting refractory sulphur compounds to sulfones. But the major disadvantages with the process of oxidative desulphurization are: (i) the oxidant used for the oxidative desulphurization is expensive and (ii) the separation of sulfones is an energy intensive process. Adsorptive desulphurization is an energy efficient process yielding clean fuel free from S under modest process conditions. Zeolite based adsorbents are not a viable option as such process necessitates the requirement of hydrogen for producing fuels meeting the Euro III/IV norms. Carbon materials being multifunctional in terms of structural, textural and surface properties, they can be tuned to match the requirement for the adsorption of S containing compounds including refractory compounds.

The objective of the investigation is to develop a regenerable carbon based adsorbent to reduce sulfur in SR Diesel (CBR) from about 737 ppm to less than 200 ppm. The feed employed is the SR feed of the Narimanam, Tamil Nadu. The adsorbent should be capable of desulphurizing the feed at mild operating conditions, e.g., low pressure (5-10 bar) and low temperatures (less than 250 ºC). Besides the adsorbent should also be easily regenerable under modest conditions of temperature and pressure by either solvent or hydrogen or air. Thus the problem of the exploitation of carbon materials as adsorbents for the desulfurization of a medium S-containing straight run diesel fraction

with a S content of 737 ppm, from Cauvery Basin Refinery (CBR), India, is taken up and elucidated in this chapter.

The physicochemical properties of the CBR diesel are summarized in Table 7.2.

Table 7.2 Properties of SR diesel from CBR distillation unit used in the studies

Property	Value
Total Sulphur content (in ppm)	737
Flash Point (°C)	93
Aniline Point (°C)	81
Viscosity (at 40 °C in cSt)	4.04
Pour Point (°C)	+6
Density (g/cc)	0.8553
Diesel Index	60
Cetane Index	53

7.2. EXPERIMENTAL

7.2.1. Adsorbents employed for desulphurization of diesel

Several commercially available activated carbon materials of varying physical and chemical properties were tested as adsorbents for the removal of organo sulphur compounds from CBR diesel.

7.2.2. Process of adsorptive desulphurization

In a typical adsorption experiment, a glass column of length 50 cm and internal diameter 1.5 cm was packed with 5.0 g of carbon sorbent placed between glass wool and glass beads on either side. Diesel was fed on top of the sorbent bed. The first 20 mL of the product collected at the outlet was analyzed for S. From the S content remaining in the product and subtracting the same from the S content in the feed diesel (737 ppm), the S removed by the carbon was obtained. The S content in the product was analyzed by using an Oxford XRF analyzer. The feed and the product diesel were also analyzed (in some experiments) for individual sulphur compounds using a GC-PFPD (Gas Chromatography – Pulsed Flame Photometric Detector) to know the nature of the actual S-compounds being removed in the adsorptive desulphurization process.

7.3 RESULTS AND DISCUSSION

7.3.1 Screening of carbon materials to choose the best

Different commercially available activated carbons, namely, IG 18 x 40, IG 12 x 10, IG 8 x 30, AC 4 x 8, AC 6 x 12, Ac 12 x 30, calgon carbon as received and adsorbent carbon as received were used as adsorbents for S containing compounds present in SR diesel. The results obtained on the studies with the afore mentioned adsorbents are given in Table 7.3. The amount of S removed (in ppm) from 20 mL deisel by 5.0 g of sorbent is shown in extreme right column of Table 7.3. Among the eight carbons studied Adsorbent carbon as received and Calgon carbon as received were superior to the others for the adsorption of S-compounds in diesel. Hence, Adsorbent carbon (A) and Calgon carbon (B) were selected for further studies.

Table 7.3 S removal capacity of different commercial activated carbon materials

Activated Carbon as Sorbent	*ml-diesel treated/g of adsorbent	S removed (ppm)
IG 18 x 40	4	134
IG 12 x 10	4	81
IG 8 x30	4	76
AC 4 x 8	4	12
AC 6 x 12	4	73
AC 12 x 30	4	92
Calgon carbon as received	4	181
Adsorbent carbon	4	229

* 20 mL initial product collected from the column packed with 5.0 g activated carbon and analyzed for S

7.3.2 Tailoring the surface properties of carbon samples (Adsorbent carbon (A) and Calgon carbon (B))

7.3.2.1 Activation with conc. HNO$_3$

HNO$_3$ treatment changes the surface chemistry of carbon materials. Such oxidative treatment results in the formation of oxygen containing surface functional groups (carbonyl and carboxyl). The presence of such surface functional groups, in most cases, enhances the adsorption capacity of carbon materials (Noh and Schwarz, 1990). Two commercial activated carbon materials, namely, the adsorbent carbon (A) and the calgon carbon (B) were treated with conc. HNO$_3$. The wt.%/wt.% ratio of carbon to conc. HNO$_3$

was 1:5. The oxidative treatment of carbon with conc. HNO_3 was carried out at 60 °C for 2 h under refluxing conditions in a 2 liter RB flask. The contents were then cooled to room temperature, washed with water and dried at 110 °C for 2 h.

7.3.2.2 Activation under Ar atmosphere

Ar activation involved the thermal activation of nitric acid treated carbon materials A and B at a temperature of 800 °C under Ar atmosphere for 2 h in a quartz tube. The carbon samples after activation were termed as nitric acid treated Ar activated carbon materials.

7.3.3 Characterization of adsorbents for desulphurization application

7.3.3.1 Structural (crystallographic) properties of carbon materials - XRD analysis

X-ray diffraction patterns of adsorbent carbon as received, adsorbent carbon treated with conc. HNO_3 and adsorbent carbon treated with conc. HNO_3 followed by subsequent activation in Ar atmosphere are shown in Figs. 7.1. (a), (b) and (c) respectively where in two broad diffraction peaks centered at 2θ values of 25.4 and 43.4 are observed. The afore mentioned peaks could be indexed, respectively, to (002) and (10) planes characteristic of activated carbon materials.

The phase structure of adsorbent carbon remained unaltered on nitric acid treatment (Fig. 7.1. (a) and (b)). But in the case of adsorbent carbon treated with nitric acid followed by activation in Ar atmosphere an additional intense and narrow diffraction peak is seen at $2\theta = 26.7$ (Fig. 7.1. (c)) attributable to the (002) reflection from highly crystalline graphitic carbon (Macia-Agullo *et al*., 2007). Nitric acid treated and Ar activated adsorbent carbon (Fig. 7.1. (c)) is more crystalline than either adsorbent carbon

as received or adsorbent carbon treated with nitric acid alone. Thus Ar activation at 1073 K, improved the crystallinity of nitric acid treated adsorbent carbon.
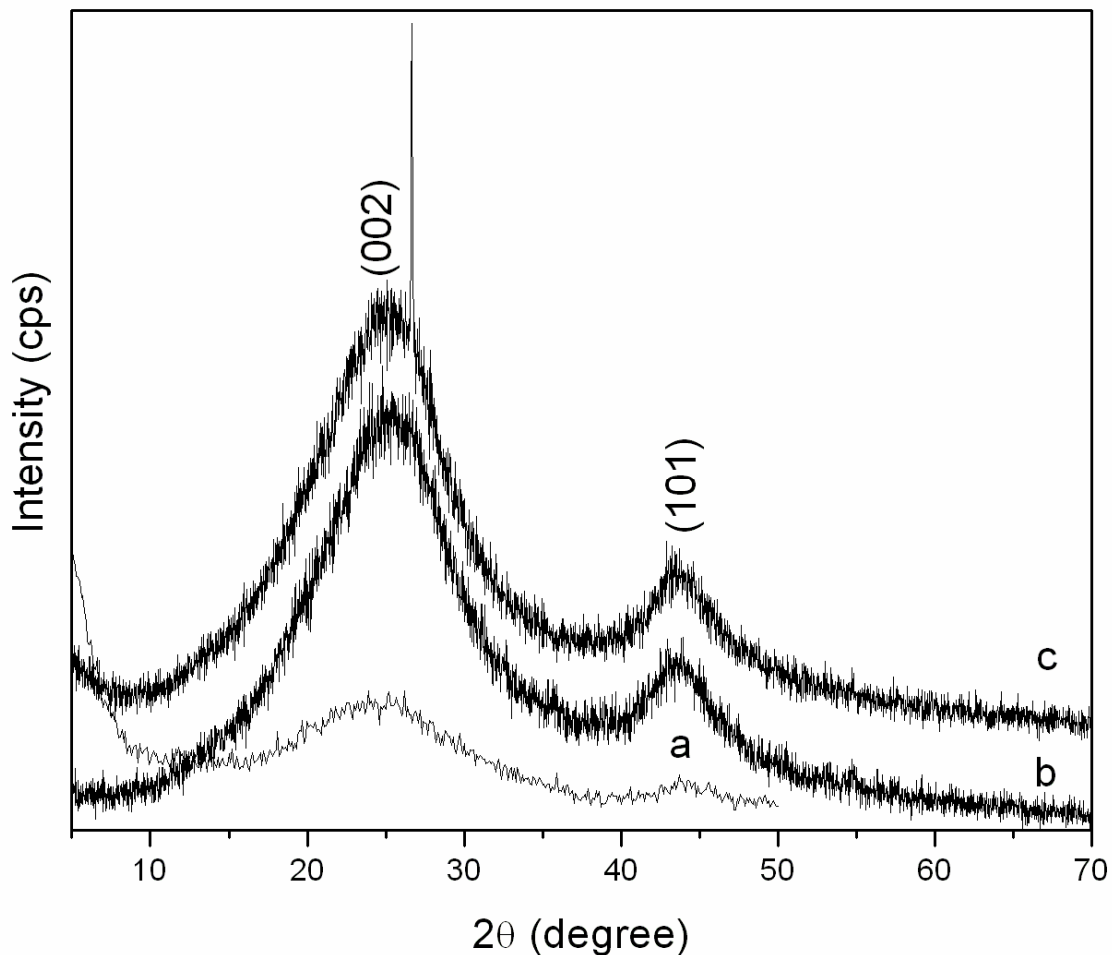
Fig. 7.1 XRD patterns of (a) Adsorbent carbon as received, (b) Adsorbent carbon treated with HNO_3 and (c) Adsorbent carbon treated with HNO_3 and activated with Ar

X-ray diffraction patterns of calgon carbon as received, calgon carbon treated with HNO_3 and calgon carbon treated with HNO_3 followed by Ar activation are shown in Fig. 7.2. (a), (b) and (c) respectively. The diffraction peaks arising from each of these carbon samples are all indexed and are typical of graphitic carbon structure (Macia-Agullo *et al.*, 2007). neither HNO_3 treatment (Fig. 7.1. (b)) nor HNO_3 treatment with subsequent Ar

activation (Fig. 7.2. (c)) significantly altered the structure of the original calgon carbon sample (Fig. 7.2. (a)). thus, neither HNO_3 treatment nor Ar activation has much influence on the phase structure of calgon carbon.
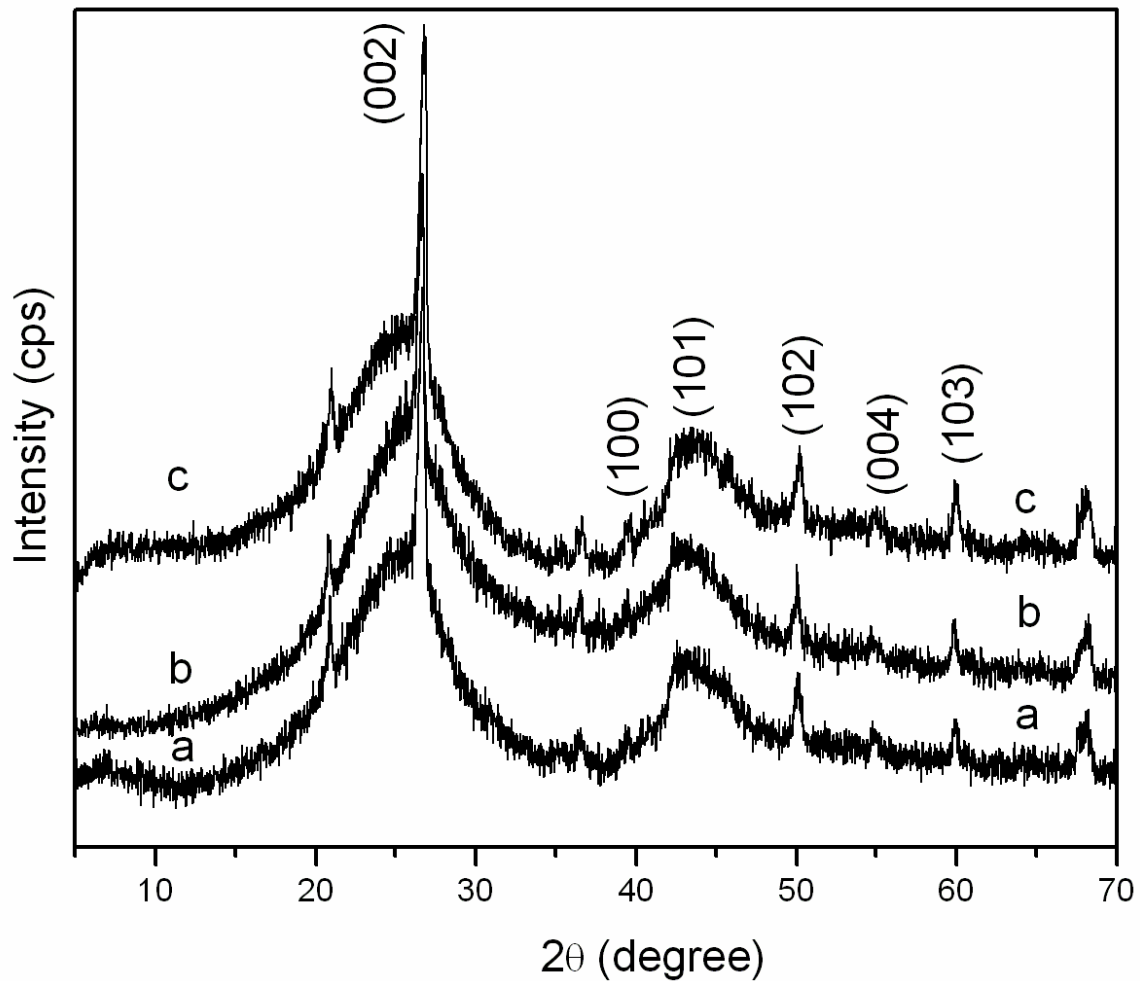
Fig. 7.2 XRD patterns of (a) Calgon carbon as received, (b) Calgon carbon treated with HNO_3 and (c) Calgon carbon treated with HNO_3 followed by Ar activation

There is a marked difference in the structural order between Adsorbent carbon and Calgon carbon. No diffraction peaks resulted from Adsorbent carbon or its modified forms beyond $2\theta = 50^\circ$ (Fig. 7.1.) in sharp contrast to the characteristic diffraction peaks

resulting from Calgon and modified Calgon carbon above $2\theta = 50^\circ$ ((Fig. 7.2) Thus, Calgon carbon appears to be structurally more ordered than Adsorbent carbon.

7.3.3.2 Textural properties of carbon materials - BET Sorptometric Studies

The N_2 adsorption-desorption isotherms of the different treated Adsorbent carbons were typically of the type I (characteristic of microporous materials) while those of the Calgon based samples were slightly different in that some multilayer adsorption was also noticed suggesting the presence of larger (meso) pores (Fig. 7.3).

Table 7.4 Surface area and pores volumes of Adsorbent carbon, Calgon carbon and their modified forms

Carbon	Specific Surface Area (m^2/g)	Total Pore Volume (cm^3/g)
Adsorbent carbon as received	950	0.451
Adsorbent carbon treated with Conc. HNO_3	882	0.398
Adsorbent carbon treated with Conc. HNO_3 followed by Ar activation	1048	0.523
Calgon carbon as received	1014	0.587
Calgon carbon treated with Conc. HNO_3	649	0.387
Calgon carbon treated with Conc. HNO_3 followed by Ar activation	996	0.598
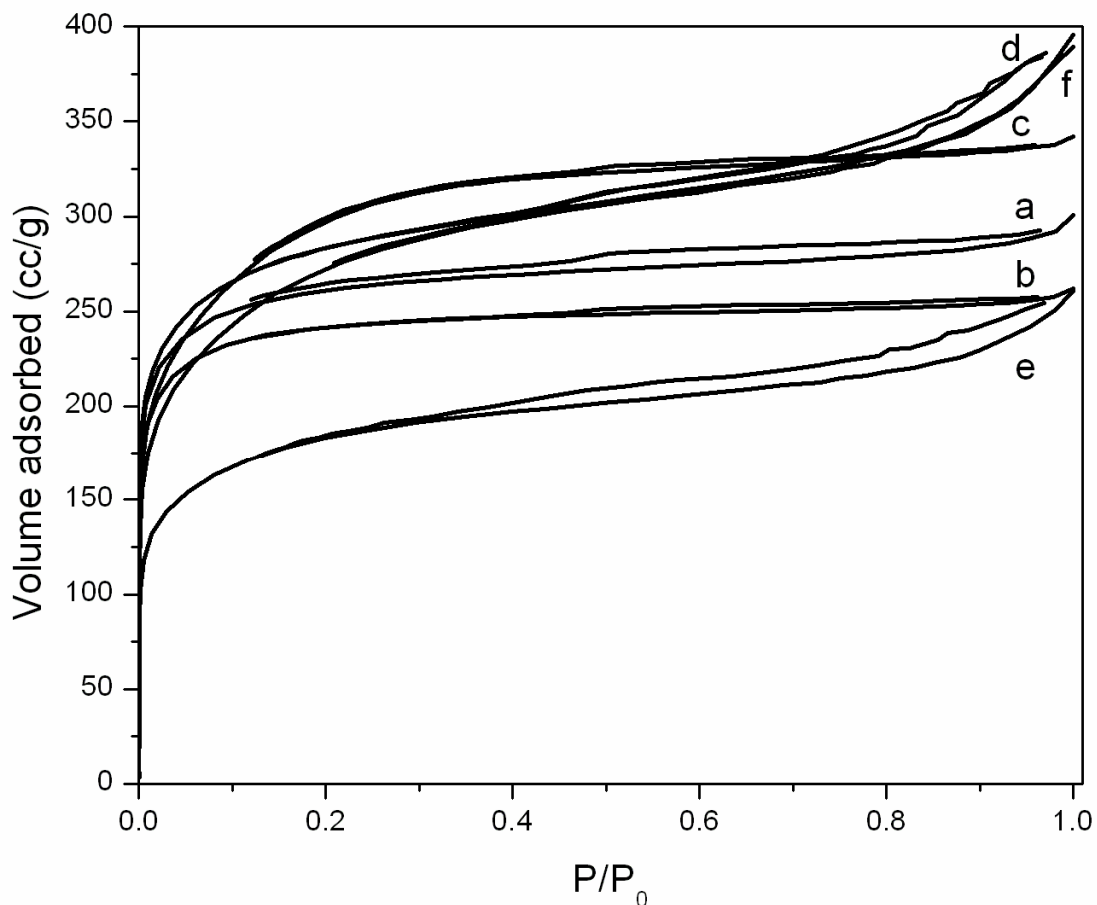
Fig. 7.3 Nitrogen adsorption-desorption isotherms of (a) Adsorbent carbon as received, (b) Adsorbent carbon treated with HNO_3, (c) Adsorbent carbon treated with HNO_3 followed by Ar activation, (d) Calgon carbon as received, (e) Calgon carbon treated with HNO_3 and (f) Calgon carbon treated with HNO_3 followed by Ar activation

The surface area and pore volumes of the different samples are presented in Table 7.4. Analysis of data in Table 7.4 reveals that irrespective of the parent carbon material, HNO_3 treatment essentially reduces specific surface area values and the total pore volume. It is observed both in the case of adsorbent carbon as well as calgon carbon that upon treatment with conc. HNO_3, the surface area values which were originally 950 and 1014 m^2/g were reduced to 882 and 649 m^2/g respectively. Subsequent activation in Ar

atmosphere at 800 °C for 2 h facilitated regaining of the original surface area values in the case of both adsorbent carbon and calgon carbon. Thus Ar activation is inevitable for keeping intact the original textural and porous characteristics of the carbon materials even after treatment with conc. HNO_3 which essentially results in loss of pore volume and in turn specific surface area values.

7.3.3.3 Nature of the surface functional groups on carbon materials - FT - IR studies

The FT-IR spectra of Adsorbent carbon and Calgon carbon, as received, treated with HNO_3 and treated with HNO_3 followed by Ar activation are presented in Figs. 7.4 and 7.5. The main distinguishing feature observed in the Activated carbon samples after nitric acid treatment is the generation of a shoulder at 1749 cm^{-1} (Fig. 7.4. (b)) attributed to the stretching vibration of C=O bond (aldehydes, ketones, lactones or carboxyl groups). This shoulder at 1749 cm^{-1} becomes intense and develops into a sharp peak upon activation in Ar atmosphere (Fig. 7.4. (c)) (Budinova *et al.*, 2006; Ishizaki and Marti, 1981). But for this difference all the three samples showed similar but rich surface chemistry with a variety of oxygen containing functional groups. A number of functional groups are common to Adsorbent carbon and its modified forms (Figs. 7.4. (a), (b) and (c)). These are: a sharp band at 3738 cm^{-1} is ascribed to isolated OH groups, a broad, intense band in the range of 3200-3600 cm^{-1} with a maximum at about 3440 cm^{-1} assigned to the O-H stretching mode of hydroxyl groups and adsorbed water (Madhava Rao *et al.*, 2006) two sharp, narrow and intense bands at 2922 and 2855 cm^{-1} as a result of, respectively, the asymmetric and symmetric C-H stretching vibrations of the methylene group (Puziy *et al.*, 2003; Puziy *et al.*, 2005; Achaw and Afrane, 2008), a

sharp intense peak at 1640 cm^{-1} attributed to the carbonyl groups in quinine, broad bands

observed in the range of 1300 – 1000 cm^{-1} attributed to C-O stretching in acids, alcohols,

phenols, ethers and esters and lastly, broad bands in the range of 600 – 800 cm^{-1} as a

result of the out of plane deformation mode of C-H in various substituted benzene rings

(Madhava Rao *et al.*, 2006; Puziy *et al.*, 2003).
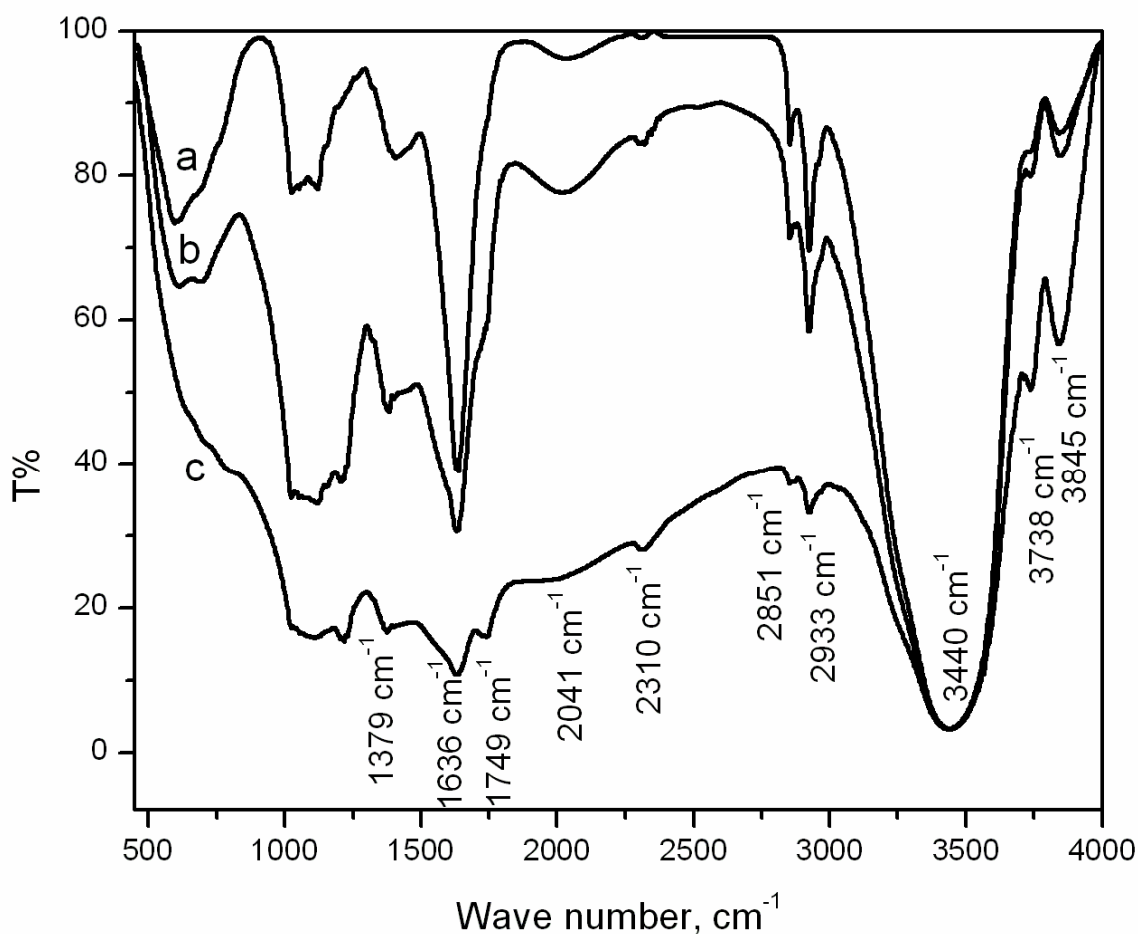
Fig. 7.4 FT-IR spectra of (a) Adsorbent carbon as received, (b) Adsorbent carbon treated
with HNO_3 and (c) Adsorbent carbon treated with HNO_3 and activated with Ar

In the case of the Calgon carbon samples (Fig. 7.5), activation with conc. HNO_3 creates

new bands at 3790, 2305 and 1387 cm^{-1} attributable to isolated O-H groups, ketone

surface groups (Macias-Garcia *et al.*, 2006) and the in-plane bending vibration of C-H in

methyl group (Yang and Lua, 2006) respectively (Fig. 7.5). In addition to the generation of -OH, C=O and –CH$_3$ groups, a broad featureless shoulder is observed in the range 2910-2990 cm^{-1}, due to aliphatic C-H stretching in methylene and methyl groups.

Ar activation of Conc. HNO$_3$ treated Calgon carbon induces certain specific changes into the spectral features. The first and foremost change is the appearance of a broad shoulder at 1753 cm^{-1} attributable to the C=O group of carboxylic acid groups Fig. 7.5 (c). Also, the broad featureless shoulder present in the HNO$_3$ treated Calgon carbon (in the range 2910-2990 cm^{-1}) develops into two clear sharp peaks centered at 2956 and 2918 cm^{-1}, which are attributed to the asymmetric and symmetric stretching vibrations of C-H in methylene groups indicating the generation of hydrophobic methylene C-H groups on the surface of calgon carbon on activation with Ar. In spite of the several striking changes brought about, as discussed above, into the surface functionality of Calgon carbon upon treatment with conc. HNO$_3$ and subsequent Ar activation, some inherent functional groups of parent Calgon carbon remained unaltered even after modification. The spectral features common to all the three samples (Fig. 7.5 (a), (b) and (c)) are as follows: a broad intense transmission peak centered at 3450 cm^{-1} corresponding to OH stretching mode of hydroxyl groups and adsorbed water and a broad intense peak centered at 1075 cm^{-1}, which can be attributed to C-O stretching in acids, alcohols, phenols, ethers and esters (Puziy *et al.*, 2005).
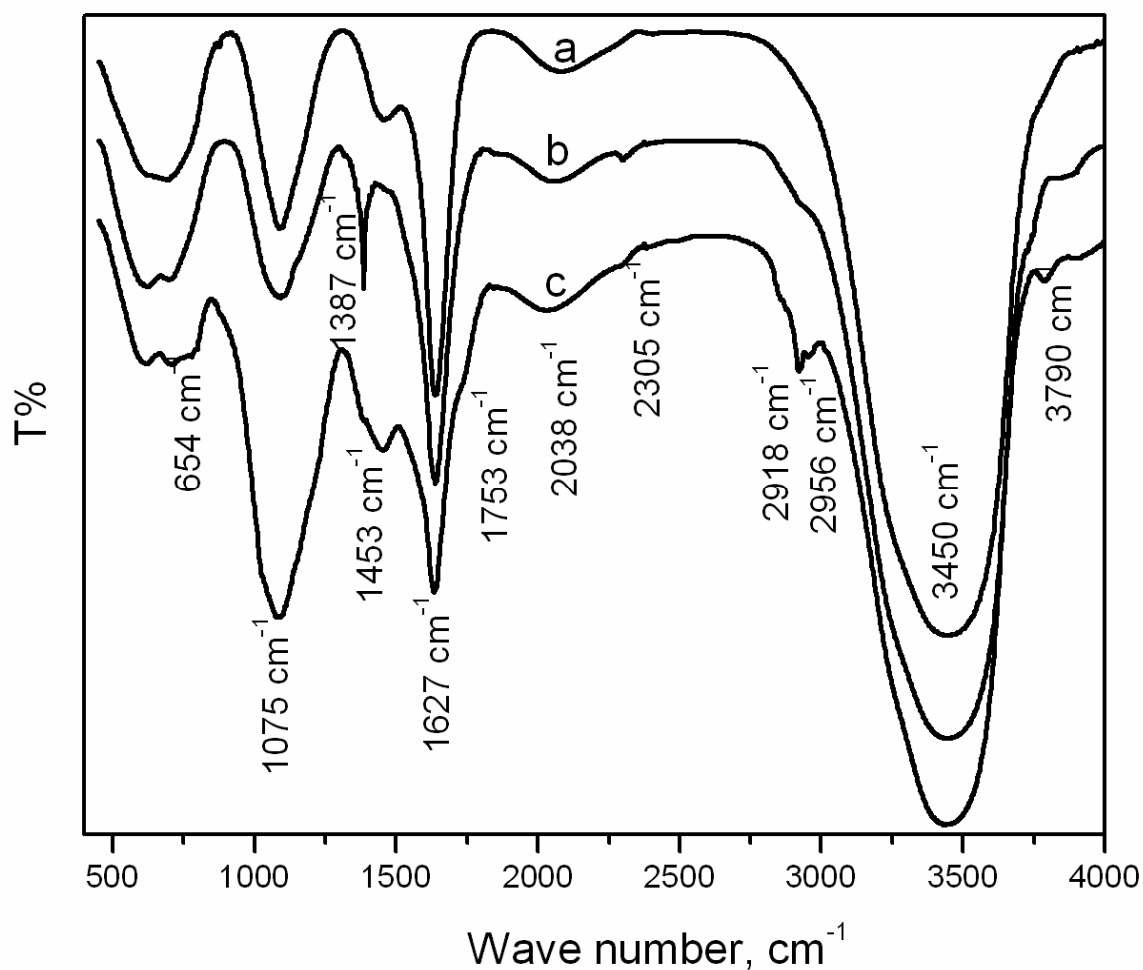
Fig. 7.5 FT-IR spectra of (a) Calgon carbon as received, (b) Calgon carbon treated with HNO$_3$ and (c) Calgon carbon treated with HNO$_3$ followed by Ar activation

7.3.4. Adsorptive desulphurization studies

7.3.4.1. Evaluation of the adsorptive desulphurization potential of adsorbent and calgon based carbon materials

The results of the adsorptive desulphurization experiments carried out on modified carbon materials (acid treatment and Ar activation) are presented in Table 7.5. Both nitric acid treatment and subsequent Ar activation enhanced the S adsorption ability of the carbon samples, the Ar activated samples being more active for adsorption. Combination

of nitric acid treatment and Ar activation induces suitable surface functionality, polarity (surface hydrophilic and hydrophobic functional groups), phase structure (discussed under XRD) and pore structure into the carbon adsorbents facilitating enhanced adsorption of the organo-sulphur compounds present in the diesel feed stocks.

Table 7.5 S sorption capacity of the different carbon samples

Carbon	S removed*, (in ppm)
Adsorbent carbon as received	410
Adsorbent carbon treated with HNO_3	577
Adsorbent carbon treated with HNO_3 followed by Ar activation	586
Calgon carbon as received	451
Calgon carbon treated with HNO_3	488
Calgon carbon treated with HNO_3 followed by Ar activation	619

*S romoved from the first 20 mL diesel after passing through the sorbent bed; S content in the diesel feed – 737 ppm; Carbon loading: 15.0 g

The nature of the S components present in the product diesel was analyzed using GC – PFPD and the results obtained over 15.0 g sorbent bed using modified Adsorbent carbon (A) and Calgon carbon (B) are shown in Table 7.6.

Table 7.6 Type and amount of the S compounds in the feed and the product diesel (after passing through the carbon bed) as analyzed by GC – PFPD

Sulphur Species	S content (in ppm)		
	CBR diesel (Feed)	Adsorbent carbon HNO_3 followed by Ar treatment, 15.0 g	Calgon carbon, HNO_3 followed by Ar treatment, 15.0 g
C_1BT	4.6	Nil	Nil
C_2BT	119.6	Nil	Nil
C_3BT	137.5	75.2	67.2
C_3^+BT	79.6	68.9	47.4
DBT	91.5	2.6	1.3
C_1DBT	157.7	Nil	Nil
C_2DBT	116.7	Nil	Nil
C_3DBT	29.5	4.3	2.1
Total S	737	151	118

*C_1, C_2, C_3, C_3^+ BT and DBT - mono, di, tri and multi alkyl substituted benzothiophene and dibenzothiophenes

It is observed that the most highly refractive compounds (C_2BT and C_2DBT) present in the feed prior to desulphurization process are absent in the product diesel after the adsorption process exemplifying the utility and usefulness of the process in selectively adsorbing the refractory S-compounds that are difficult to desulfurize over conventional hydrotreating catalysts.

7.3.4.2 Method of regeneration of adsorbent
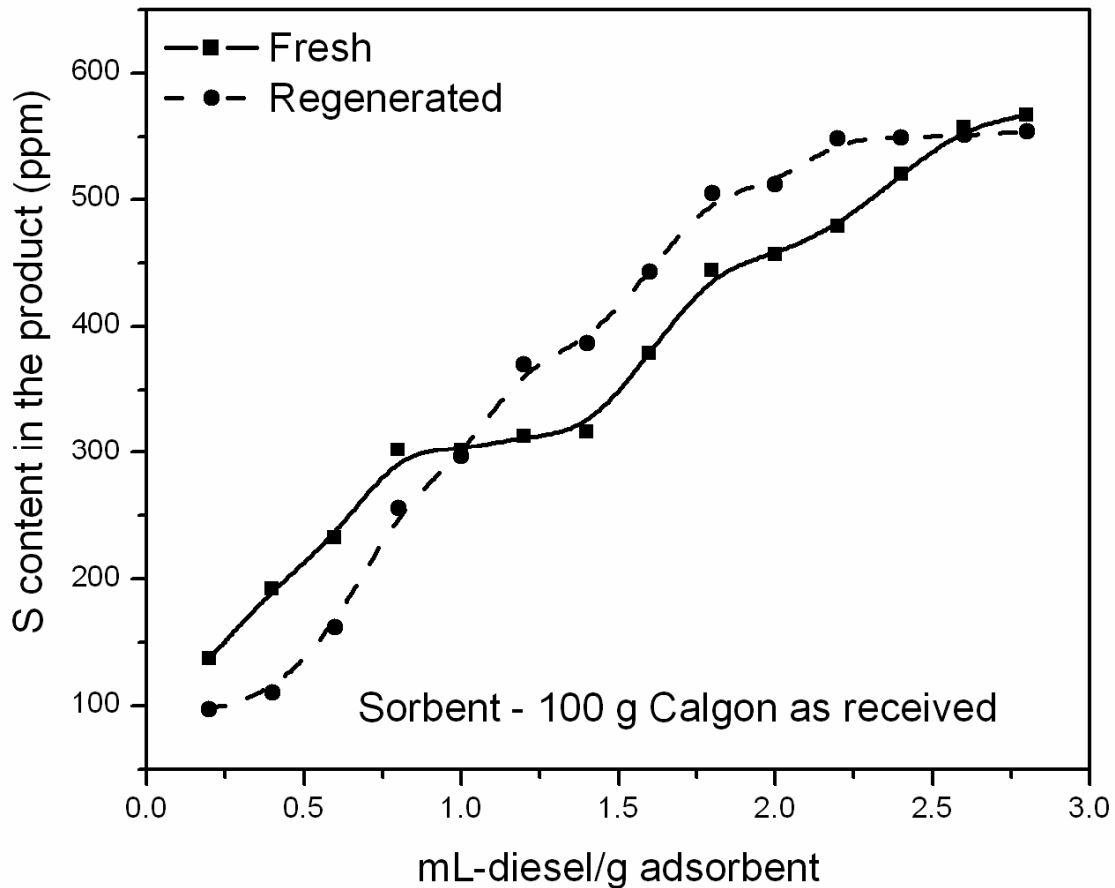
Fig. 7.6 Plot of S removal capacity of fresh Vs toluene regenerated sorbent (100 g Calgon
carbon used as received)

The carbon samples after S-adsorption could be regenerated by washing with toluene
(500 mL for 100 g spent carbon) at room temperature followed by drying the sorbent bed
at 110 °C. The results of the adsorption experiments over neat and solvent regenerated
Calgon carbon (without modification) are shown in Fig. 7.6. It is evident from the
adsorption plots that the regenerated sorbents performance is on par with that of the fresh
Calgon carbon as received. Thus an efficient and environmentally benign regeneration

method and a process for the adsorptive desulfurization appear to be feasible based on carbon materials.

7.4 CONCLUSION

An efficient desulphurization process based on adsorption, operated under modest conditions of temperature (room temperature) and pressure (atmospheric) is developed. New method of activation, which is a unique combination of nitric acid treatment and Ar activation, of carbon based adsorbents to induce desired surface functionality, polarity, phase structure and pore texture is adopted for the first time. It is found that subsequent Ar activation of nitric acid treated carbon adsorbents is inevitable to derive the best out of oxidative modification of carbon surface chemistry. For the first time the utility of adsorbent carbon as well as calgon carbon and their tailored forms as adsorbents for organo sulphur compounds is nicely elucidated. The highly refractive compounds such as substituted di benzothiophenes which are difficult to be removed by conventional HDS process, have been effectively eliminated from the diesel feed. The process of adsorptive desulphurization is scaled upto 100 g (adsorbent) batch. In addition to the successful removal of appreciable amounts of S from diesel feed stocks using tailored carbon based adsorbents, simple, inexpensive, efficient, environmentally benign and reliable solvent (toluene) based regeneration has also been developed. From the studies, it can be anticipated that newer and promising desulphurization technologies are not too far to the refinery industry.

CHAPTER – 8

SUMMARY AND CONCLUSIONS

1. A carbon precursor, a biopolymer from the stems of *Calotropis gigantea*, was exploited for the production of activated carbon with uniform and preferred physico-chemical properties. A variety of activating agents, namely, alkali metal carbonates, alkali metal chlorides, transition metal compounds, carboxylic acids and alkali metal salts of carboxylic acids were evaluated for tuning the textural and morphological features of the activated carbon derivable. Chemical activation with K_2CO_3 as activating agent resulted in the activated carbon material with the highest S_{BET} (1296 m^2/g) and Vp (0.73 cc/g) values. The activated carbon material produced by employing the stems of *Calotrpis gigantea* as a biopolymer resulted in activated carbon material (Cg potassium carbonate 3) with textural properties superior to commercial activated carbon materials (Black Pearl 2000, Vulcan XC 72 R and CDX 975). The activated carbon material possessed unique surface morphology with uniform spherical pores distributed through out the carbon particle. The activated carbon thus obtained was successfully employed as support for dodeca tungstophosphoric acid and the solid acid catalyst derived (10 wt.% HPW/Cg potassium carbonate 3) exhibited superior performance for the synthesis of tert amyl methyl ether (TAME) from methanol and tert amyl alcohol (TAA) compared to Black Pearl 2000 (10 wt.% HPW/Black Pearl 2000) and Vulcan XC 72 R (10 wt.% HPW/Vulcan XC 72 R) counterparts. Thus a widely available, inexpensive carbon precursor was successfully transformed into a value added activated carbon material and

the same was exploited for the design of solid acid catalyst (10 wt.% HPW/Cg potassium carbonate 3) for the synthesis of TAME.

2. Activated carbon (C_{Bf} potassium carbonate 1) with a high S_{BET} (1070 m^2/g) and Vp (0.55 cc/g) values was produced from the male flower spikes of *Borassus flabellifera* by the chemical (K_2CO_3) activation method. The activated carbon material was employed as a support for dodecatungsto phosphoric acid (HPW). The HPW/C_{Bf} potassium carbonate 1 catalyst was exploited for the vapour phase methyl tert butyl ether (MTBE) synthesis from methanol and tert butyl alcohol (TBA). The effect of various reaction parameters like temperature and the mole ratio of the reactants (methanol:TBA) was evaluated. The optimum reaction conditions were found to be as follows: Reaction temperature – 373 K; mole ratio of methanol:TBA – 10:1. The flow rate of the feed and the carrier gas were 10 mL/h and 30 mL/min respectively. Mesoporous silica (SBA-1) with S_{BET} (918 m^2/g) and Vp (0.46 cc/g) values comparable to those of the activated carbon material was prepared using CTMAB as surfactant and TEOS as silica source. For comparison, the performance of mesoporus silica (SBA-1) supported HPW for the synthesis of MTBE relative to carbon supported HPW was evaluated. The performance (activity, selectivity and stability) of 20 wt.% HPW/C_{Bf} potassium carbonate 1 was found to be on par with 20 wt.% HPW/SBA-1. Thus an economically viable, environmentally benign and industrially adoptable solid acid catalyst (20 wt.% HPW/C_{Bf} potassium carbonate 1) was developed for the synthesis of MTBE from methanol and TBA.

3. High specific surface area activated carbon, C_{WA} (698 m^2/g) was prepared from the shells of *Limonea acidissima* by chemical activation with KOH and HNO$_3$. The carbon material was found to possess turbostratic graphitic structure. The surface of the activated carbon is rich in oxygen containing (carbonyl, C=O, 1637 cm^{-1}) functional groups. Even though, both ordered (graphitic) and disordered carbon structures were present in the activated carbon material, the Raman intensity ratio (R=1.408) was found to be characteristic of disordered carbon material analogous to the glassy carbon. The activated carbon material was employed as support for Pt and the supported catalysts (5, 10 and 20 wt.% Pt/C_{WA}) produced by the method of dry impregnation followed by reduction in H$_2$ atmosphere were exploited for the electro oxidation of methanol for possible electrode (anode) applications in Direct Methanol Fuel Cells. Pt metal on the carbon support was found to be in *fcc* lattice. The lattice constant value of ~ 0.39 nm correlated well with the *fcc* lattice of Pt metal on the carbon support. The crystallite size of Pt in 5, 10, 20 wt.% Pt/C_{WA} catalysts were respectively, 5.0, 10.2 and 10.4 nm. Thus the crystallite size of Pt which is the critical parameter governing the electro catalytic property of Pt/C catalysts was found to be dependent on the Pt loading and also the nature of the carbon support employed. For comparison, Vulcan XC 72 R carbon black was also employed as support and 20 wt.% Pt/Vulcan XC 72 R catalyst was prepared under identical condition and the crystallite size of Pt in this case was found to be 13.1 nm. Relatively smaller crystallite size values of Pt derivable on carbon support produced from *Limonea acidissima* by chemical activation is attributed to the oxygen containing surface functional groups and also to the higher specific surface area value. The S_{BET} values of Pt/C_{WA} catalysts decreased from 505 to 123 m^2/g as the wt.% loading of Pt increased

from 5 to 20 wt.%. The electro oxidation reaction of methanol carried out on Pt/C catalysts was monitored by cyclic voltammetry. Irrespective of the carbon support and the amount of the active component, two anodic peaks, one in the forward scan and the other in the reverse scan respectively attributable to the oxidation of methanol and the removal of the incompletely oxidized carbonaceous species formed in the forward scan. Among different electro catalysts evaluated, the 5 wt.% Pt/C$_{WA}$ exhibited high current density value (69 mA/cm^2) which is an indication of higher electro chemical catalytic activity at a relatively lower onset potential value (0.21 V). In addition to the high current density and the lower onset potential values, the ratio of the anodic peak current densities in the forward (i_f) and the reverse (i_b) scans is an order of magnitude higher (14.4) in the case of 5 wt.% Pt/C$_{WA}$ compared to either 10 wt.% Pt/C$_{WA}$ (1.45), 20 wt.% Pt/C$_{WA}$ (1.60) or 20 wt.% Pt/Vulcan XC 72 R (0.96). A higher i_f/i_b value is a reflection of better CO tolerance. Only 24 % loss in the initial activity at the end of 3 h was observed in the case of 5 wt.% Pt/C$_{WA}$ compared to 36 and 89 % activity losses observed in the case of 10 wt. % Pt/C$_{WA}$ and 20 wt.% Pt/CWA as indicated from the chronoamperometric studies implying better long term stability of 5 wt.% Pt/C$_{WA}$. The high activity, stability and CO tolerance of 5 wt.% Pt/C$_{WA}$ are as a result of the small Pt crystallites (5.0 nm) distributed through out the carbon surface because of the high specific surface area as well as the richness of oxygen containing surface functional groups. Thus a highly active, stable and CO tolerant anode electro catalyst was developed at a modest wt.% loading of Pt over the activated carbon support produced from the shells of *Limonea acidissima*.

4. Removal of 55.6 mg Hg (II) per g of S functionalized activated carbon produced from *Ipomoea carnea* was achieved in a batch mode adsorption process. The adsorption capacity of the activated carbon from Ipomoea carnea was found to be greater than several other adsorbents, namely, activated carbon materials from *Cieba pentandra* hulls (25.88 mg/g), *Phaseolus aureus* hulls (23.66 mg/g), *Cicer arietinum* (22.88 mg/g) Bolluca coal (37.0 mg/g), carbon cloth (37 mg/g) and used tyre rubber (14.6 mg/g). S functionalization (generation of C=S groups, 1165 cm^{-1}) of activated carbon material improved the sorption capacity of activated carbon material. Unadsorbed Hg (II) remaining in solution was estimated by a simple and reliable method based on spectrophotometry wherein Hg (II) species were allowed to form complex (R_2HgI_4) with Rhodamine 6 G (R) reagent and KI as a result of which pink colouration is developed. The absorbance of R_2HgI_4 complex is at 575 nm. Process parameters such as the effect of pH, sorbent dosage, initial Hg (II) concentration, Hg (II) concentration and contact time on the adsorption of Hg (II) were evaluated. The equilibrium adsorption data were analyzed by Freundlich and Langmuir adsorption models. The equilibrium data fitted well with both Freundlich and Langmuir adsorption models. The Langmuir constants were found to be : q_m = 55.6 mg/g; b = 0.095 L/mg; R_L = 0.51. The Freundlich constants were found to be : K_F = 8.3 mg$^{1-1/n}$ L$^{1/n}$g^{-1} ; 1/n = 0.51. Thus a low cost and effective carbon based adsorbent for the removal of Hg (II) was developed from the stems of *Ipomoea carnea*.

5. Several commercially available activated carbon materials, namely, IG 18 x 40, IG 12 x 10, IG 8 x 30, AC 4 x 8, AC 6 x 12, AC 12 x 30, Adsorbent carbon and Calgon carbon

with varying physico chemical properties were evaluated as sorbents for the reduction of S from 737 ppm to less than 200 ppm in the straight run (SR) diesel from Cauvery Basin Refinery (CBR), Narimanam, Tamil Nadu. Preliminary screening studies indicated the potential of adsorbent and calgon based carbon for the adsorptive elimination of S containing species from the diesel under modest conditions of temperature and pressure by a simple fixed bed adsorption process. The S content in the product after the adsorption process was analyzed by XRF studies. In addition, the individual sulphur compounds present in the feed as well as the products were also analyzed using a Gas Chromatography – Pulsed Flame Photometric Detector (GC-PFPD) so as to know the nature of the actual S – compounds which were adsorbed on the sorbent bed and removed in the adsorptive desulphurization process. The surface of the adsorbent and calgon carbon materials was tailored to enhance the sorption capacity for S compounds in the diesel. Oxygen containing surface functional groups are known to enhance the sorption of organo sulphur compounds. Treatment of both calgon and adsorbent carbon materials with nitric acid resulted in the formation of carboxylic acid groups (1745-1755 cm^{-1}) on the carbon surface. In addition to HNO_3 treatment subsequent thermal activation in Ar atmosphere resulting in the generation of methylene groups that impart the required hydrophobicity to the carbon surface is inevitable. Such a modification of carbon surface enhanced the sorption capacity of both adsorbent and calgon carbon materials and the use of the modified calgon and adsorbent carbon materials as sorbent in the fixed bed reactor has effectively reduced the S content of the feed to less than 200 ppm fulfilling the desired objective. More over, the highly refractive compounds such as substituted dibenzothiophenes were completely and effectively eliminated from the diesel feed. The

241

process of adsorptive desulphurization was scaled upto 100 g batch where the modified calgon and adsorbent carbon sorbents showed promising performace. Toleune based regeneration process of the sorbent bed was developed. Thus a promising, adoptable and inexpensive desulphurization process based on adsorption was developed.

Salient features of the work include:

♥ Activated carbon materials with desired properties were synthesized from novel lignocellulosic materials, such as, *Calotropis gigantea* stems, *Borassus flabellifera* male flower spikes, *Limonea acidissima* shells, *Ipomoea carnea* stems.

♥ The properties and performance of the carbon materials produced were evaluated relative to commercially available activated carbon materials like Black Pearl 2000, Vulcan XC 72 R, Nuchar, Calgon, Adsorbent and CDX 975.

♥ The carbon materials developed were successfully exploited as sorbent (for mercury from aqueous solution and organo sulphur compounds from diesel) and as catalyst support (for Pt and HPW) in designing catalysts for the methanol electro oxidation (Pt/C) and also for the synthesis gasoline additives such as MTBE and TAME (HPW/C).

The contents of the present thesis thus deal with the exploitation of common carbon materials from natural sources for strategically important reactions.

It is finished
St. John 19 : 30

REFERENCES

1.   **Aburto, J., A. Mendez-Orozco** and **S. L. Borgne** (2004) Hydrogels as adsorbents of organosulphur compounds currently found in diesel. *Chem. Eng. Process*., **43**, 1587-1595.

2.   **Acharya, J., J. N. Sahu, C. R. Mohanty** and **B. C. Meikap** (2009a) Removal of lead (II) from wastewater by activated carbon developed from Tamarind wood by zinc chloride activation. *Chem. Eng. J*., **149**, 249-262.

3.   **Acharya, J., J. N. Sahu, B. K. Sahoo, C. R. Mohanty** and **B. C. Meikap** (2009b) Removal of chromium (VI) from wastewater by activated carbon developed from Tamarind wood activated with zinc chloride. *Chem. Eng. J*., **150**, 25-39.

4.   **Achaw, O. W.** and **G. Afrane** (2008) The evolution of the pore structure of coconut shells during the preparation of coconut shell – based activated carbons. *Microporous Mesoporous Mater*., **112**, 284-290.

5.   **Adams, M. D**. (1991) The mechanism of adsorption of $Hg(CN)_2$ and $HgCl_2$ onto activated carbon. *Hydrometallurgy*, **26**, 201-210.

6.   **Agarwal, A. K., A. K. Bansal, M. N. Ansari, M. C. Jain** and **J. S. Upadhyaya** (1992) Non-wood fibrous plants for pulp and paper manufacture (Adhatoda vasica, Ipomoea carnea and Ricinus communis) – Chemical and anatomical studies. *Chimica Acta Turcica*, **20**, 253-258.

7.   **Agueda, V. I., J. L.Sotelo, M. A. Uguina** and **R. Rodriguez** (in press) Synthesis of mesoporous aluminophosphates impregnated with metals and their application in gas oil desulphurization by adsorption. *J. Mater. Sci.,* (in press)

8.   **Alcaniz-Monge, J., M. A. D. Casa-Lillo, D. Cazorla - Amoros** and **A. Linares-Solano** (1997) Methane storage in activated carbon fibres. *Carbon*, **35**, 291-297.

9.   **Alcaniz-Monge, J., G. Trautwein, S. Parres-Esclapez** and **J. A. Macia-Agullo** (2008) Influence of microporosity of activated carbon as a support of polyoxometalates. *Microporous Mesoporous Mater*., **115**, 440-446.

10.   **Alhamed, Y. A.** and **H. S. Bamufleh** (2009) Sulfur removal from model diesel fuel using granular activated carbon from dates' stones activated by $ZnCl_2$, *Fuel*, **88**, 87-94.

11.   **Ali, M. A., B. J. Brisdon** and **W. J. Thomas** (2000) Intrinsic kinetics of MTBE synthesis from methanol and isobutene using a synthesized MFI type zeolite. *Appl. Catal. A : Gen*., **197** , 303-309.

12. **Al-Muhtaseb, S. A., M. H. El-Naas** and **S. Abdallah** (2008) Removal of aluminum from aqueous solutions by adsorption on date-pit and BDH activated carbons. *J. Hazard. Mater*., **158**, 300-307.

13. **Alvarez, P., C. Blanco** and **M. Granda** (2007) The adsorption of chromium (VI) from industrial waste water by acid – base – activated lignocellulosic residues. *J. Hazard. Mater*., **144**, 400-405.

14. **Ancillotti, F.** and **V. Fattore** (1998) Oxygenate fuels : Market expansion and catalytic aspect of synthesis. *Fuel Process. Technol.,* **57**, 163-194

15. **Ania, C. O., J. B. Parra, A. Arenillas, F. Rubiera, T. J. Bandosz** and **J. J. Pis** (2007) On the mechanism of reactive adsorption of dibenzothiophene on organic waste derived carbons. *Appl. Surf. Sci.* **253**, 5899-5903.

16. **Anirudhan, T. S., L. Divya** and **M. Ramachandran** (2008) Mercury (II) removal from aqueous solutions and wastewaters using a novel cation exchanger derived from coconut coir pith and its recovery. *J. Hazard. Mater*., **157**, 62-627.

17. **Aranda, A., R. Murillo, T. Garcia, M. S. Callen** and **A. M. Mastral** (2007) Steam activation of tyre pyrolytic carbon black : Kinetic study in a thermo balance. *Chem. Eng. J*., **126**, 79-85.

18. **Arivoli, S., M. Sumathi, K. Bharathiraja, S. Santhilkumar** and **T. Rajachandrasekar** (2007) Adsorption kinetics and thermodynamics of copper metal ion onto acid activated low cost carbon. *Oriental Journal of Chemistry*, **23**, 523-532.

19. **Attia, A. A., B. S. Girgis** and **N. Fathy** (2008) Removal of methylene blue by carbons derived from peach stones by H_3PO_4 activation : Batch and column studies. *Dyes and Pigments,* **76**, 282-289.

20. **Babich, I. V.** and **J. A. Moulijn** (2003) Science and technology of novel processes for deep desulphurization of oil refinery streams : a review. *Fuel*, **82**, 607-631.

21. **Bagotzky, V. S., Y. B. Vassiliev** and **O. A. Khazova** (1977) Generalized scheme of chemisorption, electro-oxidation and electro-reduction of simple organic compounds on Pt group metals. *J. Electroanal. Chem*., **81**, 229-238.

22. **Basar, C. A.** (2006) Applicability of the various adsorption models of three dyes adsorption onto activated carbon prepared from waste apricot. *J. Hazard. Mater*., **B135**, 232-241.

23. **Battistoni, P., S. Bompadre** and **G. Fava** (1984) Commercial activated carbon acidified by nitric acid oxidation. Effect of particle and pore size on the production of surface oxide structures. *Mater. Chem. Phys.* **11**, 339-350.

24. **Bedia, J., J. M. Rosas, J. Marquez, J. Rodriguez – Mirasol** and **T. Cardero** (2009) Preparation and characterization of carbon based acid catalysts for the dehydration of 2 – propanol. *Carbon*, **47**, 286-294.

25. **Behera, N. C.** and **K. N. Tiwary** (1980) Preliminary studies on the utilization of Ipomoea carnea Jacq. for pulp and paper. *Indian Pulp and Paper*, **34**, 7-9.

26. **Benaddi, H., T. J. Bandosz, J. Jagiello, J. A. Schwarz, J. N. Rouzaud, D. Legras** and **F. Beguin** (2000) Surface functionality and porosity of activated carbons obtained from chemical activation of wood carbon. *Carbon*, **38**, 669-674.

27. **Bhadra, A., J. M. Scharer** and **M. Moo-Young** (1987) Microbial desulphurization of heavy oils and bitumen. *Biotechnol., Adv.*, **5**, 1-27.

28. **Bhalerao, S. A.** and **S. B. Chaphekar** (2009) Ipomea carnea Jacq. for immobilization of solid wastes. *Nature, Environment and Pollution Technology*, **8**, 105-110.

29. **Bhudinova, T., N. Petrov, J. Parra** and **V. Baloutzov (2008)** Use of an activatead cabron from antibiotic waste for the removal of Hg (II) from aqueous solution. *J. Environ. Manage.*, **88**, 165-172.

30. **Bonardet, J. L., J. Fraissaid, G. B. Mc Garvey** and **J. B. Moffat** (1995) Comparative study of the microporosity of the ammonium and cesium salts of 12-tungtophosphoric, 12-molybdophosphoric and 12-tungstosilicic acids by Xe^{129} NMR. *J. Catal.*, **151**, 147-154.

31. **Boonamnuayvitaya, V., S. Sae-ung** and **W. Tanthapanichokoon** (2005) Preparation of activated carbons from coffee residue for the adsorption of formaldehyde. *Sep. Purif. Technol.*, **42**, 159-168.

32. **Borah, D**. (2005) Cleavage of C-S bond in thourea by electron transfer process with Cu^+ ion as a model study of sulphur removal and recovery. *Sep. Purif. Technol.*, **43**, 215-219.

33. **Boz, N., T. Dogu, K. Murtezaoglu** and **G. Dogu** (2005) Mechanism of TAME and TAEE synthesis from diffuse-reflectance FTIR analysis, *Catal. Today,* **100**, 419-424.

34. **Brader, M. L., E. W. Ainscough, E. N. Baker** and **A. M. Brodie** (1989) Copper (II) promoted desulphurization of N-Phenyl thio urea. The synthesis and X-ray structure of [{Cu(bipy)(pc)2}2] (bipy = 2, 2' – bipyridine, pc = phenyl cyanamide). *Polyhedron*, **8**, 2219-2221.

35. **Breysse, M., G. Djega-Mariadassou, S. Pessayre, C. Geantet, M. Vrinat, G. Perot and M. Lemaire** (2003) Deep desulfurization : reactions, catalysts and technological challenges. *Catal. Today*, **84**, 129-138.

36. **Brown, G. M., M. R. Noe-Spirlet, W. R. Busing** and **H. A. Levy** (1977) Dodecatungsto phosphoric acid hexa hydrate, $(H_5O_2^+)_3$ $(PW_{12}O_{40}^{3-})$: The true structure of Keggin's 'pentahydrate' from single crystal X-ray and neutron diffraction data. *Acta. Crystallogr.*, B, **33**, 1038-1046.

37. **Bruckman, K., J. M. Tatibouet, M. Che, E. Serwicka** and **J. Haber** (1993) Catalytic behaviour of unsupported $H_{3+n}PV_nMO_{12-n}O_{40}$. Heteropoly acids in the test reaction of CH_3OH oxidation. *J. Catal.*, **139**, 455-467.

38. **Budinova, T., E. Ekinci, F. Yardim, A. Grimm, E. Bjornbom, V. Minkova** and **M. Goranova** (2006) Characterization and application of activated carbon produced by H_3PO_4 and water vapour activation. *Fuel Process. Techonol.*, **87**, 899-905.

39. **Budinova, T., E. F. Yardim, A. Grimm, E. Bjornbom, V. Minkova** and **M. Goranova** (2006) Characaterization and application of activated carbon produced by H_3PO_4 and water vapour activation. *Fuel Process. Techonol.*, **87**, 899-905.

40. **Caballero, J. A., A. Marcilla** and **J. A. Conesa** (1997) Thermogravimetric analysis of olive stones with sulphuric acid treatment. *J. Anal. Appl. Pyrolysis,* **44**, 75-88.

41. **Cao, Q., K. Chang, Y. Lv** and **W. Bao** (2006) Process effects on activated carbon with large specific surface area from corn cob. *Bioresour. Technol.*, **97**, 110-115.

42. **Cao, B., W. Shen** and **Y.Liu** (2008) Adsorption desulphurization of gasoline by silver loaded onto modified activated carbons. *Adsorpt. Sci. Technol.,* **26**, 595-609.

43. **Carrasco-Marin, F., M. A. Alvarez-Merino** and **C. Moreno-Castilla** (1996) Microporous activated carbons from a bituminous coal. *Fuel*, **75**, 966-970.

44. **Carrette, L., K. A. Friedrich** and **U. Stimming** (2001) Fuel cells-Fundamentals and applications. *Fuel cells*, **1**, 5-39.

45. **Carrott, P. J. M., M. M. L. R. Carrott** and **J. M. V. Nabais** (1998) Influence of surface ionization on the adsorption of aqueous mercury chloro complexes by activated carbons. *Carbon*, **36**, 11-17.

46. **Castro, B., M. J. Whitcombe, E. N. Vulfeon, R. Vazquez-Duhalt** and **E. Barzana** (2001) Molecular imprinting for the selective adsorption of organo sulphur compounds present in fuels. *Anal. Chim. Acta*, **435**, 83-90.

47. **Caturla, F., M. Molina-Sabio** and **F. Rodriguez-Reinoso** (1991) Preparation of activated carbon by chemical activation with $ZnCl_2$. *Carbon,* **29**, 999-1007.

48. **Centeno, T. A.** and **H. F. Stoeckli** (2006) Method of producing activated carbons from apple pulp for use as electrodes in electric double – layer capacitors (EDLC), PCT Int Appl., Pat. No. W02006103310.

49. **Chandra, T. C., M. M. Mirna, Y. Sudaryanto** and **S. Ismadji** (2007) Adsorption of basic dye onto activated carbon prepared from durian shell : Studies of adsorption equilibrium and kinetics, *Chemical Eng. J.*, **127**, 121-129.

50. **Chauvert, O.** and **L. Forro** (1995) Magnetic anisotropies of aligned carbon nanotubes.. *Phys. Rev. B Condens. Mater.,* **52**, R6963-R6966.

51. **Chen, X., S. Jeyaseelan** and **N. Graham** (2002) Physical and chemical properties study of the activated carbon made from sewage sludge. *Waste Management,* **22**, 755-760.

52. **Chen, Y. X., A. Miki, S. Ye, H. Sakai** and **M. Osaka** (2003) Formate, an active intermediate for direct oxidation of methanol on Pt electrode. *J. Am. Chem. Soc.*, **125**, 3680-3681.

53. **Chimienti, M. E., L. R. Pizzio, C. V. Caceres** and **M. N. Blanco** (2001) Tungstophosphoric and tungstosilicic acids on cabron as acidic catalysts. *Appl. Catal., A : Gen.*, **208**, 7-19.

54. **Chuang, C. L., M. Fan, M. Xu, R. C. Brown, S. Sung, B. Saha** and **C. P. Huang** (2005) Adsorption of arsenic (V) by activated carbon prepared from oat hulls. *Chemosphere*, **61**, 478-483.

55. **Chu, W., X. Yang, X. Ye** and **Y. Wu** (1996) Vapour phase esterification catalyzed by immobilized dodecatungsto silicic acid (SiW_{12}) on activated carbon. *Appl., Catal. A : Gen.,* **145**, 125-140.

56. **Collignon, F., M. Mariani, S. Moreno, M. Remy** and **G. Poncelet** (1997) Gas phase synthesis of MTBE from methanol and isobutene over dealuminated zeolites. *J. Catal.,* **166**, 53-66.

57. **Collins, F. M., A. R. Lucy** and **C. Sharp** (1997) Oxidative desulphurization of oils via hydrogen peroxide and heteropoly anion catalysis. *J. Mol. Catal. A., Chem.* **117**, 397-403.

58. **Corcho-Corral, B., M. Olivares - Marin, C. Fernandez-Gonzalez, V. Gomez-Serrano** and **A. Macias-Garcia** (2006) Preparation and textural characterization of activated carbon from vine shoots (Vitis vinifera) by H_3PO_4 - chemical activation. *Appl. Surf. Sci.*, **252**, 5961-5966.

59.   **Corma, A.** (1997) Solid acid catalysts, *Curr. Opin. Solid State and Mater. Sci*., **2**, 63-75.

60.   **Cotton, F. A.** and **G. Wilkinson** Basic Inorganic Chemistry, John Wiley & Sons, 1976.

61.   **Dai, L., Y. Teng, K. Tabata, E. Suzuki** and **T. Tatsumi** (2001) Catalytic applications of Mo-incorporated SBA-1 mesoporous molecular sieves to partial oxidation of methane. *Microporous Mesoporous Mater*., **44**, 573-580.

62.   **Dai, W., Y. Zhou, S. Wang, L. Long** and **L. Zhong** (2007) Catalytic oxidation of thiophenes with air and PW/SBA-15. *Adsorpt. Sci. Technol.,* **25**, 385-394.

63.   **Daifullah, A. A. M., S. M., Yakout** and **S. A. Elreefy** (2007) Adsorption of fluoride in aqueous solutions using $KMnO_4$ - modified activated carbon derived from steam pyrolysis of rice straw. *J. Hazar. Mater*., **147**, 633-643.

64.   **Danwanichakul, P., D. Dechojarasrri, S. Meesumrit** and **S. Swangwareesakul** (2008) Influence of sulfur-crosslinking in vulcanized rubber chips on mercury (II) removal from contaminated water. *J. Hazard. Mater*., **154**, 1-8.

65.   **Dastgheib, S. A.** and **D. A. Rockstraw** (2001) Pecan shell activated carbon : Synthesis, characterization and application for the removal of copper from aqueous solution. Carbon 39, 1849-1855.

66.   **Davini, P.** (1999) Desulphurization properties of active carbons obtained from petroleum pitch pyrolysis. *Carbon*, **37**, 1363-1371.

67.   **Demirbas, E., M. Kobya** and **M. T. Sulak** (2008) Adsorption kinetics of a basic dye from aqueous solutions onto apricot stone activated carbon. *Bioresour. Technol*., **99**, 5368-5373.

68.   **Devarly, P., Y. Kartika, N. Indraswati** and **S. Ismadji** (2008) Activated carbon from jack fruit peel waste by H_3PO_4 chemical activation: Pore structure and surface chemistry characterization. *Chem. Eng. J*., **140**, 32-42.

69.   **Diaz, R., A. Hernandex, R. Quintana, C. Cabrera** and **E. Diaz** (2001) Development of kinetic models for gas phase MTBE production. *Catal. Today*, **65**, 373-380.

70   **Dickinson, A. D**. Great Leaders of the world - Stories of Achievement, Garden City Publishing Co, Inc. Garden city, New York, 1937.

71.   **Dicks, A. L**. (2006) The role of carbon in fuel cells. *J. Power Sources*, **156**, 128-141.

72. **Donnet, J. B., R. Bansal** and **M. Wang** (1993) Carbon Black – Science and Technology. Second Edition, Revised and Expanded, CRC publications.

73. **Eisch, J. J., L. E. Hallenbeck** and **M. A. Lucarelli** (1985) Desulphurization and denitrogenation of SRC liquids by transition metals on solid supports. *Fuel*, **64**, 440-442.

74. **Ekinci, E., T. Budinova, F. Yardim, N. Petrov, M. Razvigorova** and **V. Minkova** (2002) Removal of mercury ion from aqueous solution by activated carbons obtained from biomass and coals. *Fuel Process. Technol*., **77-78**, 437-443.

75. **El-Hendaway, A. A.** (2003) Influence of HNO_3 oxidation on the structure and adsorptive properties of corncob based activated carbon. *Carbon*, **41**, 713-722.

76. **Endo, M., C. Kim, K. Nishimura, T. Fujino** and **K. Miyashita** (2000) Recent development of Carbon materials for Li ion batteries. *Carbon*, **38**, 183-197.

77. **Endo, M., T. Matsumoto, J. Kubota** and **C. Hirose** (2000) Formation of formate in the deep oxidation of methanol on Pt (111) under UHV condition studied by IRAS. *J. Phys. Chem., B*, **104**, 4916-4922.

78. **Endo, M., T. Matsumoto, J. Kubota** and **C. Hirose** (2001) In situ IRAS observation of catalytic deep oxidation of MeOH on Pt (111) under amibient pressure conditions. *J. Phys. Chem. B*., **105**, 1573-1577.

79. **Fan, M., W. Marshall, D. Daugaard** and **R. C. Brown** (2004) Steam activation of chars produced from oat hulls and corn stover. *Bioresour. Technol*., **93**, 103-107.

80. **Filho, N. L. D., W. L. Polito** and **Y. Gushikem** (1995) Sorption and preconcentration of some heavy metals by 2-mercaptobenzothiazole – clay. *Talanta*, **42**, 1031-1036.

81. **Freitas, J. C. C., T. J. Bonagamba** and **F. G. Emmerich** (2001) Investigation of biomass-and polymer-based carbon materials using ${}^{13}C$ high-resolution solid-state NMR. *Carbon*, **39**, 535-545.

82. **Freitas, J. C. C., G. F. Emmerich** and **T. J. Bonagamba** (2000) High-resolution solid-state NMR study of the occurence and thermal transformation of silicon-containing species in biomass materials. *Chem. Mater*., **12**, 711-718.

83. **Freitas, J. C. C., J. B. Tito** and **F. G. Emmerich** (2001) Investigation of biomass and polymer-based carbon materials using ${}^{13}C$ high-resolution solid-state NMR. Carbon, **39**, 535-545.

84.	**Ganan, J., J. F. Gonzalez, C. M. Gonzalez-Garcia, A. Ramiro, E. Sabio** and **S. Roman** (2006) Air-activated carbons from almond tree pruning : Preparation and characaterization. *Appl. Surf. Sci*., **252**, 5988-5992.

85.	**Ganpat, P.V., M. Menachem and G. Aharon, C.M Jose** and **Y. Masahiro** (2004) Carbon spherules : Synthesis, properties and mechanistic elucidation. *Carbon*, **42**, 111-116.

86.	**Gercel, O., A. Ozcan, A. S. Ozcan** and **H. F. Gercel** (2007) Preparation of activated carbon from a renewable bio-plant of Euphorbia rigida by H_2SO_4 activation and its adsorption behaviour in aqueous solutions. *Appl. Surf. Sci*., **253**, 4843-4852.

87.	**Ghosh, A. K.** and **J. B. Moffat** (1986) Acidity of heteropoly compounds. *J. Catal.*, **101**, 238-245.

88.	**Gil, A., G. D. Puente** and **P. Grange** (1997) Evidence of textural modifications of an activated carbon on liquid – phase oxidation treatments. *Microporous Mater*., **12**, 51-61.

89.	**Girgis, B. S., A. A. Attia** and **N. A. Fathy** (2007) Modification in adsorption characteristics of activated carbon produced by H_3PO_4 under flowing gases. *Colloids Surf., A: Physico Chem. Eng. Aspects*, **299**, 79-87.

90.	**Girgis, B. S., S. S. Yunis** and **A. M. Soliman** (2002) Characteristics of activated carbon from peanut hulls in relation to conditions of preparation. *Materials Letters,* **57**, 164-172.

91.	**Gokam, A. N.** and **N. V. Sankpal** (2000) An improved process for the manufacture of activated carbon, Patent No. IN 2000DE01216.

92.	**Gomez-Serrano, V., M. Acedo-Ramos, A. J. Lopez-Peinado and C. Valenzuela-Calahorro** (1997) Mass and surface changes of activated carbon with nitric acid. Thermal behaviour of the samples. *Thermochim., Acta,* **291**, 109-115.

93.	**Gomez-Serrano, V., E. M. Cuerda-Correa, M. C. Fernandez-Gonzalez, M. F. Alexandre-Franco** and **A. Macias-Garcia** (2005) Preparation of activated carbons from chestnut wood by phosphoric acid – chemical activation study of microporosity and fractal dimension. *Mater. Lett*., **59**, 846-853.

94.	**Gomez-Sarrano, V., E. M. Cuerda-Correa, M. C. Fernandez-Gonzalez, M. F. Alexandre-Franco** and **A. Macias-Garcia** (2005) Preparation of activated carbons from walnut wood : A study of microporosity and fractal dimension. *Smart Mater. Struct*., **14**, 363-368.

95. **Gomez-Serrano, V., A. Macias-Garcia, A. Espinosa-Mansilla** and **C. Valenzuela-Calahorro** (1998) Adsorption of mercury, cadmium and lead from aqueous solution on heat treated and sulphurized activated carbon. *Wat. Res*., **32**, 1-4.

96. **Gomez-Serrano, V., J. Pastor-Villegas, C. J. Duran-Valle,** and **C. Valenzuela-Calahorro** (1996) Heat treatment of rockrose char in air. Effect of surface chemistry and porous texture. *Carbon*, **34**, 533-538.

97. **Gomez-Serrano, V., F. Piriz-Almeida, C. J. Duran-Valle** and **J. Pastor-Villegas** (1999) Formation of oxygen structures by air activation. A study by FT – IR spectroscopy. *Carbon*, **37**, 1517-1528.

98. **Gonzalez, J. F., J. M. Encinar, C. M. Gonzalez – Garcia, E. Sabio, A. Ramiro, J. L. Canito** and **J. Ganan** (2006) Preparation of activated carbons from used tyres by gasification with steam and carbon dioxide. *Appl. Surf. Sci.,* **252**, 5999-6004.

99. **Gonzalez, J. C., M. T. Gonzalez, M. Molina-Sabio, F. Rodriguez-Reinoso** and **A. Sepulveda-Escribano** (1995) Porosity of activated carbons prepared from different lignocellulosic materials. *Carbon*, **33**, 1175-1177.

100. **Gonzalez-Vilchez, P., A. Linares-Solano, J. de D. Lopez-Gonzalez and F. Rodriguez-Reinoso** (1979) The controlled reaction of active carbons with air at 350 °C – I : Reactivity and changes in surface area. *Carbon*, **17**, 441-446.

101. **Gregg, S. J.** and **K. S. W. Singh** (1982) Adsorption, Surface Area and Porosity. 2nd edition, Academic Press, London.

102. **Guo, J.** and **A. C. Lua** (2002) Microporous activated carbons prepared from palm shell by thermal activation and their application to sulphur dioxide adsorption. *J. Colloid Interface Sci*., **251**, 242-247.

103. **Guo, Y.** and **D. A. Rockstraw** (2007) Activated carbons prepared from rice hull by one-step phosphoric acid activation. *Microporous Mesoporous Mater*., **100**, 12-19.

104. **Guo, Y.,** and **D. A. Rockstraw** (2007) Physicochemical properties of carbons prepared from pecan shell by phosphoric acid activation. *Bioresour. Technol*., **98**, 1513-1521.

105. **Guo, Y., J. Qi, S. Yang, K. Yu, Z. Wang** and **H. Xu** (2002a) Adsorption of Cr (VI) on micro- and mesoporous rice husk-based active carbon. *Mater. Chem. Physics*, **78**, 132-137.

106. **Guo, Y., S. Yang, K. Yu, J. Zhao, Z. Wang** and **H. Xu** (2002b) The preparation and mechanism studies of rice husk based porous carbon. *Mater. Chem. Physics*, **74**, 320-323.

107. **Guo, Y., S. Yang, W. Fu, J. Qi, R. Li, Z. Wang** and **H. Xu** (2003) Adsorpion of malachite green on micro- and mesoporous rice husk-based active carbon. *Dyes and Pigments*, **56**, 219-229.

108. **Guo, Y., J. Zhao, H. Zhang, S. Yang, J. Qi, Z. Wang,** and **H. Xu** (2005) Use of rice husk-based porous carbon for adsorption of Rhodamine B from aqueous solutions. *Dyes and Pigments*, **66**, 123-128.

109. **Hameed, B. H., A. T. M. Din** and **A. L. Ahmed** (2007) Adsorption of methylene blue onto bamboo-based activated carbon : Kinetics and equilibrium studies. *J. Hazard. Mater*. **141**, 819-825.

110. **Hamnett, A**. (1997) Mechanism and electrocatalysis in the direct methanol fuel cell. *Catal. Today*, **38**, 445-457.

111. **Hassan, S. S. M., N. S. Awwad** and **A. H. A. Aboterika** (2008) Removal of mercury (II) from waste water using camel bone charcoal. *J. Hazard. Mater*., **154**, 992-997.

112. **Hayashi, J., A. Kazehaya, K. Muroyama** and **A. P. Watkinson** (2000) Preparation of acativated carbon from lignin by chemical activation. *Carbon*, **38**, 1873-1878.

113. **Hayashi, H.** and **J. B. Moffat** (1983) Conversion of MeOH into hydrocarbons over ammonium 12-tungstophoshate. *J. Catal*., **83**, 192-204.

114. **Heschel, W.,** and **E. Klose** (1995) On the suitability of agricultural by-products for the manufacture of granular activated carbon. *Fuel,* **74**, 1786-1791.

115. **Hu, Z**., and **E. F. Vansant** (1995) A new composite adsorbent produced by chemical activation of Elutrilithe with zinc chloride. *J. Colloid Interface Sci*., 176, 422-431.

116. **Hu, C., C. Wang, F. Wu** and **R. Tseng** (2007) Characterization of pistachio shell – derived carbons activated by a combination of KOH and CO_2 for electric double – layer capacitors. *Electrochim. Acta*, **52**, 2498-2505.

117. **Huang, C. P.** and **D. W. Blankenship** (1984) The removal of mercury (II) from dilute aqueous solution by activated. *carbon*, **18**, 37-46.

118. **Hubaut, R., J. Altafulla, A. Rives** and **C. Scott** (2007) Characterization and HDS activities of mixed Fe-Mo sulphides on alumina and carbon. *Fuel*, **86**, 743-749.

119. **Huo, Q., D. I. Margolese** and **G. D. Stucky** (1996) Surfactant control of phases in the synthesis of mesoporous silica-based materials. *Chem. Mater*., **8**, 1147-1160.

120. **Inbaraj, B.** and **N. Sulochana** (2006) Mercury adsorption on a carbon sorbent derived from fruit shell of Terminalia catappa. *J. Hazard. Mater*., **B 133**, 283-290.

121. **Inbaraj, B. S., J. S. Wang, J. F. Lu, F. Y. Siao** and **B. H. Chen** (2009) Adsorption of toxic mercury (II) by an extracellular biopolymer poly(γ-glutamic acid). *Bioresour. Technol*., **100**, 200-207.

122. **Ishizaki, C.** and **I. Marti** (1981) Surface oxide structures on a commercial activated carbon. *Carbon*, **19**, 409-412.

123. **Ismadji, S., Y. Sudaryanto, S. B. Hartono, L. E. K. Setiawan** and **A. Ayucitra** (2005) Activated carbon from char obtained from vacuum pyrolysis of teak sawdust : Pore structure development and characterization. *Bioresour. Technol*., **96**, 1364-1369.

124. **Izumi, Y., R. Hasebe** and **K. Urabe** (1983) Catalysis by heterogeneous supported heteropoly acid. *J. Catal.,* **84**, 402-409.

125. **Izumi, Y. and K. Urabe** (1981) Catalysis of heteropoly acids entrapped in activated carbon. *Chem. Lett.*, 663-666.

126. **Jagtoyen, M.** and **F. Derbyshire** (1998) Activated carbons from yellow poplar and white oak by H_3PO_4. *Carbon*, **36**, 1085-1097.

127. **Janik, M. J., R. J. Davis** and **M. Neurock** (2004) A first principle analysis of the location and affinity of protons in the secondary structure of phosphotungstic acid. *J. Phys. Chem. B*., **108,** 12292-12300.

128. **Jasienko-Halat, M.** and **K. Kedzior** (2005) Comparison of molecular sieve properties in microporous chars from low-rank bituminous coal activated by steam and carbon dioxide. *Carbon*, **43**, 944-953.

129. **Ji, Y. B., T. Li, L. Zhu, X. Wang** and **Q. Lin** (2007) Preparation of activated carbons by microwave heating KOH activation. *Appl. Surf. Sci*., **254**, 506-512.

130. **Ji, D., T. Ren, L. Yan** and **J. Suo** (2003) Synthesis of Ti-incorporated SBA-1 cubic mesoporous molecular sieves. *Mater. Lett*., **57**, 4474-4477.

131. **Ji, D., R. Zhao, G. Lv, G. Qian, L. Yan** and **J. Suo** (2005) Direct synthesis, characterization and catalytic performance of Ti-SBA-1 cubic mesoporous molecular sieves. *Appl. Catal., A : Gen*., **281**, 39-45.

132. **Jia, Y., G. Li, G. Ning** and **C. Jin** (2009) The effect of N-containing compounds on oxidative desulphurization of liquid fuel. *Catalysis Today*, **140**, 192-196.

133. **Jogtoyen, M.** and **F. Derbyshire** (1993) Some consideration of the origins of porosity in carbons from chemically activated wood. *Carbon*, **31**, 1185-1192.

134. **Jozefowicz, L. C., H. G. Karge, E. Vasilyeva** and **J. B. Moffat** (1993) A Microcalorimetric investigation of heteropoly acids. *Microporous Mater.*, **1**, 313-322.

135. **Jyotikusum, A., J. N. Sahu, C. R. Mohanty** and **B. V. Meikap** (2009) Removal of lead (II) from waste water by activated carbon developed from tamarind wood by zinc chloride activation. *Chem. Eng. J.,* **149**, 49-62.

136. **Kadirvelu, K., M. Kavipriya, C. Karthika, N. Vennilamani** and **S. Pattabhi** (2004) Mercury (II) adsorption by activated carbon made from sago waste. *Carbon*, **42**, 745-752.

137. **Kalderis, D., D. Koutoulaskis, P. Paraskeva, E. Diamadopoulos, E. Otal, J. O. D. Valle** and **C. Fernandez-Pereira** (2008) Adsorption of polluting substances on activated carbons prepared from rice husk and sugar cane bagasse. *Chem. Eng. J.*, **144**, 42-50.

138. **Kannan, A.** and **S. Thambidurai** (2007) Removal of lead (II) from aqueous solution using palmyra palm fruit seed carbon. *Journal of Environmental, Agricultural and Food Chemistry*, **6**, 1803-1819.

139. **Kannan, A.** and **S. Thambidurai** (2008) Removal of hexavalent chromium from aqueous solution using activated carbon derived from palmyra palm fruit seed. *Bull. Chem. Soc. Ethiopia.*, **22**, 183-196.

140. **Kao, H., C. Ting, A. S. T. Chiang, C. Teng** and **C. Chen** (2005) Facile synthesis of stable cubic mesoporous silica SBA-1 over a broad temperature range with the air of D-fructose. *Chem. Commun.*, 1058-1060.

141. **Karthikeyan, S., G. Bhuvaneswari, S. Malathi, P. Maheswari** and **B. Sivakumar** (2007) Studies on the removal of textile effluents using Ipomoea carnea stem waste activated carbon. *Journal of Indian Council of Chemistry*. **24**, 63-67.

142. **Kastening, B., M. Hahn, B. Rabanus, M. Heins** and **U. Zum Felde** (1997) Electronic properties and double layer of activated carbon, *Electrochem. Acta*, **18**, 2789-2800.

143. **Kayembe, N.** and **A. H. Pulsifer** (1976) Kinetics and catalysis of the reaction of coal char and steam. *Fuel*, **55**, 211-216.

144. **Kazanskii, L. P., E. A. Tarchenkova and V. I. Spitsyn** (1974) Structural principles in the chemistry of heteropoly compounds. *Russian Chem. Rev*., **43**, 1137-1159.

145. **Kazemipour, M., M. Ansari, S. Tajrobehkar, M. Majdzadeh** and **H. R. Kermani** (2008) Removal of lead, cadmium, zinc and copper from industrial wastewater by carbon developed from walnut, hazelnut, almond, pistachio shell and apricot stone. *J. Hazard. Mater*., **150**, 322 -327.

146. **Kim, Y., B. Lee, H. Suezaki, T. Chino, Y. Abe, T. Yanagiura, K. C. Park** and **M. Endo** (2006) Preparation and characterization of bamboo based activated carbons as electrode materials for electric double layer capacitors. *Carbon* **44**, 1592-1616.

147. **Kim, M. J.** and **R. Ryoo** (1999) Synthesis and pore size control of cubic mesoporous silica SBA-1. *Chem. Mater*., **11**, 487-491.

148. **Kinoshita, K.** (1988) Carbon - Electro chemical and physico chemical properties, John Wiley & Sons, New York, p. 32.

149. **Kobya, M., E. Demirbas, E. Senturk** and **M. Ince** (2005) Adsorption of heavy metal ions from aqueous solution by activated carbon prepared from apricot stone. *Bioresour. Technol*., **96**, 1518-1521.

150. **Konishi, Y., K. Sakata, M. Misono** and **Y. Yoneda** (1982) Catalysis by heteropoly compounds IV. Oxidation of methacrolein to methacrylic acid on 12-molybdophosphoric acid. *J. Catal*., **77**, 169-179.

151. **Kopp, O. C., E. L. Fuller, C. R. Sparks, M. R. Rogers** and **M. L. McKinney** (1997) Coal properties and their influence on air activation. *Carbon*, **35**, 1765-1779.

152. **Kozhevnikov, I. V**. (1987) Advances in catalysis by heteropoly acids. *Russian Chem. Rev*., **56**, 811-825.

153. **Kozhevnikov, I. V.** (1995) Heteropoly acids and related compounds as catalysts for fine chemical synthesis. *Catal. Rev. – Sci. Eng*., **37**, 311-352.

154. **Kozhevnikov, I. V**. (1998) Catalysis by heteropoly acids and multicomponent polyoxometalates in liquid-phase reactions. *Chem. Rev.,* **98**, 171-198.

155. **Kozhevnikov, I. V. and K. I. Matveev** (1982) Heteropoly acids in catalysis. *Russian Chemical Reviews*, **51**, 1075-1088.

156. **Kozhevnikov, I. V., A. Sinnema** and **H. V. Bekkum** (1995) Proton sites in Keggin heteropoly acids from ^{17}O NMR. *Catal. Lett.,* **34**, 213-221.

157. **Kozhevnikov, I. V., A. Sinnema, H. V. Bekkum and M. Fournier** (1996) ^{17}O MAS NMR study of 12-molybdophosphoric acid. *Catal. Lett.*, **41**, 153-157.

158. **Kozhevnikov, I. V., A. Sinnema, R. J. J. Jansen and H. V. Bekkum** (1994) ^{17}O NMR determination of proton sites in solid heteropoly acid $H_3PW_{12}O_{40}$. *Mendeleev Communications*, 92-93.

159. **Krishnan, K. A.** and **T. S. Anirudhan** (2002) Removal of mercury (II) from aqueous solutions and chlor-alkali industry effluent by steam activated and sulphurized activated carbon prepared from bagasse pith : Kinetics and equilibrium studies. *J. Hazard. Mater.*, **B 92**, 161-183.

160. **Kruk, M., B. Dufour, E. B. Celer, T. Kowalewski, M. Jaroniec and K. Matyjaszewski** (2005) Synthesis of mesoporous carbons using ordered and disordered mesoporous silica templates and polyacrylonitrile as carbon precursor. *J. Phys. Chem. B*, **109**, 9216-9225.

161. **Kruk, M.** and **M. Jaroniec** (1999) Characterization of high-quality MCM-48 and SBA-1 mesoporous silicas. *Chem. Mater.*, **11**, 2568-2572.

162. **Kubo, S., Y. Uraki** and **Y. Sano** (1989) Preparation of carbon fibers from softwood lignin by atmospheric acetic acid pulping. *Carbon*, **36**, 1119-1124.

163. **Labana, S., G. Pandey** and **R. K. Jain** (2005) Desulphurization of dibenzothiophene and diesel oils by bacteria. *Lett. Appl. Microbiol.,* **40**, 159-163.

164. **Laine, J., A. Calafat** and **M. Labady** (1989) Preparation and characterization of activated carbons from coconut shell impregnated with phosphoric acid. *Carbon*, **27**, 191-195.

165. **Langmuir, I.** (1918) The adsorption of gases on plane surfaces of glass, mica and platinum. *J. Am. Chem. Soc.*, **40**, 1361-1403.

166. **Laszlo, K., A. Bota** and **L. G. Nagy** (1997) Characaterization of activated carbons from waste materials by adsorption from aqueous solutions. *Carbon*, **35**, 593-598.

167. **Lazaro, M. J., M. E. Galvez, S. Artal, J. M. Palacios** and **R. Moliner** (2007) Preparation of steam-activated carbons as catalyst supports. J. Anal. Appl. Pyrolysis, **78**, 301-315.

168. **Lecea, C. S. D.,** and **A. Linares – Solano** (1981) Development of porosity and surface heterogeneity upon air activation of graphitized carbon black. *Carbon*, **19**, 65-70.

169. **Lei, Z., L. An, L. Dang, M. Zhao, J. Shi, S. Bai** and **Y. Cao** (2009) Highly dispersed platinum supported on nitrogen – containing ordered mesoporous carbon for methanol electrooxidation. *Microporous Mesoporous Mater.,* **119**, 30-38.

170. **Lei. Z., S. Bai, Y. Xiao, L. Dang, L. Au, G. Zhang** and **Q. Xu** (2008) CMK 5 mesoporous carbon synthesised via chemical vapour desposition of ferrocene as catalyst support for methanol oxidation. *J. Phys. Chem. C.,* **112**, 722-731.

171. **Lespade, P., R. Al-Jishi and M. S. Dresselhaus** (1982) Model for Raman Scattering from incompletely graphitized carbons. *Carbon*, **20**, 427-431.

172. **Li, W., J. Peng, L. Zhang, K. Yang, H. Xia, S. Zhang** and **S. Guo** (2009) Preparation of activated carbon from coconut shell chars in pilot-scale microwave heating equipment at 60 kW. *Waste Management*, **29**, 756-760.

173. **Li, W., K. Yang, J. Peng, L. Zhang, S. Guo** and **H. Xia** (2008) Effects of carbonization temperatures on characteristics of porosity in coconut shell chars and activated carbons derived from carbonized coconut shell chars. *Industrial Crops and Products*, **28**, 190-198.

174. **Lim, D., W. Lee** and **H. Lee** (2008) Highly dispersed and nano-sized Pt-based electrocatalysts for low-temperature fuel cells. *Catal. Surv. Asia*, **12**, 310-325.

175. **Lin, M. L., C. C. Huang, M. Y. Lo** and **C. Y. Mou** (2008) Well-ordered mesoporous carbon thin film with perpendicular channels : Application to Direct Methanol Fuel Cell. *J. Phys. Chem. C*, **112**, 867-873.

176. **Lin, L., Y. King, J. Yang, D. Shi, K. Xie** and **Y. Zhang** (2007) Scale-up of pervaporation for gasoline desulphurization. *J. Membrane Sci.,* **298**, 1-13.

177. **Lin, L., Y. Kong, K. Xie, F. Lu, R. Liu, L. Guo, S. Shao, J. Yang, D. Shi** and **Y. Zhang** (2008) Polyethylene glycol, polyurethane blend membranes for gasoline desulphurization by pervaporation technique. *Sep. Purif. Technol*., **61**, 293-300.

178. **Liu, Z., J. Y. Lee, W. Chen, M. Han.** and **L. M. Gan** (2004) Physical and electrochemical characterization of microwave – assisted polyol preparation of carbon-support PtRu nanoparticles. *Langmuir* **20**, 181-187.

179. **Liu, Z., X. Y. Ling, X. Su** and **J. Y. Lee** (2004) Carbon – supported Pt and PtRu nanoparticles as catalysts for a direct methanol fuel cell. *J. Phys. Chem. B*., **108**, 8234-8240.

180. **Liu-Cai, F. X., B. Sahut, E. Faydi, A. Auroux** and **G. Herve** (1999) Study of the acidity of carbon supported and unsupported heteropoly acid catalysts by ammonia sorption microcalorimetry. App. Catal., A : Gen., **185**, 75-83.

181. **Loan, M. B., A. Singh, D. C. Rupainwar** and **D. N. Dhar** (2008) Studies on efficiency of gauva (Psidium guajava) bark as bioadsorbent for renoval of Hg (II) from aqueous solutions. *J. Hazard. Mater*., **59**, 626-629.

182. **Loan, M. B., A. Singh, D.C. Rupainwar** and **D. N. Dhar** (2008) Studies on efficiency of gauva (Psidium guajava) bark as bioadsorbent for renoval of Hg (II) from aqueous solutions. *J. Hazard. Mater.*, **59**, 626-629.

183. **Lozano-Castello, D., D. Cazorla-Amoros** and **A. Linares-Solano** (2002) Can highly activated carbon be prepared with a homogeneous micropore size distribution. *Fuel Process. Technol.*, **77**, 325-330.

184. **Lu, A.** and **J. Zheng** (2001) Study of microstructure of high-surface-area polyacrylonitrile activated carbon fibers, *J. Colloid Interface Sci.*, **236**, 369-374.

185. **Lua, A. C.** and **J. Guo** (2000) Activated carbon prepared from oil palm stone by one – step CO_2 activation for gaseous pollutant removal. *Carbon*, **38**, 1089-1097.

186. **Lyubchik, S. B., R. Benoit** and **F. Beguin** (2002) Influence of chemical modification of anthracite on the porosity of the resulting activated carbons. *Carbon*, **40**, 1287-1294.

187. **Ma, X., S. Velu, J. H. Kim** and **C. Song** (2005) Deep desulphurization of gasoline by selective adsorption over solid adsorbents and impact of analytical methods on ppm level sulphur quantification for fuel cell applications. *Appl. Catal. B : Environ.*, **56**, 137-147.

188. **Macedo, J. S., L. Otubo, O. P. Ferreira, I. D. F. Gimenez, I. O. Mazali** and **L. S. Barreto** (2008) Biomorphic activated porous carbons with complex microstructures from lignocellulosic residues. *Microporous Mesoporous Mater.*, **107**, 276-285.

189. **Macia-Agullo, J A, B. C. Moore, D. Cazoria-Amoros** and **A. Linares-Solana** (2007) Influence of carbon fibres crystallinities on their chemical activation by KOH and NaOH. *Microporous Mesoporous Mater.*, **101**, 397-405.

190. **Macias-Garcia, A., M. A., Diaz-Diez, E. M. Cuerda-Correa** and **M. Olivares-Marin** (2006) Study of the pore size distribution and fractal dimension of HNO_3 – activated treated carbons. (2006) *Appl. Surf. Sci.*, **252**, 5972-5975.

191. **Macias-Garcia, a., M. A. Diaz-Diez, V Gomez-Serrano** and **M. C. Fernandez Gonzalez** (2003) Preparation and characterization of activated arbons made up from different woods by chemical activation with H_3PO_4. *Smart Mater. Struct.*, **12**, N24-N28.

192. **Madhava Rao, M., D. H. K. Kumar Reddy, P. Venkateswarlu** and **K. Seshaiah** (2009) Renoval of mercury from aqueous solutions using activated carbon prepared from agricultural by-product/waste. *J. Environ. Manage.*, 90, 634-643.

193. **Madhava Rao, M., A. Ramesh, G. Purna Chandra Rao** and **K. Seshaiah** (2006) Removal of copper and cadmium from the aqueous solutions by activated carbon derived from Ceiba Pentandra hulls. *J. Hazard. Mater.*, **B129**, 123-129.

194. **Mahamad, M. M**. (2007) Textural changes during CO_2 activation of chars : A fractal approach. *Appl. Surf. Sci.*, **253**, 6019-6031.

195. **Makay, D. M.** and **P. V. Roberts** (1982) The dependence of char and carbon yield on lignocellulosic precursor composition. *Carbon*, **20**, 87-94.

196. **Malecka, A., J. Pozniczek, A. Micek-Linicka** and **A. Bielanski** (1999) Gas phase synthesis of MTBE on dodecatungsto silicic acid as the catalyst. *J. Mol. Catal. A: Chem*. **138**, 67-81.

197. **Malik, P. K**. (2004) Dye removal from waste water using activated carbon developed from sawdust : adsorption equilibrium and kinetics. *J. Hazar. Mater.*, **B113**, 81-88.

198. **Mancharan, R.** and **J. B. Goodenough** (1992) Methanol oxidation in acid on ordered NiTi. *J. Mater. Chem.,* **2**, 875-888.

199. **Manivannan, A., M. Chirila, C. N. Giles** and **M. C. Seehra** (1999) Microstructure, dangling bonds and impurities in activated carbon. Carbon, **37**, 1741-1747.

200. **Manoli, J. M., P. D. Costa, M. Brun, M. Vrinat, F. Mauge** and **C. Potvin** (2004) Hydrodesulphurization of 4, 6 – dimethyl dibenzothiophene over promoted (Ni, P) alumina – supported molybdenum carbide catalysts : activity and characterization of active sites. *J. Catal.*, **221**, 365-377.

201. **Marsh, H.** and **F. Rodriguez-Reinoso** (2006) Activated Carbon, Elsevier Science & Technology.

202. **Marsh, J. H.** and **S. W. Orchard** (1992) Voltammetric studies of glassy carbon electrodes activated in air and steam. *Carbon*, **30**, 895-901.

203. **Marsonia, P. J.** and **K. P. Goswami** (1994) Evaluation of Ipomoea carnea as alternate feed stock for the biogas production. *Journal of Energy, Heat and Mass transfer*. **16**, 289-293.

204. **Martin-Gullon, I., J. P. Marco-Lozar, D. Cazorla-Amoros** and **A. Linores-Salano** (2004) Analysis of the microporosity shrinkage upon thermal post-treatment of H_3PO_4 activated carbons. Carbon, **42**, 1339-1343.

205. **McKay, G., H. S. Blair** and **J. R. Gardener** (1982) Adsorption of dyes on chitin I. Equilibrium studies. *J. Appl. Polym. Sci*., 27, 3043-3057.

206. **McKee, W. D**., (1983) Mechanism of the alkalimetal catalysed gasification of carbon. *Fuel*, **62**, 170-175.

207. **McKee, D. W.** and **D. Chatterji** (1978) The catalyzed reaction of graphite with water vapour. *Carbon*, **16**, 53-57.

208. **Meenakshi, G.** and **R. Amutha** (2008) Adsorption of Hg (II) ions from water by activated carbons. *Res. J. Chem. Environ*., **12**, 76-83.

209. **Meng, X., Z. Hua, D. Dermatas, W. Wang** and **H. Y. Kuo** (1998) Immobilization of mercury (II) in contaminated soil with used tire rubber. *J. Hazard. Mater*., **57**, 231-241.

210. **Merzougui, Z.** and **F. Addoun** (2008) Effect of oxidant treatment of date pit activated carbons application to the treatment of water. *Desalination*, **222**, 394-403.

211. **Mie, H., B. W. Mei** and **T. F. Yen** (2003) A new method for obtaining ultra-low sulphur diesel fuel via ultrasound assisted oxidative desulphurization. *Fuel*, **82**, 405-414.

212. **Miguel, G. S., G. D. Fowler** and **C. J. Sollars** (2003) A study of the characteristics of activated carbons produced by steam and carbon dioxide activation of waste tyre rubber. *Carbon*, **41**, 1009-1016.

213. **Misono, M**., Characterization of acidic properties of heteropoly compounds in relation to heterogeneous catalysis. pp. 147-156. In **B. Imelic, C. Naccache, G. Coudurier, Y. Ben Taarit and J. C. Vedrine** (eds.), *Catalysis by Acids and Bases*, Elsevier, Amsterdam, 1985.

214. **Misono, M.,** (1992) Heterogeneous catalysis by heteropoly compounds. An attempt of molecular design of practical solid acid catalysts. *Catal. Lett*., **12**, 63-72.

215. **Misono, M**. (1987) Heterogeneous catalysis by heteropoly compounds of molybdenum and tungsten. *Catal. Rev. – Sci. Eng*., **29**, 269-321.

216. **Misono, M.** (2001) Unique acid catalysis of heteropoly compounds (heteropolyoxometalates) in the solid state. *Chem. Commun*., 1141-1152.

217. **Misono, M.** and **T. Okuhara** (1993) Solid superacid catalysts. *Chem., Tech*., 23-29.

218. **Mochida, I., E. Nakamura, K. Maeda** and **K. Takeshita** (1975) Carbonization of aromatic hydrocarbons – III : Carbonization catalyzed by alkali metals. *Carbon*, **13**, 489-493.

219. **Mochida, I., E. Nakamura, K. Maeda** and **K. Takeshita** (1976) Carbonization of aromatic hydrocarbons – IV : Reaction path of carbonization catalyzed by alkali metals. Carbon, **14**, 123-129.

220. **Moffat, J. B**. (1986) Cation-anion effects in heteropoly compounds with Keggin structures. *Tetrahedron*, **5**, 261-269.

221. **Moffat, J. B.** *Heteropoly compounds : Solid acids with guarded protons*. Pp. 157-166. In **B. Imelic, C. Naccache, G. Coudurier, Y. Ben Taarit and J. C. Vedrine** (eds.), *Catalysis by Acids and Bases*, Elsevier, Amsterdam, 1985.

222. **Moffat,   J.   B**.   (1989)   Implicit   and   explicit   microporosity   in heteropolyoxometalates. *J. Mol. Catal*., **52**, 169-191.

223. **Mohan, D., K. P. Singh** and **V. K. Singh** (2006) Trivalent chromium removal from wastewater using low cost activated carbon derived from agricultural waste material and activated carbon fabric cloth. *J. Hazard. Mater*., **B135**, 280-295.

224. **Mohanty, K., D. Das** and **M. N. Biswas** (2005) Adsorption of phenol from aqueous solutions using activated carbon prepared from Tectona grandis sawdust by $ZnCl_2$ activation. *Chem. Eng. J*., **115**, 121-131.

225. **Mohindar S. S.** and **A. S. Pavlovic** (1993) X-ray diffraction, termal expansion, electrical conductivity and optical microscopy studies of coal-based graphites. *Carbon* **31**, 557-564.

226. **Molina-Sabio, M.** and **F. Rodriguz-Reinoso** (2004) Role of chemical activation in the development of carbon porosity. *Colloids Surf., A: Physicochem. Eng. Aspects*, **241**, 15-25.

227. **Molina-Sabio, M., F. Rodriguez - Reinoso, F. Caturla** and **M. J. Selles** (1995) Porosity in granular carbons activated with phosphoric acid. *Carbon*, **33**, 1105-1113.

228. **Molina-Sabio, M., F. Rodriguez-Reinoso, F. Caturla** and **M. J. Selles** (1996) Development of porosity in combined phosphoric acid – carbon dioxide activation. *Carbon*, **34**, 457-462.

229. **Morey, M. S., A. Davidson** and **G. D. Stucky** (1998) Silica-based, cubic mesostructures : synthesis, characterization and relevance for catalysis. *J. Porous. Mater*., **5**, 195-204.

230. **Mrozowski, S**. (1979) ESR of carbon in the transition range – 1. Carbon, **17**, 227-236.

231. **Nabais, J. V., P. J. M. Carrott, M. M. L. R. Carrott, M. Belchior, D. Boavida, T. Diall,** and **I. Gulyartlu** (2006) Mercury removal from aqueous solution and flow gas by adsorption on activated carbon fibres. *Appl. Surf. Sci.,* **252**, 6046-6052.

232. **Namasivayam, C.** and **K. Kadirvelu** (1999) Uptake of mercury (II) from wastewater by activated carbon from an unwanted agricultural solid by-product : Coir pith. *Carbon*, **37**, 79-84.

233. **Namasivayam, C.** and **D. Sangeetha** (2008) Application of coconut coir pith for the removal of sulfate and other anions from water. *Desalination*, **219**, 1-13.

234. **Nikolopoulos, A. A., A. Kogelbauer, J. G. Goodwin Jr.,** and **G. Marcelin** (1996) Gas phase synthesis of MTBE on triflic-acid modified zeolites. *J. Catal.*, **158**, 76-82.

235. **Ng, F. T. T.** and **I. K. Milad** (2000) Catalytic desulphurization of benzothophene in an emulsion via in situ generated H_2. *Appl. Catal., A : Gen.*, **200**, 243-254.

236. **Ngamcharussrivichai, C., C. Chatratananon, S. Nuntang** and **P. Prasassarakich** (2008) Adsorptive removal of thophene and benzothiophene over zeolites from Mae Moh coal fly ash. *Fuel*, **87**, 2347-2351.

237. **Niu, J. J., J. N. Wang, L. Zhang** and **Y. Shi** (2007) Electro catalytical acitivity on oxidizing hydrogen and methanol of novel carbon nanocages of different pore structures with various platinum loadings. *J. Phys. Chem. C.,* **111**:10329-10335.

238. **Noh, J. S.** and **J. A. Schwarz** (1990) Effect of HNO_3 treatment on the surface acidity of activated carbon. *Carbon*, **28**, 675-682.

239. **Obali, Z.** and **T. Dogn** (2008) Activated carbon – tungstophosphoric acid catalysts for the synthesis of tert – amyl ethyl ether (TAEE). *Chem. Eng. J.,* **138**, 548-555.

240. **Okada, K. N. Yamamoto, Y. Kameshima** and **A. Yasumori** (2003) Porouss properties of activated carbons from waste newspaper prepared by chemical and physical activation. *J Colloid Interface Sci.*, **262**, 179-193.

241. **Olivares-Marin, M., C. Fernandez-Gonzalez, A. Macias-Garcia,** and **V. Gomez-Serrano** (2006) Preparation of activated carbon from cherry stones by chemical activation with $ZnCl_2$. *Appl. Surf. Sci.*, **252**, 5967-5971.

242. **Onal, Y., C. Akmil-Basar and C. Sarici-Ozdemir** (2007) Elucidation of the naproxen sodium adsorption onto activated carbon prepared from waste apricot : Kinetic, equilibrium and thermodynamic characterization. *J. Hazard. Mater.*, **148**, 727-734.

243. **Ono, Y**., Heteropoly acid catalysis – a unique blend of acid – base and redox properties. Pp. 431-463. In **J. M. Thomas and K. Z. Zamarae**v (eds.), *Perspectives in Catalysis*, Blackwell, London, 1992.

244. **Osbaldiston, R. J. C.** and **E. J. Markel** (1994) Thiophene desulfurization by Co/carbon catalyst synthesized by reaction of $Co(C_5H_5)_2$ and the carbon support. *J. Mol. Catal.*, **91**, 91-106.

245. **Otto, K.** and **M. Shelef** (1977) Catalytic steam gasification of graphite : Effects of intercalated and externally added Ru, Rh, Pd and Pt. *Carbon*, **15**, 317-325.

246. **Oubagaranadin, J. U. K., N. Satyamurthy** and **Z. V. P. Murhty (2007)** Evaluation of Fuller's earth for the adsorption of mercury from aqueous solutions : A comparative study with activated carbon. *J. Hazard. Mater.,* **142**, 165-174.

247. **Owen, K**. Introduction, pp. ix-x, Volume 50; In K. Owen (ed.) Critical reports on applied chemistry – gasoline and diesel fuel additives. John Wiley, 1989.

248. **Pandolfo, A. G.** and **A. F. Hollenkamp** (2006) Carbon properties and their role in super capacitors. *J. Power Sources*, **157**, 11-27.

249. **Paredas, J. I., F. Suarez-Garcia, A. Martinez – Alonso** and **J. M. D. Tascon** (2006) A microscopic view of physical and chemical activation in the synthesis of porous carbons. *Langmuir*, **22**, 9730-9739.

250. **Paakkonen, P. K.** and **A. O. I. Krause** (2003) Comparative study of TAME synthesis on ion-exchange resin beads and a fibrous ion-exchange catalyst. *React. Funct. Polym.*, **55**, 139-150.

251. **Pandey, R. A., S. Malhotra, A. S. Rajvaidya, S. Sharma, S. Peshwe, V. K. Raman** and **A. S. Bal** (2004) Chemo-biochemical desulphurization of various gaseous streams on bench scale. *Water, Air and Soil Pollution*, **154**, 1-4.

252. **Parra, D., J. F. Izquierdo, F. Cunill, J. Tejero, C. Fite, M. Iborra** and **M. Vila** (1998) Catalytic activity and deactivation of acidic ion-exchange resins in methyl tert – butyl ether liquid – phase synthesis. *Ind. Eng. Chem. Res.,* **37**, 3575 - 3581.

253. **Pathak A. K.** and **A. Argal** (2007) Analgesic activity of Calotropis gigantea flower. *Fitoterapia,* **78**, 40–42.

254. **Pastor-Villegas, J.** and **C. J. Duran-Valle** (2002) Pore structure of activated carbons prepared by carbon dioxide and steam activation at different temperatures from extracted rock rose. *Carbon*, **40**, 397-402.

255. **Pearson, P. G**. (1988) Absolute electro negativity and hardness : Application to inorganic chemistry. *Inorganic Chem*., **27**, 734-740.

256. **Pinto, S., L. D'Ornelas** and **P. Betancourt** (2008) Synthesis and characterization of vanadium nanoparticles on activated carbon and their catalytic activity in thiophene hydrodesulphurization. *Appl. Surf. Sci.,* **254**, 5390-5393.

257. **Puziy, A. M., O. I. Poddubnaya, A. Martinez-Alonso, F. Suarez-Garcia** and **J. M. D. Tascon** (2002) Characterization of synthetic carbons activated with phosphoric acid. *Appl. Surf. Sci*., **200**, 196-202.

258. **Puziy, A. M., O. I. Poddubnaya, A. Martinez-Alonso, F. Suarez-Garcia** and **J. M. D. Tascon** (2003) Synthetic carbons activated with phosphoric acid III. Carbons prepared in air. *Carbon*, **41**, 1181-1191.

259. **Puziy, A. M., O. I. Poddubnaya, A. Martinez-Alonso, F. Suarez-Garcia** and **J. M. D. Tascon** (2005) Surface chemistry of phosphorus – containing carbons of lignocellulosic origin. *Carbon*, **43**, 2857-2868.

260. **Puziy, A. M., O. I. Poddubnaya, B. Gawdzik, M. Sobiesiak** and **M. M. Tsyba** (2007) Phosphoric acid activation – Functionalization and porosity modification. *Appl. Surf. Sci*., **253**, 5736-5740.

261. **Qian, Q., M. Machida,** and **H. Tatsumoto** (2007) Preparation of activated carbons from cattle-manure compost by zinc chloride activation. *Bioresour. Technol*., **98**, 353-360.

262. **Qingrong, Q., M. Motoi,** and **T. Hideki** (2007) Preparation of activated carbons from cattle manure compost by zinc chloride activation. *Bioresour. Technol*., **98**, 353-360.

263. **Rahman, I. A.** and **B. Saad** (2003) Utilization of guava seeds as a source of activated carbon for removal of methylene blue from aqueous solution. *Malaysian J. Chem*., 5, 008-014.

264. **Rahman, I. A., B. Saad, S. Shaidan** and **E. S. S. Rizal** (2005) Adsorption characteristics of malachite green on activated carbon derived from rice husks produced by chemical-thermal process. *Bioresour. Technol*., **96**, 1578-1583.

265. **Rajesh, B.** (2002) Methanol oxidation anodes based on conducting polymers and carbon nanotubes supported noble metal (s) for possible applications in DMFC, Ph. D., Thesis, Indian Institute of Technology Madras.

266. **Ramakrishna, T. V., G. Aravamudan** and **M. Vijayakumar** (1976) Spectrophotometric determination of mercury (II) as the ternary complex with rhodamine 6G and iodine. *Anal. Chim. Acta*, **84**, 369-375.

267 **Ranganathan, K.,** and **N. Balasubramanian** (2002) Testing of sulfide loaded activated carbon for uptake of Hg (II) from aqueous solution. *Engineering in life sciences*, **2**, 127-129.

268. **Reddy, K. O., B. R. Guduri** and **A. Varadarajulu** (2009) Structural characterization and tensile properties of Borassus fruit fiber. *J. Appl. Polymer Sci.*, **114**, 603-611.

269. **Ren B, X. Q. Li, C. X. She, D. Y. Wu** and **Z. Q. Tian** (2000) Surface Raman spectroscopy as a versatile technique to study methanol oxidation on rouge Pt electrodes. *Electrochim. Acta.*, **46**, 193-205.

270. **Rheinberg, O. V., K. Lucka, H. Kohne, T. Schade** and **J. T. Andersson** (2008) Selective removal of sulphur in liquid fuels for fuel cell applications. *Fuel*, **87**, 2988-2996.

271. **Rials, T. G.** and **W. G. Glasser** (1989) Multiphase materials with lignin. IV. Blends of hydroxypropyl cellulose with lignin. J. *Appl. Polym. Sci.*, **37**, 2399-2415.

272. **Rocha, J. D., A. R. Coutinho** and **C. A. Luengo** (2002) Biopitch produced from Eucalyptus wood pyrolysis liquids as a renewable binder for carbon electrode manufacture. *Braz. J. Chem. Eng.*, **19**, 127-132.

273. **Rodriguez, G., A. Lama, R. Rodriguez, A. Jimenez, R. Guillen** and **J. Fernandez – Bolanos** (2008) olive stone an attractive source of bioactive and valuable componds. *Bioresour. Technol.*, **99**, 5261-5269.

274. **Rodriguez-Reinoso, F., J. D. D. Lopez - Gonzalez** and **C. Berenguer** (1982) Activated carbons from almond shells – I : Preparation and characterization by nitrogen adsorption. *Carbon*, **20**, 513-518.

275. **Ruland, W**. (1990) Carbon Fibers. *Adv Mater.*, **2**, 528-536.

276. **Ruland, W.** and **B. Smarsly** (2002) X-ray scattering of non-graphitic carbon: an improved method of evaluation. *J Appl Crystallogr.*, **35**, 624-33.

277. **Salvador, F., M. Jesus Sanchez-Montero, J. Montero** and **C. Izquierdo** (2008) Activated carbon fibers prepared from a phenolic fiber by super critical water and steam activation. *J. Phys. Chem. C*, **112**, 20057-20064.

278. **Samant, P. V., C. M. Rangel, M. H. Romero, J. B. Fernandes** and **J. L. Figueiredo** (2005) Carbon supports for methanol oxidation catalyst. *J. Power Sources*, **151**, 79-84.

279. **Sanchez, A. R., A. A. Elguezabal** and **L. D. L. T. Saenz** (2001) CO_2 activation of char from Quercus agrifolia wood waste. *Carbon*, **39**, 1367-1377.

280. **Sano, Y., K. Choi, Y. Korai** and **I. Mochida** (2004) Adsorptive removal of sulphur and nitrogen species from a straight run gas oil over activated carbon for its deep hydrodesulphurization. *Appl. Catal., B : Environ.*, **49**, 219-225.

281. **Sano, Y., K. Sugahara, K. Choi, Y. Korai** and **I. Mochida** (2005) Two-step adsorption process for deep desulphurization of diesel oil. *Fuel*, **84**, 903-910.

282. **Saraswathi, K., K. V. Lakshmi** and **P. Prameela** (1997) Semi-automatic determination of elemental sulphur in rubber. *J. Automatic Chem.*, **19**, 153-158.

283. **Sarathi, R., P. Rajesh Kumar** and **R. H. Sahu** (2007) Analysis of surface degradation of epoxy nanocomposite due to tracking under AC and DC voltages. *Polymer Degradation and Stability*, **92**, 560-568.

284. **Sarkar, S.** and **B. Adhikari** (2001) Synthesis and characterization of lignin – HTPB copolyurethane. *Eur. Polym. J.*, **37**, 1391-1401.

285. **Savithramma N,, Ch. Sulochana** and **K.N. Rao** (2007) Ethnobotanical survey of plants used to treat asthma in Andhra Pradesh, *India. J. Ethnopharmacol*, **113**,54-61.

286. **Schwegler, M. A., P. Vinke, M. V. Eijk** and **H. V. Bekkum** (1992) Activated carbon as a support for heteropoly anion catalysts. *Appl. Catal., A : Gen.*, **180**, 41-57.

287. **Selvavathi, V., V. Chidambaram, A. Meenakshisundaram, B. Sairam** and **B. Sivasankar** (2009) Adsorptive desulphurization of diesel on activated carbon and nickel supported systems. *Catal. Today*, **141**, 99-102.

288. **Sevilla, M., C. Sanches , T. Valdos-Sols, E. Morallon** and **A. B. Fuertes** (2007) Synthesis of graphitic carbon nanostructures from sawdust and their application as electrocatalyst supports. *J. Phys. Chem. C,* **111**, 9749-9756.

289. **Sentorun-Shalaby, C., M. G. Ucak-Astarhoglu, L. Artok** and **C. Sarici** (2006) Preparation and characterization of activated carbons by one-step steam pyrolysis/activation from apricot stones. *Microporous Mesoporous Mater.*, **88**, 126-134.

290. **Shen, Z.** and **R. Xue** (2003) Preparation of activated mesocarbon microbeads with high mesopore content. *Fuel Process. Technol*., **84**, 95-103.

291. **Shim, J., S. Park** and **S. Ryu** (2001) Effect of modification with HNO_3 and NaOH on metal adsorption by pitch-based activated carbon fibers. *Carbon*, **39**, 1635-1642.

292. **Shukala, R. N., S. P. Sharma** and **R. M. Shrivastava** (1991) Studies on chemical analysis and papermaking of Ipomea carnea Jacq., *Vijnana Parishad Anusandhan Patrika*. **34**, 115-125.

293. **Shobha R. S.**, **K. Govind**, **B. Biju**, **S. Chandan**, **S. Manmohan** (2007) Pregnancy interceptive activity of the roots of Calotropis gigantea Linn. in rats. *Contraception*, **75**, 318–322.

294. **Singer, L. S.** and **G. Wagoner** (1968) Linewidth and relaxation in the conduction electron spin resonance of polycrystalline graphite. *Carbon*, **6**, 199-241.

295. **Singh, J** and **K. Jain** (2002) Biomethanation of fresh and dry leaves of Ipomoea carnea. *Journal of Ecophysiology and Occupational Health*. **2**, 255-264.

296. **Skodras, G., Ir. Diamantopoulou, G. Pantoleontos** and **G. P. Sakellaropoulos** (2008) Kinetic studies of elemental mercury adsorption in activated carbon fixed bed reactor. *J. Hazard., Mater*., **158**, 1-13.

297. **Sobkowski, J., K. Franaszczuk** and **K. Dobrowolska** (1992) Effect of anions and pH on the adsorption and oxidation of methanol on a platinum electrode. *J. Electroanal. Chem*., **330**, 529-540.

298. **Soleimani, M.** and **T. Kaghazchi** (2008a) Activated hard shell of apricot stones : A promising adsorbent in gold recovery. *Chin. J. Chem. Eng*., **16**, 112-118.

299. **Soleimani, M.** and **T. Kaghazchi** (2008b) Adsorption of gold ions from industrial waste water using activated carbon derived from hardshell of apricot stones – an agricultural waste. *Bioresour. Technol*., **99**, 5374-5383.

300. **Solum, M. S., R. J. Pugmire, M. Jagtoyen** and **F. Derbyshire** (1995) Evolution of carbon structure in chemically activated wood. *Carbon*, **33**, 1247-1254.

301. **Sonia, A. C., Carabineiro** and **D. T. Thompson** (2007) Catalytic Applications of Gold Nanotechnology in Nanoscience and Technology, Nanocatalysis, U. Heiz, U. Landman (Eds.), Springer-Verlag, Berlin Heidelberg, p. 463.

302. **Sotelo, J. L., M. A. Uguina** and **V. I. Agueda** (2007) Fixed bed adsorption of benzothiophene over zeolites with faujasite structure. *Adsorption*, **13**, 331-339.

303. **Srilatha, C. H., N. R. G. Naidu** and **P. R. Rao** (1997) Pathology of Ipomoea carnea toxicity in goats. *Indian Journal of Animal Sciences*, **67**, 253-254.

304. **Stephen, B., S. D. Lola, W. D. Edwards** and **T. Edward** (1940) On a theory of the van der Waals adsorption of gases. *J. Am. Chem. Soc.,* **62**, 1723-1732.

305. **Stoeckli, H. F**. (1990) Microporous carbons and their characterization : The present state of the art. *Carbon*, **28**, 1-6.

306. **Suarez-Garcia, F., A. Martinez-Alonso** and **J. M. D. Tascon** (2002) Pyrolysis of apple pulp : Chemical activation with phosphoric acid. *J. Anal. Appl. Pyrolysis*, **63**, 283-301.

307. **Suresh, B. V.** and **M. S. Seehra** (1996) Modeling of disorder and X-ray diffraction in coal based graphitic carbons. *Carbon*, **34**, 1259-1265.

308. **Suarez-Garcia, F., A. Martinez-Alonso** and **J. M. D. Tascon** (2002) Pyrolysis of apple pulp : Effect of operation conditions and chemical additives. *J. Anal. Appl. Pyrolysis*, **62**, 93-103.

309. **Susan E**, **S. Shraddha**, **T. Vidya**, **C.P. Kaushik**, **R. Kanwar** and **S.F. D'Souza** (2006) Phytoremediation of radiostrontium (^{90}Sr) and radiocesium (^{137}Cs) using giant milky weed (Calotropis gigantea R. Br.) plants. *Chemosphere*, **65**, 2071-2073.

310. **Syna, N.** and **M. Valix** (2003) Assessing the potential of activated bagasse as gold adsorbent for gold-thiourea. *Miner. Eng.,* **16**, 511-518.

311. **Taarit and J. C. Vedrine** (eds.), *Catalysis by Acids and Bases*, Elsevier, Amsterdam, 1985.

312. **Taguchi, A.** and **F. Schuth** (2005) Ordered mesoporous materials in catalysis. *Microporous Mesoporous Mater.*, **77**, 1-45.

313. **Tancredi, N. T. Cordero, J. Rodriguez-Mirosol** and **J. J. Rodriguez** (1996) Activated carbon from Uruguayan eucalyptus wood. *Fuel*, **75**, 1701-1706.

314. **Tang, M. M.** and **R. Bacon** (1964) Carbonization of cellulose fibers-1. Low temperature pyrolysis. *Carbon*, **2**, 211-214.

315. **Teng, H., J. A. Ho** and **Y. F. Hsu** (1997) Preparation of activated carbon from bituminous coals with CO_2 activation – Influence of coal oxidation. *Carbon*, **35**, 275 -283.

316. **Thouvenot, R., M. Fournier and C. Rocchiccioli-Deltcheff** (1991) Catalysis by polyoxometalates : Part 2 – ^{29}Si Nuclear magnetic resonance : Evidence for 12-molybdosilicate in silica supported molybdenum catalysts. *J. Chem. Soc. Faraday Trans.*, **87**, 2829-2935.

317. **Timothy R. G.** and **W. G. Glasser** (1989) Multiphase materials with lignin. IV. Blends of hydroxyl propyl cellulose with lignin. *J. Appl. Polym. Sci.*, **37**, 2399-2415.

318. **Toles, C. A., W. E. Marshall** and **M. M. Johns** (1999) Surface functional groups on acid-activated nutshell carbons. *Carbon*, **37**, 1207-1214.

319. **Tonini, P. E. D. R., D. A. Gauvin, R. W. Soffel** and **W. P. Freeman** (2003) Achieving low mercury concentration in chlor-alkali waste waters. *Environ. Prog.*, **22**, 167-173.

320. **Torrgrosa, R.** and **J. M. Martin-Martinez** (1991) Activation of lignocellulosic materials : A comparison between chemical, physical and combined activation in terms of porous texture. *Fuel*, **70**, 1173-1180.

321. **Toteva, V., A. Georgiev** and **L. Topalova** (2009) Oxidative desulhurization of light cycle oil : Monitoring by FT – IR spectroscopy. *Fuel Process. Technol.,* **90**, 965-970.

322. **Tsai, W. T., C. Y. Chang** and **S. L. Lee** (1998) A low cost adsorbent from agricultural waste corn cob by zinc chloride activation. *Bioresour. Technol.*, **64**, 211-217.

323. **Tsai, W. T., C. Y. Chang, S. Y.Wang, C. F. Chang, S. F. Chien** and **H. F. Sun** (2001) Preparation of activated carbons from corn cob catalyzed by potassium salts and subsequent gasification with CO_2. *Bioresour. Technol.,* **78**, 203-208.

324. **Tseng, R.** (2007) Physical and chemical properties and adsorption type of activated carbon prepared from plum kernels by NaOH activation. *J. Hazard. Mater.,* **147**, 1020-1027.

325. **Tseng, R.** and **S. Tseng** (2006) Characterization and use of high surface area activated carbons prepared from cane pith for liquid-phase adsorption. *J. Hazard. Mater.*, **B 136**, 671-680.

326. **Tuntawiroon, N.**, **P. Samootsakorn** and **G. Theeraraj** (1984) The environmental implications of the use of calotropis gigantea as a textile fabric. *Agri Ecosystem Environ.*, **11,** 203-212.

327. **Turmuzi, M., W. R. W. Daud, S. M. Tasirin, M. S. Takriff** and **S. E. Iyuke** (2004) Production of activated carbon from candlenut shell by CO_2 activation. *Carbon*, **42**, 453 – 455.

328. **Ugurlu, M., A. Gurses** and **M. Acikyildiz** (2008) Comparison of textile dyeing effluent adsorption on commercial activated carbon and activated carbon prepared from olive stone by $ZnCl_2$ activation. *Microporous Mesoporous Mater*., **111**, 228-235.

329. **Ukkirapandian, V., V. Sadasivam** and **B. Sivasankar** (2008) Oxidation of dibenzothiophene and desulphurization of diesel. *Pet. Sci. Technol.,* **26**, 423-435.

330. **Usmani, T. H., T. W. Ahmed** and **A. H. K. Yousufzai** (1994) Preparation and liquid-phase characterization of granular activated carbon from rice husk. *Bioresour. Technol*., **48**, 31-35.

331. **Valix, M., W. H. Cheung** and **K. Zhang** (2008) Role of chemical pre-treatment in the development of super-high surface areas and hetero atom fixation in activated carbons prepared from bagasse. *Microporous and Mesoporous Materials*. **116**, 513-523.

332. **Vaughan, T., C. W. Seo** and **W. E. Marshall** (2001) Removal of selected metal ions from aqueous solution using modified corncobs. *Bioresour. Technol*., **78**, 133-139.

333. **Vecht, A., D. A Davies** and **D. Smith** (1998) A novel method for the prepration of sulfindes and selenides and its applications for phosphor synthesis. *Mater. Res. Innovations*, **2**, 176-180.

334. **Viboon S., P. Chiravoot, A. Duangdao** and **A. Duangduen** (2008) Preparation and characterization of activated carbon from the pyrolysis of physic nut (Jatropha Curcas L.) waste. *Energy and Fuels*, **22**, 31-37.

335. **Vinke, P., M. V. D. Eijk, M. Verbree, A. F. Voskamp** and **H. Van Bekkum** (1994) Modification of the surfaces of a gas activated carbon and a chemically activated carbon with nitric acid, hypochlorite and ammonia. *Carbon*, **32**, 675-686.

336. **Vinu, A., T. Krithiga, N. Gokulakrishnan, P. Srinivasu, S. Anandan, K. Ariga, V. Murugesan, V. V. Balasubramanian** and **T. Mori** (2007) Halogen-free acylation of toluene over Fe-SBA-1 molecular sieves. *Microporous Mesoporous Mater*., **100**, 87-94.

337. **Viswanathan, B.** (2009) Architecture of carbon support for Pt anodes in direct methanol fuel cells. *Catal. Today*, **141**, 52-55.

338. **Viswanathan, B.** and **M. Aulice Scibioh** (2006) Fuel Cells: Principles and Applications, Universities Press.

339 **Viswanathan, B., M. J. Omana** and **T. K. Varadarajan** (1989) Acidity of heteropoly compounds from XPS measurements. *Catal. Lett*., **3**, 217-221.

340. **Wang, S., Y. Tzon, Y. Lu** and **G. Sheng** (2007) Removal of 3-chlorophenol from water using rice-straw-based carbon. *J. Hazar. Mater*., **147**, 313-318.

341. **Wang, H. J., H. Yu, F. Peng** and **P. Lv** (2006) Methanol electrocatalytic oxidation on highly dispersed Pt/sulfomated - carbon nanotube catalysts. *Electrochem. Commun*., **8**, 499-504.

342. **Wang, X., N. Zhu** and **B.Yin** (2008) Preparation of sludge-based activated carbon and its applications in dye waste water treatment. *J. Hazard. Mater*., **153**, 22-27.

343. **West, A. R**. (1984) Solid State Chemistry and its Applications, Wiley, Chichester, p. 734.

344. **Wu, F.** and **R. Tseng** (2006) Preparation of highly porous carbon from fir wood by KOH etching and CO_2 gasification for adsorption of dyes and phenols form water. *J. Colloid Interface Sci*., **294**, 21-30.

345. **Wu, G.** and **B. Q. Xu** (2007) Carbon nanotube supported Pt electrodes for methanol oxidation : A comparison between multi - and single - walled carbon nanotubes. *J Power Sources,* **174**, 148-158.

346. **Yaji, H. J. Baosheng, Z. Zhaoping, Z. Wenqi** and **X. Rui** (2008) Characteristics and mercury adsorption of activated carbon produced by CO_2 activation of chicken waste. *J. Environ. Sci.*, **20**, 291-296.

347. **Yamashita, Y.** and **K. Ouchi** (1982) Influence of alkali on the carbonization process – III : Dependence on type of alkali and alkali earth compounds. *Carbon*, **20**, 55-58.

348. **Yang, T.** and **A. C. Lua** (2003) Characteristics of activated carbons prepared from pistachio-nut shells by physical activation. *J. Colloid Interface Sci*., **267**, 408-417.

349. **Yang, T**. and **A. C. Lua** (2006) Textural and chemical properties of zinc chloride activated carbons prepared from pistachio-nut shells. *Mater. Chem. Phys*., **100**, 438-444.

350. **Yoshikawa, M., F. Xu, T. Morikawa, Y. Pongpiriyadacha, S. Nakamura, Y. Asao, A. Kumahara** and **H. Matsuda** (2007) Medicinal flowers XII. New spirostane – type steroid saponius with antidiabetogenic activity from Borassus flabellifera. *Chemical and Pharmaceutical Bulletin*, **55**, 308-316.

351. **Yu, G., S. Lu, H. Chen** and **Z. Zhu** (2005) Diesel fuel desulphurization with hydrogen peroxide promoted by formic acid and catalyzed by activated carbon. *Carbon*, **43**, 2285-2294.

352. **Yu, C., J. S. Qiu, Y. F. Sun, X. H. Li, G. Chen** and **B. Zhao** (2008) Adsorption removal of thiophene and dibenzothiophene from oils with activated carbons as adsorbent : effect of surface chemistry. *J. Porous. Mater.*, **15**, 151-157.

353. **Yun, C. H., Y. H. Park** and **C. R. Park** (2001) Effects of pre-carbonization on porosity development of activated carbons from rice straw. *Carbon*, **39**, 559-567.

354. **Zabaniotou, A., P. Madau, P. D. Oudenne, C. G. Jung, M. P. Delplancke** and **A. Fontana** (2004) Active carbon production from used tire in two-stage procedure : industrial pyrolysis and bench scale activation with $H_2O – CO_2$ mixture. *J. Anal. Appl. Pyrolysis*, **72**, 289-297.

355. **Zhang, F., H. Ma, J. Chen, G. Li, Y. Zhang** and **J. Chen** (2008) Preparation and gas storage of high surface area microporous carbon derived from biomass source cornstalks. *Bioresour. Technol.*, **99**, 4803-4808.

356. **Zhang, F. S.** and **H. Itoh** (2003) Adsorbents made from waste ashes and post – consumer PET and their potential utilization in waste water treatment. *J. Hazard. Mater.*, **B 101**, 323-337.

357. **Zhang, F., J. O. Nriagu** and **H. Itoh** (2005) Mercury removal from water using activated carbons derived from organic sewage slude. *Wat. Res.*, **39**, 389-395.

358. **Zhang, Z. Y., T. B. Shi, C. Z. Jai, W. J. Ji, Y. Chen** and **M. Y. He** (2008) Adsorptive removal of aromatic organosulphur compounds over the modified Na-Y zeolites. *Appl. Catal., B. Environ.*, **82**, 1-10.

359. **Zhang, T., W. P. Walawander, L. T. Fan, M. Fan, D. Daugaard** and **R. C. Brown** (2004) Preparation of activated carbon from forest and agricultural residues through CO_2 activation. *Chem. Eng. J.*, **105**, 53-59.

360. **Zhao, N., N. J. Li, Z. Qiao, J. Cui** and **F. He** (2005) Surface properties of chemically modified activated carbons for adsorption rate of Cr (VI). *Chem. Eng. J.*, **115**, 133-138.

361. **Zhao, D., R. Liu, J. Wang** and **B. Liu** (2008) Photochemical oxidation – ionic liquid extraction coupling technique in deep desulphurization of light oil. *Energy Fuels*, **22**, 1100-1103.

362. **Zhao, X.** and **X. Wang** (2006) Synthesis, characterization and catalytic applications of Cr-SBA-1 mesoporous molecular sieves. *J. Mol. Catal., A : Chem.*, **261**, 225-231.

363. **Zheng, S., J. Hu, L. S. Zhong, L. J. Wan** and **W. G. Song** (2007) In situ one-step method for preparing carbon nanotubes and Pt composite catalysts and their performance for MeOH oxidation. *J. Phys. Chem., C* **111**, 11174-11179.

364. **Zhuo, O., R. M. Fleming, D. W. Murphy, C. H. Chen, R. C. Haddon, A. P. Ramirez,** and **S. H. Gharum** (1994) Defects in carbon nanostructures. *Science*, **263**, 1744-1747.

LIST OF PUBLICATIONS BASED ON RESEARCH WORK

I REFEREED JOURNALS

1. **B. Viswanathan, P. Indra Neel** and **T. K. Varadarajan** (2009) Development of carbon materials for energy and environmental applications, *Catalysis Surveys from Asia*, **13**, 164-183.

2. **B. Viswanathan, P. Indra Neel** and **T. K. Varadarajan** (2009) The role of activating agents in the preparation of carbon materials, Indian Journal of Chemistry Section A (communicated).

II PATENT

1. **B. Viswanathan, T. K. Varadarajan** and **P. Indra Neel** (2008) A process for the preparation of activated carbon from botanical sources, Indian Patent IN 2007CH00376 A 20081128, 2008.

III NATIONAL/INTERNATIONAL CONFERENCE

1. **P. Indra Neel, B. Viswanathan** and **T. K. Varadarajan** (2005) Preparation, characterization and evaluation of catalytic activity of dodeca tungsto phosphoric acid (HPW) and dodeca tungsto silicic acid (HSiW) supported on SBA-1 mesoporous silica, 17th National Symposium on Catalysis, 18-20th January, 2005, CSMCRI, Bhavnagar, Gujarat, India.

2. **P. Indra Neel, B. Viswanathan** and **T. K. Varadarajan** (2005) Spectroscopic analysis of supported heteropoly acid catalysts, International Conference on Spectrophysics, INCONS-2005, 9-12th February, 2005, Pachaiyappa's college, Chennai, Tamil Nadu, India

3. **P. Indra Neel, B. Viswanathan** and **T. K. Varadarajan** (2005) Nanoclusters of polyoxometalates dispersed on SBA-1 mesoporous silica for the production of gasoline additives, National Symposium and Conference on Solid State Chemistry, ISCAS-2005, 1-3rd December, 2005, University of Goa, Goa, India.

4. **P. Indra Neel, B. Viswanathan** and **T. K. Varadarajan** (2007) Hydrogenation behaviour of W/C systems, 18th National Symposium on Catalysis, 16-18th April, 2007, IIP Dehradun, India.

CURRICULUM VITAE

1. NAME   : PULIDINDI INDRA NEEL

2. ADDRESS   : Research Scholar
National Centre for Catalysis Research
Department of Chemistry
Indian Institute of Technology Madras
Email: indraneelp@rediffmail.com

3 DATE OF BIRTH   : 08-08-1980

4 EDUCATIONAL QUALIFICATIONS

1997-2000   Bachelor of Science

                     Institution   : Government College, Rajahmundry

2000-2002   Master of Science

                     Institution   : Andhra University, Visakhapatnam

                     Specialization   : Nuclear Chemistry

Doctor of Philosophy (Ph.D.)

                     Institution   : Indian Institute of Technology Madras

                     Registration Date : 29-07-2002

DOCTORAL COMMITTEE

CHAIR PERSON   :   **Prof. R. Dhamodharan**

Head, Department of Chemistry

Indian Institute of Technology Madras

GUIDE   :   **Prof. T. K. Varadarajan**

Department of Chemistry

Indian Institute of Technology Madras

MEMBERS   :   **Prof. M. V. Sangaranarayanan**

Department of Chemistry

Indian Institute of Technology Madras

Prof. U. V. Varadaraju

Department of Chemistry

Indian Institute of Technology Madras

Prof. K. Vidyasagar

Department of Chemistry

Indian Institute of Technology Madras

Prof. V. Sankaranarayanan

Department of Physics

Indian Institute of Technology Madras